Extreme Floods in Switzerland

Hydrological scenarios for large catchments

Daniel Viviroli · Maria Staudinger · Martina Kauzlaric

Zürich, 18.11.2025

Universität Zürich[UZH]

Universität Bern

Commissioned by the Federal Office for the Environment (FOEN) and the Swiss Federal Office of Energy (SFOE)

Extreme Floods in Switzerland

Hydrological scenarios for large catchments

Daniel Viviroli · Maria Staudinger · Martina Kauzlaric

Date	18.11.2025
Commissioned by	Federal Office for the Environment (FOEN) Swiss Federal Office of Energy (SFOE)
Contractor	Department of Geography, University of Zurich Institute of Geography, University of Bern
Authors	Martina Kauzlaric, University of Bern Maria Staudinger, University of Zurich Daniel Viviroli, University of Zurich
FOEN / SFOE support	Emmanuel Brocard, FOEN Alexandre Pachoud, SFOE
Cover image	Reuss at Gebenstorf / Windisch, 23.08.2005 Bildarchiv ETH-Bibliothek Zürich, doi:10.3932/ethz-a-001308389
Suggested citation	Viviroli D, Staudinger M, Kauzlaric M, 2025. Extreme Floods in Switzerland: Hydrological scenarios for large catchments. Project report commissioned by the Federal Office for the Environment (FOEN) and the Swiss Federal Office of Energy (SFOE). Department of Geography, University of Zürich, and Institute of Geography, University of Bern.

Universität Zürich[UZH]

UNIVERSITÄT BERN

Executive summary

Flood estimates are critically important for a wide range of applications, including hazard mapping, hydraulic engineering and safety assessments of critical infrastructure. They are essential for preventing human and economic damage and for designing safe and cost-effective hydraulic structures. However, several challenges complicate flood estimation, primarily due to the comparatively short length of discharge observations at a site of interest or, in many cases, the complete absence of discharge data for direct extrapolation.

The project on Extreme floods in Switzerland (EXCH) addresses these challenges and targets hydrometeorological fundamentals for catchments across all of hydrological Switzerland. EXCH is a follow-up to the Extreme flood events on the River Aare (EXAR) project and further develops methods established in EXAR. Although the project name may suggest otherwise, the flood estimates achieved in EXCH (and also in EXAR) are valuable across a wide range of return periods, ranging from floods with recurrence intervals in the range of 10 to a few 100 years to exceedingly rare and extreme floods with recurrence intervals in the order of 1 000 to 10 000 years.

For methodological reasons, it is not possible to follow one single approach consistently across all relevant scales. Instead, the work had to be divided into two modules: one focusing on “large” catchments (greater than ~1 000 km^2) and another focusing on “small” (~10 to 1 000 km^2) and “very small” (~1 to 10 km^2) catchments. In the transition area between the two modules, discontinuities in the results are expected, as the currently available methods do not allow for seamless processing across all scales being considered.

For the large catchments addressed in this report, the focus is on sub-catchments of Switzerland’s main river basins, similar to the sub-catchments considered in EXAR for the Aare River. Specifically, a total of 60 output sites are covered, with a scale range of approximately 920 to 35 900 km^2. Of these sites, 24 are weirs under the supervision of the Swiss Federal Office of Energy (SFOE), while the remaining 36 concern gauging sites operated by the Federal Office for the Environment (FOEN), with some overlap between the weir and gauging sites.

EXCH follows a continuous simulation approach, employing simulations with a hydrometeorological model chain that in the case of large catchments consists of three links. In a first step, hourly scenarios of precipitation and temperature with a total aggregated length of 300 000 years are generated with the weather generator GWEX. The parameters of GWEX are fitted to data from the period 1930–2019. An alternative weather generator SCAMP as well as reforecast data are explored as alternatives. In a second step, the weather scenarios are forcing the bucket-type catchment model HBV for 330 sub-catchments covering all of hydrological Switzerland. Disaggregated weather observations 1931–2019 are forcing HBV for a control simulation. In a third step, HBV simulations for the individual sub-catchments were combined with hydrological routing using the RS Minerve model. The immediate hydrological results encompass 300 000 years of continuous discharge hydrographs at an hourly time-step for each site. These simulated hydrographs can be analysed similarly to observed hydrographs and are used in this project to derive exceedance curves of annual peak discharge. No further extrapolation is necessary at this stage, as extrapolation was already performed for precipitation and temperature in weather generation. The scope of the results, primarily determined by the configuration of the weather generator, applies to catchments with an area of more than roughly 1 000 km^2, and return periods of up to roughly 10 000 years. All results apply to current conditions, whereas climate change and future river engineering projects are deliberately not accounted for in this project.

The results of the control simulation with observed weather show good to very good agreement of observed and simulated flood peaks for many sites. The validity of the approach is demonstrated for floods with return periods of approximately 100 to 300 years, where assessments against observations (and their extrapolations) are possible. Some deviations from the observed behaviour can be attributed to hydraulic engineering changes during the observation period. These changes are not yet fully reflected in the discharge observations, but are implemented in the model chain in their current state. Some of the output sites examined have a catchment area smaller than 1 000 km^2, and underestimations are indeed noted in some of these cases due to the weather generator approaches used.

The long continuous simulations on the basis of weather scenarios also show good agreement with observations as well as with control simulations. Disagreement is, however, possible and no reason for dismissing the long continuous simulations, which sample the possible hydrometeorological behaviour of a catchment differently – and far more comprehensively – than discharge observations. Also, the extrapolation via meteorology (time series of precipitation and temperature) rather than via hydrology (time series of discharge) necessarily leads to different flood estimates. With increasing return period, uncertainty also increases, and events with a recurrence interval of 1 000 years and considerably more cannot be verified or validated quantitatively due to a lack of sufficiently long observations for comparison. In this range of recurrence intervals, the simulated flood peaks are partly higher than what could be expected from a frequency analysis of discharge observations. However, this disagreement is not surprising because of the limited length, representativeness and homogeneity of the flood records. A comprehensive evaluation of the model chain has not revealed important shortcomings that would question the plausibility of results. Cautious interpretation is recommended, however, for some catchments with extremely high peak flows. These values could be unrealistically high, but on the other hand might also indicate behaviour involving potential process changes that have not yet been observed.

The long continuous simulation approach followed in EXCH offers several key advantages over common flood estimation methods such as extreme value statistics or event-based simulation. These include the extrapolation of meteorological instead of hydrological observations (generally with longer observation periods and easier interpolation in space); the avoidance of assumptions about antecedent conditions such as soil moisture, snow cover and lake levels (facilitating the estimation of return levels and allowing a broad range of precipitation patterns to be paired with an equally broad range of antecedent condition patterns); the comprehensive exploration of unobserved but possible spatial and temporal configurations of conditions (indicating flood extremes that clearly exceed the range covered by discharge observations); the consistency of flood estimates in time and space across the large river basins considered (avoiding the influence of available hydrological records and differing flood estimation approaches employed); and the availability of full continuous hydrographs rather than peak flow estimates alone (enabling bivariate flood statistics or the identification of representative hydrograph shapes).

At the same time, limitations and uncertainties are present. In addition to the general uncertainties associated with observations and their extrapolation – relevant in any flood estimation approach –, specific limitations and uncertainties pertain to the hydrometeorological simulations. These include, in particular, model choice, model parametrization, and model calibration. These uncertainties increase with the return period considered and are challenging to quantify due to the lack of suitable observational data for comparison and the substantial computational demand required to run sensitivity experiments.

As each approach to flood estimation has its own advantages and limitations, it would not make sense to replace all current flood estimates with values derived from EXCH where available. Also, the EXCH approach cannot reach the level of site-specific tailoring that is achieved with a detailed hydrological study directed toward an individual catchment. Rather, it is suggested that EXCH results be viewed as an alternative that circumvents some of the limitations of traditional flood estimation but obviously is also subject to specific limitations and uncertainties. In this sense, the EXCH results should ideally be used in conjunction with other approaches. Important decisions regarding design or safety values should consider all available methods in a specific case, and where necessary a more detailed hydrological study should be undertaken.

Zusammenfassung

Hochwasserabschätzungen sind von entscheidender Bedeutung für eine Vielzahl von Anwendungen, einschliesslich der Gefahrenkartierung, des Wasserbaus und der Sicherheitsbeurteilung von kritischer Infrastruktur. Sie sind zentral, um menschlichen und wirtschaftlichen Schaden zu verhindern und um sichere und kostenwirksame Schutzbauten zu dimensionieren. Verschiedene Herausforderungen erschweren allerdings die Hochwasserabschätzung, hauptsächlich aufgrund der vergleichsweise kurzen Abflussbeobachtungen an einem interessierenden Standort oder, in vielen Fällen, des Fehlens von Abflussdaten für eine direkte Extrapolation.

Das Projekt Extremhochwasser Schweiz (EXCH) befasst sich mit diesen Herausforderungen und zielt auf hydrometeorologische Grundlagen für Einzugsgebiete in der gesamten hydrologischen Schweiz ab. EXCH ist eine Fortsetzung des Projekts Extremhochwasser an der Aare (EXAR) und entwickelt die dort etablierten Methoden weiter. Auch wenn der Projektname eine andere Erwartung wecken könnte, sind die aus EXCH (und auch EXAR) resultierenden Hochwasserabschätzungen für ein breites Spektrum von Wiederkehrperioden wertvoll, von Hochwassern mit Wiederkehrperioden im Bereich von 10 bis 100 Jahren bis hin zu sehr seltenen und extremen Hochwassern im Bereich von 1 000 bis 10 000 Jahren Wiederkehrperiode.

Aus methodischen Gründen ist es nicht möglich, einen einzigen Ansatz konsequent über alle betrachteten Skalen hinweg zu verfolgen. Anstattdessen mussten die Arbeiten in zwei Module unterteilt werden: Eines mit Fokus auf „grosse“ (mehr als ~1 000 km^2) Einzugsgebiete, und eines mit Fokus auf „kleine“ (~10 bis 1 000 km^2) und „sehr kleine“ (~1 bis 10 km^2) Einzugsgebiete. Im Übergangsbereich zwischen den beiden Modulen sind Diskontinuitäten in den Ergebnissen zu erwarten, da die derzeit verfügbaren Methoden keine nahtlose Bearbeitung über alle betrachteten Skalen hinweg erlauben.

Für die grossen Einzugsgebiete, die in diesem Bericht behandelt werden, liegt der Schwerpunkt auf den Teileinzugsgebieten der grossen Flussgebiete der Schweiz, ähnlich den in EXAR für die Aare betrachteten Teileinzugsgebieten. Insgesamt werden 60 Abflussstandorte abgedeckt, mit einer Fläche im Bereich von etwa 920 bis 35 900 km^2. Von diesen Standorten sind 24 Wehre unter der Aufsicht des Bundesamtes für Energie (BFE), während die verbleibenden 36 Standorte Messstationen betreffen, welche vom Bundesamt für Umwelt (BAFU) betrieben werden. Zwischen Wehr- und Messstandorten bestehen einige Überschneidungen.

EXCH folgt einem Ansatz der kontinuierlichen Simulation, welcher eine hydrometeorologische Modellkette als Grundlage verwendet. Für die grossen Einzugsgebiete umfasst diese Modellkette drei Elemente: In einem ersten Element werden mit Hilfe des Wettergenerators GWEX stündliche Szenarien von Niederschlag und Temperatur mit einer aggregierten Gesamtlänge von 300 000 Jahren generiert. Die Parameter von GWEX wurden auf Basis des Zeitraums 1930 bis 2019 geschätzt. Ein zweiter Wettergenerator SCAMP sowie Reforecast-Daten werden als Alternativen untersucht. Im zweiten Element dienen diese Wetterszenarien als Input für das hydrologische Modell HBV in 330 Teileinzugsgebieten, welche die gesamte hydrologische Schweiz abdecken. Disaggregierte Wetterbeobachtungen 1931–2019 treiben HBV für eine Kontrollsimulation an. Im dritten Element werden die HBV-Simulationen für die einzelnen Teileinzugsgebiete mit der hydrologischen Routing-Komponente des Modells RS Minerve kombiniert. Die unmittelbaren hydrologischen Resultate umfassen 300 000 Jahre simulierte kontinuierliche Abflusshydrographen in stündlicher Auflösung für jeden Standort. Diese simulierten Hydrographen können gleich wie beobachtete Hydrographen analysiert werden und dienen in diesem Projekt dazu, Hochwasserhäufigkeitskurven herzuleiten. Eine weitere Extrapolation ist in diesem Schritt nicht erforderlich, da die Extrapolation bereits bei der Erzeugung der Wetterszenarien geschieht. Der Anwendungsbereich der Ergebnisse wird hauptsächlich durch die Eigenschaften des Wettergenerators bestimmt und umfasst Einzugsgebiete mit einer Fläche von mehr als ungefähr 1 000 km^2 und Wiederkehrperioden von bis zu ungefähr 10 000 Jahren. Alle Ergebnisse gelten für gegenwärtige Bedingungen, während Klimawandel und zukünftige Flussbauprojekte in diesem Projekt bewusst nicht berücksichtigt werden.

Die Ergebnisse der Kontrollsimulation mit beobachtetem Wetter zeigen an vielen Standorten eine gute bis sehr gute Übereinstimmung der beobachteten und simulierten Hochwasserspitzen. Die Anwendbarkeit des Ansatzes wird für Hochwasser mit Wiederkehrperioden von etwa 100 bis 300 Jahren aufgezeigt, wo eine Beurteilung anhand von Beobachtungen (und deren Extrapolationen) möglich ist. Einige Abweichungen vom beobachteten Verhalten können auf wasserbauliche Veränderungen im Verlauf des Beobachtungszeitraums zurückgeführt werden. Diese Veränderungen sind in den Abflussbeobachtungen noch nicht umfassend abgebildet, sind aber in der Modellkette implementiert. Einige der untersuchten Abflussstandorte haben ein Einzugsgebiet von weniger als 1 000 km^2, und dort wurden fallweise tatsächlich Unterschätzungen festgestellt, die auf die Details der Wettergenerierung zurückzuführen sind.

Die langen kontinuierlichen Simulationen auf Basis von Wetterszenarien zeigen ebenfalls eine gute Übereinstimmung mit den Beobachtungen sowie mit den Kontrollsimulationen. Abweichungen sind möglich und kein Grund, die Simulationen zu verwerfen, da letztere das hydrometeorologische Verhalten eines Einzugsgebiets anders – und erheblich umfassender – abbilden als Abflussbeobachtungen. Auch die hier vorgenommene Extrapolation über die Meteorologie (Zeitreihen von Niederschlag und Temperatur) anstelle der Hydrologie (Zeitreihen des Abflusses) führt zwangsläufig zu unterschiedlichen Hochwasserabschätzungen. Mit zunehmender Wiederkehrperiode nimmt auch die Unsicherheit zu, und Ereignisse mit einer Wiederkehrperiode von 1 000 Jahren und mehr können aufgrund des Fehlens ausreichend langer Beobachtungen nicht mehr direkt quantitativ überprüft werden. In diesem Jährlichkeitsbereich fallen die simulierten Hochwasserspitzen teilweise höher aus, als aufgrund einer Häufigkeitsanalyse der Abflussbeobachtungen zu erwarten wäre. Diese Diskrepanz ist jedoch nicht überraschend, da Länge, Repräsentativität und Homogenität der Hochwasserdaten limitiert sind. Eine umfassende Überprüfung der Modellkette hat keine wesentlichen Probleme offenbart, welche die Plausibilität der Ergebnisse in Frage stellen würden. Für einige Einzugsgebiete mit extrem hohen Spitzenabflüssen wird jedoch eine vorsichtige Interpretation empfohlen. Diese Werte könnten unrealistisch hoch sein, könnten aber auch auf mögliche Prozessänderungen hinweisen, welche bisher noch nicht beobachtet wurden.

Der im EXCH verfolgte Ansatz der langen kontinuierlichen Simulation bietet entscheidende Vorteile gegenüber gängigen Hochwasserschätzmethoden wie der Extremwertstatistik oder der ereignisbasierten Simulation. Dazu gehört, dass die Extrapolation über meteorologische anstatt hydrologische Daten geschieht (mit in der Regel längeren verfügbaren Beobachtungen und einfacher Interpolation im Raum); dass keine Annahmen über Anfangsbedingungen wie Bodenfeuchtigkeit, Schneedecke und Seepegel gemacht werden müssen (womit die Schätzung von Wiederkehrperioden erleichtert wird und eine breite Palette von Niederschlagsmustern mit einer ebenso breiten Palette von Anfangsbedingungen kombiniert wird); dass unbeobachtete, aber mögliche räumliche und zeitliche Konfigurationen von Bedingungen umfassend ausgelotet werden (mit Hinweisen auf Hochwasserextreme, welche das durch Abflussbeobachtungen abgedeckte Spektrum deutlich übersteigen); dass die Hochwasserabschätzungen in den betrachteten grossen Flussgebieten zeitlich und räumlich konsistent sind (womit standortspezifische Unterschiede in den verfügbaren hydrologischen Beobachtungen und Diskrepanzen aus unterschiedlichen methodischen Ansätzen zur Hochwasserabschätzung vermieden werden); und dass vollständige kontinuierliche Ganglinien verfügbar sind anstatt nur Schätzungen des Spitzenabflusses (womit bivariate Hochwasserstatistiken oder die Ableitung repräsentativer Ganglinienformen möglich werden).

Zu betonen sind jedoch auch Einschränkungen und Unsicherheiten. Neben den allgemeinen Unsicherheiten, welche mit Beobachtungen und deren Extrapolation verbunden sind – was bei jeder Methode zur Hochwasserabschätzung von Bedeutung ist –, bestehen spezifische Einschränkungen und Unsicherheiten, welche die hydrometeorologischen Simulationen betreffen. Dazu gehören insbesondere die Wahl, Parametrisierung und Kalibrierung der eingesetzten Modelle. Diese Unsicherheiten nehmen mit der betrachteten Wiederkehrperiode zu und sind nur schwer zu quantifizieren, da es an geeigneten Vergleichsbeobachtungen fehlt und Sensitivitätsanalysen erhebliche Rechenressourcen erfordern.

Da jede Methode zur Hochwasserabschätzung ihre spezifischen Vorteile und Einschränkungen hat, erscheint es nicht sinnvoll, alle aktuellen Hochwasserabschätzungen durch die aus EXCH abgeleiteten

Werte zu ersetzen, wo solche verfügbar sind. Auch kann der hier verwendete Ansatz nicht das Mass an standortspezifischer Anpassung erreichen, welches etwa mit einer detaillierten hydrologischen Studie eines einzelnen Einzugsgebiets möglich ist. Es wird vielmehr vorgeschlagen, die Ergebnisse von EXCH als Alternative zu betrachten, welche einige der Einschränkungen konventioneller Hochwasserabschätzungen umgeht, jedoch ebenfalls spezifische Einschränkungen und Unsicherheiten beinhaltet. In diesem Sinne sollten die Ergebnisse von EXCH idealerweise in Verbindung mit anderen Ansätzen verwendet werden. Wichtige Entscheidungen hinsichtlich Bemessungs- oder Sicherheitswerten sollten zudem alle im jeweiligen Fall verfügbaren Methoden berücksichtigen, und wo nötig sollte eine detailliertere hydrologische Studie durchgeführt werden.

Résumé exécutif

Les estimations des crues sont d'une importance cruciale pour un large éventail d'applications, y compris les cartes des dangers, l'ingénierie hydraulique et les évaluations de sécurité des infrastructures critiques. Elles sont essentielles pour prévenir les dommages humains et économiques, ainsi que pour concevoir des ouvrages hydrauliques sûrs et économiquement efficaces. Cependant, plusieurs défis compliquent l'estimation des crues, principalement en raison de la courte durée des observations de débit à un site d'intérêt ou, dans de nombreux cas, de l'absence complète de données de débit pour une extrapolation directe.

Le projet Crues Extremes en Suisse (EXCH) aborde ces défis et cible les fondamentaux hydrométéorologiques pour des bassins versants dans toute la Suisse hydrologique. EXCH est une suite du projet Crues extrêmes de l'Aar (EXAR) et poursuit le développement des méthodes établies dans EXAR. Bien que le nom du projet puisse donner une autre impression, les estimations des crues obtenues dans EXCH (et aussi dans EXAR) sont précieuses pour une large gamme de périodes de retour, allant des crues de l'ordre de 10 à 100 ans d'intervalle de retour, jusqu'aux crues très rares et extrêmes de l'ordre de 1 000 à 10 000 ans d'intervalle de retour.

Pour des raisons méthodologiques, il n'est pas possible de suivre une approche unique de manière cohérente à toutes les échelles pertinentes. Le travail a donc dû être divisé en deux modules : l'un axé sur les « grands » bassins versants (supérieurs à ~1 000 km^2), et l'autre sur les « petits » (~10 à 1 000 km^2) et « très petits » (~1 à 10 km^2) bassins versants. Dans la zone de transition entre les deux modules, des discontinuités dans les résultats sont attendues, car les méthodes actuellement disponibles ne permettent pas un traitement fluide à toutes les échelles envisagées.

Pour les grands bassins versants traités dans ce rapport, l'accent est mis sur les sous-bassins des principaux bassins fluviaux de la Suisse, similaires aux sous-bassins considérés dans EXAR pour l'Aar. Plus précisément, un total de 60 sites sont couverts, avec une gamme de taille allant d'environ 920 à 35 900 km^2. Parmi ces sites, 24 sont des barrages sous la supervision de l'Office fédéral de l'énergie (OFEN), et 36 sites concernent des stations de jaugeage de l'Office fédéral de l'environnement (OFEV), avec un certain chevauchement entre les barrages et les stations de jaugeage.

EXCH suit une approche de simulation continue, employant des simulations avec une chaîne de modèles hydrométéorologiques qui, dans le cas des grands bassins versants, comporte trois maillons. Dans le premier maillon, des scénarios horaires de précipitations et de températures d'une durée totale cumulée de 300 000 ans sont générés avec le générateur météorologique GWEX. Les paramètres de GWEX sont estimés pour la période 1930–2019. Un autre générateur météorologique, SCAMP, ainsi que des données de réforecast sont également explorés en tant qu'alternatives. Dans le deuxième maillon, les scénarios météorologiques alimentent le modèle hydrologique de type « seau d'eau » HBV pour 330 sous-bassins couvrant toute la Suisse hydrologique. Des observations météorologiques désagrégées de 1931 à 2019 alimentent HBV pour une simulation de contrôle. Dans le troisième maillon, les simulations de HBV pour les sous-bassins individuels sont combinées avec un routage hydrologique utilisant le modèle RS Minerve. Les résultats hydrologiques immédiats comprennent 300 000 années d'hydrographes de débit continu à une résolution horaire pour chaque site. Ces hydrographes simulés peuvent être analysés de manière similaire aux hydrographes observés et sont utilisés dans ce projet pour dériver des courbes d'excédence des débits de crue annuels. Aucune extrapolation supplémentaire n'est nécessaire à cette étape, car l'extrapolation est réalisée pour les précipitations et les températures dans la génération météorologique. La portée des résultats, principalement déterminée par la configuration du générateur météorologique, s'applique aux bassins versants d'une superficie de plus de 1 000 km^2 environ, et pour des périodes de retour allant jusqu'à 10 000 ans environ. Tous les résultats s'appliquent aux conditions actuelles, tandis que les effets du changement climatique et les futurs projets d'aménagement fluvial ne sont délibérément pas pris en compte dans ce projet.

Les résultats de la simulation de contrôle avec les conditions météorologiques observées montrent une bonne à très bonne concordance entre les pics de crue observés et simulés pour de nombreux sites. La validité de l'approche est démontrée pour des crues avec des périodes de retour d'environ 100 à 300 ans, où une évaluation par rapport aux observations (et leurs extrapolations) est possible. Plusieurs écarts par rapport au comportement observé peuvent être attribuées à des changements en génie hydraulique pendant la période d'observation. Ces changements ne sont pas encore largement reflétés dans les observations de débit, mais ils sont mis en œuvre dans la chaîne de modèles dans leur état actuel. Certains des sites examinés possèdent un bassin versant inférieur à 1 000 km^2, et des sous-estimations ont effectivement été observées à certains de ces sites en raison des approches de génération météorologique utilisées.

Les simulations longues et continues basées sur des scénarios météorologiques montrent également une bonne concordance avec les observations ainsi qu'avec les simulations de contrôle. Une divergence est cependant possible, mais ce n'est pas une raison pour rejeter les simulations longues et continues, qui échantillonnent le comportement hydrométéorologique possible d'un bassin versant de manière différente – et bien plus complète – que les observations de débit. En outre, l'extrapolation via la météorologie (séries de précipitations et de températures) plutôt que via l'hydrologie (séries de débits) conduit nécessairement à des estimations de crues différentes. À mesure que la période de retour augmente, l'incertitude augmente également, et les événements ayant un intervalle de retour de 1 000 ans ou plus ne peuvent plus être vérifiés ou validés quantitativement en raison du manque de données d'observation suffisamment longues pour la comparaison. Dans cet intervalle de retour, les pics de crue simulés sont partiellement plus élevés que ce qui pourrait être attendu d'une analyse de fréquence des observations de débit. Cette divergence, toutefois, n'est pas surprenante en raison de la limitation de la longueur, de la représentativité et de l'homogénéité des enregistrements des crues. Une évaluation complète de la chaîne de modèles n'a pas révélé de défauts importants qui remettraient en question la plausibilité des résultats. Cependant, une interprétation prudente est recommandée pour certains bassins versants avec des pics de crue extrêmement élevés. Ces valeurs pourraient être irréalistes, mais d'autre part, elles pourraient aussi indiquer des changements de processus possibles qui n'ont jusqu'à présent jamais été observés.

L'approche de simulation continue à long terme suivie dans EXCH présente plusieurs avantages clés par rapport aux méthodes courantes d'estimation des crues, telles que les statistiques des valeurs extrêmes ou la simulation basée sur des événements. Parmi ces avantages figurent l'extrapolation des observations météorologiques plutôt qu'hydrologiques (généralement avec des observations plus longues disponibles et une interpolation spatiale plus facile) ; l'évitement des hypothèses sur les conditions antécédentes telles que l'humidité du sol, la couche de neige et les niveaux des lacs (ce qui facilite l'estimation des niveaux de retour et associe une large gamme de configurations de précipitations à une gamme tout aussi large de conditions antécédentes) ; l'exploration exhaustive des configurations spatiales et temporelles non observées mais possibles (indiquant des extrêmes de crue qui dépassent clairement la plage couverte par les observations de débits) ; la cohérence des estimations de crue dans le temps et l'espace à travers les grands bassins fluviaux considérés (évitant l'influence des données hydrologiques disponibles et des différentes approches d'estimation des crues employées) ; et la disponibilité d'hydrogrammes continus complets plutôt que de simples estimations des débits de pointe (permettant des statistiques bivariées des crues ou l'identification de formes représentatives d'hydrogrammes).

En même temps, des limitations et des incertitudes existent. En plus des incertitudes générales associées aux observations et à leur extrapolation – pertinentes dans toute approche d'estimation des crues – des limitations et incertitudes spécifiques concernent les simulations hydrométéorologiques. Celles-ci incluent en particulier le choix, la paramétrisation et la calibration des modèles. Ces incertitudes augmentent avec la période de retour considérée et sont difficiles à quantifier en raison du manque de données d'observation adéquates pour comparaison, et en raison des exigences de calcul substantielles nécessaires pour effectuer des analyses de sensibilité.

Comme chaque approche d'estimation des crues présente ses propres avantages et limitations, il ne serait pas judicieux de remplacer toutes les estimations actuelles des crues par des valeurs dérivées de EXCH lorsque celles-ci sont disponibles. De plus, l'approche EXCH ne peut pas atteindre le niveau d'adaptation spécifique au site qui est obtenu avec une étude hydrologique détaillée pour un bassin versant individuel. Il est plutôt suggéré de considérer les résultats d'EXCH comme une alternative qui contourne certaines des limitations des méthodes traditionnelles d'estimation des crues, mais qui est également soumise à des limitations et des incertitudes spécifiques. En ce sens, les résultats d'EXCH devraient idéalement être utilisés en conjonction avec d'autres approches. Des décisions importantes concernant les crues de dimensionnement ou des crues de sécurité devraient tenir compte de toutes les méthodes disponibles dans un cas spécifique, et, si nécessaire, une étude hydrologique plus détaillée devrait être entreprise.

Contents

Nomenclature

Acronyms and abbreviations

AMF	annual maximum flood
CS	continuous simulation
ECMWF	European Centre for Medium-Range Weather Forecasts
EDF	Électricité de France
ENSI	Swiss Federal Nuclear Safety Inspectorate
EGP3D	extended generalized Pareto type 3 distribution
EGPD	extended generalized Pareto distribution
EXAR	Extreme flood events on the River Aare
EXCH	Extreme floods in Switzerland
FDC	flow duration curve
FOCP	Federal Office for Civil Protection
FOEN	Federal Office for the Environment
GEV	Generalized Extreme Value
GPD	Generalized Pareto distribution
GWEX	Generator of Weather EXtremes
HBV	Hydrologiska Byråns Vattenbalansavdelning
IWG	Institut für Wasser und Gewässerentwicklung
KGE	Kling-Gupta efficiency
KGE-NP	Non-parametric Kling-Gupta efficiency
MAP	mean areal precipitation
MAR	multivariate autoregressive model
MAT	mean areal temperature
MeteoSwiss	Federal Office of Meteorology and Climatology
NSE	Nash-Sutcliffe efficiency
OF	objective function
OBS	observations
PMF	Probable Maximum Flood
PMP	Probable Maximum Precipitation
RCM	Regional Climate Model
RF	reforecast
RMSE	root mean square error
RS Minerve	Routing System Minerve
SCAMP	Sequential Construction of atmospheric Analogs for Multivariate Weather Predictions
SEP	skew exponential power
SFOE	Swiss Federal Office of Energy
Swisstopo	Federal Office of Topography
WSL	Swiss Federal Institute for Forest, Snow and Landscape Research

1 Introduction

In 2013, the Federal Office for the Environment (FOEN), the Swiss Federal Office of Energy (SFOE), the Swiss Federal Nuclear Safety Inspectorate (ENSI), the Federal Office for Civil Protection (FOCP) and the Federal Office of Meteorology and Climatology (MeteoSwiss) jointly commissioned the Extreme flood events on the River Aare (EXAR) project to establish a unified and harmonized basis for assessing the risk of extreme flooding on the Aare river, including possible failure processes of hydraulic structures in addition to river flows. The project was conducted under the lead of the FOEN, coordinated by the Swiss Federal Institute for Forest, Snow and Landscape Research (WSL), and accompanied by a board of external experts. Its final results (Andres et al., 2021) were presented in 2021. A method to derive representative hydrographs useful for dam safety assessments was developed for the SFOE (Staudinger et al., 2021) in the last phase of EXAR, although it did not account for specific hydraulic conditions upstream or for scales smaller than those for which EXAR was developed.

FOEN and SFOE then took initiative to commission the development of similar hydrometeorological foundations – albeit without failure processes and detailed hydraulic analyses – for all of Switzerland, starting from approaches developed in EXAR and further developing methods where necessary. This work was conducted within the Extreme floods in Switzerland (EXCH) project, with the primary goal of determining site-specific exceedance frequencies of peak flows under current conditions.

Based on meteorological and hydrological observations, exceedingly long continuous simulations of precipitation, temperature and runoff are derived for selected sites all over Switzerland. These simulations then serve as a basis for extreme value analyses. Following experience from EXAR, reliable statements are expected for return periods up to 1 000 years, and indicative statements up to 10 000 years. The uncertainty of flood estimates increases with return period, and further extrapolation to even rarer events is not advisable due to the large uncertainties. In addition to statements on precipitation intensities and peak discharges, the simulation results can also be analysed for runoff volumes or the spatial extent of flood events, and can serve as a basis for further evaluations such as representative hydrographs or flood maps, although these aspects were not part of the present project.

The EXCH project is intended to cover a wide range of catchment sizes, with particular emphasis on the dams under supervision of SFOE. For methodological reasons, it was not possible to pursue a single approach that was consistently applicable from small (larger than 5–10 km^2) to large (smaller than ~35 000 km^2) catchments. Rather, the work had to be divided into a project module on “large” catchments and a module of “small” catchments, with a scale limit of about 1 000 km^2. For large catchments (approximately 1 000–35 000 km^2), the focus was on sub-basins of Switzerland’s main rivers, and methods from EXAR were used with adjustment and refinement where indicated. For small catchments (approximately 10–1 000 km^2), where the dams in the Alps were of particular interest, the approach for generating weather had to be further developed considerably to adequately represent the relevant temporal and spatial scales of precipitation. Due to methodological differences, discontinuities must be expected between the estimations for small and large catchments, and results in the vicinity of 1 000 km^2 should not be expected to align. For “very small” catchments in the scale range of 1–10 km^2, intensity-duration-frequency relationships of precipitation will be available based on the methods developed in the module on small catchments. In addition to these main analyses, two further feasibility studies were part of the project: On the one hand, it was explored whether reforecasts can serve as an alternative source for unobserved precipitation events with high intensities. On the other hand, the impact of uncertainties in weather generator and hydrological model on the resulting flood estimates was investigated. Both of these additional studies were carried out for a set of test catchments only due to high computational cost.

The exceedingly long continuous simulations (CSs) pursued in this project offer considerable advantages to estimate floods across a broad range of magnitudes. In contrast to event-based approaches, it avoids assumptions about antecedent conditions and their spatial patterns, and also about patterns of spatial and temporal development of flood-triggering meteorological conditions. Furthermore, the explicit consideration of important processes of flood generation and routing (snow accumulation, snow melt, soil moisture storage, bank overflow, lake and floodplain retention) is a substantial advantage of the approach pursued here. This allows for a comprehensive exploration of possible yet unobserved spatial and temporal patterns of hydrometeorological behaviour, which is particularly valuable in the river basins considered here since the complex interactions of flows from individual tributaries and lake regulations are typically not well captured in streamflow observations. As shown in Viviroli et al. (2022), the framework is suitable for both estimating frequent as well as rare floods in large catchments. It can on the one hand cover values required in hazard mapping and hydraulic engineering, while also ensuring spatial consistency of flood estimates – a key advantage in this context. On the other hand, the framework can be used to estimate dimension and safety floods for critical infrastructure such as dams and weirs. A further major advantage is that the approach does not only deliver peak flow estimates, but rather full continuous hydrographs. These can be used for bivariate flood statistics that include the flood event volume (Brunner et al., 2016), or further analysed to identify representative hydrograph shapes for different return periods (Staudinger et al., 2021). Such analyses are valuable for assessments concerning, for example, retention volumes, levee stability or bedload transport, but are not part of the present project.

Despite the advantages of the CS-based approach to flood estimation presented here, it should be kept in mind that results are subject to specific uncertainties and limitations (see Chapter 10). These are to an important part due to the limited length of meteorological and hydrological observations available and can thus not be fully amended with additional computational resources and a higher number of simulated scenarios. Nevertheless, the more conventional approaches to flood estimation, including extrapolation of observed discharge, also entail specific uncertainties and limitations. The approach introduced here is therefore not intended to replace other flood estimation methods, but should rather complement them towards a more comprehensive picture.

The present report covers the hydrological parts of the project module on large catchments and summarises other parts of that module as far as necessary for overview and interpretation of results. Details for the meteorological inputs are provided in the technical reports by Mas et al. (2023) for the weather generator scenarios and by Jury et al. (2024) for the reforecasts. The results from sensitivity analyses will be reported separately. After describing the data (Chapter 2) and methods (Chapter 3), two precipitation inputs to the model are juxtaposed (Chapter 4), and the hydrological simulations are validated as far as possible using observational data (Chapter 5). The flood estimates based on the main weather generator are then presented and discussed for selected sites in all major river basins (Chapter 6). Flood estimations from all sites are subsequently evaluated jointly in the context of envelope curves (Chapter 7), and, for the Aare River, compared to EXAR results (Chapter 8). Additionally, comparisons are made using two alternative meteorological inputs (Chapter 9). Following a discussion of advantages and limitations (Chapter 10) and an assessment of the lifetime of results (Chapter 11), the report concludes with a summary and outlook (Chapter 12).

2
Data

2.1. Meteorological data

The continuous meteorological data encompass records from stations operated by MeteoSwiss as well as records from all neighbouring countries (see Mas et al., 2023). For precipitation, daily records with a maximum extent of 1931–2019 were available at 1 706 sites, and hourly records with a maximum extent of 1990–2019 were available at 677 sites. For temperature, daily records with a maximum extent of 1931–2019 were available at 657 sites, and hourly records with a maximum extent of 1990–2019 were available at 497 sites. These sets were subsequently reduced with a view to data consistency and suitability for use in the weather generator GWEX (see Chapter 3.2.1 for details). A list of the precipitation and temperature stations selected is found in Tables D.1 and D.2, respectively. Precipitation extreme value analyses by MeteoSwiss for individual stations were taken from Fukutome et al. (2018).

For the period with only daily continuous records (1931–1989), hourly precipitation and temperature values were obtained by disaggregation. This disaggregation used the temporal structure of the respective variable observed, either for the same day if available at a nearby station, or for an analogous day in the period with hourly continuous observations. The analogy was specified using surface weather for the region, and applying constraints to preserve season and class of intensity following Breinl and Di Baldassarre (2019). For details, the reader is referred to Viviroli et al. (2022) and Mas et al. (2023).

2.2. Hydrological data

The hydrological data encompass continuous discharge records with a resolution of at least one hour. A total of 550 stations were gathered from the FOEN, the cantons of Aargau, Appenzell Ausserrhoden, Bern, Basel-Land, Fribourg, Genève, Glarus, Graubünden, Luzern, Neuchâtel, St. Gallen, Schaffhausen, Solothurn, Thurgau, Ticino, Vaud, Valais and Zürich, from relevant authorities in Austria, Germany, France and Italy, and from the LamaH-CE (LArge-SaMple DAta for Hydrology and Environmental Sciences for Central Europe) dataset (Klingler et al., 2021). Of these 550 stations, the 463 listed in Table C.1 were suitable for calibration of the catchment model HBV and yielded sufficiently good calibration results (see Section 3.3). The other 87 stations mostly relate to large catchments beyond the scope of HBV, for example because of complex lake regulation or simply because their catchment areas are too large for a lumped modelling approach. The calibration data usually fall within the period 1974–2019, with a median length of 45 years and a range of 16–47 years.

Records of annual maximum floods (AMFs) were available for the stations operated by the FOEN. These records often date back further than the continuous measurements, with a median length of 94 years and a range of 32–111 years. Extrapolations from these data were done following the FOEN approach based on a Generalized Extreme Value (GEV) distribution (see Baumgartner et al., 2013).

A total of 41 major water bodies were modelled, for which various types of data were collected and analysed: two large natural unregulated lakes, nine large natural regulated lakes and thirty reservoirs, all utilized for hydropower production.

For the two large natural and unregulated lakes (Lake Walensee, surface area 24.1 km^2; Lake Constance, 536 km^2), stage measurements were collected from FOEN in addition to the discharge measured at the outlet.

Regulation rules for the large natural and regulated lakes (Lake Biel, 39.8 km^2; Lake Brienz, 29.8 km^2; Lake Geneva, 581.3 km^2; Lake Lucerne, 113.6 km^2; Lake Lugano, 48.7 km^2; Lake Maggiore, 212.3 km^2; Lake Thun, 48.4 km^2; Lake Zug, 113.6 km^2; Lake Zürich, 90.1 km^2) were provided by the respective authorities. Where necessary, regulations were estimated based on this information in combination with stage-discharge measurements from FOEN (Lake Geneva, Lake Lugano), or from previous studies (Andres et al., 2016; Stucki et al., 2018) combined with stage-discharge measurements (Lake Maggiore, using measurements provided by both FOEN and Italian authorities). Depending on the lake, the rules are aimed at diverse and partly contradicting goals such as protecting settlements downstream from floods, avoiding inundation of the lakeside areas, providing cooling water for nuclear power plants, providing water for irrigation, preserving habitats, mimicking natural stage fluctuations and ensuring lake navigation. The information available ranged from detailed stage-discharge diagrams at a daily or monthly scale to rough indications of target discharge values for different intervals of lake level. For two small regulated lakes (Lake Ägeri, 7.2 km^2; Lake Lauerz, 3.1 km^2), the impact of regulation on flows at the critical sites was considered minor and thus neglected, also because in both of these cases, another regulated lake with considerably larger surface area is located downstream.

Regulation rules for reservoirs, defining the turbinated water volumes and annual operations, were derived, where possible, from internal reports on the calibration and set-up of the hydrological model WaSim ETH (Schulla, 2009; Schulla and Jasper, 2007) used for flood forecasting at the FOEN (Karsten Jasper, personal communication, 5 April 2021). These rules were digitized and simplified, typically by defining two seasonal rules – one for winter, one for summer – rather than using more precise calendar day rules. When available, additional rules were collected from the literature (e.g., Verbunt et al., 2005) or other sources, such as the Centre de recherche sur l'environnement alpin (CREALP) in Valais which develops Routing System Minerve (RS Minerve) and provided theoretic hourly turbined discharge at points of interest, as used in their forecasting model for the Rhone River.

Water intakes and transfers also had to be taken into account in some cases to reliably simulate the water balance of the reservoirs. Here we combined information from the residual flow map (Bundesamt für Umwelt (BAFU), 2013), the Hydrological Atlas of Switzerland (Baumgartner et al., 2007) and sources providing direct tributary catchment areas for reservoirs (e.g., Swiss Committee on Dams (swissdams), 2022).

The following reservoirs were explicitly considered (see Section 3.4 for more details):

- Aare River basin (including rivers Reuss and Limmat): Rossens, Schiffenen and Sihl
- Alpine Rhine River basin: Curnera, Davoser See, Marmorera, Nalps, Santa Maria, Sufers, Valle di Lei, Zervreila
- Rhone River basin: Emosson, Les Toules, Grande Dixence, Mauvoisin, Mattmark, Moiry, Salanfe, Vieux Emosson and Zeuzier
- Ticino River basin: Cavagnoli, Luzzone, Naret, Palagnedra, Ritom, Robièi, Sambuco, Sfundau, Vogorno, Zött

The bi-weekly filling levels for various regions of Switzerland, available since 2000 (Bundesamt für Energie (BFE), 2022), provided an indicative basis for assessing the plausibility of the simulated reservoir storage levels in the different large basins.

Finally, reconstructions of the historical floods of 1480, 1570, 1852 and 1876 were available from the EXAR project (Baer and Schwab, 2020; Viviroli et al., 2022; Wetter, 2015), of which the estimate for Aare at Brugg corresponds to a site also examined in EXCH. These floods cover different seasons and are indicative of extreme events in the Are River, although it has to be stressed that major river corrections (e.g., diversion of Kander River to Lake Thun 1714; diversion of Aare River to Lake Biel, 1878) have altered the hydrological system fundamentally in the meantime. Reliable estimates for the return periods of these events under current conditions are thus not feasible.

3

Methods

3.1. Model set-up

3.1.1. Modelling chain

This project employs a hydrometeorological modelling chain developed in the course of the EXAR project (Andres et al., 2021; Staudinger and Viviroli, 2020). As in EXAR, it here operates with a time step of one hour and comprises three main components (see Viviroli et al., 2022):

1. The weather generators GWEX (Section 3.2.1) and SCAMP (Section 3.2.2) were used to generate scenarios of precipitation and temperature with a total aggregated length of 300 000 years. The use of two weather generators aimed to assess the structural uncertainty in the meteorological part of this study. Unlike in the EXAR project, where the use of SCAMP was limited to a selection of 3 425 major precipitation events for reasons of computational cost, it was here possible to utilize the full 300 000 years of SCAMP scenarios for the project as well. In addition, the feasibility of utilizing reforecast (RF) data for estimation of rare events was explored.
2. The full mean areal precipitation (MAP) and mean areal temperature (MAT) outputs of GWEX and SCAMP were used as input for the bucket-type catchment model HBV (Section 3.3), run at an hourly time-step for all 330 sub-catchments that cover hydrological Switzerland (see Section 3.1.2). MAP and MAT derived from disaggregated observations 1931–2019 were used as a basis for a control simulation.
3. HBV simulation results from the individual sub-catchments were routed downstream using the hydrological routing components of RS Minerve (Section 3.4). The final simulation outputs span 300 000 years at an hourly time-step and cover 60 output sites (see Section 3.1.2).

As explained in Viviroli et al. (2022), the choice of models was motivated by the specific requirements of continuous simulation (CS), namely to cover a wide range of possible meteorological and hydrological conditions rather than the upper ranges of precipitation and discharge only. In addition, the model chain had to be suitable for application across all of Switzerland, especially regarding the specific challenges of mountainous environments that include rain-snow partitioning of precipitation, representation of snow accumulation and snow melt, as well as suitable simulation of glaciers. In addition, the models have to represent a considerable number of hydrological and hydraulic complexities such as lake retention and regulation, reservoir management, bank overflow and floodplain retention. Another important factor was the computational efficiency of all model chain links due to the vast extent of hourly simulations for a large number of sub-catchments. This requirement ruled out the use of models with more detailed physical process formulations. While the overall focus was on rare flood events, the model chain also represents normal conditions in sufficient quality so that the CSs provide realistic initial conditions for extreme events. The periods 1931–2019 (meteorology) and 1990–2019 (hydrology) serve as a reference for the hydrometeorological observations.

Note that each of the large river basins (Rhine including Aare, Reuss and Limmat; Rhone including Doubs; Ticino; Inn; see Figure 3.1) had an individual modelling chain and was treated independently. This was necessary to keep the complexity of multi-site weather generation manageable and does not entail limitations for flood estimation in the individual river basins. As a minor limitation, the simultaneous occurrence of floods in more than one of the major river basins cannot be studied.

All components of the modelling chain have been further developed and adjusted from the state reported by Viviroli et al. (2022) for EXAR in order to refine the methods, to account for recent scientific developments, and to accommodate the extended application framework of EXCH that covers a considerably larger area and makes use of much more observational data. A comprehensive overview of the most succinct differences to EXAR is given in Section 8.3.

As in EXAR, this implementation is not expected to be suitable for catchments smaller than approximately 1 000 km^2, due to both the initial three-day cycle of GWEX and the hourly temporal resolution of the simulations. Smaller catchments, where convective events become more decisive for flood behaviour (Sikorska et al., 2015), will be handled in the small catchments module of EXCH.

Advantages and limitations of this approach are discussed in more detail in Chapter 10.

3.1.2. Spatial distribution and output sites

For the present study, hydrological Switzerland was subdivided into 330 sub-catchments at the meso scale with a median surface area of 90.7 km^2 (range: 8.2 – 1 973 km^2) (Figure 3.1). Of these 330 sub-catchments, 141 have calibrated model parameters and 189 regionalised model parameters (see Section 3.3 for details). Of the regionalised sub-catchments, 72 are complete catchments including headwaters, 64 are intermediate catchments without headwaters, 15 are lake areas, and 38 are leftover tributaries to lakes, i.e., smaller catchments including headwaters that were merged to larger tributary areas. These sub-catchments formed the basis for the hydrological modelling as described further below in Section 3.3. They cover all regime types occurring in Switzerland (Weingartner and Aschwanden, 1992), and 53 of them have a glacier cover of at least 1 %, with a median glacier cover of 4.7 % in these glaciated catchments. The simulations for these sub-catchments were subsequently combined with hydrological routing (see Section 3.4) to simulate a total of 51 sites, of which 25 concern selected weirs under supervision of SFOE (Table A.1) and 26 concern selected gauging stations operated by FOEN (Table A.2). In addition, 10 further FOEN gauging stations are located close to SFOE sites and have only a slightly smaller or larger catchment area, so that results can be easily derived by applying a scaling factor, assuming similar specific discharge (see Table A.3). Results are thus available for a total of 61 sites. A list of sites that were considered but discarded in consultation with SFOE and FOEN is found in Table A.4.

3.2. Meteorological inputs

3.2.1. Weather generator GWEX

GWEX (Generator of Weather EXtremes) is a multi-site, two-part stochastic weather generator for precipitation and temperature that relies strongly on the structure proposed by Wilks (1998). GWEX aims to reproduce the statistical behaviour of weather events at different temporal and spatial resolutions, with a focus on extremes. Since comparatively long events are relevant in the main river basins of Switzerland considered here, GWEX generates three-day precipitation amounts in a first step. These amounts are then disaggregated to daily and ultimately hourly values using meteorological analogs.

The precipitation occurrence process of GWEX is represented for each site by a two-state first-order Markov chain that generates three-day sequences with or without precipitation. The seasonality of this occurrence process is considered by estimating model parameters independently for each month of the year. Inter-site correlations between precipitation occurrence are introduced using a multivariate Gaussian distribution. For three-day sequences with precipitation, the extended generalized Pareto type 3 distribution (EGP3D) (Papastathopoulos and Tawn, 2013) is then used to generate three-day precipitation amounts at each site. This distribution can be described by a smooth transition between a gamma-like distribution and a heavy-tailed Generalized Pareto distribution (GPD) and has been shown to adequately model precipitation intensities (Naveau et al., 2016).

The shape parameter of the distribution was estimated with a robust regional advanced method (Evin et al., 2016). Spatial and temporal dependence of three-day precipitation amounts was represented using a first-order multivariate autoregressive model (MAR). A Student copula represents the dependence structure of innovations in the MAR and introduces a tail dependence between at-site extremes. Similar

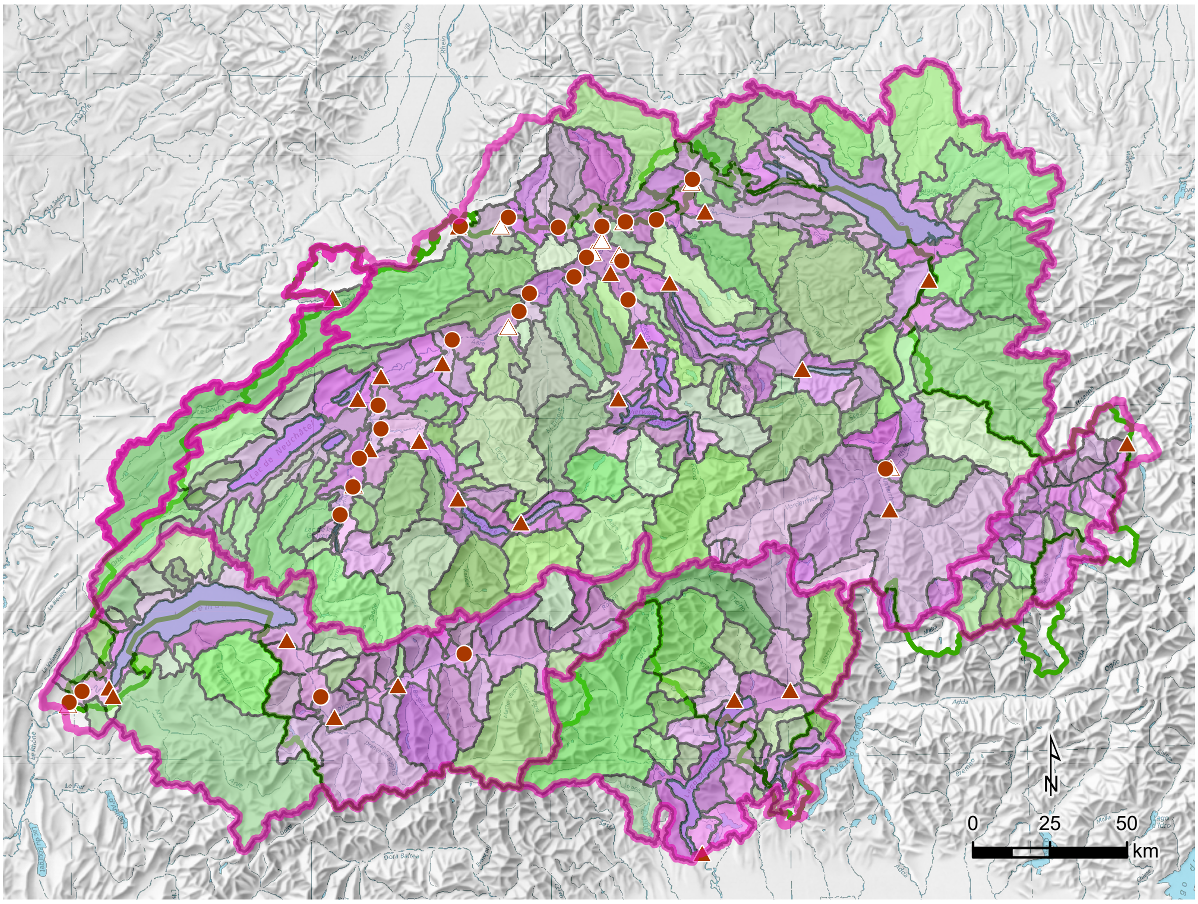

Figure 3.1: Overview map of hydrological Switzerland, showing the division into sub-catchments simulated by the HBV catchment model. The model parameters of HBV were calibrated for the sub-catchments shown in green hues, and regionalised for the sub-catchments shown in purple hues. Red circles show output nodes at selected weirs under supervision of SFOE, red triangles show output nodes at selected gauging stations operated by FOEN. Red triangles with white fill refer to FOEN sites that do not have an output node, but are very close by a SFOE site. Large river basins (each with a separate parametrisation of the weather generator GWEX) are shown with purple outlines. Base map ©Swisstopo.

to the occurrence process, the seasonality of the precipitation intensity was taken into account by fitting the model for each month using a three-month moving window.

As a further development after EXAR, GWEX was conditioned on four different weather types. Type 1 represents days with anticyclonic conditions over central Europe and very low rainfall intensities; type 4 corresponds to days with the highest rainfall intensities; and types 2 and 3 represent intermediate conditions, with more precipitation in the Southeast (Alps) for type 2 and more precipitation in the Northwest (Jura and plateau) for type 3. These types were aggregated from the nine types proposed by Weusthoff (2011). The conditioning was applied to the GWEX parameters determining multi-site occurrence and intensity dependency, whereas the extended generalized Pareto distribution (EGPD) had to be parametrised independently of weather types. For generating scenarios, a series of weather types was generated first. Further details are found in Mas et al. (2023).

For temperature, GWEX uses the skew exponential power (SEP) distribution (Fernandez and Steel, 1998) to model the standardized daily temperature at each station and a MAR model to represent the spatial and temporal dependence structures simultaneously. The seasonal cycles are accounted for with non-parametric functions and the generation is additionally conditioned on precipitation of the current generation day.

To achieve the sub-daily data needed for the hydrological simulations. a temporal disaggregation based on weather analogs was employed. For each day in the simulation period, the daily weather variables obtained with GWEX were disaggregated according to the spatial and temporal structure of an analogous day for which hourly observations were available in the period 1990–2019. The analog day candidates were identified using the root mean square error (RMSE) which measures the similarity between the regional weather situation of the target generated day and that of the observations. The regional weather situation of a given day was described by the spatial field of the weather variable considered, namely the daily value of the variable available at the multiple gauge stations in the area.

The mean areal values of precipitation and temperature (MAP and MAT) for a given sub-catchment – to be handed over to HBV as lumped meteorological inputs – were obtained using the Thiessen (1911) polygon method applied to the weather scenarios produced at the multiple sites. More advanced interpolation methods were considered, especially in view of the issue of conditional bias (for more see Beguería et al., 2016; Fantini et al., 2018; Frei and Isotta, 2019; Gervais et al., 2014). Together with experts from MeteoSwiss, it was however concluded that conditional bias is unlikely to be an issue in the scale range considered here, and that more complex approaches to interpolation can be dismissed, not least due to limited time and resources available for the present project module. In the EXCH project module devoted to small catchments (approximately 10–1 000 km^2), conditional bias is relevant, but will be avoided by using the MeteoSwiss product CombiPrecip that combines weather radar and gauge data (Sideris et al., 2014) to provide raster maps of precipitation.

Note that the initial set of precipitation stations (1 706 with daily data 1931–2019; 677 with hourly data 1990–2019; see Section 2.1) was first reduced to 969 sites where disaggregation from daily to hourly values and fitting GWEX was feasible. Of these, 451 sites contributed to the interpolation of MAP in at least one catchment in the final simulation set-up (see Table D.1). Similarly, the initial set of temperature stations (657 daily 1931–2019; 497 hourly 1990–2019) was reduced to 160 sites, of which 109 contributed to the interpolation of MAT in at least one catchment (see Table D.2).

Further details on GWEX are available in Evin et al. (2018, 2019) and Viviroli et al. (2022). A documentation of the refined set-up used in the present project is found in Mas et al. (2023), along with a comprehensive evaluation against observations.

3.2.2. Weather generator SCAMP

SCAMP (Sequential Construction of atmospheric Analogs for Multivariate Weather Predictions) is a hybrid weather generator based on atmospheric and weather analogues. It is methodologically fully independent of GWEX (Chardon et al., 2018; Raynaud et al., 2020, 2017). SCAMP generates long series of synoptic weather over Europe in a first step, using the ERA-20C atmospheric reanalysis 1900–2010 (Poli et al., 2016) as point of departure. New atmospheric trajectories are possible by rearranging the atmospheric sequences observed within the 110 years covered by ERA-20C. A detailed description of the simulation process is given in Chardon et al. (2016) and Raynaud et al. (2020). The resulting long series of synoptic weather are then used to generate daily weather over the application domain. To this end, a stochastic downscaling model based on atmospheric analogues is applied (Chardon et al., 2016; Raynaud et al., 2020). It employs the K-nearest neighbor (K-NN) method, where similar atmospheric conditions are identified based on historical records (see e.g., Gangopadhyay et al., 2005). For each day within the long time series of synoptic weather, the K-nearest atmospheric analogue days are identified in the archive period 1930–2010 where both ERA-20C data and station records are available. The regional weather scenario for the day in question is then generated from the statistical distribution of the regional weather observed for those K-analogues. As shown by Mezghani and Hingray (2009) and Chardon et al. (2014), the accuracy of statistically downscaled weather scenarios typically increases with spatial aggregation. For the present application, the K-nearest analogue days are thus used to generate the regional weather, namely mean areal precipitation (MAP) and mean areal temperature (MAT) for the relevant sub-catchments. For the current generation day, the regional weather scenario was generated from the statistical distribution of the regional weather observed for those K-nearest analogue days (Chardon et al., 2018). The criterion used to identify the nearest analogues is a measure of the similarity of 1) the dynamic of atmospheric circulation at a synoptic scale and 2) the thermodynamic state of the atmosphere at a regional scale. For this, we considered in a two-step identification process 1) the spatial shape of fields of geopotential heights at 1 000 hPa and 500 hPa and 2) the mean regional-scale vertical velocity at 600 hPa and the September–May temperature at 2 m. In summer, large-scale precipitation is used instead of vertical velocity since it has better predictive power for convective phenomena at the coarse resolution of the reanalysis data.

To achieve the sub-daily data, an approach similar to that used for GWEX was applied (see Section 3.2.1 above). For SCAMP, however, the regional weather situation was described with the regional MAP and MAT scenarios generated in the first step of the generation process. This disaggregation approach directly exploits past observed spatio-temporal structures and imposes the relative distribution of the candidate day (i.e., the sub-daily distribution of the precipitation and temperature values, as well as the sub-regional distribution, so-called fragments) on the day of interest. This approach, also called the "method of fragments" (Buishand and Brandsma, 2001), is described in detail in Appendix 10.2 of Staudinger and Viviroli (2020) for GWEX scenarios and in Mezghani and Hingray (2009) for the simulation context of SCAMP.

SCAMP was adopted from EXAR without modifications, but re-parametrised for the project domain of EXCH. Mas et al. (2023) give a comprehensive evaluation against observations.

3.2.3. Reforecasts

In the sense of a feasibility study, it was explored within EXCH whether reforecast (RF) data can be exploited to provide physically consistent and plausible time series of weather conditions that have not actually occurred (see e.g., Kelder et al., 2022, 2020; Thompson et al., 2017). These reforecasts (also called hindcasts) are weather model runs for past dates, where perturbation of the initial simulation conditions is used to create an ensemble simulation that can evolve towards unobserved conditions, including unobserved extremes. The approach is thus largely independent from the weather generators introduced above and allows for the investigation of atmospheric dynamics in the range of several 1 000 years. The following description closely follows Jury et al. (2024), where further details and an in-depth evaluation are found.

In processing the raw RF data obtained from the European Centre for Medium-Range Weather Forecasts (ECMWF), the first 15 days of each ensemble run were discarded to ensure independence of the individual ensemble members. Then, a statistical spatial downscaling approach was applied to cover a number of test catchments of different sizes (see Table 3.1). This downscaling is largely based on a stochastic weather generator developed by Switanek et al. (2022), which has been shown to perform well in bridging the gap between gridded data (in our case with a grid length of 0.5°) and data at the point scale. This stochastic weather generator was further developed within EXCH to account for specifics of the project and the corresponding data. For the bias adjustment, a transfer function was built by estimating the distribution of RF data from non-overlapping samples that are of the same length as the observed data. This ensures that unprecedented extreme events are preserved. Daily data had to be disaggregated to the hourly scales required for hydrological modelling, and single RFs with a length of between two and four weeks had to be combined in order to derive longer (here yearly) time series that can be used for hydrological modelling.

The approach achieved good key statistics (annual cycle, wet day frequency, one-day and three-day precipitation extremes, sub-daily and multi-day precipitation) at the catchment scale for large, medium and some small catchments, and thus the scale relevant for the large catchments module of EXCH. Shortcomings were identified for some small and all very small catchments, rooted in a smaller station count and the coarse resolution of the RFs.

The at-station downscaled RF data were treated similarly to the GWEX at-station data to compute time series of MAP and MAT, using temperature lapse rate, precipitation adjustment factor and Thiessen interpolation (see Section 3.2.1).

The concatenation of individual RF runs for use as continuous time-series in HBV led to some temperature jumps at the splices (see Jury et al., 2024), but verification of the HBV simulations did not show extraordinary behaviour in these time regions (see Section 5.1.3).

Unobserved extreme seasons and years are not reflected well, mainly because the concatenation of single RF was aimed at minimizing temperature differences at the splices. Moreover, the RF data have been produced over a period with positive phase of the Atlantic Multidecadal Oscillation (AMO) (Na-

Table 3.1: Test catchments for development and evaluation of RF data.

ID12	*ID6*	*River and site*	*Area [km^2]*
600710198000	AarBrn	Aare @ Bern, Schönau	2 965.1
613230179280	AarThu	Aare @ Thun	2 459.3
608710148300	AllAde	Allenbach @ Adelboden	28.8
582550103270	DdBLeC	Drance de Bagnes @ Le Châble, Villette	253.7
670467153932	GonOwd	Goneri @ Oberwald	38.4
795800165910	InnSCh	Inn @ S-Chanf	615.9
693120116720	IsoMsg	Isorno @ Mosogno	124.7
617790168400	KanHon	Kander @ Hondrich	490.7
663700213630	KEmEmm	Kleine Emme @ Emmen	478.3
644500119420	KruKlu	Krummbach @ Klusmatten	19.4
629130140910	LonBla	Lonza @ Blatten	77.4
703100113860	MagLcn	Maggia @ Locarno, Solduno	926.9
704425215310	MinEut	Minster @ Euthal, Rüti	59.1
718810167690	RdSSum	Rein da Sumvitg @ Sumvitg, Encardens	21.8
684970135960	RdCCav	Riale di Calneggia @ Cavergno, Pontit	23.9
642220129630	SalBrg	Saltina @ Brig	76.5
573520161345	SarBro	Sarine @ Broc, Château d'en bas	636.3
741133228784	ThuASJ	Thur @ Alt St. Johann, Unterwasser, Chlostobel	42.3
693510272500	ThuAnd	Thur @ Andelfingen	1 701.6
723675252720	ThuJon	Thur @ Jonschwil, Mühlau	492.9

tional Center for Atmospheric Research (NCAR), 2023). This boundary condition cannot be overcome by statistical downscaling.

Overall, the processing of RF data provided 9 920 annual (360-day calendar) time-series of hourly precipitation and temperature. These were used as inputs for hydrological modelling and subsequently applied to flood estimation. Contrary to initial expectations, the long span of RF data that could be made available allowed for corresponding continuous hydrological simulations, and thanks to these, return periods could be estimated for the simulated AMFs.

In addition to the stochastic downscaling of ECMWF RF data explained above, a dynamical downscaling was pursued as well. For this, it was envisaged to use a Regional Climate Model (RCM) with a resolution of a few kilometres, to achieve better resolution of small-scale extremes such as thunderstorms. However, this approach ultimately had to be abandoned because the RF data available from the ECMWF did not provide sufficient resolution in time and in space: Relevant parts of data are stored at 12-hour intervals only, and the need for strong interpolation can lead to underestimation of short-time precipitation amounts. Furthermore, it was not feasible to reliably select large-scale events from these data that would also lead to extreme small-scale events, whereas downscaling all events was beyond feasibility due to the high computational cost of running RCM simulations. Dynamical downscaling would have been feasible at a larger scale (more than ~500 km^2), but in this scale range, statistical downscaling is sufficiently accurate already.

3.3. Hydrological model (HBV)

The HBV (Hydrologiska Byråns Vattenbalansavdelning) model (Bergström, 1972, 1992; Seibert and Bergström, 2022) was employed for the hydrological simulations, using the version HBV light (Seibert, 1997; Seibert and Vis, 2012). The choice of HBV was motivated by its fast processing speed (necessary for running exceedingly long CS for a large number of sub-catchments) and its well-documented suitability for flood estimation in Switzerland (Horton et al., 2022). HBV is a semi-distributed bucket-type model that uses time series of mean areal precipitation and mean air temperature as inputs. These inputs were distributed within the catchment along predefined elevation zones.

For temperature, we used common lapse rates for each of six large river basin regions, namely Aare and Doubs; Rhine upstream of confluence with the Aare River; Reuss and Limmat; Rhone; Ticino; and Inn. In calibration and control simulation, the lapse rate was specific for every hour. In long CS with weather generator input, the lapse rate was specific for every hour of every calendar day (see Mas et al., 2023, for details). For precipitation, we used a constant adjustment factor with a linear increase of 5% for every 100 m increase in elevation (see e.g., Farinotti et al., 2012; Ménégoz et al., 2020; Ruelland, 2020; Viviroli et al., 2022). For both temperature and precipitation, the values at the individual stations were first adjusted to mean catchment elevation and then interpolated to derive MAP and MAT.

The precipitation adjustment factor mentioned above is necessary to compensate for gauge undercatch (Kochendorfer et al., 2017) and the lack of representativeness of the gauging network for high elevations (Shahgedanova et al., 2021; Viviroli et al., 2011). While gauge undercatch – which is higher for snow than for rain – can partly be compensated by HBV's multiplicative snowfall correction factor SFCF, the insufficient representativeness of precipitation gauges can still result in an unrealistic water balance in many cases. As a consequence, further HBV parameters, such as those for soil moisture and evapotranspiration, may attempt to compensate for the water balance mismatch. This can lead to unrealistic parameter values and model behaviour, which is much less desirable than setting an adjustment factor. The adjustment factor of 5 % per +100 m, used here based on experience in EXCH, aligns well with the orders of magnitude reported by Ménégoz et al. (2020) and Ruelland (2020), who found rates in a range of approximately 30–40 % km^{-1}, and Farinotti et al. (2012), who reported rates of 0.00–0.07 % m^{-1} over nine catchments, with a mean value of 0.035 % m^{-1}. However, it should be noted that these rates refer to long-term climatology, and that it is difficult to estimate more realistic rates (Evin et al., 2024). Differentiated rates might be more appropriate for single events (see e.g., Gottardi et al., 2012), but this information is difficult to extract for the observation period and not available for scenarios. A differentiation by weather type was considered but dismissed due to some types not occurring frequently enough to achieve robust factors.

The standard version of HBV consists of four main routines that represent snow processes, soil moisture, groundwater and streamflow routing in the channel. These routines entail 15 tuneable parameters. For sub-catchments with a glacier cover of 1% or more, an additional glacier routine with five tuneable parameters was activated (see Seibert et al., 2018; Stahl et al., 2008), assuming a constant glacier extent equivalent to that of year 2000. The long-term accumulation of snow in glacier-free areas – so-called "snow towers" (Freudiger et al., 2017) – was avoided by using the snow redistribution by Freudiger et al. (2021). In contrast to EXAR, where the standard response routine of HBV was used, we here employed the updated response routine of HBV-96 (Lindström et al., 1997). This updated routine improves the behaviour of fast runoff and avoids the discontinuous behaviour of flood exceedance curves that was occasionally found in sub-catchment simulations for EXAR. Actual evapotranspiration was estimated from the long-term daily mean of potential evaporation in combination with observed temperature and simulated soil moisture. Potential evaporation in turn was estimated with the approach of Hamon (1961), deriving the empirical factor from land cover classes in the catchment following Farinotti et al. (2012). Mean catchment elevation and elevation zones were derived from EU-DEM v1.1 (European Environment Agency (EEA), 2018), land cover classes (including glacier cover) from CORINE 2000 (European Union Copernicus Land Monitoring Service (Copernicus), 2020), and lakes from the Federal Office of Topography (Swisstopo) Vector200 map.

A total of 463 gauged sub-catchments were calibrated successfully (Table C.1), focusing on sites without major impacts from hydropower, lake regulation, bank overflow and floodplain retention. As shown in Table 3.2, all regime types (see Weingartner and Aschwanden, 1992) are represented. For calibration, a genetic algorithm (Seibert, 2000) was used with a modified Kling-Gupta efficiency (KGE) (Gupta et al., 2009) serving as the objective function (OF). The modification to KGE involves adding a bias score for the intermediate high-flow spectrum, specifically between the 50^{th} to 80^{th} percentiles. Specific emphasis on even higher peak flows is avoided, as substantial uncertainties must be assumed in their observation (Westerberg et al., 2020). To account for parameter uncertainty, four different nine-year periods (hydrological years 1983–1992, 1992–2001, 2001–2010, 2010–2019) were used, with 25 parameter sets calibrated for each period. In cases where less than 90 % of a nine-year period was covered with observations, the 25 parameter sets were randomly assigned to the other periods for calibration. If none of the fixed periods was covered with data for 90 % or more for a catchment, the longest continuous period available was chosen (up to a maximum of 9 years to remain comparable to the fixed periods). The 12 months before each period are used as warm-up period.

The resulting 100 parameter sets for each sub-catchment represent parameter uncertainty, but not all could be run with long CS due to the high computational cost. Therefore, three representative parameter sets were subsequently selected from the pool of 100 sets for each sub-catchment. Each parameter set was tested in a validation simulation for the other three available time periods. If the model performance was unsatisfactory for any parameter set in this test, it was excluded from the selection of representative parameter sets. Then, the AMFs from 10 000 years of simulations with each of the 100 parameter sets were analysed and the median, 10 % and 90 % percentiles of this ensemble were chosen following Sikorska-Senoner et al. (2020) to represent an intermediate, a low and a high response in simulated peak flows, respectively.

Table 3.2: Number of catchments calibrated in HBV per regime type (in total 463 catchments).

a-glaciaire	4
b-glaciaire	9
a-glacio-nival	12
b-glacio-nival	14
nivo-glaciaire	11
nival alpin	42
nival de transition	27
nivo-pluvial préalpin	44
pluvial supérieur	36
pluvial inférieur	107
pluvial jurassien	61
nivo-pluvial jurassien	64
nival méridional	8
nivo-pluvial méridional	14
pluvio-nival méridional	8
pluvial méridional	2

Of the 330 sub-catchments used as a basis for simulations at the output points (see Section 3.1.2), 141 have model parameters that were calibrated against observations. For the remaining 189 ungauged sub-catchments, parameters were estimated (i.e., regionalised) from the pool of calibrated sub-catchments using a clustering algorithm to identify two donor sub-catchments (Kauzlaric et al., 2020, 2021a; Viviroli et al., 2022) of the same regime type (Weingartner and Aschwanden, 1992). From each of these two donors, 12 parameter sets were randomly drawn from each of the four calibration periods, and two more were randomly drawn from all calibration periods, to give again a total of 100 parameter sets that can be transferred to the target sub-catchment. From these 100 sets, three representative sets were selected as described further above for calibrated sub-catchments. The direct tributary catchments to some relevant reservoirs were simulated as separate HBV sub-units with own regionalised parameter sets. This concerned the reservoirs Curnera, Davoser See, Marmorera, Nalps, Santa Maria, Sufers, Valle di Lei and Zervreila in the Alpine Rhine; and Emosson, Grande Dixence, Les Toules, Mauvoisin, Moiry, Salanfe and Vieux Emosson in the Rhone River basin. For other reservoirs, the tributary catchments were simulated by directly taking parameter sets from calibrated catchments and adapting the meteorological time series to represent the mean elevation of the sub-unit. This concerned Cavagnoli, Naret, Robièi, Sfundau, Sambuco and Zött in the Maggia River basin; and Mattmark in the Rhone River basin. Inflows to a few more major reservoirs were added at a later stage, obtained by simply scaling the flow simulated for the catchments in which they were nested. This approach was applied to Vogorno (Verzasca) and Ritom, both with calibrated donors, and Luzzone, with a regionalised donor.

3.4. Hydrological routing (RS Minerve)

Discharge of the individual sub-catchments simulated with HBV was finally combined and routed using Routing System Minerve (RS Minerve) (García Hernández et al., 2020) to achieve results at output nodes selected together with FOEN and SFOE (see Section 3.1.1 and especially Figure 3.1).

As with HBV, the main reasons for using RS Minerve were its speed and well-documented applications in Switzerland (Horton et al., 2022). The simplified routing representation implemented using RS Minerve emulates more detailed 2D hydraulic simulations of synthetic hydrographs, which were performed with BASEMENT (Vetsch et al., 2018). Synthetic hydrographs with return periods of 100, 300, 1 000, 10 000 and 100 000 years were derived as described by Mosimann et al. (2024) to cover a broad spectrum of possible event magnitudes and comprehensively explore the behaviour of the hydraulic system (see Staudinger and Viviroli, 2020). In some cases, estimates of extreme floods (EHQ) available from the literature or results from preliminary simulations exceeded the estimated 100 000 year return level. In these cases, hydraulic simulations were supplemented with runs using synthetic hydrographs generated for these peaks as well. This approach was taken to avoid extrapolating the hydraulic behaviour of the system for these “black swan events” (see also Montanari et al., 2024), which are often highly non-linear and may conceal unexpected effects.

Major effects of bank overflow and floodplain retention – resulting in attenuation and retardation of the flood peak – were considered across a wide range of discharges by implementing channels both in series and in parallel, as well as small idealized reservoirs at relevant sites. These channels and small reservoirs account for estimated channel flow capacity and inundated areas. Levee breaches, in contrast, have not been implemented. The inclusion of small reservoirs to emulate water retention on the floodplain for a longer time is a novel feature compared to the model configuration used in EXAR. The inclusion of this type of water retention, which is stronger than that emulated by adding side channels and resembles a form of water loss, was motivated by cases where depressions on the floodplain or specific topographical and infrastructural features – such as elevated motorways or airports – indeed create a standing retention effect rather than flowing retention. This configuration was first successfully tested on the floodplain of the Reuss River upstream of Bremgarten, and was subsequently implemented in the Thur River downstream of Halden, in the Alpine Rhine River downstream of the Ill River confluence, in the upper Inn River before and around the Flaz River confluence, in the Ticino River on the Magadino plain, and across most of the Rhone River downstream of Bramois.

For all of the major lakes and reservoirs, stage-volume relationships were extracted from digital terrain data (Bundesamt für Landestopographie (Swisstopo), 2005). For the large natural regulated lakes (see Section 2.2), regulation rules are usually expressed as stage-discharge relationships with seasonal, monthly or even daily variation. These rules were digitized and implemented into RS Minerve, where necessary in slightly simplified form. Where available and feasible, rules applied in case of flood events – i.e., deviating from business-as-usual operation – were implemented. For example, discharge in the Aare River is limited to 450 $m^3 s^{-1}$ downstream of Lake Thun in Bern and to 850 $m^3 s^{-1}$ downstream of Lake Biel in Murgenthal for as long as possible. If the level of a lake rises above the flood stage (i.e., the level above which widespread inundations occur, see flood danger levels defined by Bundesamt für Umwelt (BAFU) (2022)), stage-discharge relationships as simulated in BASEMENT assuming open weirs are used.

Reservoirs and hydropower plants can impact not only the mean discharge behaviour and its seasonality, but also potentially affect the discharge peaks, typically those with return periods of 100 to 300 years (see Zarn et al., 2017). For reservoirs that drain directly into a large natural lake or flow downstream into a lake – and do not contain any relevant output points for the project along the directly affected river section (e.g., Lake Grimsel upstream of Lake Brienz) – more detailed investigations and explicit mapping in RS Minerve were generally not conducted. Lake Vogorno on the Verzasca River, which drains directly in Lake Maggiore, is an exception. It was added in a later stage, after analysing preliminary simulation results, to improve the dynamics of Lake Maggiore, where winter inflows were often far too low, leading to too low lake stages in spring. When a reservoir reaches full capacity, the total water inflow is released directly downstream, effectively bypassing the reservoir.

Further relevant smaller reservoirs were identified by comparing their available water retention capacity with 100-year and 300-year daily precipitation intensities extracted from MeteoSwiss maps of extreme precipitation (Fukutome et al., 2018). Based on this information, it is possible to estimate how much precipitation is required to fill the reservoir or to utilise the retention potential at different filling levels. Following this analysis, several reservoirs were identified as having an important effect on flood events and were included in RS Minerve. The reservoirs selected and explicitly simulated are located in the following river catchments: Borgne (Grande Dixence), Brenno (Luzzone), Dranse (Mauvoisin, Les Toules), Hinterrhein (Davos, Marmorera, Sufers, Valle di Lei), Liène (Zeuzier), Maggia (Cavagnoli, Naret, Palagnedra, Robièi, Sambuco, Sfundau, Zött), Vispa (Mattmark), Navisence (Moiry), Saane (Rossens, Schiffenen), Salanfe (Salanfe), Sihl (Sihl), Ticino (Luzzone), Trient (Emosson, Vieux Emosson), Verzasca (Vogorno) and Vorderrhein (Curnera, Nalps, Santa Maria, Zervreila).

Due to the small size of some reservoirs and the important volumes of water turbinated between them, the following reservoirs were partly merged: In the Maggia River basin, Robièi was merged with Zött into a single reservoir, and Cavagnoli was merged with Sfundau and Narèt. In the Trient River basin, Vieux Emosson was merged with Emosson.

Water transfers between catchments were generally included for reservoirs in the Rhone and Ticino River basins, whereas these transfers were omitted in the Alpine Rhine River basin, as they often degraded simulation performance in the control period.

For the Rhone River, streamflow volumes were generally underestimated by approximately 5 to 10 %, primarily due to an insufficient representation of low-flow and baseflow conditions during winter. Typically, the simulated low-flow was about half of the observed flow, with local discrepancies reaching factors of 3 to 4. This pattern was also observed in the sub-catchments Vispa River (which contains the Mattmark reservoir) and Borgne River (which contains the Grande Dixence reservoir), where it interacted strongly with the operating rules of the reservoirs. In the case of the Vispa River, the calibration likely contributed to flow underestimation, as it was based on the observed discharge records that reflect substantial water transfers to Grand Dixence and thus to the Borgne River sub-catchment. To address this, the operating rules at Mattmark and Grande Dixence were adjusted by restricting turbination in summer. This approach allowed the reservoirs to reach full capacity by the start of the main turbination season (around September to October), enabling a gradual depletion of accumulated water through winter.

It is important to note that while most settings for the Aare River basin were adapted as defined and calibrated within the framework of EXAR, selected parts underwent further scrutiny and were modified where deemed necessary or where performance of the model could be further improved. The following four major modifications (to some extent already mentioned above) were implemented:

- Improved retention parametrisation in the floodplain of the Reuss River
- Explicit simulation of the Lake Sihl reservoir, incorporating specific operational rules that account for its connection and interdependency with Lake Zürich. Based on official regulation rules, rules were defined to allow a reduction in the volume of water turbinated towards Lake Zürich, depending on the simulated water level in Lake Zürich
- Improved regulation rules for Lake Biel in case of floods, now often preventing abrupt changes in simulated releases rates while switching between operational states. This issue occasionally arose in some scenarios simulated in EXAR and was often misinterpreted as numerical instability.
- Explicit simulation of unregulated Lake Walensee

Finally, it is important to note that the current hydraulic engineering status is consistently maintained throughout all simulations, with 2015 chosen as the reference year to align with the EXAR framework. However, substantial engineering projects are planned or already being implemented on several rivers. These include the major river regulation projects on the Alpine Rhine River (upstream of Lake Constance[1]) and the Rhone River (upstream of Lake Geneva[2]) as well as the flood relief tunnel for the Sihl River (downstream of Lake Sihl[3]). These are expected to markedly impact the future routing behaviour of the system and will render the EXCH implementation inaccurate.

[1] https://rhesi.org
[2] https://www.vs.ch/web/rhone
[3] https://www.zh.ch/de/planen-bauen/wasserbau/wasserbauprojekte/entlastungsstollen-sihl-zuerichsee.html

4

Juxtaposition of precipitation inputs

4.1. Introduction

This chapter explores jointly the results from the two fundamentally different approaches used to construct precipitation scenarios in EXCH: The weather generator GWEX and the reforecasts (RF). More detailed evaluations of the individual approaches are found in the reports by Mas et al. (2023) and Jury et al. (2024).

Three test regions were selected to represent differences in climatology as well as station density and representativeness: The Aare River basin (upstream of Bern), the Thur River basin, and the Maggia River basin. These are evaluated in terms of annual peaks of MAP. In addition, three to four meteorological stations were selected per river basin with focus on different station elevations (see Table 4.1).

Table 4.1: Meteorological stations used for juxtaposition of precipitation inputs. Their locations are given in the Swiss coordinate system (CH1903).

Code	*Name*	*x coordinate[m]*	*y coordinate [m]*	*Elevation [m a.s.l.]*
BOS	Bosco-Gurin	680 879	130 027	1 486
CEV	Cevio	689 688	130 565	417
BEP	Belp	605 140	193 805	515
FRF	Frauenfeld	709 480	270 170	393
GRH	Grimsel Hospiz	668 583	158 215	1 980
INT	Interlaken	633 019	169 093	577
LTB	Lauterbrunnen	635 851	160 291	815
MSG	Mosogno	692 803	117 050	771
SAE	Säntis	744 200	234 920	2 502
URN	Urnäsch	739 205	241 765	825

The following data were used as a basis in the juxtaposition:

– Weather generator (GWEX): 30 realizations of 10 000 years length each. Confidence intervals were computed from these 30 realizations.

– Reforecasts (RFs): 30 times stochastic downscaling of 9 920 years length each. Confidence intervals were computed from these 30 series of stochastic downscaling (i.e., the uncertainties depicted relate only to local meteorological variability, not to variability in the RFs themselves). An analysis for shorter blocks, allowing better comparison of confidence intervals, is given in Section 4.3 further below.

– Observations (OBS): A maximum of 90 years 1930–2019. Confidence intervals were computed as follows: 1) for monthly means: from 90 monthly values; 2) for annual maxima: from a parametric bootstrap (GEV distribution, fitted with L-Moments, 5 000 realizations); 3) for spell lengths: from a non-parametric bootstrap (block resampling with replacement, separately for each spell duration of D days, using a block length of D × 15 days, 5 000 realizations).

Please note the following regarding the OBS dataset and its suitability as a reference:

– GWEX has been parametrized using OBS data 1930–2019. OBS is therefore a suitable reference for assessing GWEX performance. That being said, GWEX parameters were estimated with a regional approach, where observations are pooled (Region of Influence method) to the end of reducing uncertainty and improving robustness of estimates. This could result in differences between the distributions estimated for OBS and simulated GWEX values.

– The ECMWF RF dataset covers the period 1991–2020, and the data have been bias corrected using RhiresD (MeteoSwiss, 2013) over this period. The stochastic downscaling has then been calibrated using the full available RhiresD data 1961–2019 and station data 1961–2019. Intersite dependence is modelled similar to the approach developed by Bárdossy and Plate (1992) (see Switanek et al., 2022). Stations with less than 75 % coverage in the period 1961–2019 were excluded, but obviously data for single stations are still missing for some days. The RFs thus relate to the two time periods 1961–2019 and 1991–2020, both of which are different from the full OBS period 1930–2019. Caution is therefore warranted when using OBS as a reference for RF performance. In particular, the Atlantic Multidecadal Oscillation (AMO) index went through different phases during 1930–2019 (see Trenberth et al., 2023), indicating a relevant impact of internal climate variability.

Please also note that the maximum precipitation sums have been plotted on a GEV scaled x-axis, and the corresponding return periods have been estimated using the plotting position after Gringorten (1963). In the diagrams for 1-day and 3-day precipitation sums, the latest statistics by MeteoSwiss (Fukutome et al., 2018, retrieved 27.03.2023) are shown for reference. At each station, these statistics use the entire measurement series available up to 2022.

The assessment presented below focuses on return periods covered by OBS (~150 years following the Gringorten plotting position). For larger return periods, it is merely feasible to state the results of GWEX and RF, while any further quantitative assessment is not possible due to the lack of suitable reference data.

4.2. Assessment per variable

4.2.1. Mean monthly precipitation sum

Assessment (see Figure 4.1):

– Both GWEX and RFs show good results in this evaluation. The somewhat larger differences to OBS found at stations for the RFs should be considered in the context of the observation data: The values 1930 to 2019 serve only as an indirect reference for the RFs.

Details:

– GWEX: At all precipitation measurement stations and in all test catchments considered, GWEX shows very good agreement with observed monthly precipitation sums. The regimes are reproduced accurately, and the monthly and annual sums agree well with observations. In most cases, the monthly differences are clearly smaller than 10 %, and the annual differences are always smaller than 5 %.

– RF: In comparison with the observed monthly precipitation sums at stations, the reforecasts show good agreement in many cases and mostly reproduce the monthly regime. The largest deviation is found for GRH, where the slight winter precipitation maximum is not well reproduced and sums are underestimated by up to 25 %. Part of these deviations may be caused by using the reference period 1930–2019 in the observations, which is different from the period the RFs cover with their initial conditions. However, GRH also shows a winter maximum in observed data after 2008, corresponding to the start of the RF period. The deviations for the other stations are mostly limited to a range of −20 % to +10 %. In the test catchments considered, RF results agree well for Aare-Bern (average difference −4 %) and Thur (average difference 3 %), and agree reasonably well for Maggia (higher and lower than observed values give a mean difference of −6 %). The fact that the RFs are closer to OBS at catchment level as compared to station level does not seem to indicate systematic problems in the stochastic downscaling, but might rather be due to sampling issues.

4.2.2. Maximum 1-day precipitation sum

Assessment (see Figure 4.2):

– GWEX generally shows very good agreement with OBS.

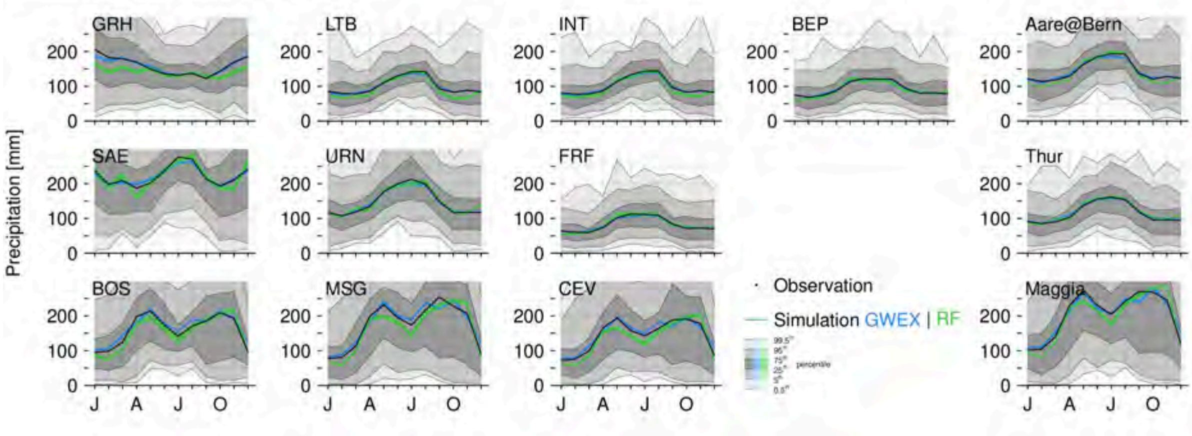

Figure 4.1: Comparison of GWEX, RF and observed mean monthly precipitation sums.

– The agreement of RFs and OBS is still well in the plausible range in most cases; one case (MSG) shows a marked disagreement.
– What seems especially relevant, but also especially difficult to assess for both GWEX and RFs is the behaviour in cases where OBS does not show a clear and continuous pattern in the figures.

Details:

– GWEX: For 1-day precipitation sums, GWEX shows generally very good agreement both at point and at catchment scale. The picture in the Ticino region is difficult to assess: Observations at station CEV and interpolated observations for catchment Maggia seem to indicate a levelling of precipitation intensities in the range of 100 years return period, whereas GWEX shows a slightly upward bent curve for return periods of 100 years and more.
– RF: The agreement between RFs and OBS is good to very good at catchment scale, and also for some of the stations considered (e.g., BEP, SAE, FRF, BOS) a good agreement is noticed. Slightly lower values are found for LTB and INT, slightly higher values for URN. For MSG, RFs show clearly lower values. In the case of GRH, the agreement between OBS and RFs is difficult to assess because OBS shows a marked increase in intensities around 20 to 50 years return period but then levels off again. The RFs agree well up to around 30 years return period. For CEV the agreement is somewhat difficult to assess as well: OBS show slightly stronger increase in intensities around 10 to 20 years return period and then again a levelling from 20 to 100 years. The RFs do not show this behaviour but fit well in the range of 1 to approximately 10 years and then again match well for the highest return period covered by OBS (~150 years).

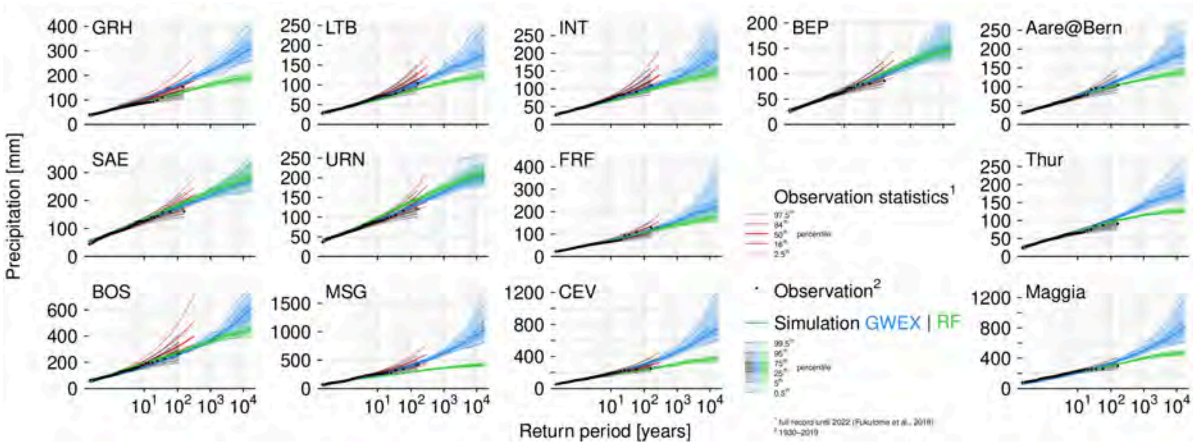

Figure 4.2: Comparison of GWEX, RF and observed maximum 1-day precipitation sums.

4.2.3. Maximum 3-day precipitation sum

Assessment (see Figure 4.3):

– GWEX shows slightly lower station values in comparison to OBS. Apart from that, the shapes of the OBS and GWEX curves usually agree well. Values in the Aare-Bern test catchment show limited disagreement, in the Thur and Maggia catchments the agreement is high.

– RFs frequently show lower values at station level, although good agreement with OBS occurs in some cases as well. At catchment scale, the agreement of RFs and OBS is generally high.

Details:

– GWEX: For 3-day precipitation sums, GWEX often shows slightly lower station values in comparison to OBS (e.g., GRH, LTB, INT, SAE, URN, FRF, BOS). In Ticino, the disagreement is larger for return periods of approximately 10 to 50 years and then becomes smaller again for return periods of approximately 100 years (BOS, MSG, CEV). A somewhat similar pattern is found for BEP, although it is less marked there. Slightly lower values in comparison to OBS are also found in the Aare-Bern catchment, especially for return periods of 20 years and more. In the Thur and Maggia catchments there is generally good agreement, although interpretation of slope and shape of the OBS curve in comparison to the GWEX fit is not straightforward.

– RF: For many of the stations considered the RF values are lower in comparison to OBS. This is most marked for GRH, MSG and CEV where the disagreement increases with increasing return period (to a lesser extent also for SAE). Other stations have uniformly lower RF values in comparison to OBS (LTB, INT), but also closer agreement is found, with only slightly lower RF values (URN, FRF). For BEP, OBS shows a levelling while RFs show a further increase of precipitation sums. At catchment scale, the agreement between OBS and RFs is good to very good, with slight disagreement only for return periods in the range 30 of 100 years.

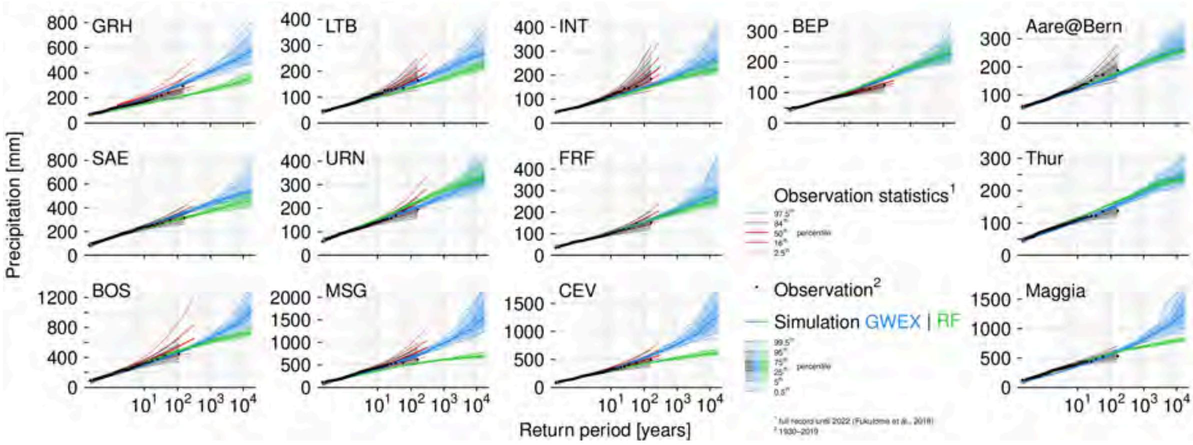

Figure 4.3: Comparison of GWEX, RF and observed maximum 3-day precipitation sums.

4.2.4. Dry spell length

Assessment (see Figure 4.4):

– GWEX shows high agreement with OBS, with only some limited disagreement for long spells (20 days and more).

– RFs generally show shorter spell lengths in comparison to OBS, and the disagreement increases slightly for long spells. The disagreement might originate from 1) biases in the original ECMWF RF data (see e.g., Lavers et al., 2021); 2) the concatenation of the single RFs; 3) the stochastic downscaling, where temporal dependency derives only from the predictors, and is downscaled separately during the month-wise stochastic downscaling.

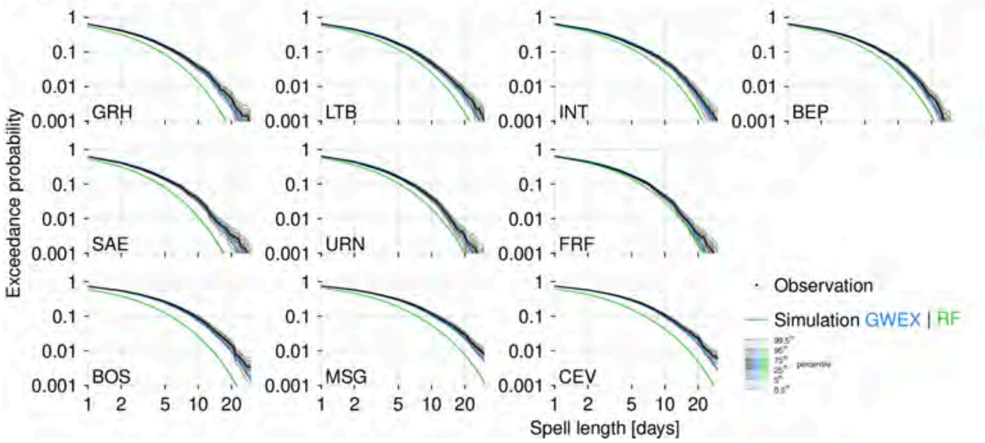

Figure 4.4: Comparison of GWEX, RF and observed dry spell lengths.

4.2.5. Wet spell length

Assessment (see Figure 4.5):

- GWEX shows – similar to dry spell length – high agreement with OBS, with only some occasional and limited disagreement.
- RF spell lengths often agree well with OBS. Disagreement is in most cases limited, with RFs showing slightly longer spells.

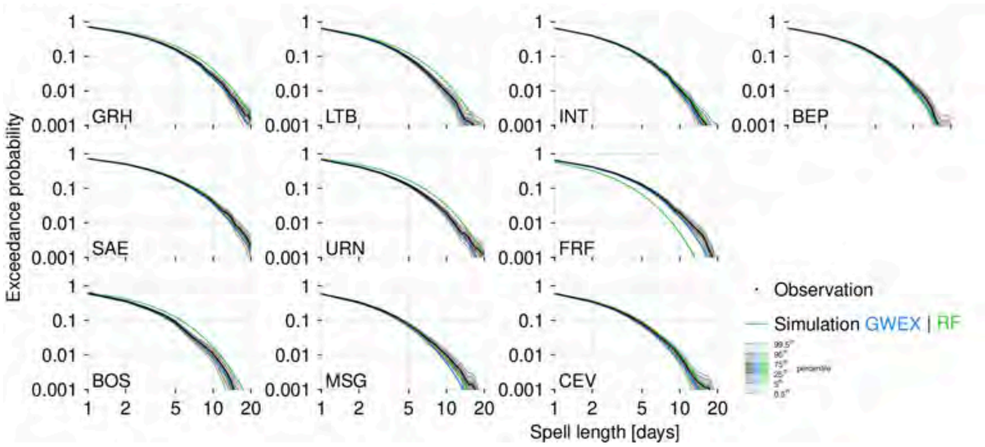

Figure 4.5: Comparison of GWEX, RF and observed wet spell lengths.

4.3. Maximum precipitation sums for shorter blocks

To achieve a consistent comparison of confidence intervals, an additional analysis of maximum 1- and 3-day precipitation sums was implemented (see Figures 4.6 and 4.7). It is based on a time series of 9 900 years for GWEX and RF each, divided into 99 blocks with a length of 100 years each. Results in most cases indicate a broader range of values in the tail of the distribution for GWEX as compared to RF, showing also that GWEX reaches higher precipitation extremes in the 9 900 years of data analysed. Given the differences between how the GWEX and RF time series were composed, it appears not possible to draw firm conclusions beyond this statement. Also, it does not appear justified to make comparisons to the range found for OBS since the latter is an uncertainty estimate derived from a maximum of 90 years of data.

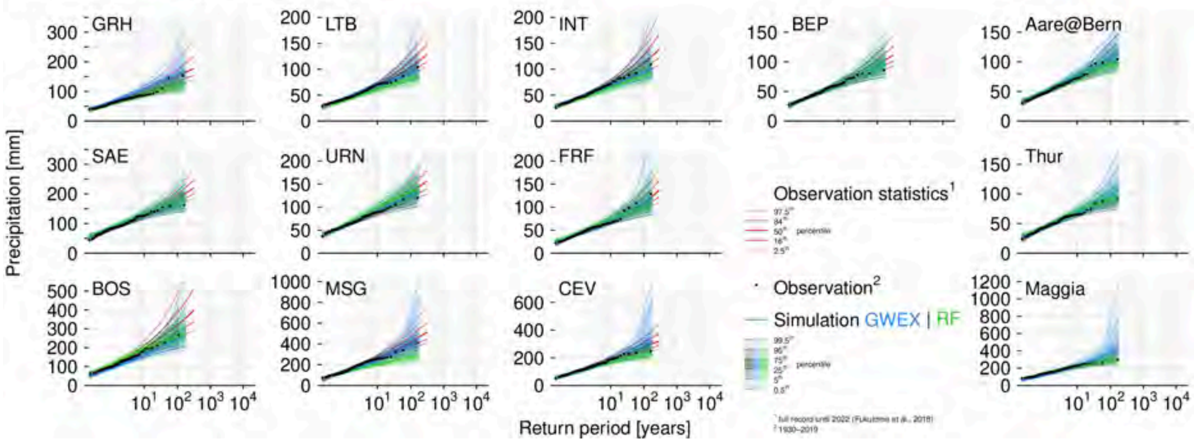

Figure 4.6: Comparison of GWEX, RF and observed maximum 1-day precipitation, here taking 9 900 years of data and dividing them into 99 blocks with length 100 years each for GWEX and RF.

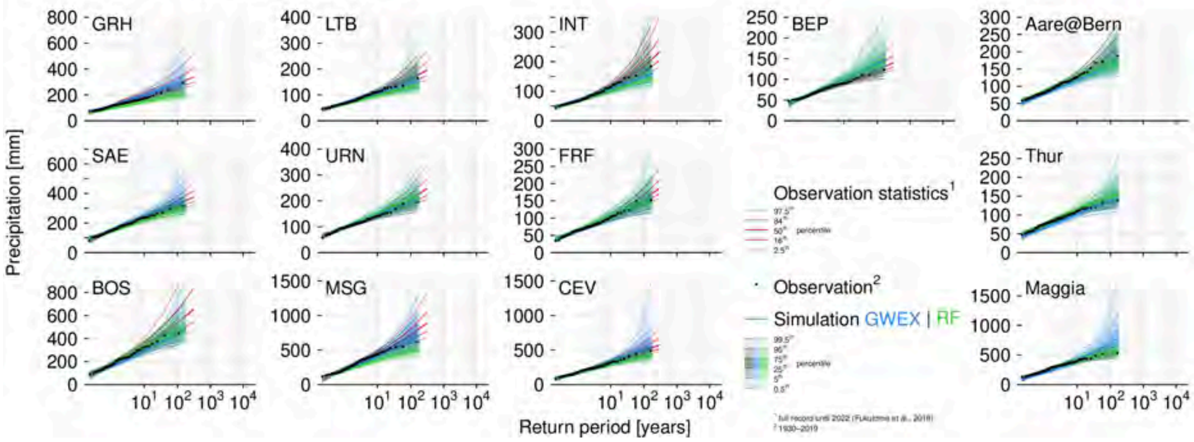

Figure 4.7: Comparison of GWEX, RF and observed maximum 3-day precipitation sums, here taking 9 900 years of data and dividing them into 99 blocks with length 100 years each for GWEX and RF.

4.4. Overall assessment

Both the weather generator (GWEX) and the stochastically downscaled reforecasts (RF) agree well or at least reasonably well with the observations (OBS). In particular, there is good agreement for maximum 1-day precipitation sums for the range of return periods covered by OBS (up to ~150 years). While the differences are larger for two stations in the Maggia River basin, agreement is high for all three test catchments considered, including the Maggia River. For large return periods considerably beyond the range of OBS (1 000–10 000 years), the results of GWEX and RFs differ from each other at various stations and in all test catchments, but based on the available data it is not possible to determine whether any of the two approaches is closer to reality. Good agreement is also noted for monthly precipitation sums and wet spell length. The sometimes slightly weaker agreement of RFs and OBS for these metrics should be seen in the context of different reference periods and the potentially different modes of internal variability; it does not necessarily indicate a poorer performance of the RFs. A somewhat more notable disagreement with OBS is visible for maximum 3-day precipitation sums at the level of meteorological stations, where GWEX and even more so RFs show lower return levels in comparison. At the scale of river basins, by contrast, both GWEX and RFs agree very well with OBS. For rare return periods (1 000–10 000 years), GWEX and RFs show similar results for both the Aare and Thur river basins, while results differ for large return periods in the Maggia River basin. As with 1-day maxima, it is not possible to determine what simulation behaviour is closer to reality. For dry spell length, GWEX agrees well with OBS, whereas the RFs show lower values at the majority of stations considered. The disagreement of RFs and OBS increases with increasing spell length and might point to limitations in the raw RF data or in their treatment. However, dry spell length is comparatively less decisive for the subsequent hydrological simulations and their evaluation towards flood peaks. Any influence would primarily affect antecedent conditions, specifically in cases of exceptionally dry catchment states prior to an initial precipitation event. This does not appear to be a critical limitation with a view to flood estimation, although it deserves attention in any potential follow-up work.

In summary, good agreement of both GWEX and RFs with OBS is noted with respect to the criteria considered here. The agreement between GWEX and OBS appears slightly higher than the agreement between RFs and OBS. This might be partly due to the fact that OBS were used to parametrize GWEX, whereas OBS are not a fully compatible reference for the RF due to different periods covered, biases in the original ECMWF RF data and challenges in bias correcting and downscaling the RFs. The evaluation of precipitation has not revealed critical limitations in either of the two approaches.

Based on these encouraging results, combining RFs and GWEX approaches to investigate the potential impacts of internal variability would be an interesting direction for future research.

5

Validation of hydrological simulations

This chapter provides selected validations for the hydrological simulations with HBV (Section 5.1) and the hydrological routing with RS Minerve (Section 5.2), exploring on the one hand disaggregated observations of precipitation and temperature as inputs for a control simulation (see Section 3.1.1), and on the other hand using meteorological inputs from the two weather generators GWEX and SCAMP (Sections 3.2.1 and 3.2.2) and the reforecasts (Section 3.2.3). The aspects examined include performance metrics, runoff coefficients, flow duration curves (FDCs), and seasonality of annual maximum floods (AMFs). Note that performance metrics can only be calculated for the control simulation, where daily and to some extent also hourly discharge observations are available for at least part of the simulation period. Furthermore, runoff coefficients are only discussed for hydrological modelling, and not for the routing, as they lose relevance in large catchments where lake regulation, lake retention and further effects strongly delay runoff response. In a similar vein, the relevance of runoff coefficients diminishes in larger sub-catchments simulated with HBV, although results are still shown in the following.

It is important to emphasize that a more comprehensive validation across the entire range of return periods considered in this project is not feasible due to a lack of suitable reference data on rare events. A detailed discussion of AMF results and corresponding exceedance curves at individual output sites is provided in Chapters 6 and 9, and a comparative evaluation of orders of magnitude follows in Chapter 7.

5.1. Hydrological modelling

5.1.1. Control simulation

The control simulations discussed in the following were done with the disaggregated meteorological input (see Section 2.1) for the entire period 1930–2019, using the first year as a warm-up. Model performance was assessed with common hydrological performance metrics such as Nash-Sutcliffe efficiency (NSE) and Kling-Gupta efficiency (KGE), comparing simulated and observed discharge data. We also analysed flow duration curves (FDCs) based on daily discharge data to evaluate model performance across the full range of discharges, from low to high flows and including larger floods. Note that the analysis of daily FDCs is more focused on flood volumes in catchments where the highest peak flows occur over markedly shorter durations than a day. The runoff coefficient of the AMFs was examined to implicitly compare runoff generation between simulations and observations. Furthermore, the distribution of the occurrence of AMFs was examined to evaluate the seasonality of the simulated floods.

Most models showed satisfactory to good performance regarding the hydrological performance metrics (Figure 5.1) ranging between NSE values of 0.6 and 0.75 and KGE values around 0.8. Figure 5.1 also shows that there are only small differences in model performance for the three representative parameter sets. These boxplots refer to data from the calibrated catchments (see Section 3.3). The performance of the regionalised catchments was less straightforward to assess because the quality of the limited observations available was sometimes questionable, among other things due to the strong impact of lake and reservoir regulation. In other cases, only peak flow data were available for comparison.

Model performance was not satisfactory for a few catchments (outliers in Figure 5.1), reaching NSE values between 0 and 0.3 only. For example, Maggia at Lodano (MagLdn) does not perform well over the entire control run period. However, the overall performance of the model appears to be worsened mainly by its behaviour during the melting season and by a simulated flow response that is absent

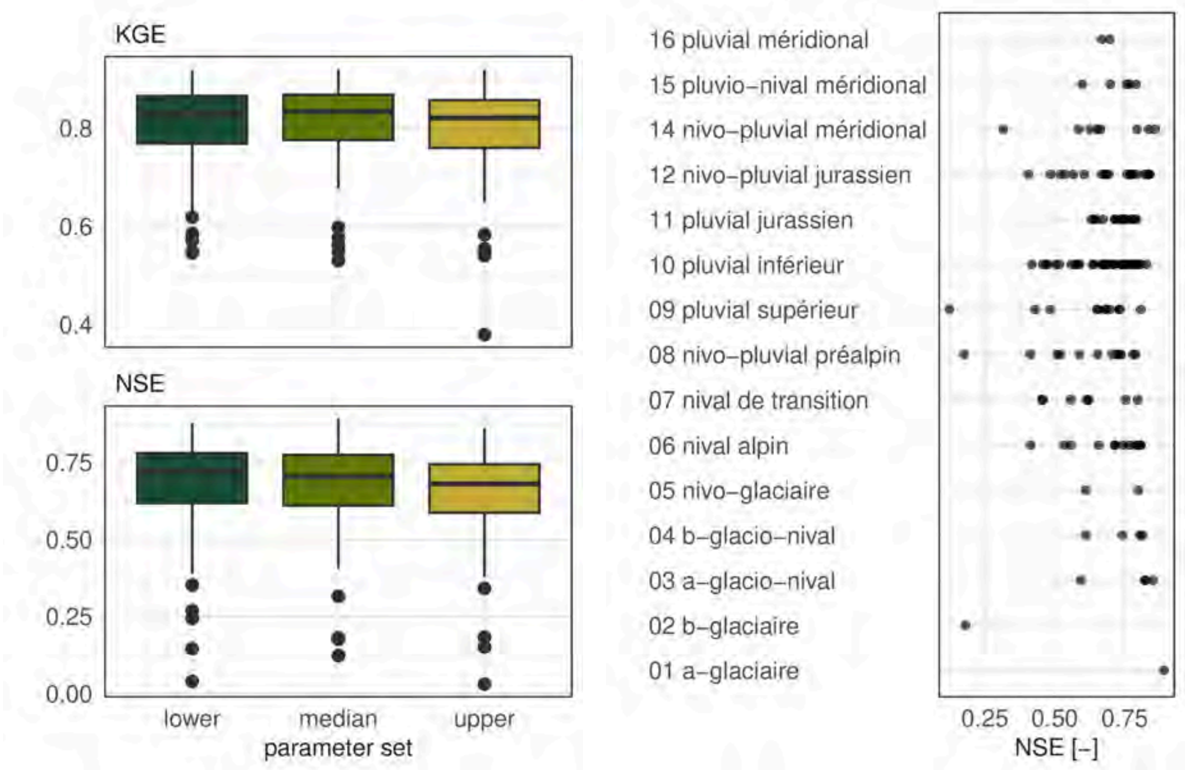

Figure 5.1: Model efficiency criteria. Left: Boxplots of the model efficiency criteria KGE and NSE. Comparison of the three simulations to the observations using three representative parameter sets (high, low, intermediate) using disaggregated precipitation 1930–2019 as input. Right: The individual model efficiency criterion NSE for all catchments grouped by streamflow regime. Results are here only shown for the intermediate representative parameter set.

in the observations. This indicates precipitation events resulting from the interpolation of station data that were not actually occurring in the catchment. It is also important to note that reservoirs are not implemented in the HBV representation of the Maggia River basin. Further insights in this context are given in the discussion of hydrological routing (Section 5.2).

No correlation was identified between model performance and streamflow regimes, indicating that no particular streamflow regime consistently shows particularly high or low performance. For example, we find very high model performances for catchments with glacier influenced streamflow regimes, but also one of the poorest performances is found for a glacier influenced catchment (Figure 5.1).

Runoff coefficients were computed using the AMFs of each year and the associated sum of precipitation 72 hours around the peak flow. To compare the runoff coefficients of the AMFs, we removed events where snow melt was a major contributor to runoff generation. We also did not compare the runoff coefficients for catchments with glacier influence, because there glacier melt is the main component of runoff in summer, and it is not possible to identify how much of the precipitation contributes directly to runoff.

Overall, the seasonal distribution of runoff coefficients is very similar for all analysed regime types, with values between 0.1 and 0.5 for nival alpin and pluvial inférieur, and 0.25 to 0.60 for nival de transition, nivo-pluvial préalpin and pluvial jurassien. For the catchments with regime types pluvial méridional and nivo-pluvial méridional found in the south of Switzerland, the distributions of the runoff coefficient are changing over the seasons and are not as similar between observed and control simulation as for the regimes in the north of Switzerland.

For most regimes, only the winter distribution for the simulations differs from the observations. For the regime types nival alpin, nivo-pluvial préalpin and nivo-pluvial méridional, the simulated winter distri-

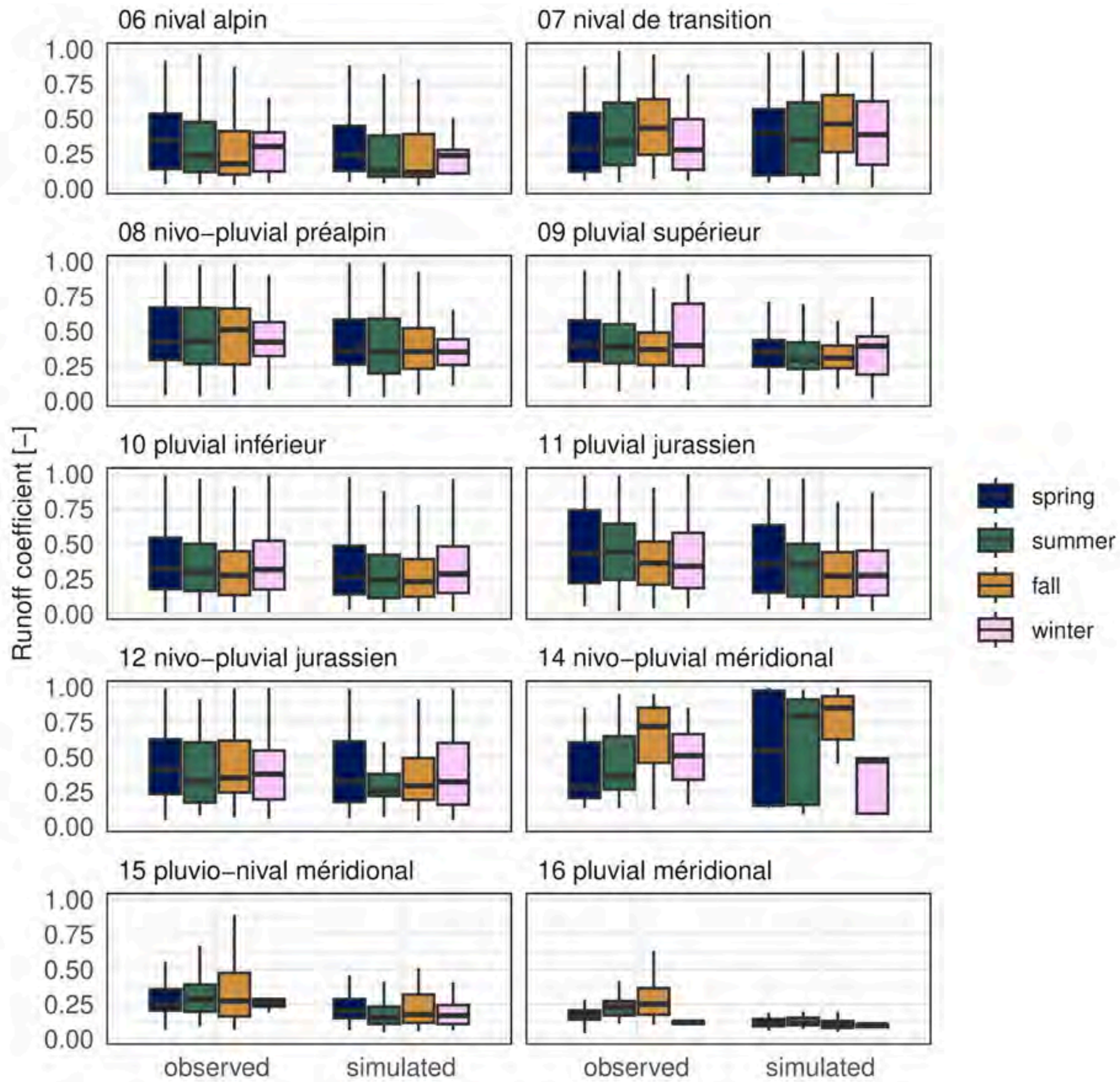

Figure 5.2: Seasonal distributions of AMF runoff coefficients for observations and simulations using the intermediate representative parameter set.

bution consists of lower runoff coefficients. For catchments with regime type nival de transition, the simulated winter distribution shows higher runoff coefficients.

While there seems to be a shift towards lower runoff coefficients in all seasons for the more precipitation-influenced regimes of the méridional family, the spread in the simulations is much higher for the type nivo-pluvial méridional, and the resulting distributions from the simulations are very different from the observed ones.

We compared the flow duration curves (FDCs) of the observations with the simulated FDCs, again based on daily discharge data (Figure 5.3). To focus more on high flows, the plots are drawn with a logarithmically scaled x-axis. The overall simulated FDCs using the disaggregated meteorological input are very similar to the observed ones, indicating that the overall flow distributions are satisfactorily simulated, which is important for the approach of using CS for flood estimation. However, the maximum flows (which were not the focus of the calibration) are often slightly over- or underestimated.

For the pluvial catchments in the river basins Rhine, Limmat, Reuss and Aare, we found only slight over- and underestimations of the highest flows (e.g., Biber at Biberbrugg (BibBib), Steinach at Steinach, Mattenhof (SacSac), Argen at Giessen (ArgGie)). The same is true for the catchments with a nival streamflow regime (including the Inn River basin). Looking at the catchments with glacier influence, we found both overestimation (e.g., Reuss at Seedorf (ReuSee)) and underestimation of the highest flows, and also very good matches (e.g., Grosstalbach at Isenthal (GroIse), Kander at Hondrich (KanHon)).

For the Rhone River basin, there were more over- than underestimations of high flows for the catchments with pluvial streamflow regime (e.g., L'Aire at Centenaire (AirCen)), but with exceptions (e.g., L'Hermance at Hermance (HrmHrm) or La Versoix at Versoix-CFF (VsYVer)). We furthermore found slight overestimation of the largest flows in the FDCs for the nival catchments (e.g., Avancon at Bex (AvaBeY)), and again under- and overestimation for the glacier influenced catchments.

The FDCs in the Ticino River basin were satisfactorily simulated for the catchments with pluvial streamflow regimes, with slight over- and underestimation for the catchments with nival regimes (e.g., Cassarate at Pregassona (CasPre) and Vedeggio at Agno (VedAgn)). Strong overestimation of high flows was found for Magliasina at Magliaso, Ponte (MglMag) and strong underestimation of high flows for Fiume Toce at Candoglia (TocCan).

We validated the seasonality of the simulations using the disaggregated meteorological data as model forcing by first grouping the catchments by regime type, discerning dominant influence of ice melt, snow melt and precipitation. The visual evaluation of all catchments with available observations is summarized in Table 5.1, showing that for most catchments there were satisfactory to good simulations with respect to the seasonality of the occurrence of AMFs. Note that five out of the eleven catchments for which the simulated seasonality was not satisfactory are catchments that contain a substantial amount of karst (20 % or more). Realistically representing karst would require detailed local data that in many cases are not available.

Table 5.1: Evaluation of the seasonality match of the AMFs between observation and control simulation.

Regime	good	satisfactory	poor
a-glaciaire	1	0	0
b-glaciaire	1	2	0
a-glacio-nival	5	3	0
b-glacio-nival	6	2	1
nivo-glaciaire	6	1	0
nival alpin	12	4	2
nival de transition	3	4	0
nivo-pluvial préalpin	6	7	1
pluvial supérieur	6	6	2
pluvial inférieur	23	19	1
pluvial jurassien	5	12	0
nivo-pluvial jurassien	12	5	3
nival méridional	3	1	0
nivo-pluvial méridional	4	7	0
pluvio-nival méridional	2	2	1
pluvial méridional	0	2	0

In the following, we present examples of the evaluation of the seasonality of the occurrence of observed and simulated AMFs by simple streamflow regimes, i.e. pluvial, nival glacial.

In the catchments with pluvial streamflow regime, AMFs occurred throughout the year, and we generally found a good to very good agreement between observations and simulations. For the catchments in the Rhine River basin, the Limmat River shows only some AMFs in winter, with most AMFs being found in spring and summer months, between May and September. For the Reuss River, the AMFs occur between May and November. For the remaining pluvial catchments in the Rhine River basin, some show AMFs mainly in winter (e.g., Biber at Buch (BbrBuc), Wiese at Basel (WieBas)), many show AMFs throughout the year (e.g., Ergolz at Liestal (ErgLie), Töss at Neftenbach (ToeNef)), and some show AMFs mainly during summer (Dornbirnerach at Lauterach (DbaLah), Goldach at Goldach, Bleiche (GolGol)) (Figure 5.4). In the Rhone and the Ticino river basins, we find some catchments that have two more distinct seasons for high flows (e.g., Le Redon at Margencel (RedMgc)), which are also well captured by the simulations (Figure 5.4).

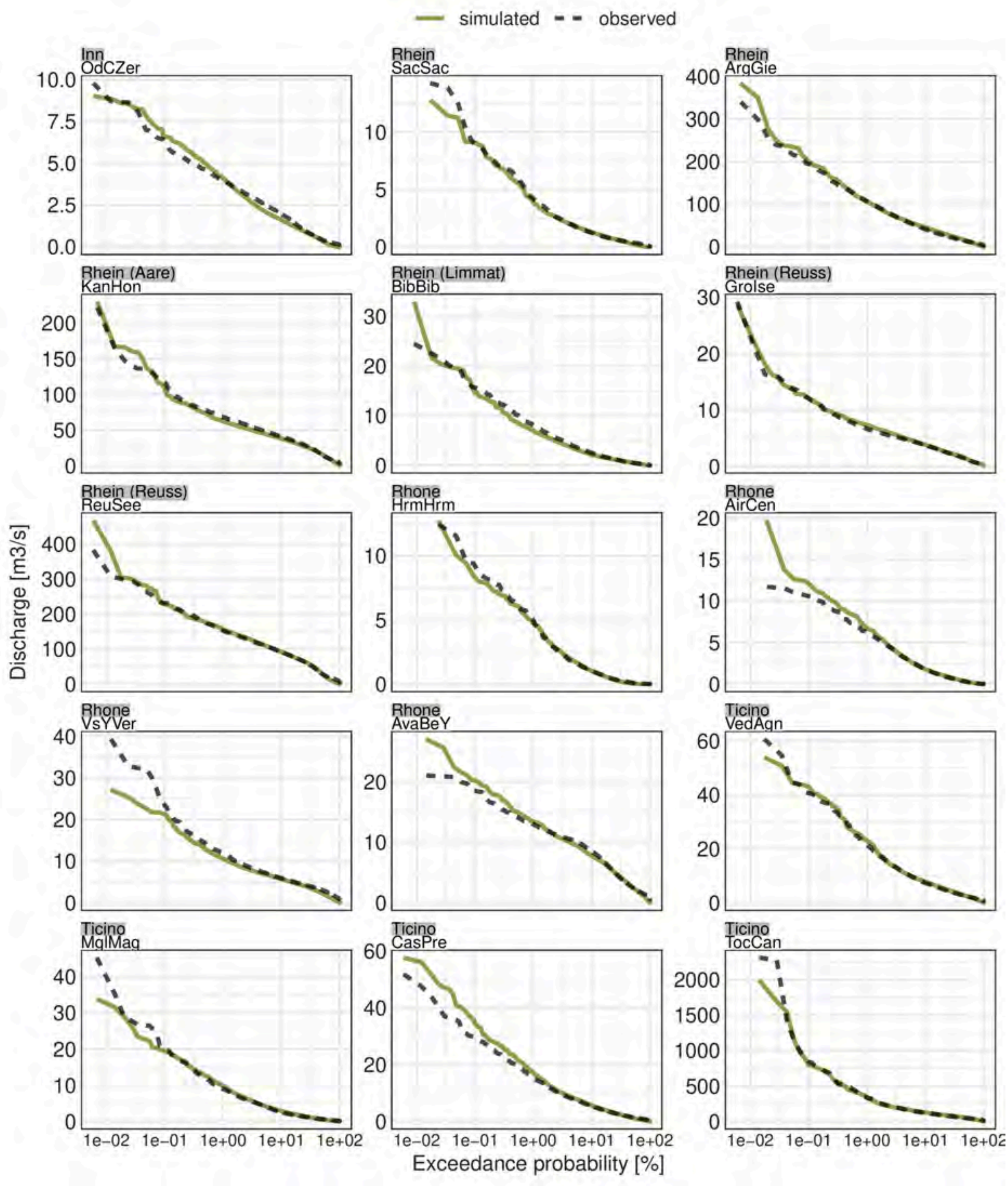

Figure 5.3: Flow duration curves of selected example catchments from the large river basins. The catchments are grouped by large river basin and within that by mean catchment elevation. Note the logarithmic x-axis.

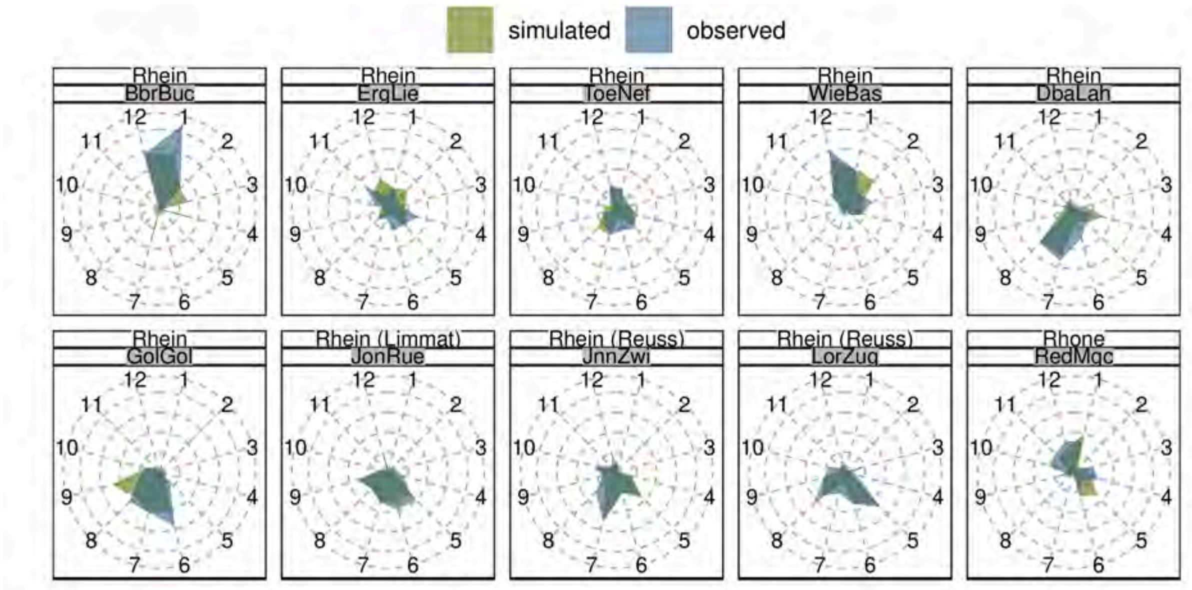

Figure 5.4: Seasonality of observed (blue) and simulated (green) AMFs, expressed in percent of occurrence for examples of catchments with pluvial streamflow regimes. For the simulation, disaggregated precipitation and air temperature was used in conjunction with the intermediate representative parameter set. For catchment abbreviations see Table C.1.

For the snow influenced catchments, the agreement between simulated and observed seasonality appears to depend on the degree of snow influence. Many catchments showed a distinct seasonal pattern, while those with more transitional snow influence often have a more complex pattern of peak flows. In these cases, the simulations only partially capture the observed seasonality (Figure 5.5). In the Rhine River basin, the observed AMFs occur between May and September, and many are well reproduced by the model. Some of the catchments show a minor amount of observed winter floods that are not or not well simulated (e.g., Thur at Jonschwil, Mühlau (ThuJon)). For the Reuss and the Limmat river basins, we found a tendency for the AMFs to be simulated about one month earlier than they were observed (e.g., Seez at Mels (SeeMls)), but apart from that, the seasonality was rather well simulated. An exception is the Kleine Emme River (KEmEmm), where a second peak season is observed, but not simulated. Instead, all AMFs are simulated in May and June for the Kleine Emme River.

For the Aare River basin, about half of the catchments show very good agreement between observed and simulated AMF seasonality both in summer (e.g., Emme at Emmenmatt (EmmEmt)) and in winter (e.g., Arnon at Grandson-Poissine (ArnGra)). Some observed seasonalities show more complexity, with multiple peak months. These cases are less well simulated, with discrepancies such as two peak flow seasons in the observations, but only one in the simulations (e.g., Giessbach at Brienz (GssBri)); two peak flow seasons simulated correctly but a temporal shift (e.g., Rotache at Oppligen (RtaOpp)); or two simulated peak flow seasons whereas one only is present in the observations (e.g., Mujon at Treycovagnes (MujTre)).

For the Inn River basin, the seasonality was well simulated, and for the Rhone River basin, seasonality was simulated satisfactorily for most catchments (e.g., Promenthouse at Gland Route Suisse (ProGla)), also with distinct summer or winter peak flow seasons and more complicated seasonality (e.g., L'Aire at Centenaire (AirCen)). For the Ticino and Adda river basins, the seasonality of the AMFs usually is centered around early summer (i.e., May and June) and fall (i.e., September, and for some November). For these southern catchments, the simulated seasonality of the AMFs was satisfactory.

All of the glacier influenced catchments have their highest annual flows in summer between May and September, as expected from their regime type. This is true for both the observations as well as the simulations. For the majority of glacier influenced catchments, the seasonality of the observed and simulated AMFs agree well. Figure 5.6 shows this seasonality match for example catchments in the Rhone River basin (Goneri at Oberwald (GonOwd)), the Rhine River basin (Linth at Mollis, Linthbrücke

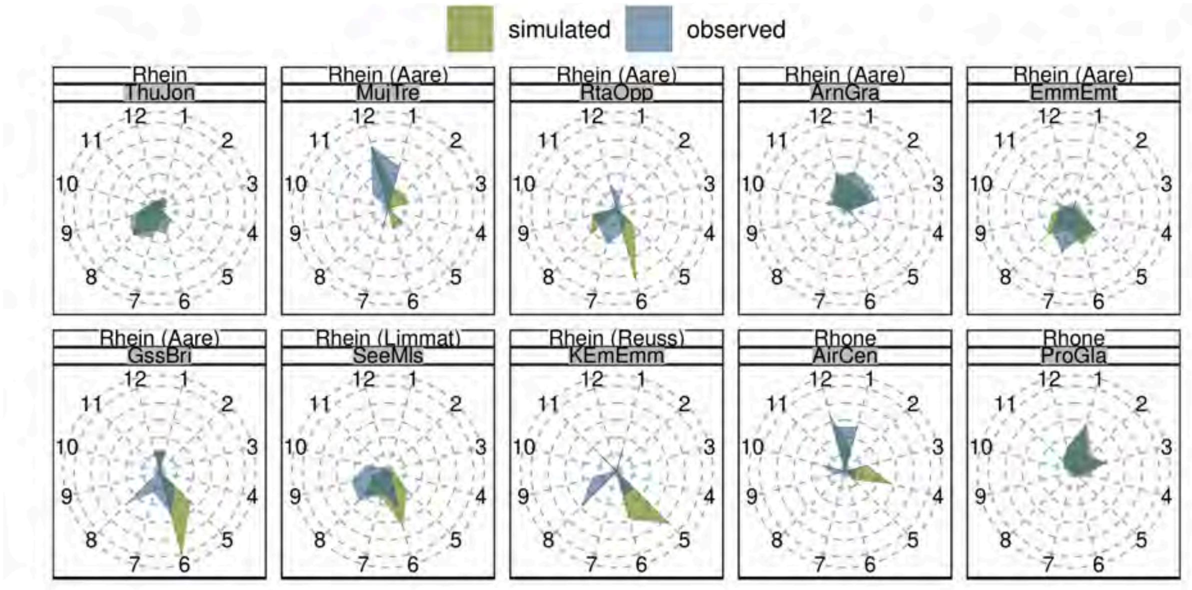

Figure 5.5: Seasonality of observed (blue) and simulated (green) AMFs, expressed in percent of occurrence for examples of catchments with nival streamflow regimes. For the simulation, disaggregated precipitation and air temperature was used in conjunction with the intermediate representative parameter set. For catchment abbreviations see Table C.1.

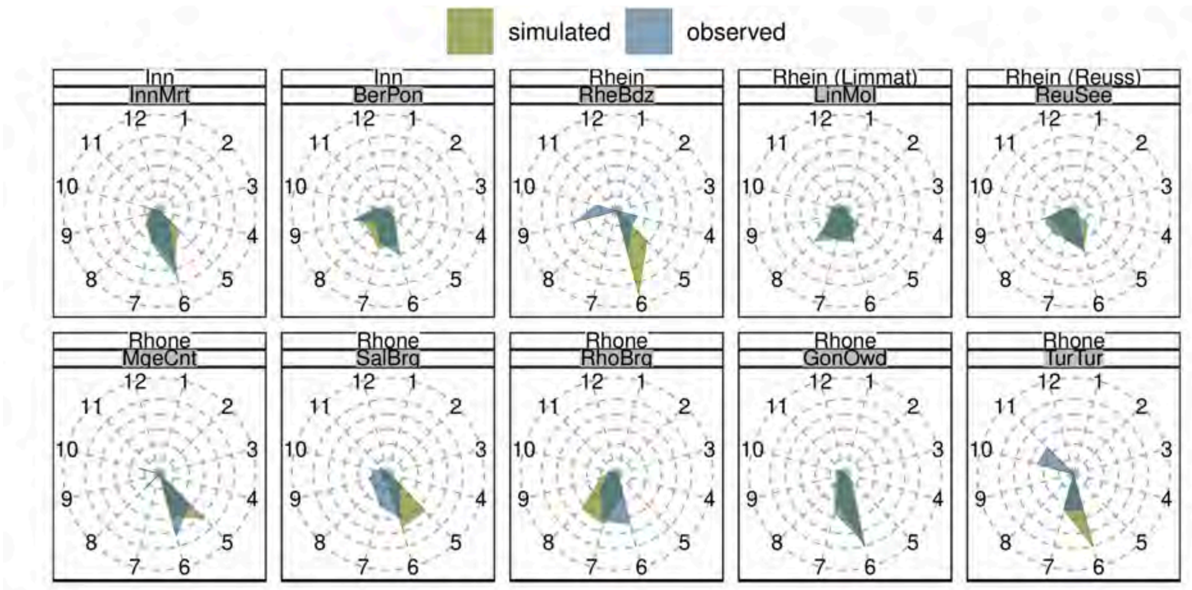

Figure 5.6: Seasonality of observed (blue) and simulated (green) AMFs, expressed in percent of occurrence for examples of catchments with glacier influenced streamflow regimes. For the simulation, disaggregated precipitation and air temperature was used in conjunction with the intermediate representative parameter set. For catchment abbreviations see Table C.1.

(LinMol), Reuss at Seedorf (ReuSee)) and the Inn River basin (Inn at Martina (InnMrt), Berninabach at Pontresina (BerPon)). For some catchments in the Rhone River basin, the simulated AMFs tend to occur approximately one month earlier (e.g., Saltina at Brig (SalBrg)) or one month later (e.g., Rhône at Brig (RhoBrg)), and for some catchments, AMFs occur in two seasons but the simulations show only one season (e.g., Turtmänna at Turtmann (TurTur)).

Overall, the control simulations over the period 1930–2019 show at least satisfactory results for most catchments in terms of efficiency criteria, flow duration curve and size and timing of the AMFs. For the few catchments where the control simulations were not satisfactory, several reasons were found for the lack of performance. These include in particular a high percentage of karst areas, impact of reservoir operation on observed streamflow, small catchment size, and a mismatch between the disaggregated precipitation events and observed floods.

5.1.2. Weather generators GWEX and SCAMP

To keep the analysis of the flow duration curves (FDCs) manageable for the long simulations using weather generator inputs (300 000 years, hourly), we again sampled daily values with length similar to that of observations for each scenario and each block of 1 000 years. From each of the samples, we calculated the exceedance probabilities separately. For plotting, we calculated the 95 % confidence intervals for each exceedance probability over the flow values and show these together with the observations (if available) and the control simulation (see previous section).

Figures 5.7 and 5.8 show the 95 % confidence intervals of all sampled FDCs. It should be noted that of course individual extreme FDCs exist beyond these confidence intervals, and that comparison of the different FDCs shown in the plot should be made with caution, as the FDCs of control simulation and observations do not include confidence intervals. We chose not to plot individual extreme FDCs from the simulations based on weather scenarios to maintain readability and focus on assessing overall agreement.

For catchments in the Limmat and Reuss river basins, such as Jona at Rüti (JonRue) and Rauti at Oberurnen (RtiObu) (Figure 5.7), there are mainly very similar FDCs from the simulations of the weather generators resampled to the size of the available observations.

The flow duration curves in the Rhine, Aare and part of the Reuss river basins show a tendency for simulations using the GWEX weather generator to be higher than those using the SCAMP weather generator for the larger flow values and especially for rare floods (Figure 5.7). Examples include the Glatt at Rheinsfelden (GlaRhs), the Reuss at Seedorf (ReuSee), the Aabach at Lenzburg (AabLen) and the Suhre at Suhr (SuhSuh). The range of intermediate to low discharge values of the FDCs is very similar for almost all catchments. Regarding their comparison with the control simulation with the disaggregated meteorological input as well as with observations, we find many catchments where the FDCs of the observations and control simulations are more similar to the FDCs of SCAMP rather than to GWEX, where they are different.

Also for the Inn, Rhone, Doubs and Ticino river basins, GWEX mostly has higher estimates and deviates to higher values in the FDC for the higher discharge values (Figure 5.8). Example catchments for higher rare floods are the Rosegbach at Pontresina (RosPon), the Verzasca at Lavertezzo (VerLav) or the Maggia at Lodano (MagLdn). However, the FDCs of the two weather generators are also very similar in many cases (Ova dal Fuorn at Zernez, Punt la Drossa (OdFZer), Arve at Genève, Bout du Monde (ArvGen), Le Doubs at Ocourt (DouOco) and Brenno at Loderio (BrnLod)). For a few catchments, the SCAMP-based simulations are slightly higher than the GWEX-based ones (e.g. Le Redon at Margencel (RedMGc)).

For some catchments, the observations and control simulations are within the 95 % confidence intervals of the weather generators. An interesting example is the Rosegbach at Pontresina (RosPon) (Figure 5.8), where the FDC confidence intervals of GWEX are similar to the observations and the FDC confidence intervals of SCAMP are similar to the control simulation. In several cases, higher values are obtained for the weather generators, especially for GWEX. This is explained by the larger pool of extreme events available, resulting from the pairing of generated precipitation events with antecedent conditions provided by the continuous simulation approach.

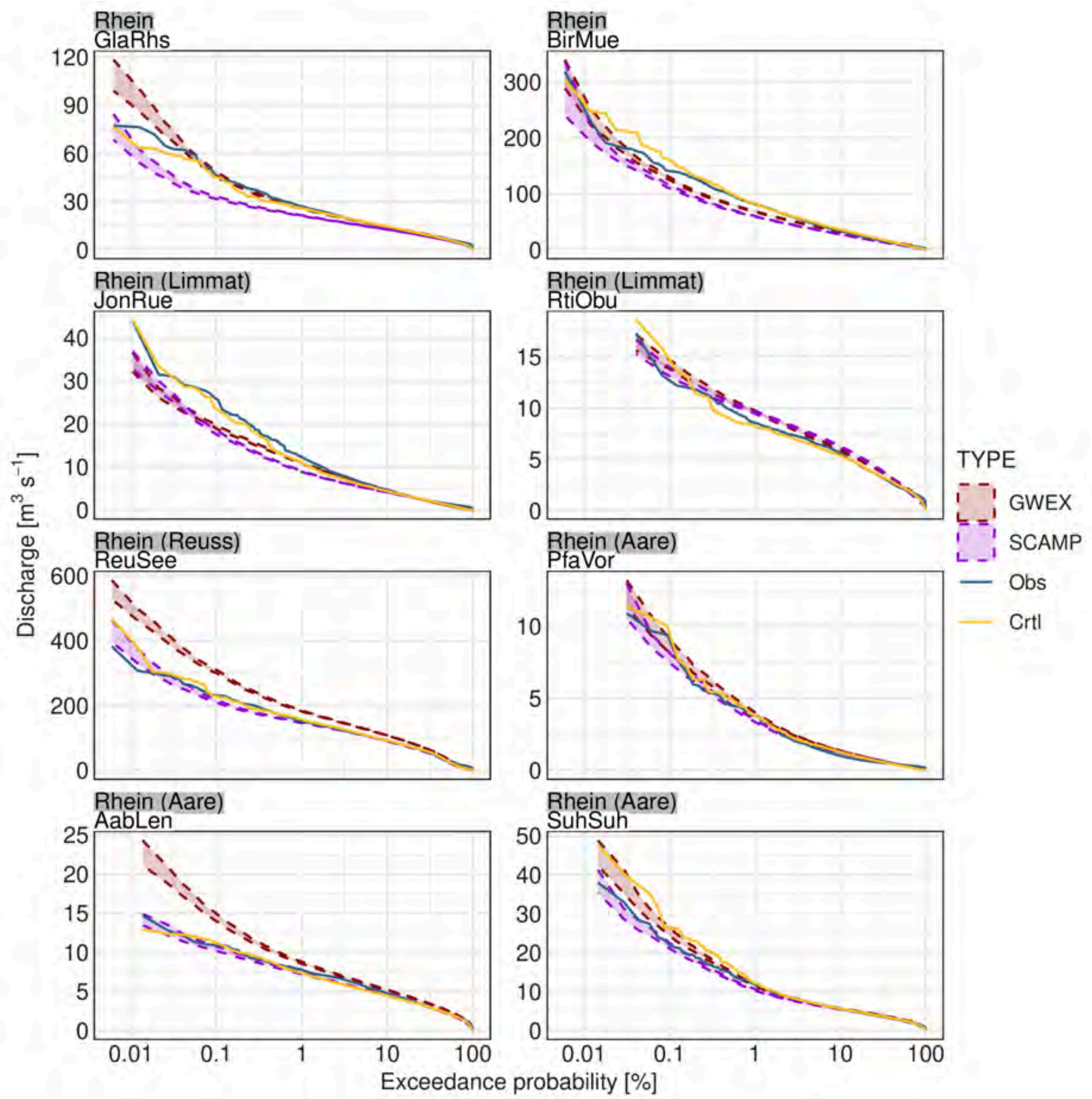

Figure 5.7: Flow duration curves (FDCs) for selected sub-catchments of the Rhine River basin (rivers Rhine, Limmat, Reuss and Aare). The flows are sampled from the simulations using GWEX and SCAMP weather scenarios, together with the FDCs from the control run (Ctrl) and the observations (Obs). The sample size is equal to the length of the observations (or the control run if its length is shorter than that of the observations). Only the results of the intermediate representative parameter set are shown. For catchment abbreviations see Table C.1.

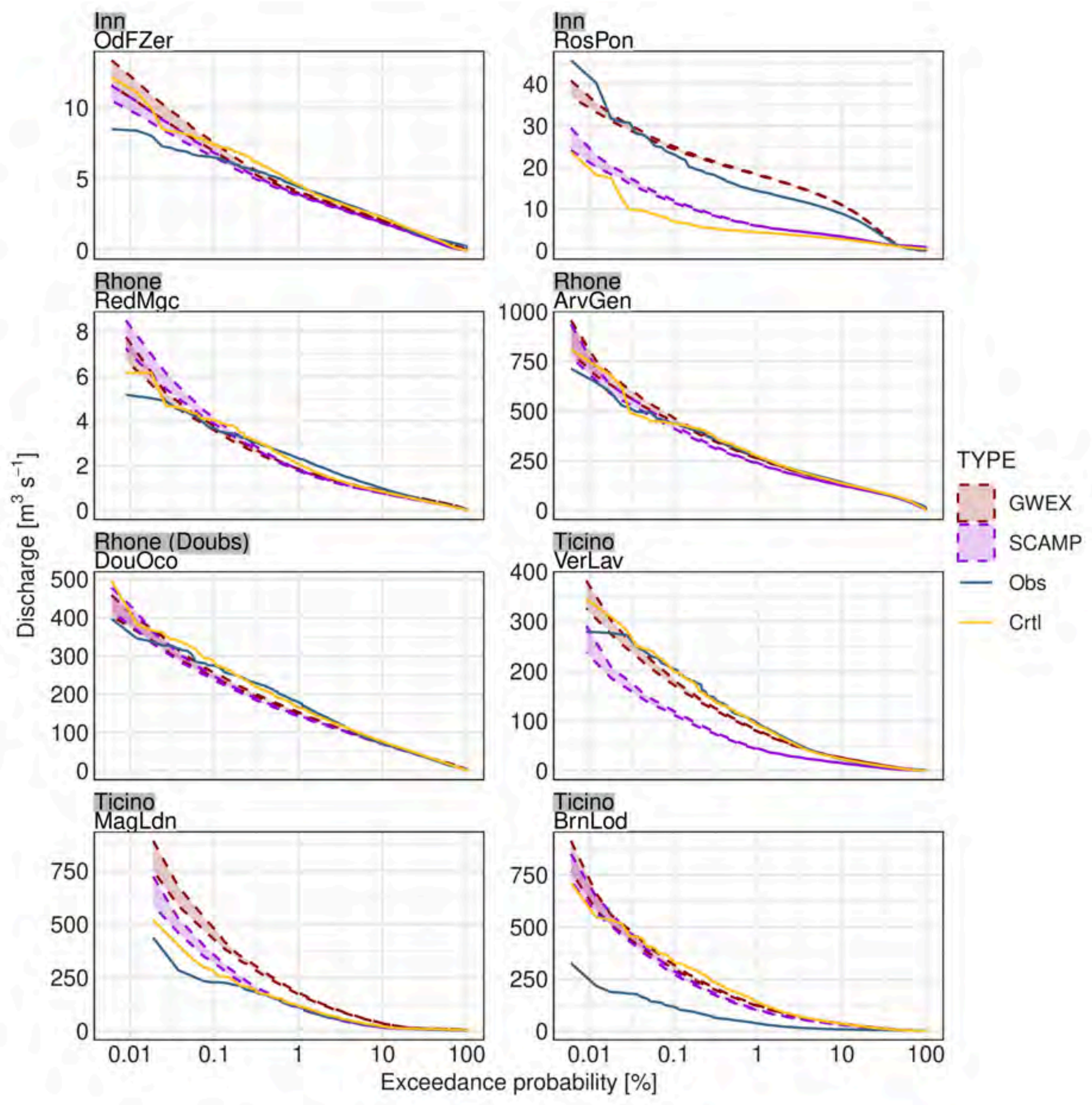

Figure 5.8: Flow duration curves (FDCs) for selected selected sub-catchments of the Rhone, Doubs, Inn and Ticino river basins. The flows are sampled from the simulations using the GWEX and SCAMP weather scenarios, together with the FDCs from the control run (Crtl) and the observations (Obs). The sample size is equal to the length of the observations (or the control run if its length is shorter than that of the observations). Only the results of the intermediate representative parameter set are shown. For catchment abbreviations see Table C.1.

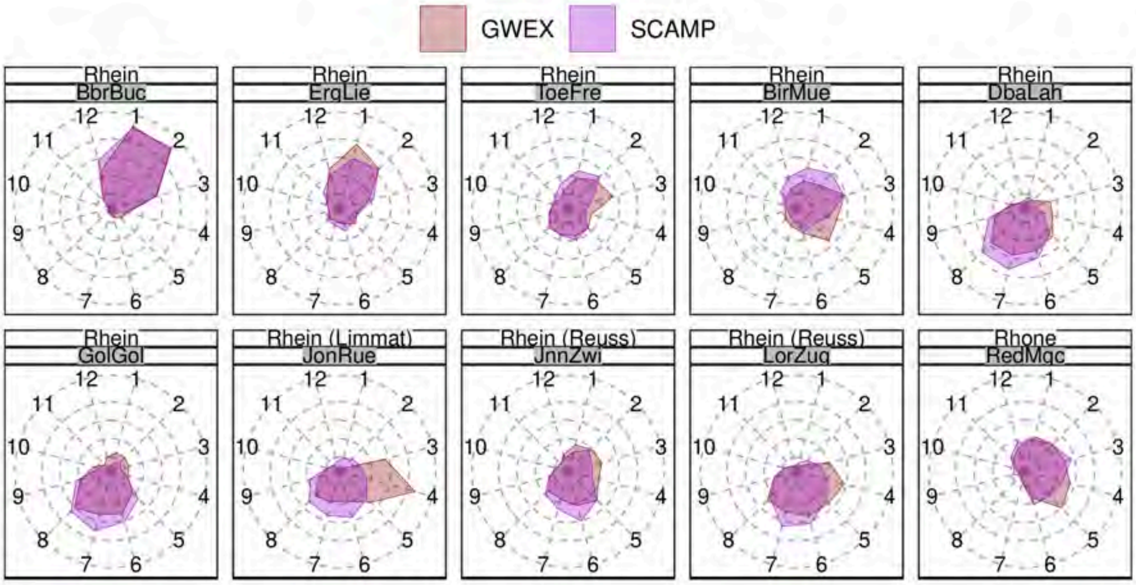

Figure 5.9: Seasonality of AMFs simulated using the weather generators GWEX and SCAMP, expressed in percent of occurrence for sample catchments with **pluvial** streamflow regimes. For catchment abbreviations see Table C.1.

In the glacier-dominated catchments, simulations using the two weather generators GWEX and SCAMP show the same distinct seasonalities for all larger basins (Figure 5.11), with the highest probability of AMFs occurring in May, June or July. There is a maximum shift of one month in either direction for the highest probability of occurrence of AMF (e.g., Berninabach at Pontresina (BerPon) and Morge at Conthey (MgeCnt)).

The same is found for the nival catchments: A seasonality that is very similar to identical between the two weather generators (Figure 5.10), here about one month earlier than in the glacier-dominated catchments. This is consistent with the runoff regimes of the catchments, where snow melt peaks earlier in the year than ice melt.

Also for the pluvial catchments, the seasonality of the two weather generators is very similar, indicating the highest probability of AMF occurrence in winter and early spring (January, February, March) (e.g., Biber at Buch (BbrBuc), Ergolz at Liestal (ErgLie)) or in summer (June, July) (e.g., Jonen at Zwillikon (JnnZwi), Goldach at Goldach, Bleiche (GolGol)), with further occurrences throughout the year (Figure 5.9). The GWEX and SCAMP weather generators are not in perfect agreement in all cases, but for many catchments have a shift of about one month in the highest probability of AMF occurrence. For some catchments, the SCAMP weather generator causes some AMFs to occur even in winter (e.g., Goldach at Goldach, Bleiche (GolGol)), while the GWEX weather generator does not cause any AMFs in this season.

The GWEX weather generator was compared in terms of FDCs with both the control simulation, the observation and the alternative weather generator SCAMP. For all catchments, the lower parts of the FDCs agree very well. For the highest flows, we found differences to the observations and the control run, mostly showing higher flow values for the GWEX weather generator, which can be explained by the larger pool of events due to the very long CS, which allows for numerous events beyond the observed range.

Compared to the alternative weather generator SCAMP, we found higher estimates for the GWEX weather generator for many catchments, but not for all catchments (Figure 5.12). When counting the sub-catchments where GWEX produced higher FDCs than SCAMP, we find that the Inn River basin shows the highest percentage of GWEX-based FDCs to be clearly higher than the ones based on SCAMP. This is true throughout the Inn River basin, with no clear indication for influence of catchment extent or elevation. Also in the Rhine River basin, we find comparatively numerous sub-catchments

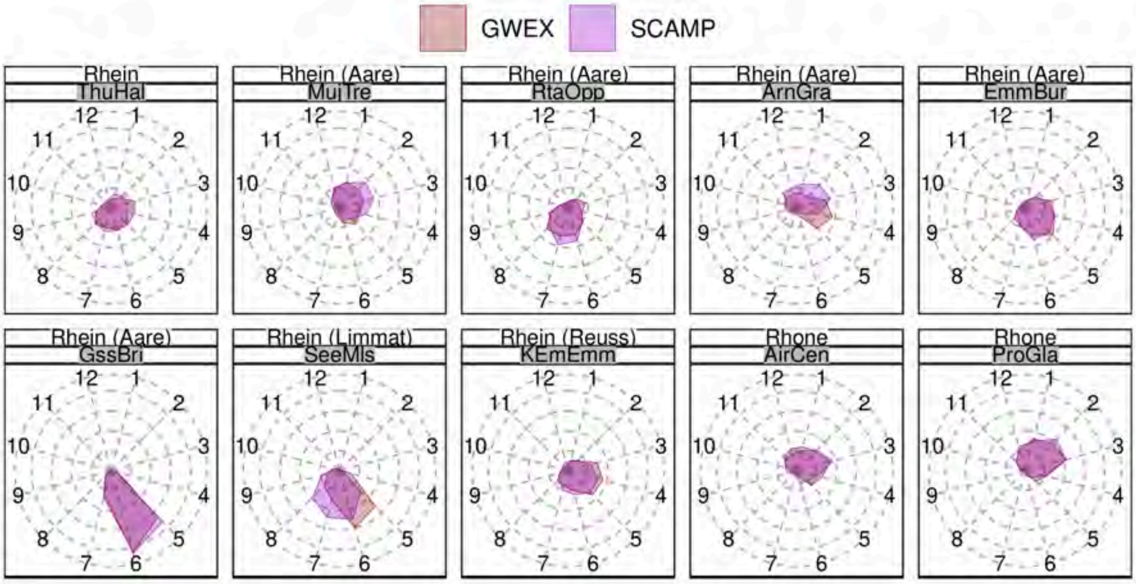

Figure 5.10: Seasonality of AMFs simulated using the weather generators GWEX and SCAMP, expressed in percent of occurrence for sample catchments with **nival** streamflow regimes. For catchment abbreviations see Table C.1.

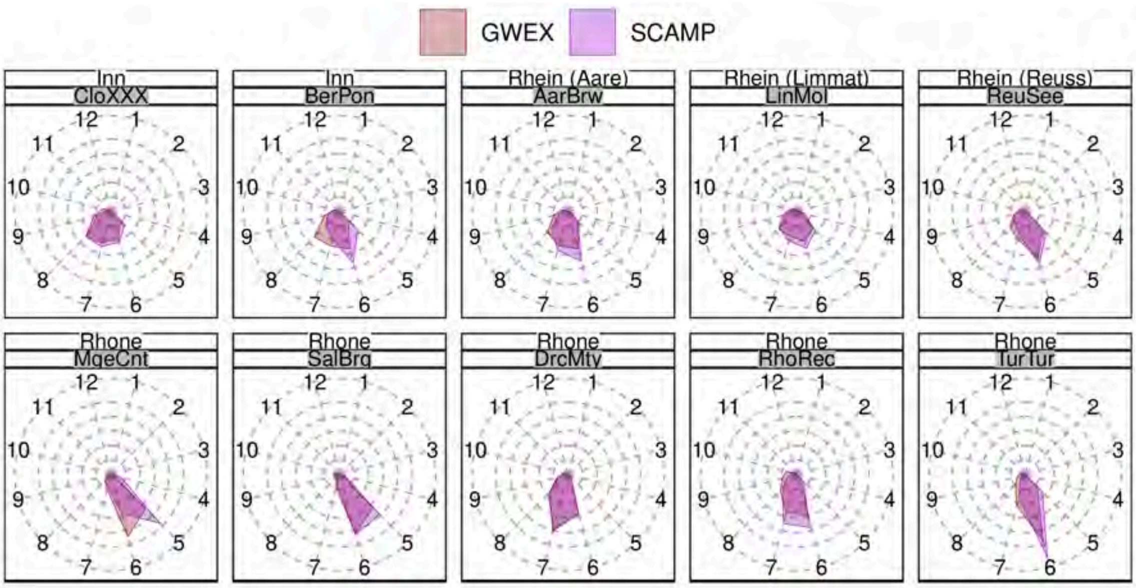

Figure 5.11: Seasonality of AMFs simulated using the weather generators GWEX and SCAMP, expressed in percent of occurrence for sample catchments with **glacier influenced** streamflow regimes. For catchment abbreviations see Table C.1.

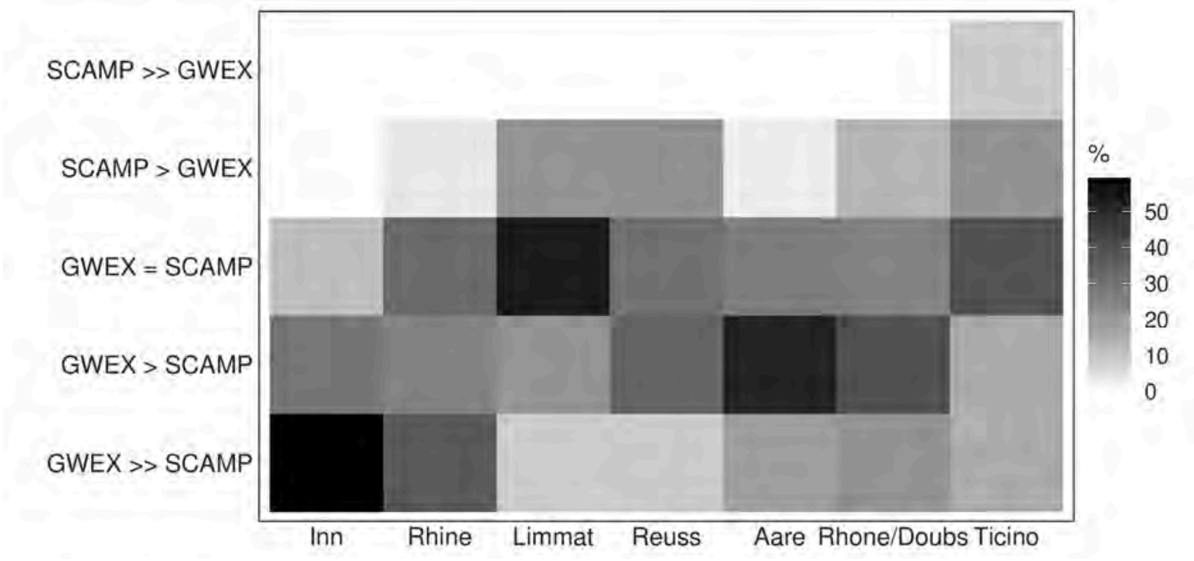

Figure 5.12: Comparison of simulated flow duration curves (FDCs) using weather generators GWEX and SCAMP for all sub-catchments in the entire simulation domain, based on visual inspection of the 95 % confidence intervals.

where the FDCs of GWEX are clearly larger than the ones from SCAMP. Here, however, we also find a considerable number of sub-catchments with very similar estimates from both weather generators. In the Limmat and Reuss river basins, results of GWEX and SCAMP are rather balanced, with many similar estimates, and the same amount of slightly larger estimates from SCAMP and from GWEX. In the Aare River basin, we find mostly slightly higher estimates from GWEX, but still many catchments show very similar FDCs from both weather generators. In the Aare River basin, lower catchment elevation seems to be linked with the more similar estimates from both weather generators. In the Rhone River basin, this relationship shows even more pronounced. For the Doubs River basin, we still find most estimates from GWEX to be slightly higher than the ones of SCAMP for the higher part of the FDCs, but also here there is a considerable amount of sub-catchments where the use of both weather generators results in very similar FDCs. In the Ticino River basin, most catchments show similar FDCs from both weather generators, but there are a few where GWEX results in much higher values in the higher part of the FDCs than SCAMP. An evaluation of SCAMP-based AMF values is found in Section 9.1.

When it comes to the seasonality of the AMF occurrence, simulations using both weather generators show very similar results.

5.1.3. Reforecasts

We calculated the FDCs of the RF-based simulations in the same way as we did for the weather generators, sampling daily values over the length of the observation for each block of about 1 000 years. The last block is smaller, summing to a total of 9 920 years. From each of the samples, we calculated the exceedance probabilities separately. For plotting, we calculated the 95 % confidence intervals for each exceedance probability over the flow values and show these together with the observations, the control run as well as the results from the two weather generators GWEX and SCAMP. This highlights the differences in FDCs when using different meteorological inputs for the hydrological model.

Comparing the AMFs resulting from reforecasts and weather generators, we find very similar behaviour for many catchments in the different large river basins. The largest differences to observations as well as to control run were again found in the higher flow ranges.

In the Aare River basin, about half of the catchments show higher simulated FDC for the RFs in comparison to the weather generators (e.g., Rotache at Oppligen (RtaOpp)). For the other half of the catch-

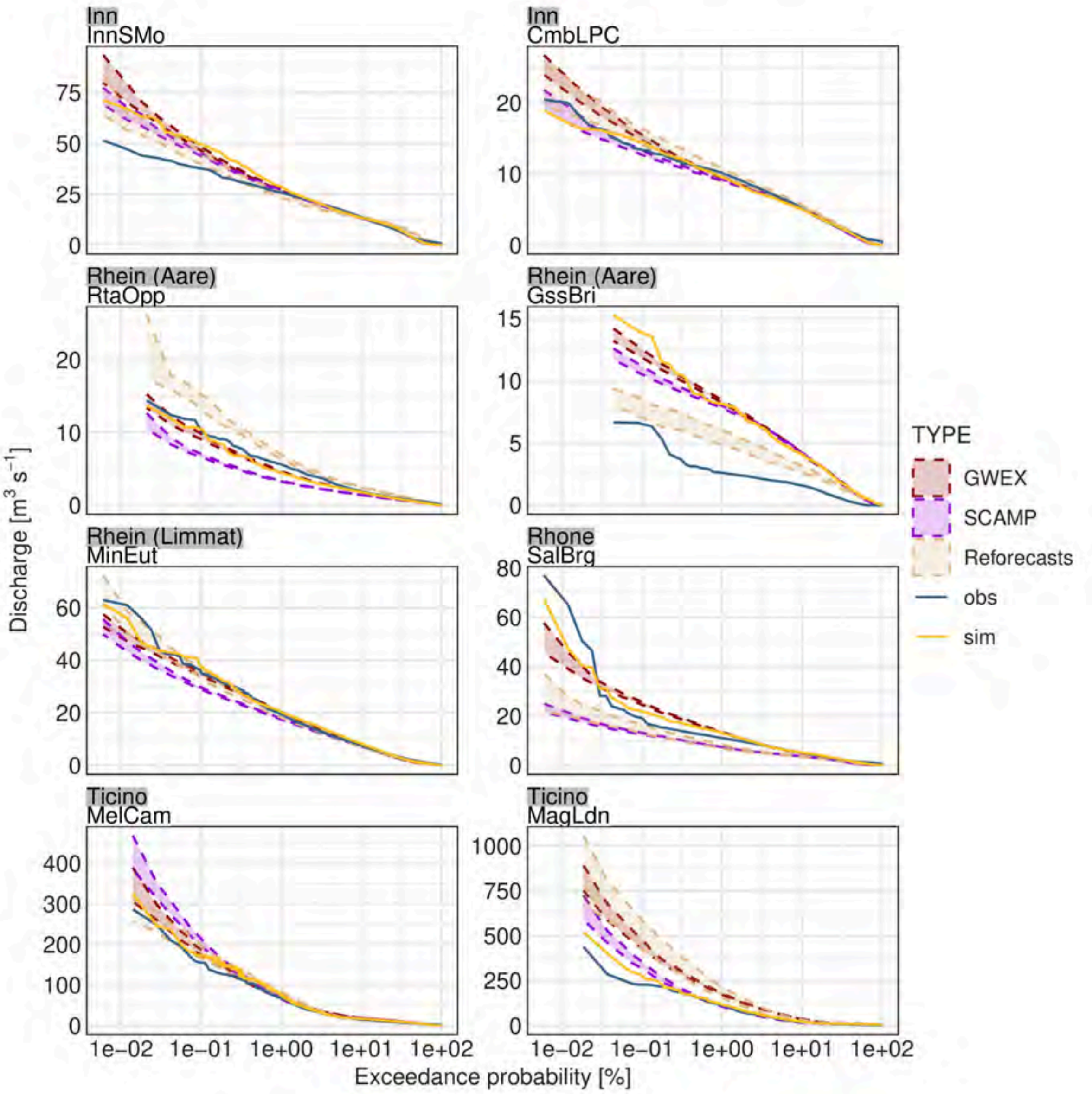

Figure 5.13: Flow duration curves (FDCs) for selected sub-catchments of the large river basins. The flows are sampled from the simulations using RFs as meteorological input and are compared to the simulations using GWEX and SCAMP weather scenarios together with the FDCs from the control run (Ctrl) and the observations (Obs). The sample size is equal to the length of the observations (or the control run if its length is shorter than that of the observations). Only the results of the intermediate representative parameter set are shown. For catchment abbreviations see Table C.1.

ments, the RFs estimates are slightly lower than those from the weather generators (e.g., Giessbach at Brienz (GssBri)), or are in a similar range.

For the Limmat, Rhine and Ticino river basins, the confidence intervals of the FDCs of weather generators and RFs overlap (e.g., Minster at Euthal, Rüti (MinEut)), or show only slightly higher or lower RFs results compared to the weather generators. In the Ticino river basin, the FDCs of the RFs for Melezza at Camedo (MelCam) are closer to those of SCAMP, and from Maggia at Lodano (MagLdn) closer to those of GWEX.

In the Inn River basin, some catchments are closer to the FDCs of SCAMP (e.g., Inn at St. Moritzbad (InnSMo)), and others closer to the FDCs of GWEX (e.g., Chamuerabach at La Punt-Chamues-ch (CmbLPc)).

Since individual RF runs were concatenated for obtaining a continuous hourly time series (see Section 3.2.3), it had to be verified whether the resulting AMFs do not show exceptional behaviour. For examining this, we compared time of occurrence and magnitude of the AMFs to the stitching dates, looking for a relationship between the two (Figure 5.14). This assessment was done for all three representative parameter sets, where Figure 5.14 only show the intermediate parameter set for a small and a larger catchment from each large river basin. For the smaller catchments, the densest occurrence of the AMFs is within a relatively narrow time window, occurring markedly after the stitching point (typically at least 100 days later). For the larger catchments, the AMFs are more widely distributed, often over the entire year after the stitching. In conclusion, the simulated AMFs seem unrelated in their magnitude and timing to the stitching points.

The seasonality of simulations using weather generators and RFs was found to be very similar, with differences occurring only in a few catchments (Figure 5.15). One example of differing behaviour is the Chiesebach at Freimettigen (CsbFrA), where the AMFs simulated with RFs not only occur from February to August (with a focus in May to July), but also show winter floods in December, with a similar probability of occurrence as in June. These winter floods were also found for other catchments, although with a slightly lower probability, such as for Rotache at Oppligen (RtaOpp), Sarine at Broc, Château d'en bas (SarBro) and Simme at Latterbach (SimLat), all located in the Aare River basin. A shift in seasonality was observed for Kleine Emme at Emmen (KEmEmm), where the RFs led to simulated floods mainly in June to August and again in December, while the GWEX and SCAMP weather scenarios led to AMFs mainly occurring in spring, from March to May. In the Ticino River basin, most of the RF seasons are similar, with most AMFs occurring in autumn (September to November), while the weather generators in this region show a slightly higher probability of AMF occurrence in late spring and summer (May and June for GWEX; June to September for SCAMP) in addition to the autumn events.

Additionally, testing the RFs as an alternative meteorological input to long CS for a number of test catchments revealed that the RFs align with the weather generators in terms of FDCs, generally falling between the two alternatives, GWEX and SCAMP. Cases where the RF show lower values can be attributed to the shorter length of the reforecasts (9 920 years) compared to the length of the weather generator scenarios (300 000 years). The RFs agree very well with the weather generators in terms of AMF seasonality, confirming the timing of major floods for specific regions and catchments.

5.2. Hydrological routing

5.2.1. Control simulation

As previously done for the hydrological modelling (see Section 5.1), the performance achieved in the control simulations is discussed here for hydrological routing, with reference to the period 1930–2019. Model performance was assessed similarly to the hydrological modelling, using standard hydrological performance metrics (NSE, KGE) to compare simulated and observed discharge data; analysing flow duration curves (FDCs) and examining the ability of the model chain to capture the seasonality of the AMFs. Additionally, the reproduction of some of the largest observed events was examined in detail, along with the effects and plausibility of the simulations involving the small artificial reservoirs.

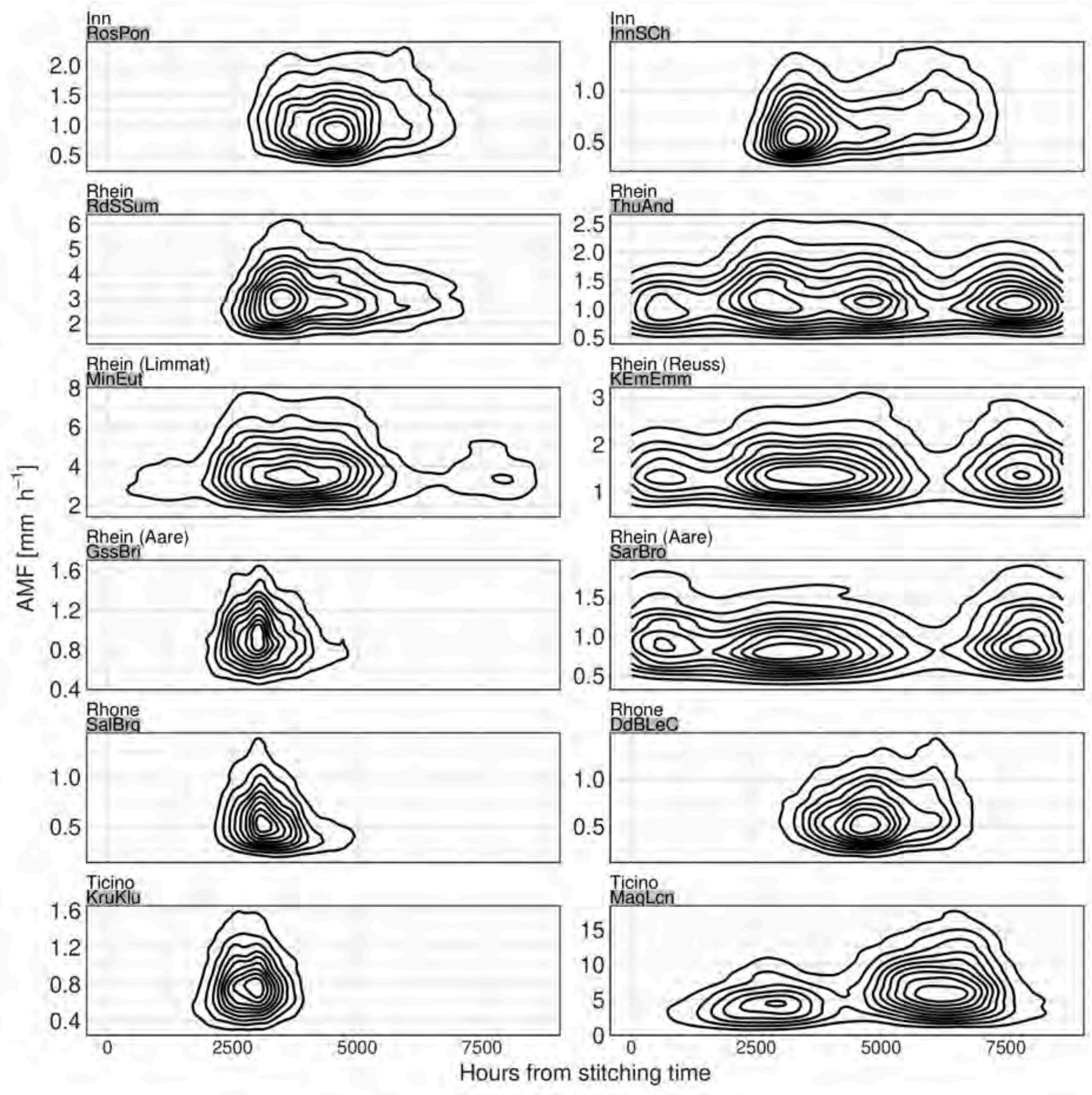

Figure 5.14: Contour density plots showing the magnitude of simulated AMFs (intermediate representative parameter set) as a function of their occurrence time relative to the stitching points of individual RFs. Where available, a smaller and a larger catchment was chosen for each river basin. For catchment abbreviations see Table C.1.

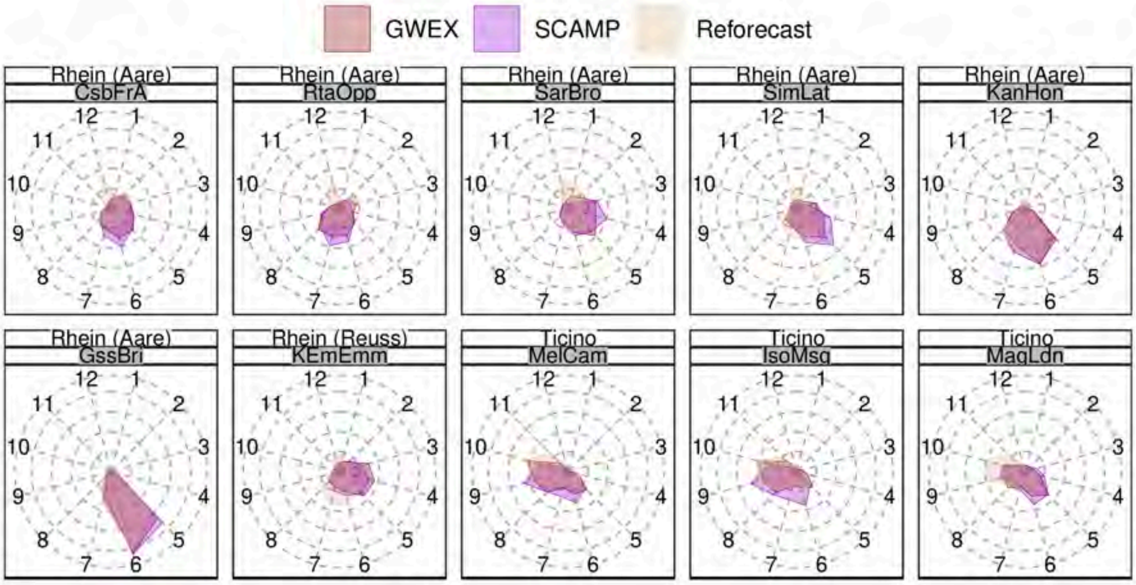

Figure 5.15: Comparison of simulated AMF seasonality of GWEX, SCAMP and RFs. For catchment abbreviations see Table C.1.

The following gauging points are assessed:

- Rhine River basin without the Aare River basin (6): Vorderrhein at Ilanz (VRhIla), Hinterrhein at Fürstenau (HRhFue), Rhein at Diepoldsau (RheDpa), Thur at Andelfingen (ThuAnd) and Rhein at Basel (RheBas).
- Aare River basin (19): Aare at Ringgenberg (AarRin), Aare at Thun (AarThu), Aare at Bern (AarBrn), Sarine at Fribourg (SarFri), Saane at Laupen (SaaLau), Aare at Hagneck (AarHag), Aare at Brügg, Aegerten (AarBre), Emme at Wiler (EmmWil), Aare at Murgenthal (AarMur), Reuss at Luzern (ReuLuz), Reuss at Mühlau (ReuMhl), Lorze at Zug (LorZug), Reuss at Mellingen (ReuMel), Aare at Brugg (AarBru), Linth at Weesen (LinWee), Sihl at Zürich (SihZue), Limmat at Zürich (LimZue), Limmat at Baden (LimBad) and Aare at Untersiggenthal (AarUnt).
- Rhone River basin (6): Rhone at Brig (RhoBrg), Rhone at Sion (RhoSio), Rhone at Branson (RhoBra), Rhone at Porte du Scex (RhoPdS), Rhone at Genève (RhoGen) and Rhone at Chancy (Chancy).
- Ticino River basin (6): Ticino at Bellinzona (TicBlz), Maggia at Bignasco (MagBig), Maggia at Lodano (MagLdn), Maggia at Locarno (MagLcn), Tresa at Ponte Tresa (TrePtr) and Ticino at Miorina (TicMio).
- Inn River basin (2): Inn at S-Chanf (InnSCh) and Inn at Martina (InnMrt).

After hydrological routing, results demonstrate satisfactory to good performance for both efficiency criteria (Figure 5.16), with NSE values ranging from 0.4 to 0.8 and KGE values ranging from 0.5 to 0.9. Figure 5.16 shows that there are some small differences in model performance for the three representative parameter sets, which are more noticeable when examining KGE. For the Inn River basin and the Rhone River basin, the goodness of fit increases with increasing percentile (from the low to the high representative parameter set). This trend is also observed for the Aare River basin, albeit less pronounced. In contrast, the Rhine River basin exhibits opposite behaviour. For the Ticino River basin, KGE initially increases from the low to the intermediate representative parameter set, but then drops to its lowest performance for the high parameter set. For the Inn River basin, the behaviour might be attributed to an underestimation of precipitation, as indicated by a negative percentage bias (where the total simulated discharge exceeds the total observed discharge) across all parameter sets. This bias decreases with increasing percentile. For the Rhine River basin, the behaviour is likely due to the interaction between the parameter sets and the artificial reservoirs in the Alpine Rhine, where marked differences in the percentage bias between different parameter sets are noted, such as a discrepancy of more than 20 % between the low and the high representative parameter sets for the Hinterrhein at Fürstenau (HinFue). In the Rhone River basin, the entire area downstream of Porte du Scex (RhoPdS) covers 5 238 km². Of this, seven sub-catchments covering a total area of 1 505 km² are calibrated (approximately 26 %), while the remaining sub-catchments are regionalised. This widespread regionalisation is why the model's performance is expected to be markedly lower compared to other regions in Switzerland. In general, there appears to be a missing volume of 5–10 %, primarily due to the underestimation of low flows (baseflow) in winter. On average, this underestimation is about half, but locally it can be as much as 3 to 4 times too low. This issue is also evident in the sub-catchments of the Vispa River, where the Mattmark reservoir is located, and the Borgne River, where the Grande Dixence reservoir is located. In these regions, the underestimation strongly interacts with the operating rules of the reservoirs. In the case of the Vispa River, the issue may also stem from the fact that the calibration was performed using a flow time series in which an important amount of water is transferred to Grande Dixence. The weakest point in the Rhone River basin is the outlet of Lake Geneva (RhoGen). This is due, on the one hand, to the markedly too low winter inflow to the lake, which results in a lower stage than expected, and on the other hand to water that is turbinated for electricity production at the lake outlet (about 40 % of the electricity used by the city of Geneva is generated here). Together, these factors can sometimes lead to an excessive depletion of the lake's water. For the Ticino River basin, the drop in performance for the high representative parameter set may be due to the larger precipitation extremes observed in this region compared to the rest of Switzerland, making the hydrological model more sensitive to changes in parametrization. It is worth noting that only half of the points considered show this clear drop in performance for the high representative parameter set, but the effect is strong enough to deteriorate the overall statistics.

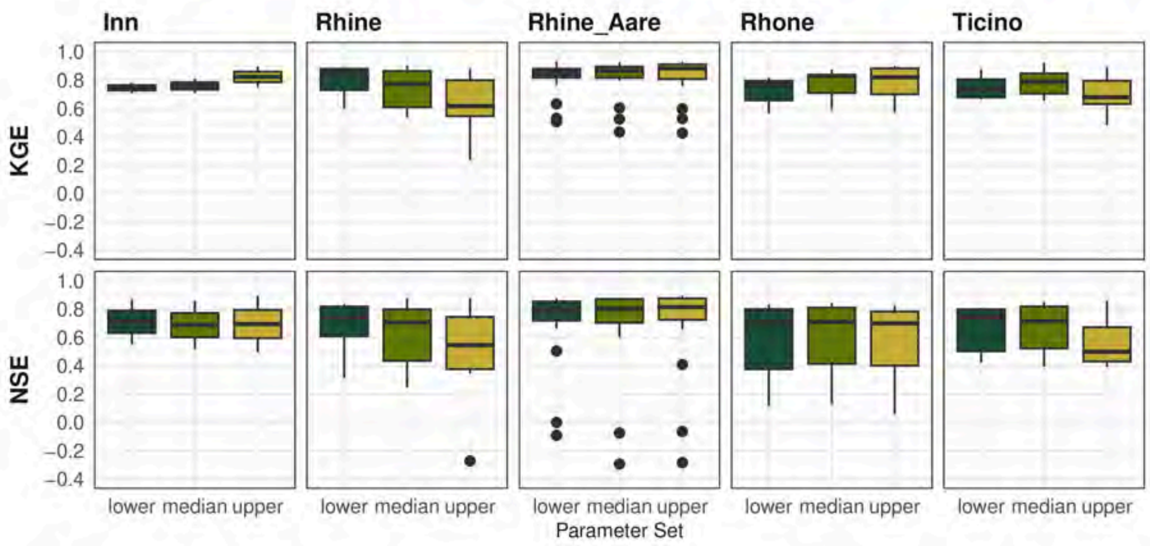

Figure 5.16: Boxplots of the model efficiency criteria KGE and NSE for five river basins. Comparison of the simulations using three representative parameter sets (high, low, intermediate) with disaggregated precipitation 1930–2019 to the observations. The label *Rhine* corresponds to the sub-basin of the Rhine River upstream of Basel without the Aare River sub-basin, while the label *Rhine_Aare* corresponds to the latter.

Overall, model performance was less satisfactory for only a few catchments, as indicated by outliers in Figure 5.16. These include NSE values between 0.3 and 0.5 for Inn at Martina (InnMrt), Vorderrhein at Ilanz (VRhIla), Rhein at Domat/Ems (RheDEm), Rhone at Chancy (Chancy), Maggia at Bignasco (MagBig) and Maggia at Lodano (MagLdn). Note that the two sites on the Maggia River are here treated differently than in Section 5.1: While they were calibrated and validated with the hydrological model at their respective gauging stations in the validation of HBV, the simulations with RS Minerve discussed here used a different configuration which, for instance, includes artificial reservoirs. The Rhone at Geneva (RhoGen) has a NSE value of about 0.1, while Hinterrhein at Fürstenau (HRhFue), Sarine et Fribourg (SarFri) and Saane at Laupen (SaaLau) all exhibit negative NSE values. These negative values can be attributed to major impact of hydropower production in the respective sub-catchments. However, this does not necessarily result in inadequate reproduction of peak flows (see e.g., Figure 5.21).

We further compared the flow duration curves (FDCs) derived from observations with those from simulations, again based on daily data. To emphasise high flows, the plots are presented with a logarithmically scaled x-axis (Figure 5.17). The overall simulated FDCs using disaggregated meteorological inputs are mostly very similar to the observed ones, indicating that the overall flow distributions are well captured by the modelling chain. Deviations are often found in sub-catchments where performance is poorer, such as for Saane at Laupen (SaaLau) and Vorderrhein at Ilanz (VRhIla). The underestimation of peaks in the Reuss River, such as at Mellingen (ReuMel), is mainly due to the underestimation of the peaks in the Kleine Emme at Emmen (KEmEmm) (see Sections 6.3.2 and 6.3.3). The overestimation of peak flows in the Ticino at Bellinzona (TicBlz) and the Rhone at Porte du Scex (RhoPdS) is not primarily due to an overestimation of the absolute peak values, but rather to an overestimation of the volume associated with some of the largest events (see also Figures 5.24 and 5.23, respectively). For the Maggia at Locarno (MagLcn), the model might appear to systematically overestimate high flows. However, observations at this gauging station should be interpreted with caution. The observation period at this site is comparatively short, and some of the largest observed peaks are missing in the available time series (Näf-Huber et al., 2021). Further details about the challenges in the Ticino River are provided in Section 6.7.

To examine whether the hydrological routing influences the reproduction of seasonality in simulations using disaggregated meteorological data as model forcing – which has generally been shown to be well captured by the hydrological model (see Section 5.1) –, we also calculated the percent of occurrence of AMFs in each month of the year. The visual evaluation of selected points (Figure 5.18) shows that for most points there is good agreement between simulations and observations regarding the seasonality of the occurrence of AMFs, with exception of Emme at Wiler (EmmWil).

In the following, the six largest observed events are presented and discussed for selected points across all four major river basins, along with additional insights for the results in the Aare River basin.

The Inn at Martina (InnMrt) is likely the most challenging and least accurate example reported here. While the simulated discharge appears to reach the peak values in absolute terms with the high representative parameter set, the peaks are generally strongly delayed, and the volume of the three largest events is underestimated. However, both the delay and the volume deficit improve when reproducing the three remaining events (Figure 5.19). This issue may be caused by several factors: partly due to an underestimation of precipitation, but also because model parameters had to be regionalised for about half of the basin, with very few calibrated sub-catchments nearby. Additionally, the basin is strongly impacted by hydropower production. Despite these challenges, the range of the simulated hydrographs still matches the observed events satisfactorily.

Examining selected points on the Aare River (Figure 5.20), a marked improvement compared to the EXAR implementation is visible in the simulation of water release at the outlet of Lake Biel (site Aare at Brügg, Aegerten (AarBre)), where the occurrence of oscillations after major events is reduced. Some abrupt changes in simulated release rates still occur while switching between operational states, such as in the flood events of 2007 and 2015. This is attributable to the underestimation of the lake inflow during the later recession phase of the flood event, leading then the regulation to switch too early from the high water regime regulation back to the regulation under normal conditions. The systematic underestimation of water released during the flood events of 1987 and 2006 is clearly reflected in the systematic underestimation of base flow at Murgenthal (AarMur). The hysteretic behaviour and the stage-discharge relationship implemented in RS Minerve, which describes the high water regime regulation, are representative of average and simplified operating rules. These rules were primarily defined by calibrating for the well-known events of 1999, 2005 and 2007. However, these rules are idealized and differ from actual operational decisions: In 2005 and 2007, for instance, systematic differences of over 100 $m^3 s^{-1}$ were applied in parts of the events, with more water being released in 2007. This likely stemmed from the distinct characteristics of the events: 2005 saw a shorter, more intense peak, while 2007 featured a more prolonged event with two major peaks. Consequently, it is not trivial to disentangle the actual reasons for deviations from observations, as lake regulation here is manual and relies on forecast-based decisions made by the engineer in charge. Both flood peaks missing in the simulations at Murgenthal (AarMur) in 1981 and 2007 are linked to the missed peaks in the Emme at Wiler (EmmWil). Furthermore, operational rules for Lake Biel were changed between 1980 and 1982,

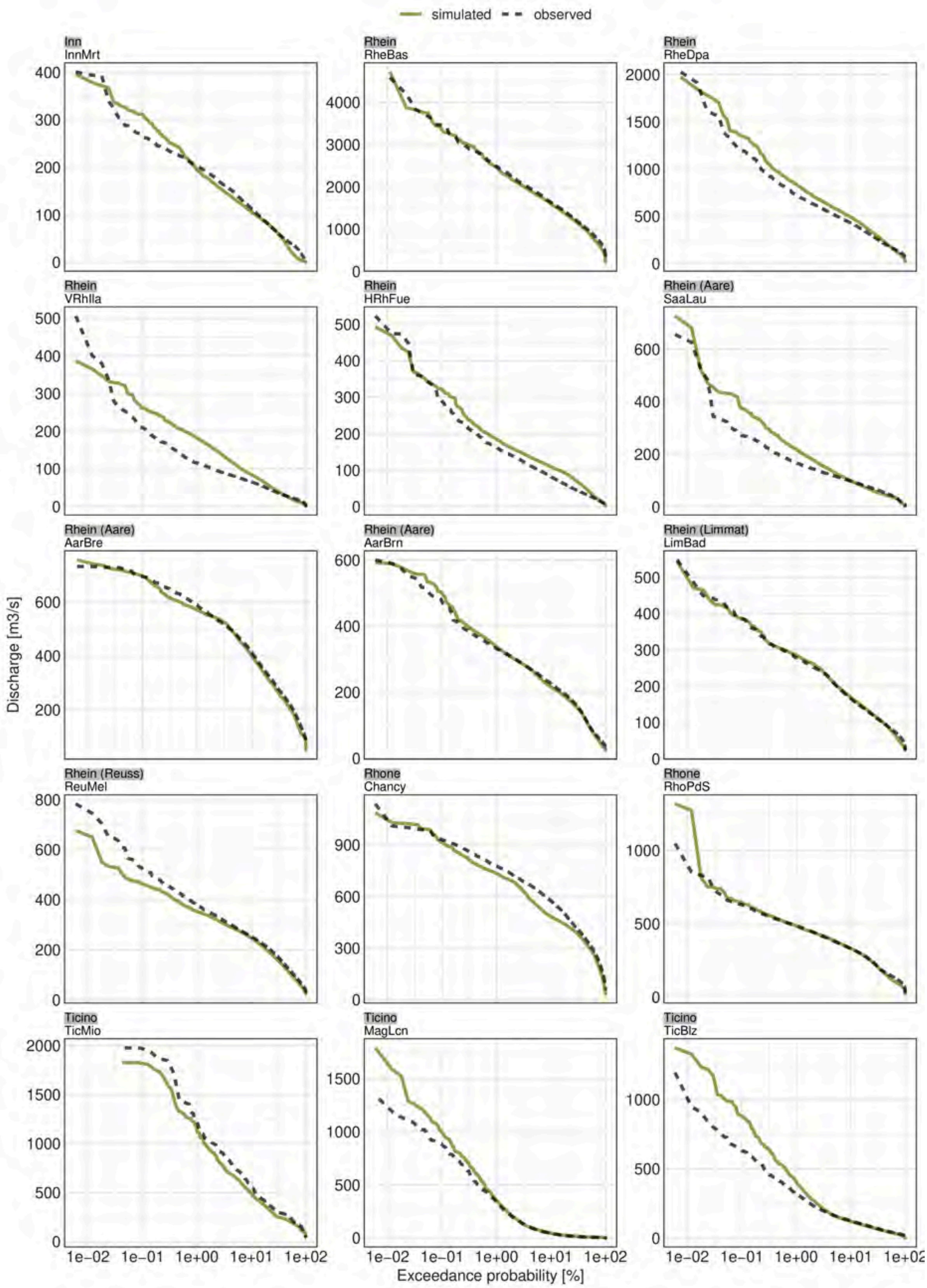

Figure 5.17: Flow duration curve of selected example catchments from the large river basins. The catchments are grouped by large river basin and within that by mean catchment elevation. Note the logarithmic x-axis. For catchment abbreviations see Table C.1.

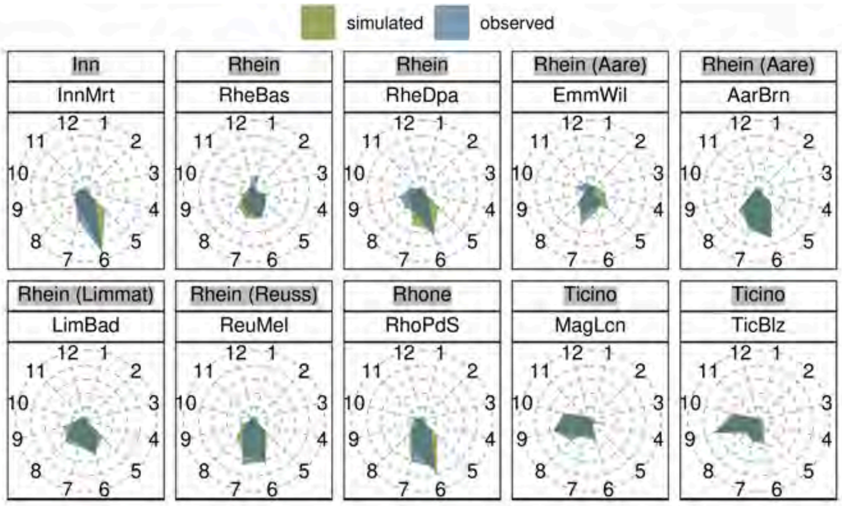

Figure 5.18: Seasonality of observed (blue) and simulated (green) AMFs, expressed in percent of occurrence for example catchments. For catchment abbreviations see Table C.1.

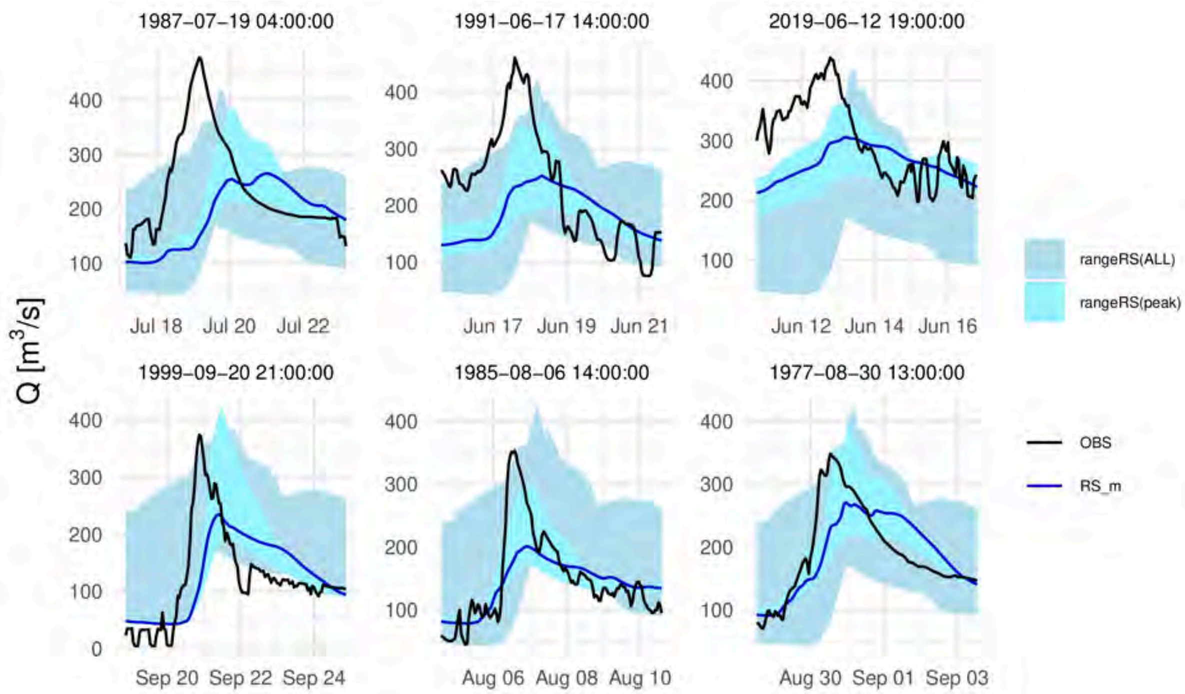

Figure 5.19: Overview of the six largest observed floods for Inn at Martina (InnMrt). The black line shows observations (OBS), the blue line shows the intermediate representative parameter set (RS_m), the light cyan area represents the range between the low and high representative parameter sets (rangeRS(peak)), and the light blue area shows the range across all six simulated peaks for all three representative parameter sets (rangeRS(ALL)).

likely contributing to the larger discrepancies between simulations and observations noted for the 1981 event.

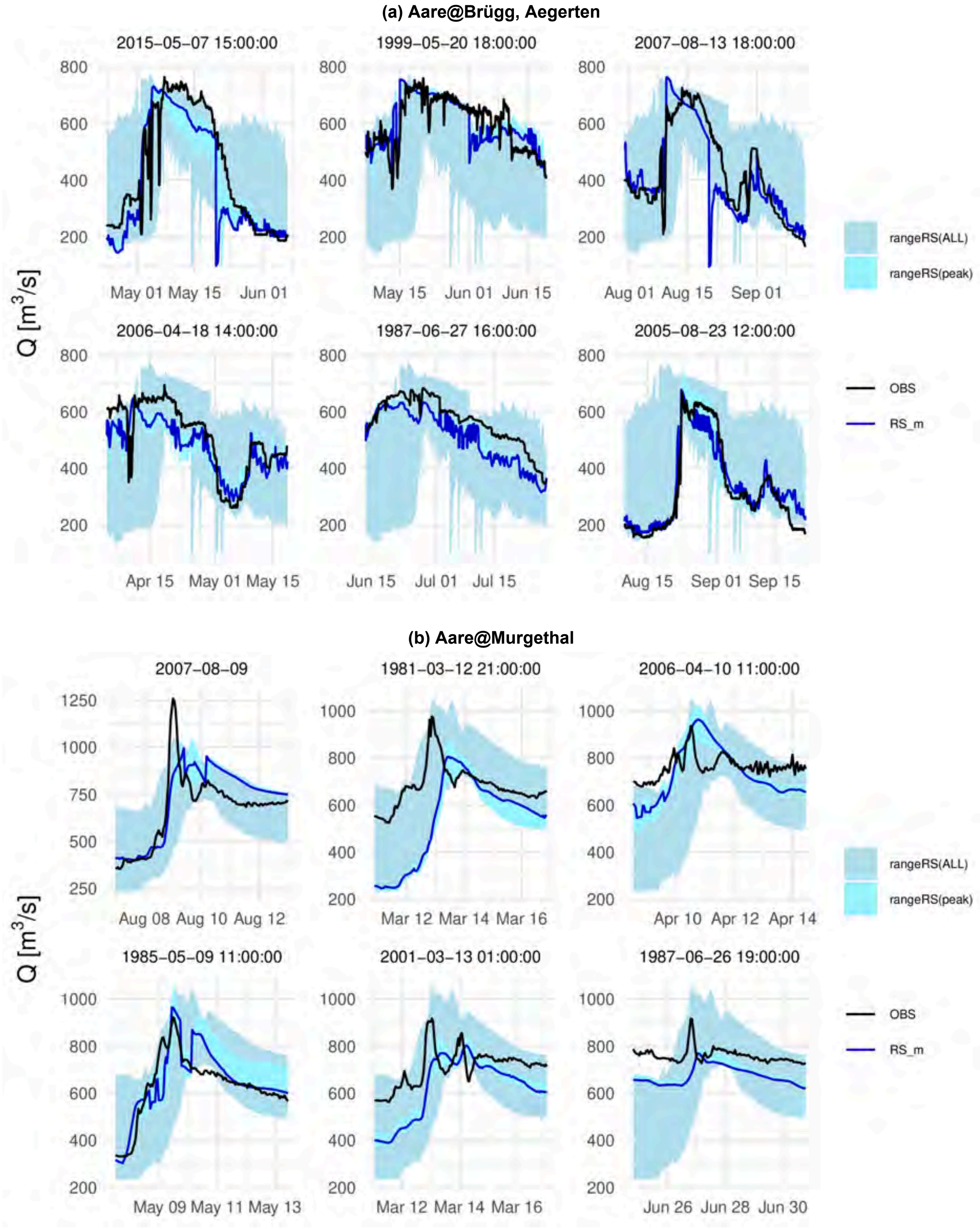

Figure 5.20: Overview of the six largest observed floods for: (a) Aare at Brügg, Aegerten (AarBre), (b) Aare at Murgenthal (AarMur). The black line shows observations (OBS), the blue line shows the intermediate representative parameter set (RS_m), the light cyan range represents the range between the low and high representative parameter sets (rangeRS(peak)), and the light blue area shows the range across all six simulated peaks for all three representative parameter sets (rangeRS(ALL)).

Sarine at Fribourg (SarFri) and Limmat at Zürich (LimZue) are both interesting points to examine in more detail (Figure 5.21). The Sarine at Fribourg is strongly affected by hydropower production from the large artificial reservoir Lake Gruyère upstream, and shows generally negative NSE values. The main reason for these negative efficiencies lies in the difficulty of correctly representing the strongly fluctuating behaviour occurring under normal conditions, characterized by the turbination regime and hydro peaking. Besides the 2005 flood event, underestimating the peak event with the high representative parameter set, all peaks are well captured by the model in terms of peak, volume, onset and recession. The second point, the Limmat at Zürich (LimZue), reflects the combined effects of hydropower production in the Sihl River catchment and lake regulation at the outlet of Lake Zürich. While a slight tendency to overestimate the largest peaks is noted here, volume, onset and recession of the events are well reproduced by the model. The tendency to overestimate peaks is linked to the overestimation of peaks in the Sihl at Zürich (SihZue), with a median of +70 $m^3 s^{-1}$ in 2005 and +50 $m^3 s^{-1}$ in 1999. It partly results from the intentionally reduced outflow from Lake Zürich, a measure implemented following lessons learned from the 1999 flood. Unfortunately, such clear but isolated and non-systematic departures from usual regulation cannot be accounted for in our modelling chain.

In the Rhine River basin, notable deficiencies are noted in the simulations of the Alpine Rhine, as illustrated by the example of Rhein at Diepoldsau (RheDpa). These deficiencies largely disappear further downstream, or are reflected as a slight delay in the representation of flood events at Basel (RheBas) (Figure 5.22). Apart from 1999 and 2005, most of the largest events exhibit the correct shape but are generally delayed. The miss in 1999 can also be linked to the underestimation of the first peak for Rhein at Domat/Ems (RheDEm), while in 2005, the underestimation is likely due to factors in the catchments downstream of this point. Overall, however, it can be concluded that for the Alpine Rhine River, the range of the largest simulated floods adequately covers the range of observed floods. The 2013 flood event at Rhein at Basel (RheBas) inherits part of its peak delay from a small delay observed in the Aare at Untersiggenthal (AarUnt). Despite the minor offset in the onset of the events, all six of the largest peaks at Rhein at Basel (RheBas) are generally well represented by the simulations. We emphasize that, as in the case of the Inn River basin, the Alpine Rhine River is a challenging domain with its generally drier climate and the the influence of hydropower reservoirs.

The Rhone River basin is an interesting example, where the reproduction of the largest flood peaks yields remarkably good results despite the challenges involved in modelling it (Figure 5.23). It was mentioned earlier already that the vast majority of the catchments upstream of Porte du Scex (RhoPdS) has regionalised HBV model parameters, and that some of the largest artificial reservoirs in the Swiss Alps are situated in this river basin. The largest observed flood event in 2000 is simulated well in terms of peak discharge, but the overall volume of the event is overestimated by the simulation. However, it remains unclear to what extent the major embankment failure at Chamoson after the first peak reshaped the rest of the observed hydrograph and reduced the actual event volume (see Jordan et al., 2004). In contrast, all other events show a tendency towards underestimation of the peak, although the peak is almost always reached by the high representative parameter set. The six largest peaks at Chancy (Chancy), downstream of Lake Geneva and of the confluence with the Arve River, show markedly worse representation of the largest flood events with respect as compared to upstream of Lake Geneva, except for the flood event in 1980. As already discussed earlier when looking at the efficiency criteria, the poor performance here is mainly attributed to the poor representation of the water released and turbinated at the outlet of Lake Geneva. However, it is difficult to assess how the performance would change if the total volume of water inflow and baseflow during winter were better represented in the models. Also, in some cases the peak is not only missed due to the challenging regulation Lake Geneva, as in 1990, when the simulations for the Arve River only reach the peak with the high representative parameter set and markedly underestimate the volume of the event. The Arve River plays an important role for most flood events taking place at Chancy, contributing up to half of the volume and peak observed there. Notably, the observed peaks at Chancy are all within a similar range, a tendency also found in the Arve River, where 9 out of the 10 largest peaks fall between 600 and 700 $m^3 s^{-1}$. If we set aside the fact that turbination still occurs at the lake outlet for most of the flood events – due to the water level not reaching the threshold needed to stop turbination –, the range of the simulated flood events closely mirrors the observations.

Eventually, results in the Southern part of the Alps are examined in the Ticino River basin, focusing on the Ticino River at Bellinzona (TicBlz) and at Miorina (TicMio) (Figure 5.24). At Bellinzona, two of

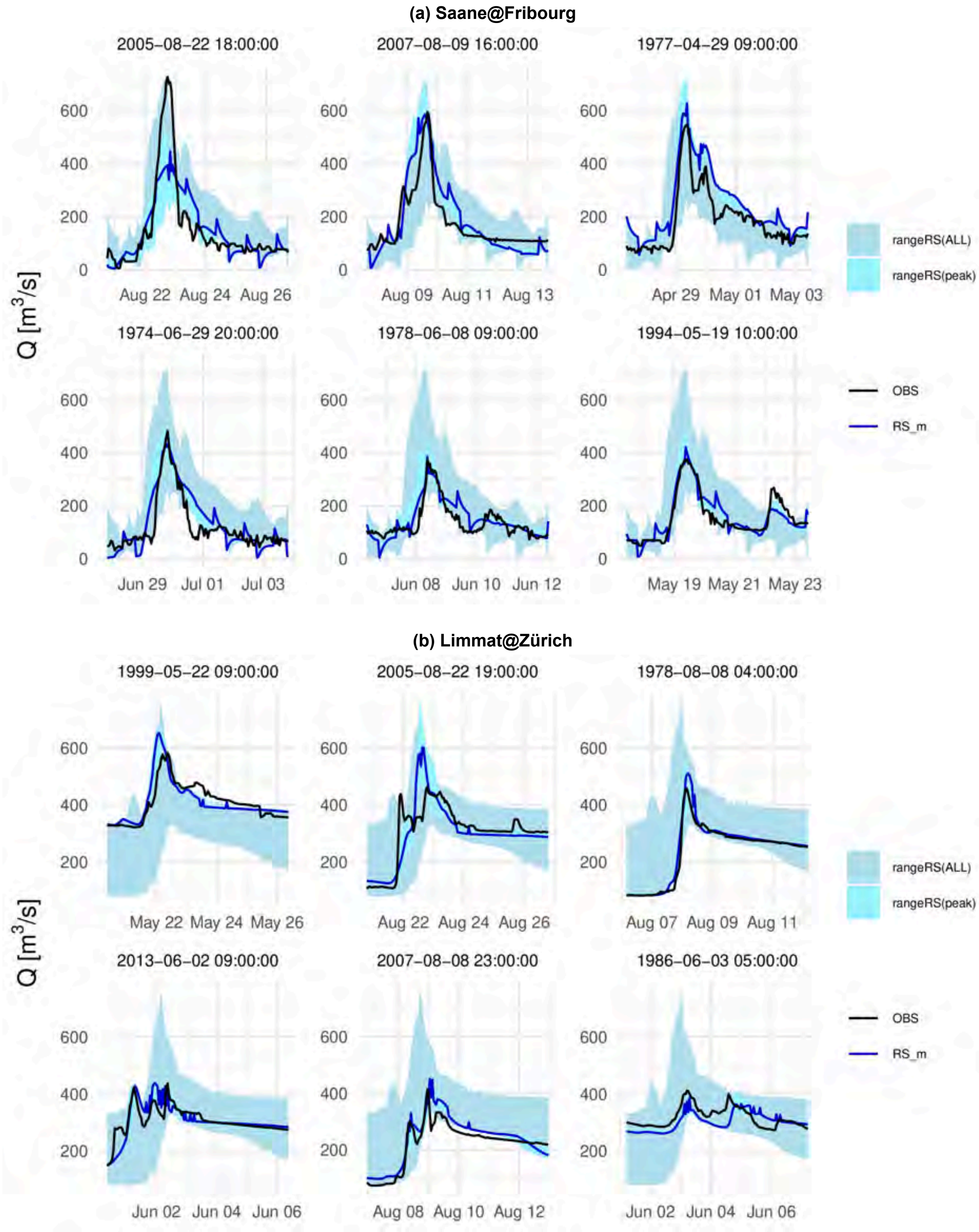

Figure 5.21: Overview of the six largest observed floods for: (a) Saane at Fribourg (SarFri), (b) Limmat at Zürich (LimZue). The black line shows observations (OBS), the blue line shows the intermediate representative parameter set (RS_m), the light cyan range represents the range between the low and high representative parameter sets (rangeRS(peak)), and the light blue area shows the range across all six simulated peaks for all three representative parameter sets (rangeRS(ALL)).

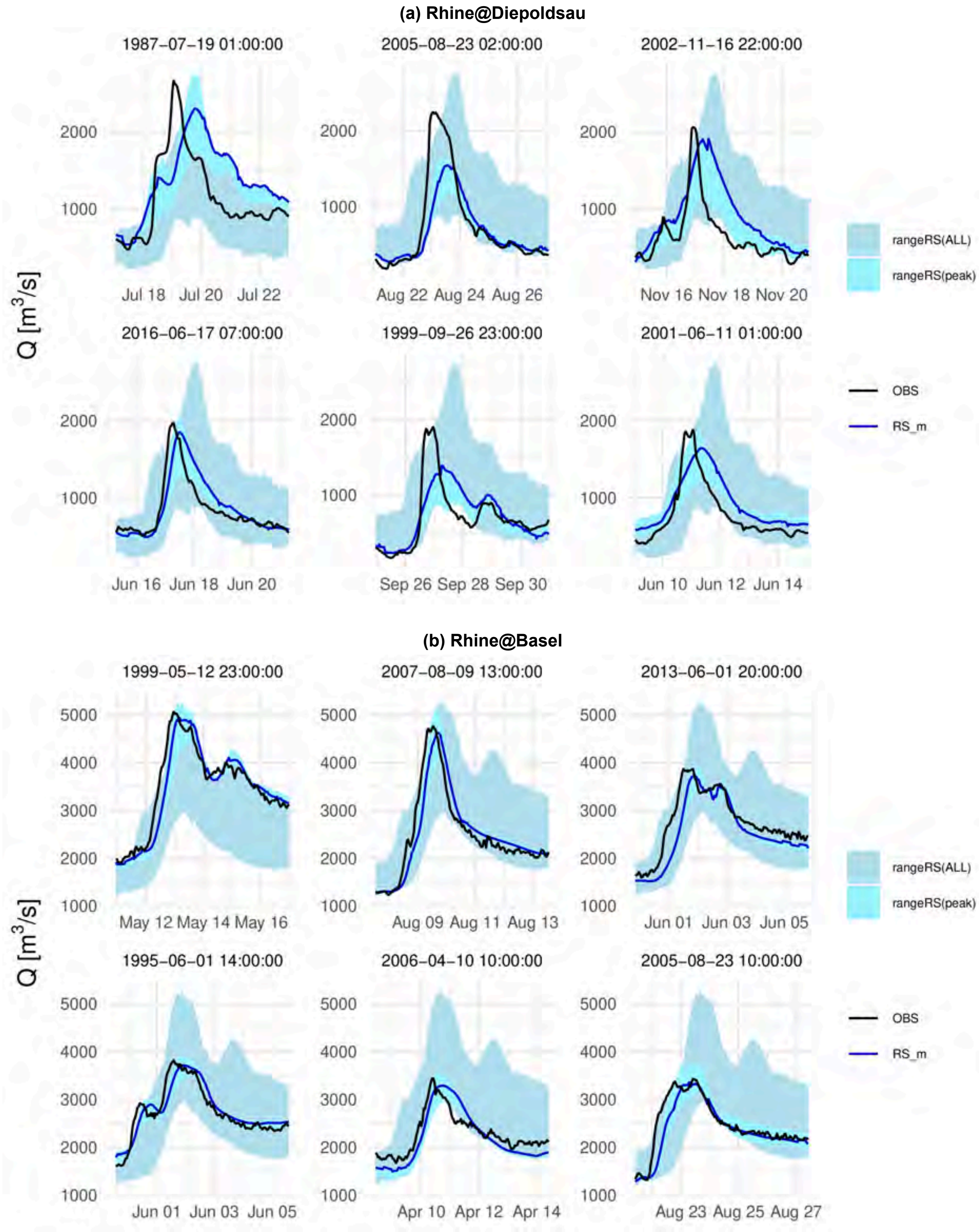

Figure 5.22: Overview of the six largest observed floods for: (a) Rhein at Diepoldsau (RheDpa), (b) Rhein at Basel (RheBas). The black line shows observations (OBS), the blue line shows the intermediate representative parameter set (RS_m), the light cyan range represents the range between the low and high representative parameter set (rangeRS(peak)), and the light blue area shows the range across all six simulated peaks for all three representative parameter sets (rangeRS(ALL)).

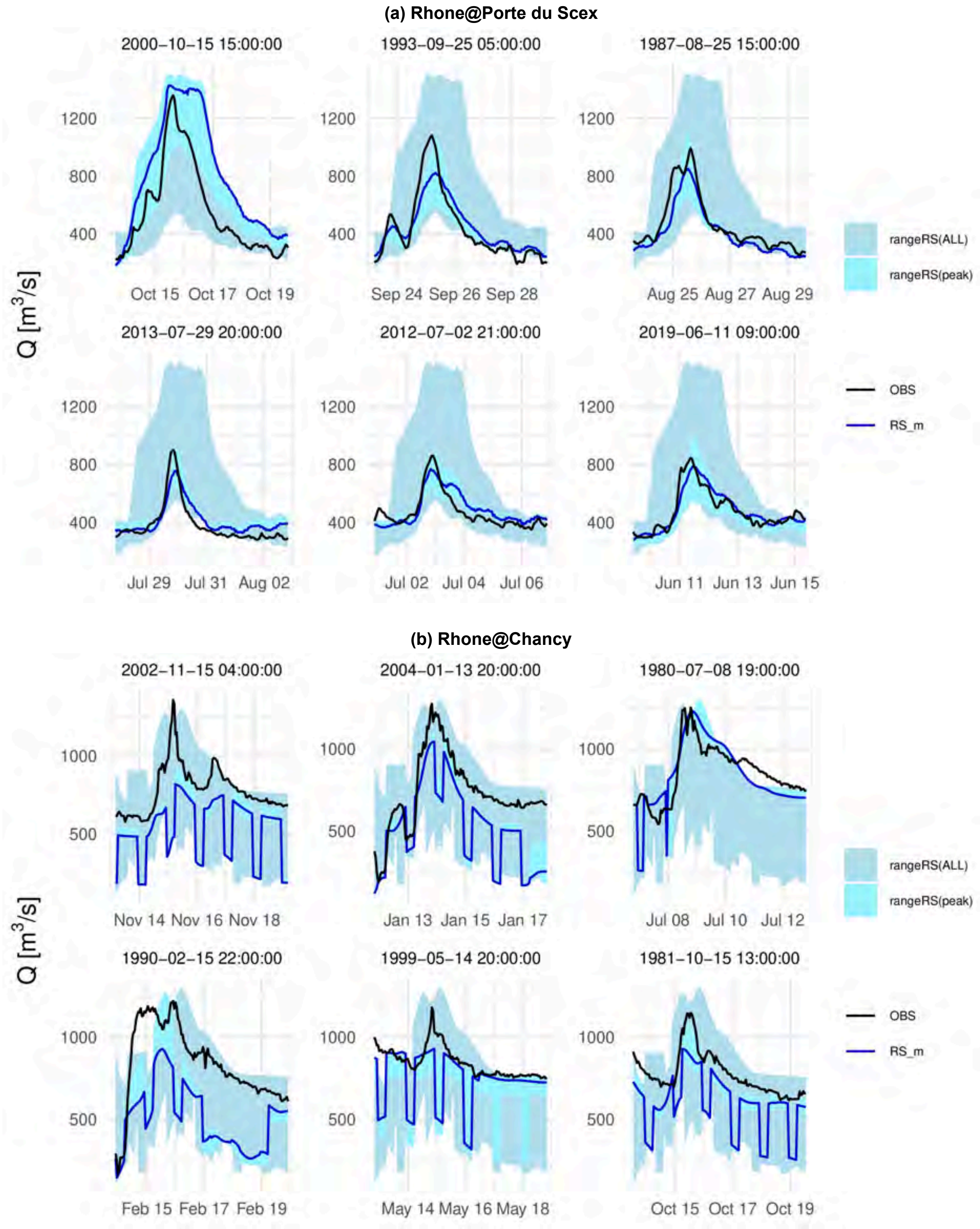

Figure 5.23: Overview of the six largest observed floods for: (a) Rhone at Port du Scex (RhoPdS), (b) Rhone at Chancy (Chancy).The black line shows observations (OBS), the blue line shows the intermediate representative parameter set (RS_m), the light cyan range represents the range between the low and high representative parameter set (rangeRS(peak)), and the light blue area shows the range across all six simulated peaks for all three representative parameter sets (rangeRS(ALL)).

the largest six floods are overestimated, while another two are underestimated by a similar order of magnitude. The results indicate a tendency to overestimate the volume related to the largest flood events. For the Ticino at Miorina (TicMio), results must be considered cautiously, as the available time series spans only seven years (2013–2019) and, apart from the flood event in 2014, does not contain any of the known major events of the past, such as the floods of 1993, 2000 and 2002. Within the short observation period, simulations agree well with observations, except for 2013.

At last, we analysed the filling of the reservoirs and their impact on flood peaks in the basins where such reservoirs are present. As a reference, we used the bi-weekly regional statistics regularly published by the SFOE since 2000 (Bundesamt für Energie (BFE), 2022). It is important to note that these statistics are regionally aggregated and include more reservoirs than those represented in RS Minerve. The comparisons presented here are primarily intended to assess whether the model captures the correct order of magnitude and seasonality.

The results reveal notable differences in how the various parameter sets interact with the annual cycle. When comparing reservoir filling patterns based on regionally aggregated statistics from the SFOE with simulations on basis of the three representative parameter sets for the Alpine Rhine, Rhone, and Ticino river basins, we find that the seasonality is captured reasonably well. However, the differences between the three river basins are substantial, and no systematic differences emerge between the parameter sets within each basin (see Figure 5.25).

In the Alpine Rhine, reservoir filling is substantially underestimated throughout the year (Figure 5.25, upper panel). The intermediate representative parameter set produces the highest filling levels, with a larger discrepancy between the low and the intermediate representative parameter sets compared to the discrepancy between the intermediate and the high representative parameter sets (Figure 5.25, upper panel). This pattern is reversed in the Rhone River basin, where the low and intermediate representative parameter sets align well with observed minimum storage, while the high representative parameter set better captures maximum storage levels (Figure 5.25, middle panel). The magnitudes of the filling follow the order of the representative parameter sets. In Ticino, the differences show a more irregular character, with some years being well represented, and others where the amplitude of the yearly cycle is underestimated (Figure 5.25, lower panel). Here, the high representative parameter set consistently produces the highest storage levels, while the low and intermediate representative parameter sets are swapped, with the low representative parameter set showing the best performance.

Considering the challenging modelling task and the large variability in the management practices of artificial reservoirs – which even increased after the liberalization of the electricity market in 2009 –, it can be concluded that the range of the yearly cycle for the Rhone and the Ticino is well reproduced. A pronounced dry bias is evident for the Alpine Rhine, as shown by the flow duration curves (FDCs) in Figure 5.17, and in agreement with the underestimation of the peaks for Vorderrhein at Ilanz (VRhIla).

Examining individual reservoirs in the Ticino River basin (see Figure 5.26), we can for some reservoirs identify a slight tendency to drift into a certain range over longer time periods. This can be attributed to the climatology, as the simulations often reflect the general climatic character of specific decades. For instance, the 1940s and 1970s were relatively dry, while the 1980s were comparatively wet.

To assess whether the low regional reservoir filling levels in the Alpine Rhine lead to implausible behaviour in peak flow simulations, we compared our findings with previous studies on flood peak attenuation caused by artificial reservoirs in this river basin (Zarn et al., 2017). For this, we removed all the reservoirs implemented in the routing for this basin and re-ran the simulations for the control period. By juxtaposing the annual maximum floods (AMFs) simulated with and without artificial reservoirs, we note a reduction of the peaks for all gauging points upstream of Rhein at Diepoldsau (RheDpa) when reservoirs are incorporated into the system (see Figure 5.27). This effect is most pronounced in the upstream part of the basin, particularly for Vorderrhein at Ilanz (VRhIla) and Rhein at Domat/Ems (RheDEm), and diminishes for Rhein at Diepoldsau (RheDpa), before the Alpine Rhine flows into Lake Constance. Zarn et al. (2017) compared observed peaks by splitting the data into two periods, before and after reservoirs construction, and estimated return periods for the corresponding flood peaks. Although our simulated results cannot be directly compared to these findings due to differences in the periods covered, general behaviour and patterns can still be appraised. We deliberately opted to analyse longer simulated time series rather than splitting them, aiming to minimize the effects introduced by

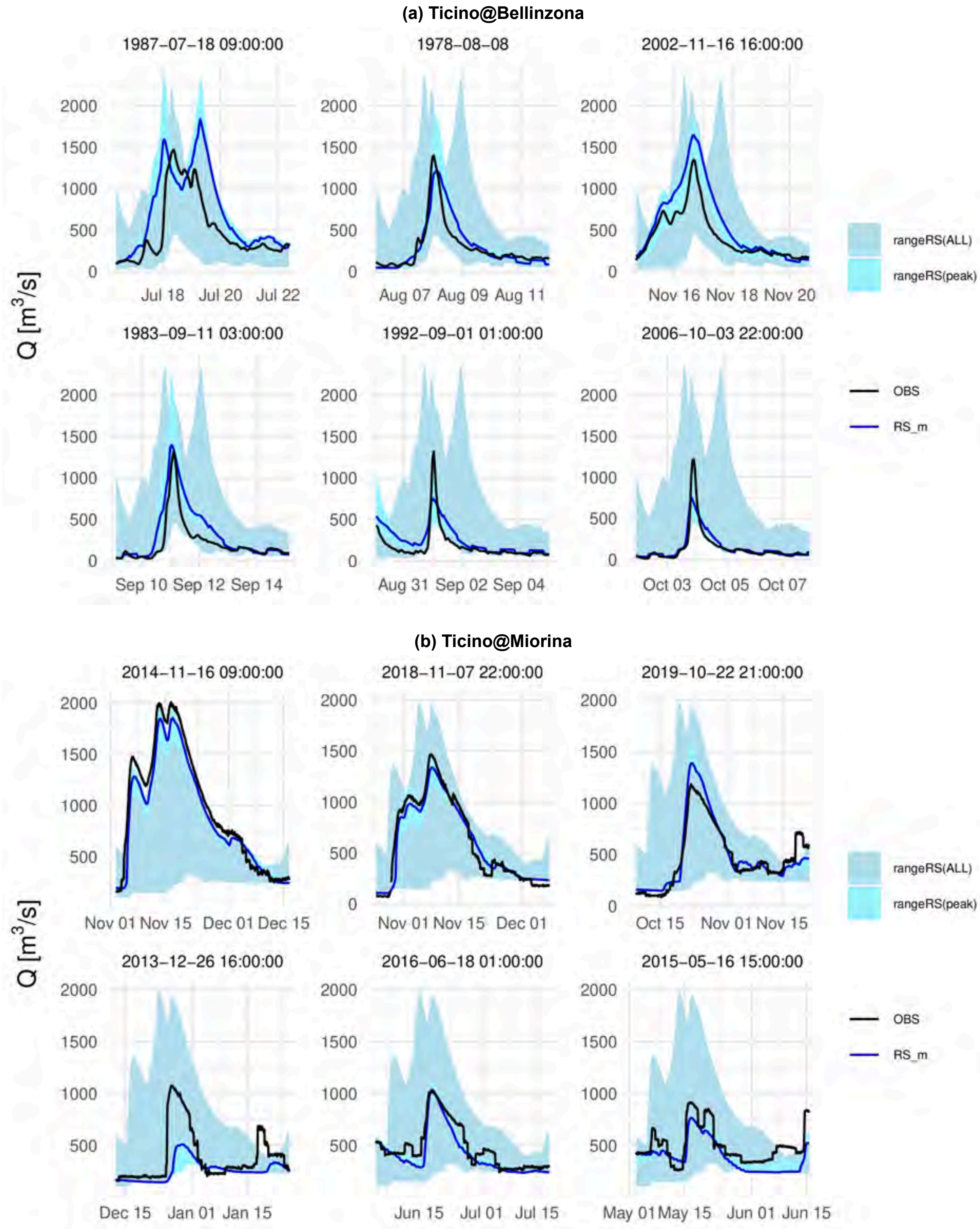

Figure 5.24: Overview of the six largest observed floods for: (a) Ticino at Bellinzona (TicBlz), (b) Ticino at Miorina (TicMio). The black line shows observations (OBS), the blue line shows the intermediate representative parameter set (RS_m), the light cyan range represents the range between the low and high representative parameter set (rangeRS(peak)), and the light blue area shows the range across all six simulated peaks for all three representative parameter sets (rangeRS(ALL)).

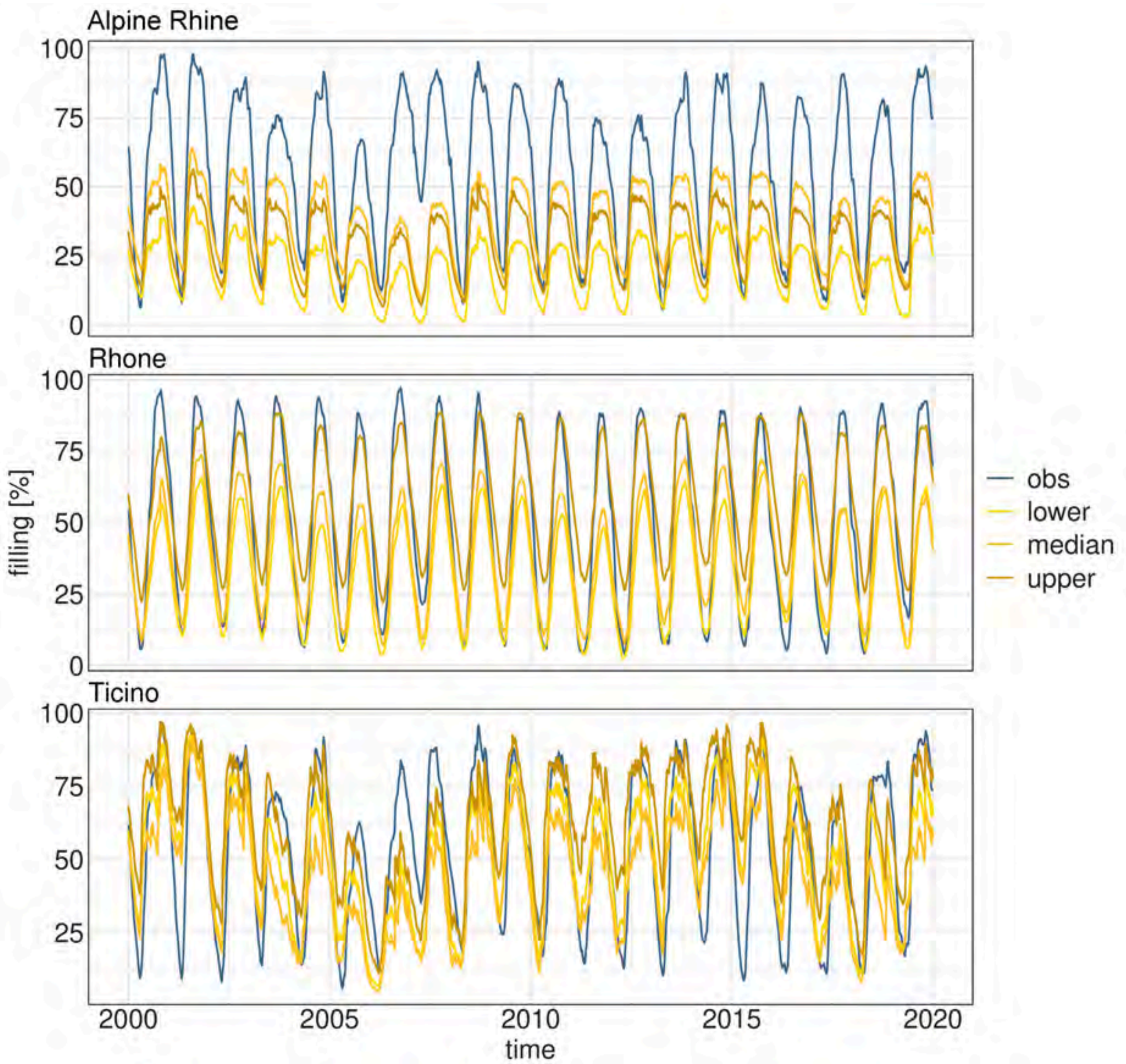

Figure 5.25: Regionally aggregated two-week reservoir filling levels between 2000 and 2019: Yellow lines as simulated using RS Minerve using disaggregated data 1931–2019, blue as simulated in the Ticino catchment using RS Minerve on the basis of observations 1981–2019, red according to SFOE statistics.

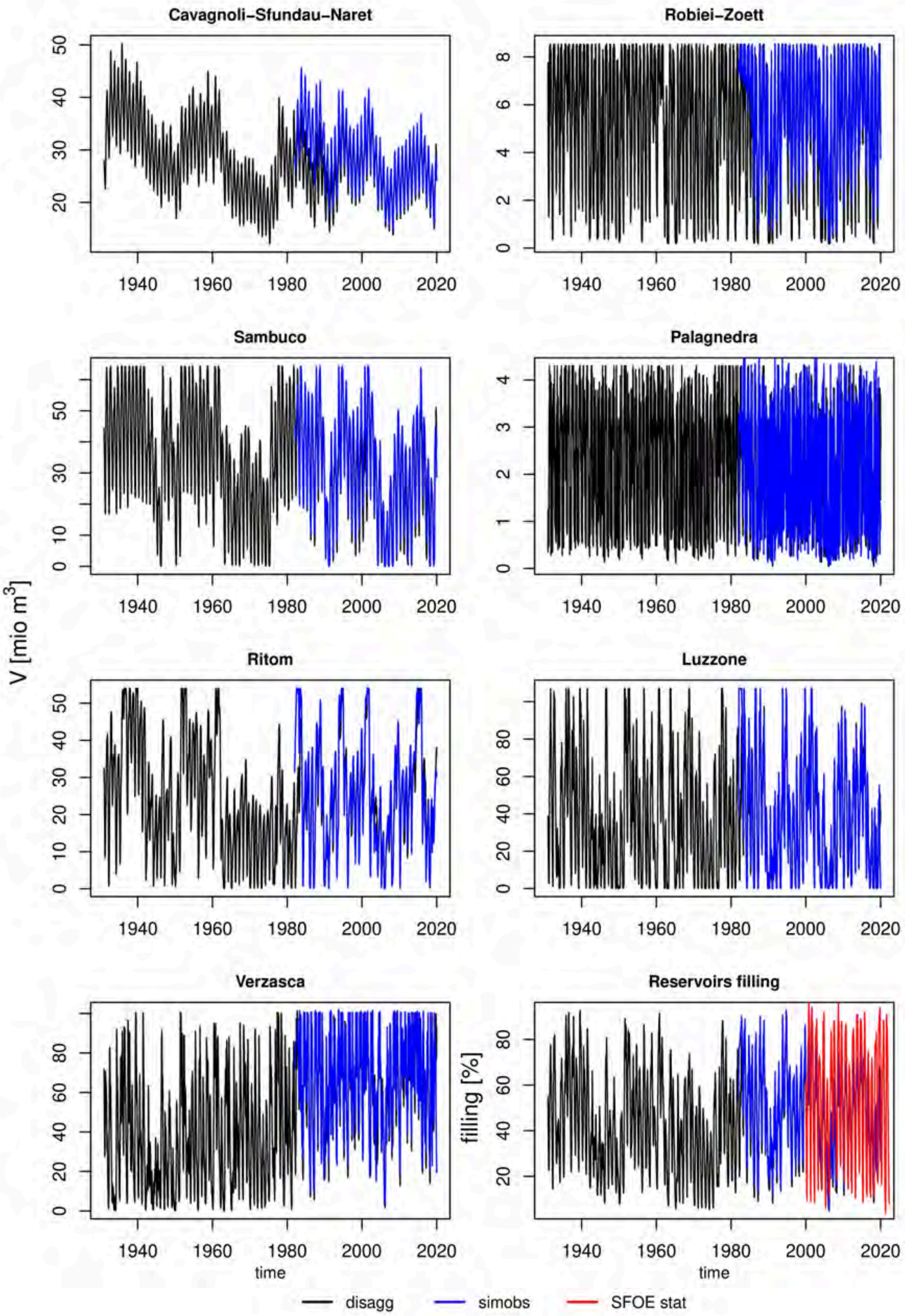

Figure 5.26: Overview of two-week reservoir filling in Ticino between 1931 and 2019. Each panel shows the reservoirs explicitly simulated in RS Minerve, except for the bottom right panel, which shows the aggregated value for the entire catchment. In black as simulated using RS Minerve with the intermediate representative parameter set using disaggregated meteorological inputs 1931–2019, in blue as simulated with the intermediate representative parameter set using observations 1981–2019, red according to aggregated SFOE statistics for Ticino.

inhomogeneities and the variability in underlying climatology and processes. This approach prioritizes robustness in the derived evidence. The maximum attenuation in the flood peak shifts depending on the parameter set: For Rhein at Domat/Ems (RheDEm), for instance, we estimated a flood peak reduction of up to 230 $m^3 s^{-1}$ for a 20-year return level with the intermediate representative parameter set, and a flood peak reduction of up to 360 $m^3 s^{-1}$ for the 30-year return level with the high representative parameter set. For Rhein at Diepoldsau (RheDpa), the reduction is approximately 200 $m^3 s^{-1}$ for the 10-year return level with the intermediate representative parameter set, and goes up to 340 $m^3 s^{-1}$ for the 45-year return level with the high representative parameter set. For the largest peaks, the reduction is around 170 $m^3 s^{-1}$ at both points for the intermediate representative parameter set, about 115 $m^3 s^{-1}$ for the low representative parameter set, and about 185 $m^3 s^{-1}$ for the high representative parameter set. If we take the intermediate representative parameter set as a reference, where the regional filling of the reservoirs is more realistic (see Figure 5.25), these reductions are smaller than those estimated by Zarn et al. (2017) based on observations, and the maximum attenuation occurs at return periods lower than 100 years. Despite these differences, both approaches consistently reveal a smaller reduction in peaks downstream of Domat/Ems (RheDEm) and a non-linear behaviour in peak attenuation.

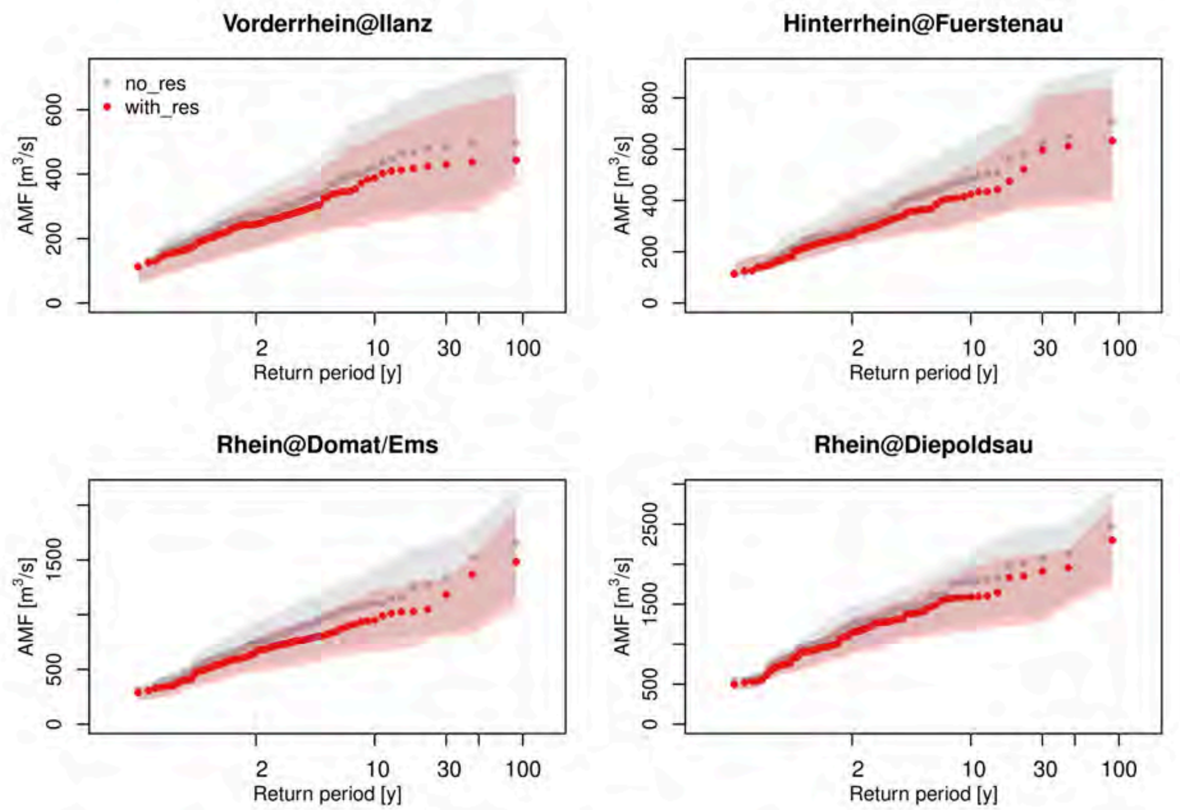

Figure 5.27: Overview of the annual maximum floods (AMFs) and their respective empirical return period for the control period 1931–2019 for four gauging points in the Alpine Rhine. Grey shows simulation results without reservoirs, red simulation results including reservoirs in the hydrological routing. Dots show results for the intermediate representative parameter set, the shaded area shows the range of results between the low and the high representative parameter sets.

We performed the same experiment described above for the Alpine Rhine to assess the effect of including reservoirs in the Rhone River basin (see Figure 5.28). For the three largest observed peaks in the Rhone River in 1987, 1993 and 2000, Jordan et al. (2004) estimated the natural simulated peaks (i.e., without reservoirs) down to Martigny using a detailed model also implemented in RS Minerve. The same values are reported and extended to include the Rhone down to Porte du Scex in a report analysing the 2000 flood both in the Rhone and the Ticino river basins (Hegg et al., 2002). We here consider the high representative parameter set as the reference, as it provides the most realistic representation of reservoir filling (see Figure 5.25) and more accurately captures the three largest peaks (see Figure 5.23). For the 1993 flood in the Rhone at Sion (RhoSio), García Hernández (2011) simulated a peak attenuation of 80 $m^3 s^{-1}$ due to the reservoirs. In contrast, Hegg et al. (2002) and Jordan et al. (2004) estimated a peak attenuation of 220–270 $m^3 s^{-1}$ for flood peaks of 1987 and 1993, which have estimated return periods of 38 and 63 years, respectively (Bundesamt für Umwelt (BAFU), 2017d). For the largest flood observed in 2000, however, Hegg et al. (2002) and Jordan et al. (2004) report a much smaller reduction of 125 $m^3 s^{-1}$ when reservoirs are included, only about half the extent of the earlier events. The flood has an estimated return period of 144 years (Bundesamt für Umwelt (BAFU), 2017d). For this site, using the high representative parameter set, we find a maximum peak reduction of 210 $m^3 s^{-1}$ for the flood event of 2000, which corresponds to a return period of 90 years. For the event in 1993, we find a reduction in the same order of magnitude as García Hernández (2011). For lower return periods, we find a weaker attenuation, with reductions of approximately 70 $m^3 s^{-1}$ for the 30-year event and 130 $m^3 s^{-1}$ for the 10-year event.

For the Rhone at Porte du Scex (RhoPdS), Hegg et al. (2002) estimated a peak attenuation of 230–260 $m^3 s^{-1}$ for the peaks of 1993 and 2000, which have an estimated return period of 72 and more than 150 years, respectively (Bundesamt für Umwelt (BAFU), 2017c). For the third-largest flood, observed in 1987, the reduction is largest with roughly 310 $m^3 s^{-1}$, for a return period corresponding to 36 years (Bundesamt für Umwelt (BAFU), 2017c). In our simulations, the largest peak reduction is found for approximately a 10-year event, amounting to 200 $m^3 s^{-1}$. For the largest flood, corresponding to the event in 2000, we find an attenuation of about half this magnitude, amounting to 100 $m^3 s^{-1}$. Jordan (2007) presents hydrographs of the events observed and simulated with reservoirs removed at Porte du Scex (RhoPdS) in 1993 and 2000, showing reductions of 110 $m^3 s^{-1}$ in 1993 and 140 $m^3 s^{-1}$ in 2000. These values are very similar to those reported by García Hernández (2011) for the same two events, and all of these are closer to our estimates.

In general, the Rhone River basin shows a similar behaviour to that observed in the Alpine Rhine, regardless of the source of information used for the simulations in a natural state. Specifically, a smaller relative reduction in peaks is noted downstream of Sion (RhoSio), although not absolute terms according to Hegg et al. (2002). In addition, the basin shows non-linear behaviour in peak attenuation.

For the Rhone River downstream of Lake Geneva (RhoGen) we could not find any references reporting the effects of the reservoirs upstream. However, it is evident that a natural regime would show more frequent high flows, to be expected from the redistribution of flows caused by the reservoirs, which artificially increase winter inflows, and decrease summer inflows. This reinforces flood peaks to diverge already at comparatively small return periods, with the largest differences occurring between 10-year and 30-year events. The attenuation then diminishes again for higher return periods.

5.2.2. Weather generators GWEX and SCAMP

As in the hydrological modelling analysis, we sampled daily values over the observation time interval for each of the 1 000 years blocks within the 300 000 −year simulation using inputs from the two weather generators. For each sample, we independently calculated the exceedance probabilities. To visualize the results, we determined the 95 % confidence intervals for the flow values corresponding to each exceedance probability and plotted these alongside the observations and the control simulation.

Figure 5.29 presents the results for nearly the same gauging points as in the previous section, where FDCs from simulations and observations were compared. Here, the 95 % confidence intervals of all sampled FDCs for GWEX and SCAMP are indicated as well. We replaced the Vorderrhein at Ilanz (VRhIla) with the Emme at Wiler (EmmWil) to illustrate a problematic catchment, where flow is consistently and markedly underestimated in all simulations. We emphasize that individual extremes going beyond the confidence intervals shown for the considered gauging points can occur. Comparisons between the different FDCs presented in this plot should be made with caution, as the FDCs from control simulation and from observations do not include confidence intervals. To enhance readability and maintain focus on the broader agreement between the different time series, we opted not to include individual extreme FDCs derived from the two weather generators.

As with the hydrological simulations (Section 5.1), it is also difficult to identify a common pattern after the hydrological routing. We generally observe almost systematically lower estimates for SCAMP compared to GWEX, and simulations of the control period being closer to those performed with GWEX.

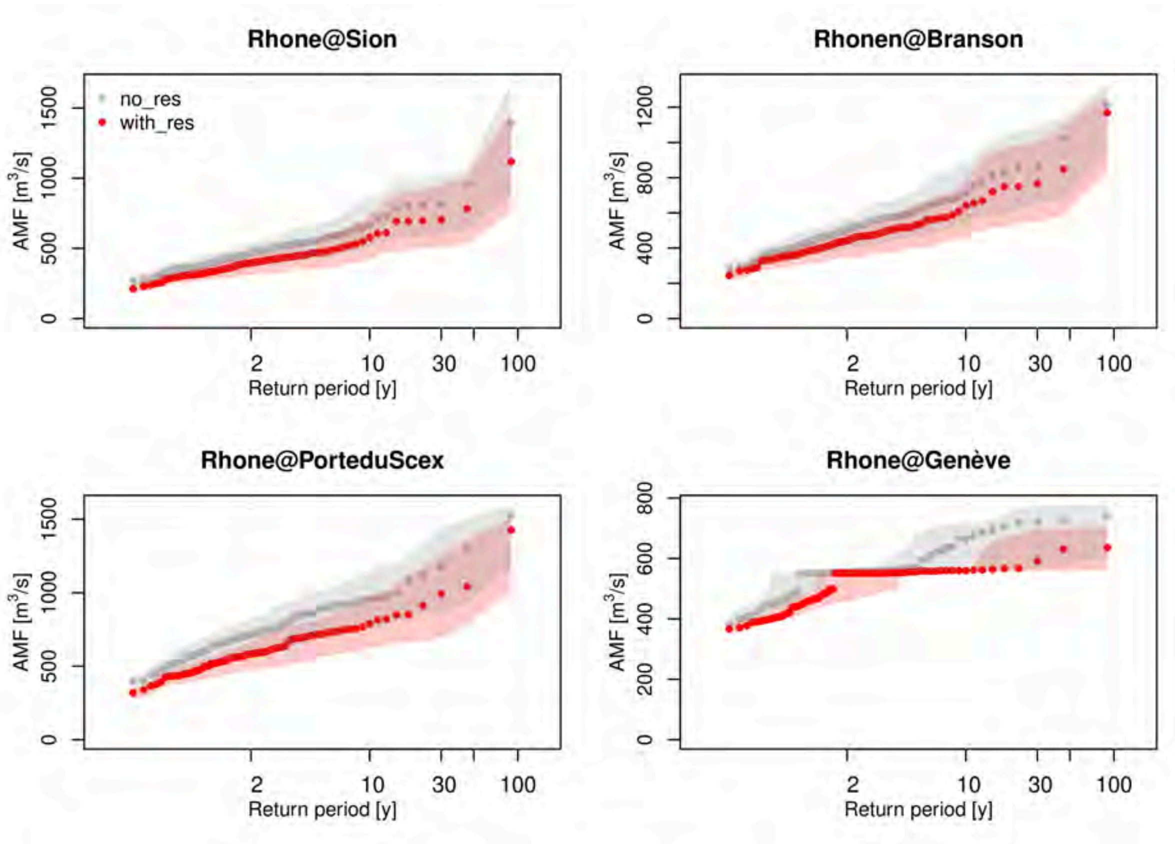

Figure 5.28: Overview of the annual maximum floods (AMFs) for four gauging points in the Rhone River basin and their respective empirical return periods for the control period 1931–2019. Grey shows simulation results without reservoirs, red simulation results including reservoirs in the hydrological routing. Dots show results for the intermediate representative parameter set, the shaded area shows the range of results between the low and the high representative parameter sets.

Only for the Limmat at Zürich (LimZue) and the Maggia at Locarno (MagLcn), the confidence intervals of GWEX and SCAMP mostly overlap. For Limmat et Zürich, the confidence intervals in addition very well entail observations and control simulation. The largest differences are found for the Inn at Martina (InnMr), where SCAMP much better agrees with observations and control period, and for the Hinterrhein at Fürstenau (HRhFue), where GWEX shows better agreement with observations and control period.

In the Rhine River basin, the largest departure between the two weather generators is found in the Alpine Rhine, and the greatest agreement between observations, control period and weather generator is found for GWEX.

In the Rhone River basin at Porte du Scex (RhoPdS), upstream of Lake Geneva, the highest flows are overestimated by GWEX as well as in the control simulation. It is important to note that for the control period, this is mainly due to the overestimation of the volume of the peak in 2000. The FDCs of SCAMP, by contrast, are closer to observations, and slightly and systematically underestimate flows. At Chancy, downstream of Lake Geneva, SCAMP is also closer to the observations for the highest flows, but considerably underestimates the flows for the remaining range.

For the Ticino River basin, the highest flows for Ticino at Bellinzona (TicBlz) and Maggia at Locarno (MagLcn) are consistently overestimated in all simulated time series. However, the largest differences in the Ticino River are found between the simulations with the weather generators and the observations, with the control simulation falling between these two. For Ticino at Miorina (TicMio), downstream of Lake Maggiore, the FDCs of observations, control simulation and GWEX are very similar for most of the flow range. However, for the highest flows, the FDCs of both observations and control period bend into the confidence interval of simulations with SCAMP. This might be due to the short observation period of only seven years.

Just as in the hydrological simulations using both weather generators, there is a strong agreement in the seasonality of the AMF occurrence in all basins (Figure 5.30).

5.2.3. Reforecasts

At last we evaluate results from the simulations with the RFs for the four selected test catchments: Inn at S-Chanf (InnSCh), Thur at Andelfingen (ThuAnd), Aare at Bern (AarBrn) and Maggia at Locarno (MagLcn). For doing this we again examined the FDCs and the seasonality of the AMFs.

We calculated the FDCs for simulations using inputs from RF in the same manner as for the weather generators, by sampling daily values over the observation period for each block of approximately 1 000 years. The final block is slightly shorter, giving a total of 9 920 years. From each sample, we calculated the exceedance probabilities individually. For visualization, we determined the 95 % confidence intervals for each exceedance probability based on the flow values, and present these alongside the observations, the control run, and the results from the two weather generators, GWEX and SCAMP (Figure 5.31). Please note that for Inn at S-Chanf (InnSCh), results from the weather generators are not present because this is not an output site.

When we compare the FDCs resulting from reforecasts and weather generators, we find mostly a very similar behaviour, with the reforecasts often showing a wider range compared to the weather generators, in particular for Aare at Bern (AarBrn). The largest differences to observations as well as to control run were usually found in the higher flow ranges. The largest discrepancy between observations, control run and reforecasts is found for Inn at S-Chanf (InnSCh). A noticeable discrepancy can also be seen for Maggia at Locarno (MagLcn). However, it appears that observations at this site might not be fully representative: As noted further above already, some of the largest floods that occurred here are missing in the records (Näf-Huber et al., 2021). The Maggia at Locarno (MagLcn) and Thur at Andelfingen (ThuAnd) show a remarkable agreement between control run and all simulations produced with long time series. For Thur at Andelfingen (ThuAnd), simulations and observations are very close, while SCAMP slightly deviates from all other simulations in the mid flows.

If we take a look at reproduction of seasonality (Figure 5.32), we see the largest agreement between weather generators and control run. The reforecasts, by contrast, sometimes miss the seasonal signal, such as for Inn at S-Chanf (InnSCh), and often overestimate its range, in particular for Aare at Thun (AarThu) and Aare at Bern (AarBrn). The best agreement is found for Maggia at Locarno (MagLcn).

5.2.4. Spatial patterns during the six largest floods

In the following, the spatial patterns of the six largest simulated events are analysed, comparing simulations produced using the two weather generators GWEX and SCAMP. Maps of simulated specific discharge are shown for three individual river basins, with reference to peak flows at the respective outlets, namely Aare at Beznau, Inn at Martina and Ticino at Miorina.

The top six GWEX events occurring at Aare at Beznau (Figure 5.33) are mainly events from May, July, August, and a winter flood in December. For SCAMP, by contrast, most of the events occur later in the year, in September and October, with only one event in July. The September and October events of the SCAMP simulations have very similar patterns of contributing sub-catchments, with highest contributions in the western part of the basin, and less from the Alpine region. The largest events identified in the GWEX simulation show a different pattern of contributing sub-catchments: Snow melt is the main contributor, with Alpine catchments playing the most important role during these events. The 3rd and 4th highest events of GWEX are more similar to the pattern found in SCAMP events, but also here the alpine catchments contribute more than in SCAMP.

For Inn at Martina (Figure 5.34), both GWEX and SCAMP are more similar in the timing of the largest events. The GWEX top events occur from May to September, and the SCAMP top events only in August and September. The pattern of contributing sub-catchments is very similar for both weather generators. In general, there are slightly higher contributions for the sub-catchments in the GWEX simulations.

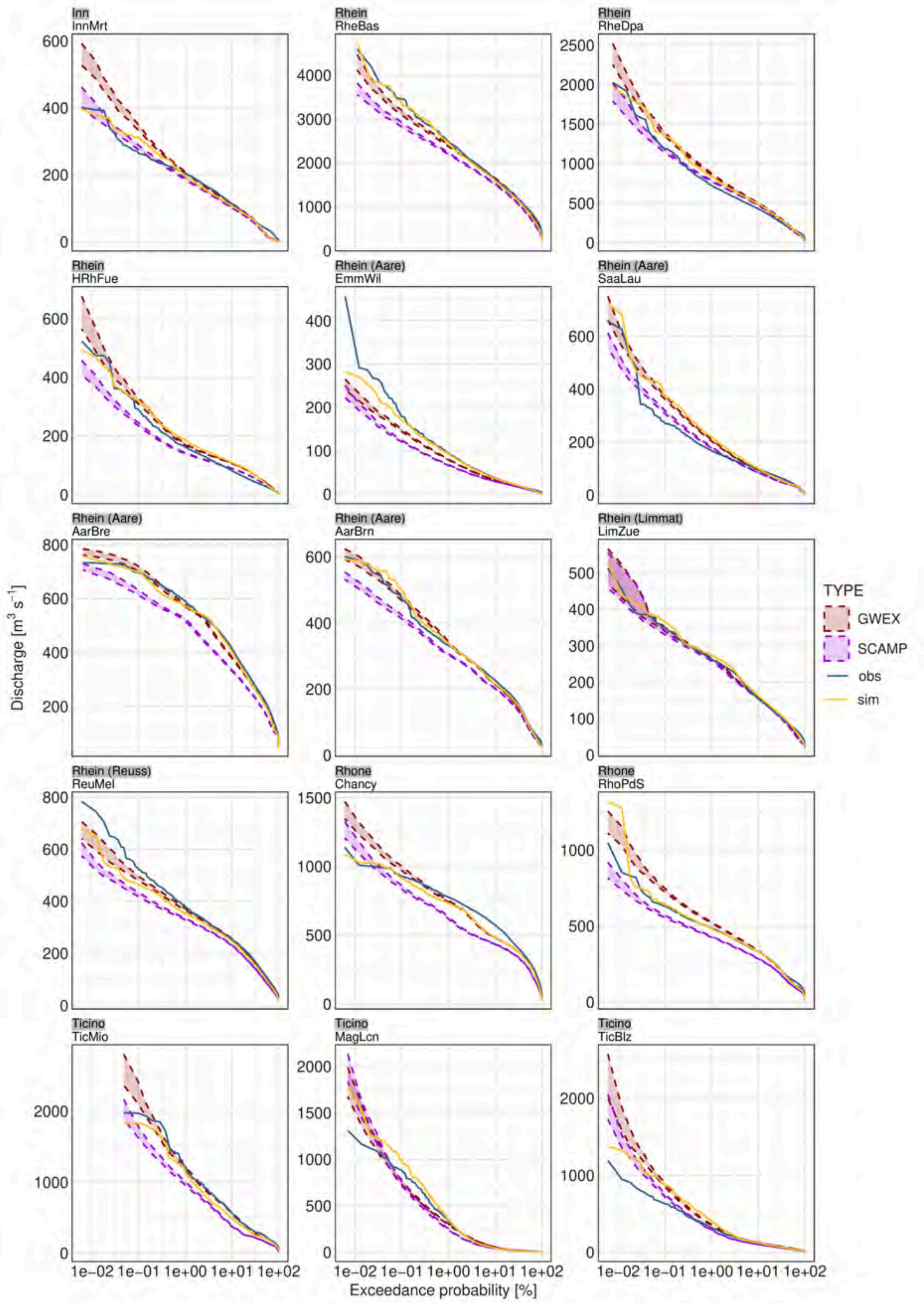

Figure 5.29: Flow duration curves of selected example catchments from the large river basins. The flows are sampled from the simulations using GWEX and SCAMP weather scenarios, together with the FDCs from the control run (sim) and the observations (obs). The sample size is equal to the length of the observations (or the control run if its length is shorter than that of the observations). Only the results of the intermediate representative parameter set are shown. For catchment abbreviations see Table C.1.

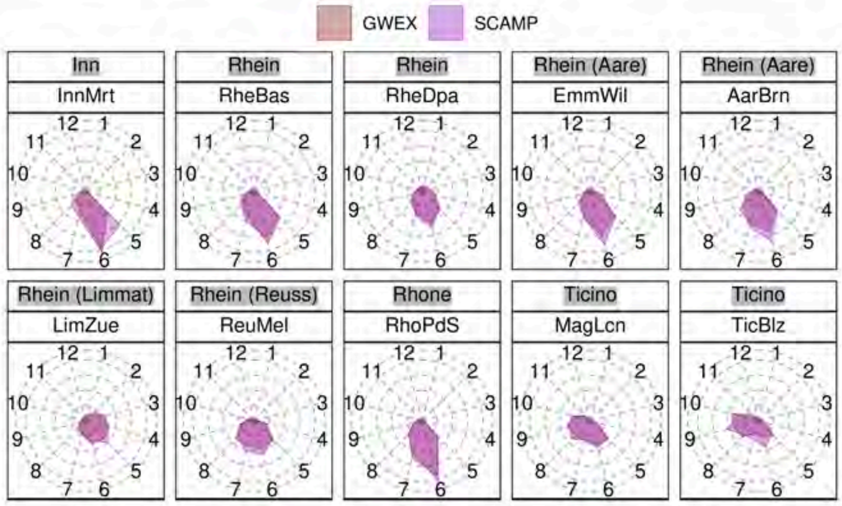

Figure 5.30: Comparison of simulated AMF seasonality of GWEX and SCAMP. For catchment abbreviations see Table C.1.

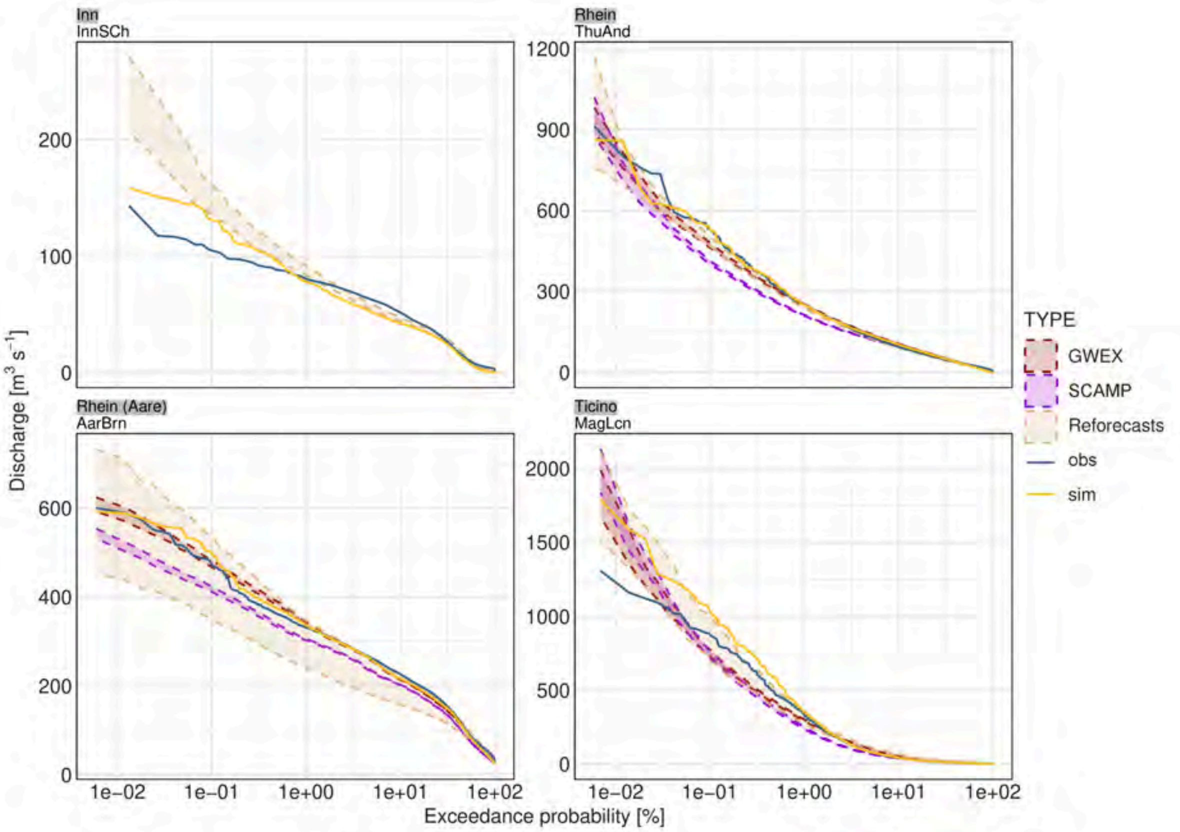

Figure 5.31: Flow duration curves (FDCs) for selected sub-catchments of the large river basins. The flows are sampled from the simulations using RFs as meteorological input and are compared to the simulations using GWEX and SCAMP weather scenarios together with the FDCs from the control run (sim) and the observations (obs). The sample size is equal to the length of the observations (or the control run if its length is shorter than that of the observations). Only the results of the intermediate representative parameter set are shown. For catchment abbreviations see Table C.1.

Figure 5.32: Comparison of simulated AMF seasonality of GWEX, SCAMP and RFs. For catchment abbreviations see Table C.1.

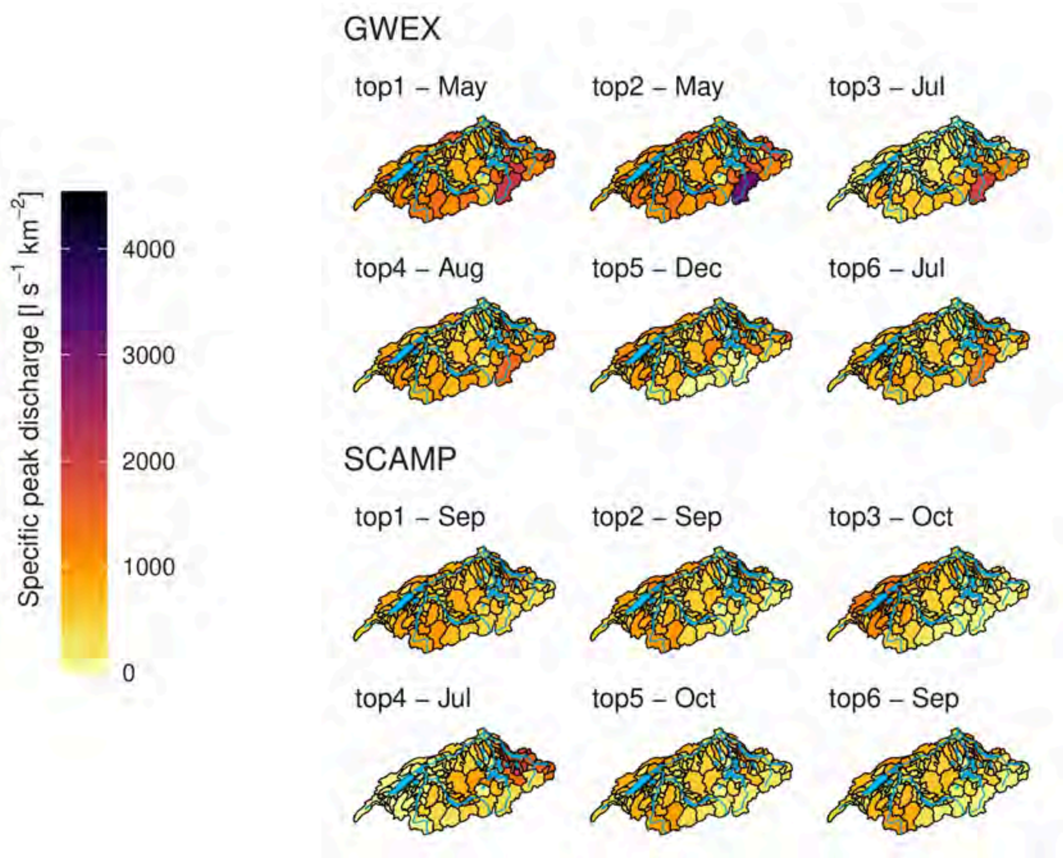

Figure 5.33: Top six peak flow events for the Aare River basin: Contributions of specific discharge of the different sub-catchments comparing simulations with GWEX and SCAMP weather scenario input. The intermediate representative parameter set was used for the simulations.

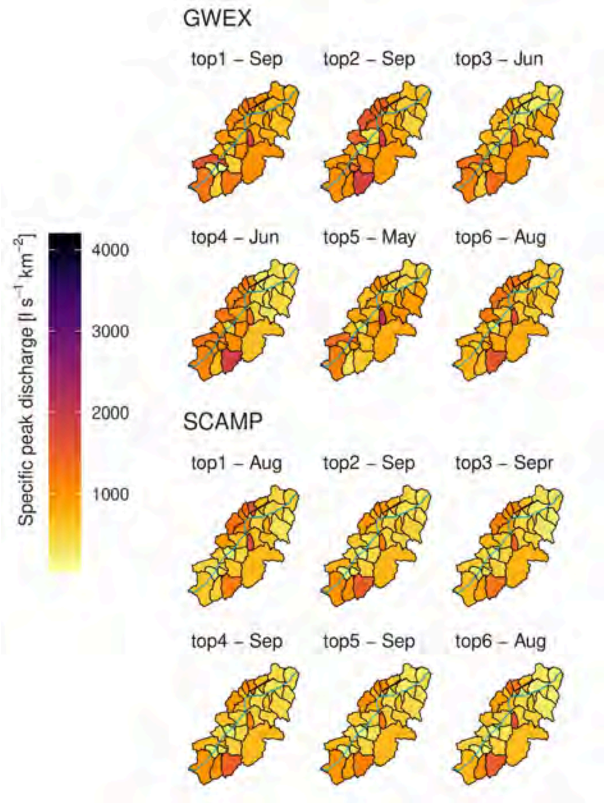

Figure 5.34: Top six extreme events for the Inn basin: Contributions of specific discharge of the different sub-catchments comparing simulations with GWEX and SCAMP weather scenario input. The intermediate representative parameter set was used for the simulations.

For Ticino at Miorina (Figure 5.35), the largest events from GWEX occur in August and October, while the largest events from the SCAMP simulations occur in June, October and November. For the largest events in Ticino, very high contributions from specific regions (sub-catchment clusters) are clearly visible, with patterns differing between the events. These patterns are not seasonal but recurrent. The contributions of the sub-catchments to the largest events in the SCAMP simulations were much smaller, and the corresponding spatial patterns also vary. While the patterns for SCAMP are very similar (4th, 5th and 6th highest events) despite occurring in different seasons, they are very different from those of GWEX. In this river basin, we find by far the largest differences between the spatial patterns of streamflow contributions for the largest events, much larger than for the Aare and especially much larger than for the Inn river basins. This highlights that the degree of differences between the two weather generators is regionally dependent.

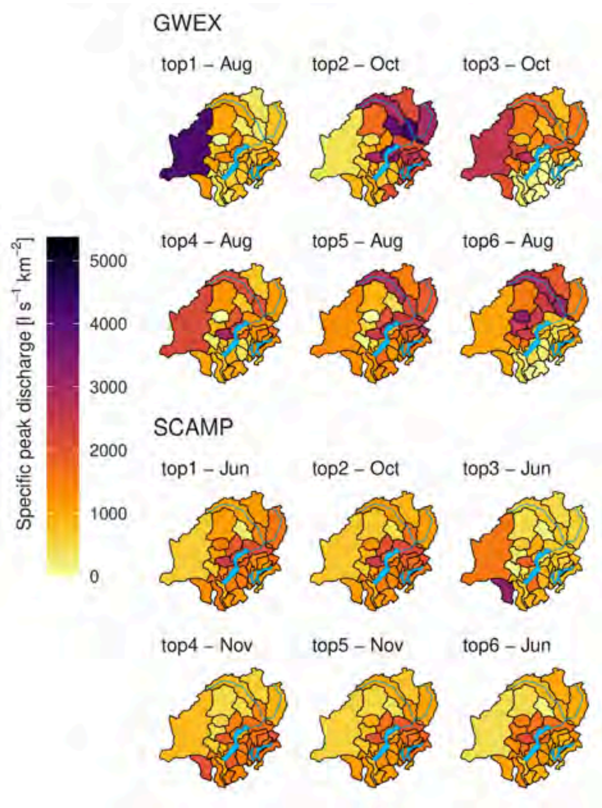

Figure 5.35: Top ten extreme events for the Ticino basin: Contributions of specific discharge of the different sub-catchments comparing simulations with GWEX and SCAMP weather scenario input. The intermediate representative parameter set was used for the simulations.

6

GWEX based flood estimates at selected sites

6.1. Introduction

The following sections show results obtained using GWEX weather scenarios (see Chapter 3) as input. These results are considered as the primary flood estimates for EXCH, given the extensive experience with GWEX in the simulation chain throughout EXAR and EXCH, as well as the characteristics of GWEX-based annual maximum floods (AMFs) compared with observations.

Simulations based on SCAMP weather scenarios can provide a second opinion and help contextualise the GWEX-based results shown here. This is especially recommended when GWEX-based AMFs show unexpected behaviour. In this sense, SCAMP results are occasionally mentioned below where relevant, whereas a more detailed appraisal of these simulations using alternative weather input is given in Section 9.1.

In a similar fashion, the use of reforecasts (RFs) as alternative weather input can provide an additional perspective and further context. Within this project, RFs have been explored in the sense of a feasibility study, examining a set of test catchments, four of which overlap with FOEN output sites (Aare at Thun, Aare at Bern, Thur at Andelfingen, Maggia at Locarno). More details on the RF results are given in Section 9.2.

The selection of sites presented in this chapter prioritizes locations with available observational data for comparison, focusing on cases of high relevance to hydrology or flood risk. Additionally, the selection includes sites where background information and contextual discussion help interpret results, particularly in the presence of specific hydrological or hydraulic conditions. Selected return levels (HQ_{30}, HQ_{100}, HQ_{300}, $HQ_{1\,000}$, $HQ_{10\,000}$) for all output sites are presented in Appendix B. These return levels were also derived from the GWEX-based simulations, using the full, 300 000-year long continuous simulation (CS).

The main figures for each site consist of three panels. The top-left panel a focuses on floods with return periods of approximately 100 years. For this, the 300 000-year long CS was subdivided into blocks corresponding to the length of the observed AMF record. The simulated AMFs are shown with median and 95 % confidence intervals. The top-right panel b focuses on rarer floods, with the continuous simulation (CS) subdivided into 300 blocks of 1 000 years each, using similar confidence intervals. The bottom-left panel c focuses on exceedingly rare floods, with the continuous simulation (CS) subdivided into 30 blocks of 10 000 years each, again with similar confidence intervals. All three panels use a Gumbel-scaled abscissa, as applied to all exceedance plots shown in this report. All simulations used are based on the intermediate representative parameter set unless stated otherwise. An uncertainty band spanning the low and high representative parameter sets (see Section 3.3) is available but not shown here. As context for interpretation, please bear in mind the uncertainties and limitations discussed in Section 10.2.

Note that the long CS can be treated either as one single realisation or subdivided into blocks of varying lengths. Reducing the block length increases the number of realisations, which results in wider confidence intervals and a shorter maximum return period (see Figure 6.1). Similarly, using a longer continuous simulation would result in wider confidence intervals and might influence the estimates for

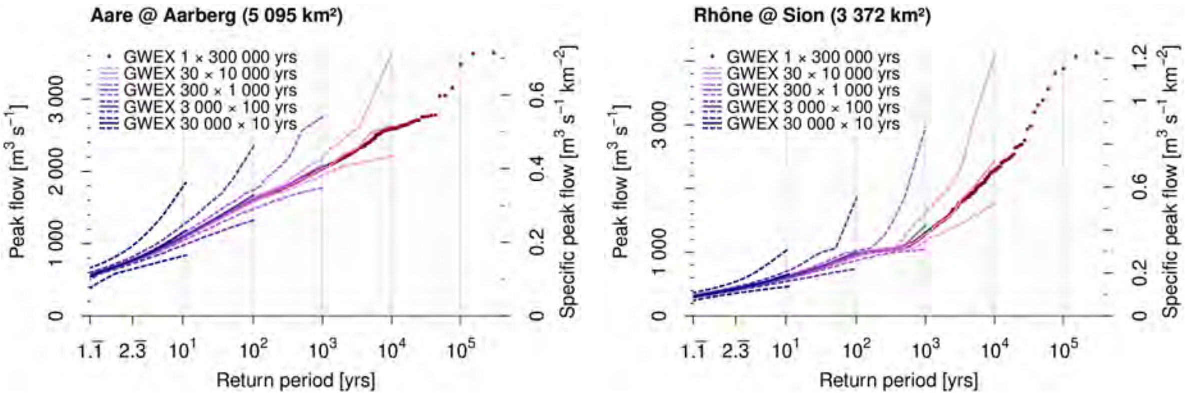

Figure 6.1: GWEX-based flood estimates for Aare at Aarberg (left; for details see Section 6.2.7) and Rhone at Sion (right; see Section 6.6.1), illustrating the impact of subdividing the 300 000-year long continuous simulation (CS) into blocks of varying lengths. The dots represent the annual maximum floods of the full CS, the lines indicate the median (solid) and 95 % confidence intervals (dashed) for the respective block subdivisions.

very rare floods. There is currently no scientific consensus on the preferred method for analysing such long CS (see e.g., Blazkova and Beven, 2004), and the choices made in the present project follow practical considerations, particularly the need for comparability with AMF observations and alignment with the return periods targeted in the present project. However, Beven (2021) generally recommends using simulations that are at least ten time times longer than the return period of interest – which here covers the highest return period in focus, namely the 10 000-year flood. Small differences in the computed return levels arise depending on whether the CSs are subdivided into blocks and, if so, on the chosen block length. These differences are generally minor and become more noticeable only for return periods close to the chosen block length, and if the chosen block length is small (see Figure 6.1). That said, panel a, based on blocks matching the length of the observed AMF record, should be regarded primarily as a diagnostic tool for comparing observed and simulated AMFs. When making such comparisons, it is important to consider any site-specific effects occurring at high discharges – such as bank overflow in the example of Rhone at Sion (Figure 6.1, right) – which become apparent only in sufficiently long blocks. It is also important to note that the confidence intervals shown in panel b and especially in panel c are rather narrow due to the smaller number of simulation blocks available, and should not be taken as an indicator of overall uncertainty.

All three panels also display AMFs from a control simulation using observed weather 1931–2019, where precipitation and temperature data have been disaggregated from daily to hourly time step (see Section 2.1).

Furthermore, the panels show observed AMFs with extrapolation and confidence intervals according to Baumgartner et al. (2013), as they can be found online in the FOEN flood statistics[1]. In this context, it is important to remember that observations and simulations do not always need to agree very closely. Reasons for disagreements can, on the one hand, include different reference periods: While the control simulations always refer to 89 years of simulations 1931–2019, the observations cover periods that vary in length and coverage depending on the station in question. When it comes to the long continuous simulations, the period used for parametrising the weather generators is also 1931–2019. And while the extrapolation of observations occurs via discharge records, the extrapolation underlying the simulations stems from the weather generator, and therefore represents a joint extrapolation of precipitation and temperature at multiple sites. The meteorological records are usually longer than the hydrological records and can be better interpolated in space. In addition, the extrapolation via weather generator explores in great depth the combination of a large spectrum of antecedent conditions (including snow cover, lake filling and soil moisture) with heavy precipitation events (Viviroli et al., 2022). On the other hand, hydraulic structures and diversions built over the decades have changed the hydraulic and hydrological conditions in some cases, leading to inhomogeneities in the observed record, or at least to changes in behaviour that shorten the period that represents the current state. We recall that

[1] https://www.hydrodaten.admin.ch

the state of the EXCH modelling system is 2015 throughout. An example for this is the Aare River at Thun, where the AMF records before 2009 do not agree well with the current state that includes a flood relief tunnel and updated lake regulation (see Section 6.2.2). The impacts of these changes are also visible for the Aare River at Bern (Section 6.2.3). Another example is the Aare River downstream of Lake Biel, where the second Jura water correction (1962–1973) has led to a slight increase in frequent floods that has an appreciable impact on the exceedance curve, including its upper tail (see e.g., Klemeš, 1986; Viviroli et al., 2022). This is considered here (and in the FOEN flood statistics available online) by not using the AMFs before 1974 (see e.g. Section 6.2.11). By contrast, it is not feasible to eliminate the impact of the many further, smaller alterations. For rare floods, it is important to note that AMF observations have a limited length spanning a few decades to a bit more than 100 years (see Section 2.2). Extrapolations are usually not recommended for return periods beyond two to three times the length of the AMF record due to large uncertainties (Baumgartner et al., 2013; Maniak, 2005), and here thus – depending on the site – not for more than 100–300 years.

As noted in Chapters 1 and 3, the CS approach used here essentially exploits precipitation and temperature records at multiple sites to parametrize a multi-site weather generator and to enable exceptionally long hydrological simulations that are finally evaluated statistically. The extrapolation to small probabilities is thus based on meteorological rather than hydrological observations, and therefore a considerably broader range of conditions can be covered than is present in the streamflow records. This concerns especially the extent, spatial configuration and temporal progress of triggering meteorological events, and the combined hydrological response of the many sub-catchments. Therefore, perfect correspondence between flood estimates derived from observations and from simulations should not be expected.

6.2. Aare River basin

6.2.1. Aare at Ringgenberg, Goldswil

Starting with the main branch of the Aare River, results for Ringgenberg (catchment area: 1 138 km^2) are presented first. This site is located between the regulated lakes Brienz and Thun. In comparing the AMF exceedance curves (Figure 6.2), the control simulation shows slightly lower values than the observations for floods exceeding the HQ_{10}, except for the highest peak, which is higher than the observed maximum discharge. This discrepancy may stem from peculiarities of lake regulation in the case of individual floods – that can deviate from the rules implemented in RS Minerve – and should be considered in light of the observation period, which, at 42 years, is less than half the 89-year period covered by the control simulation. Moreover, changes in lake regulation have occurred during this time, whereas all EXCH simulations consistently depict the current state. In the case of Ringgenberg, however, the impact of these changes appears comparatively small (Bundesamt für Umwelt (BAFU), 2017a). Very good agreement is noted between observations and long CSs.

6.2.2. Aare at Thun

For the Aare River at Thun (2 459 km^2), any assessment against observations must consider notable alterations affecting the outflow of Lake Thun: In addition to changes to the regulation of both lakes Thun and Brienz, a flood relief tunnel was taken into operation in Thun in 2009, increasing outflow capacity by approximately 100 m^3 s^{-1}. The gauging site at Thun, located downstream of the tunnel's outlet, is influenced by both alterations, and higher discharges can be expected for frequent floods due to the proactive, forecast-oriented regulation of both lakes. The observed time series is likely not stationary (Bundesamt für Umwelt (BAFU), 2020b).

As the EXCH modelling chain depicts the current state, a comparison for the period 2009–2021 is most appropriate. In this period, there is indeed a strong agreement between control simulation and observations (Figure 6.3), although the statistics of observed floods show an exceptionally wide confidence interval due to the short record length. The continuous simulation has a pattern similar to that of the control simulation, whereas the exceedance curve temporarily flattens for recurrence intervals between approximately 100 to 550 years, where the effect of the flood relief tunnel is exhausted. For even higher recurrence intervals, a steady further extrapolation of observations 1906–2021 would point in a similar direction as the long continuous simulations.

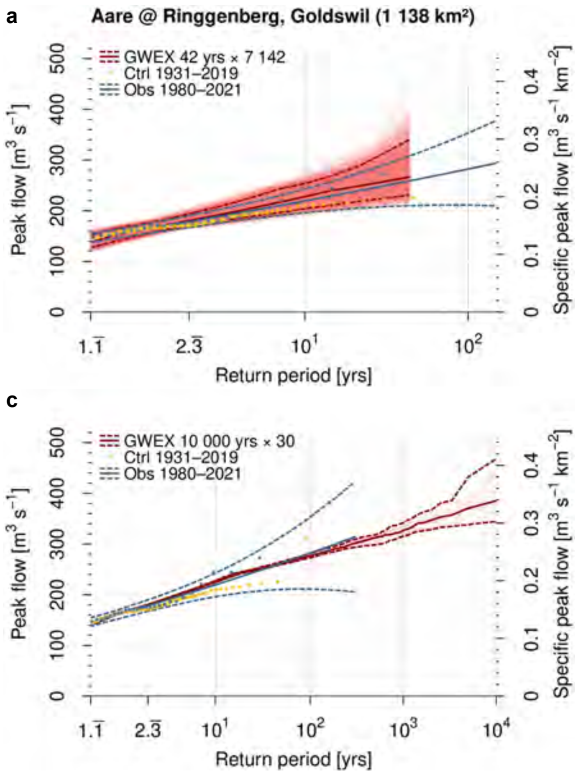

Figure 6.2: GWEX-based flood estimates for Aare at Ringgenberg, with simulations subdivided into blocks as follows: panel a, blocks similar in length to the annual peak flow record; panel b, 300 blocks of 1 000 years; panel c, 30 blocks of 10 000 years. For interpretation and important background information see Chapter 10.

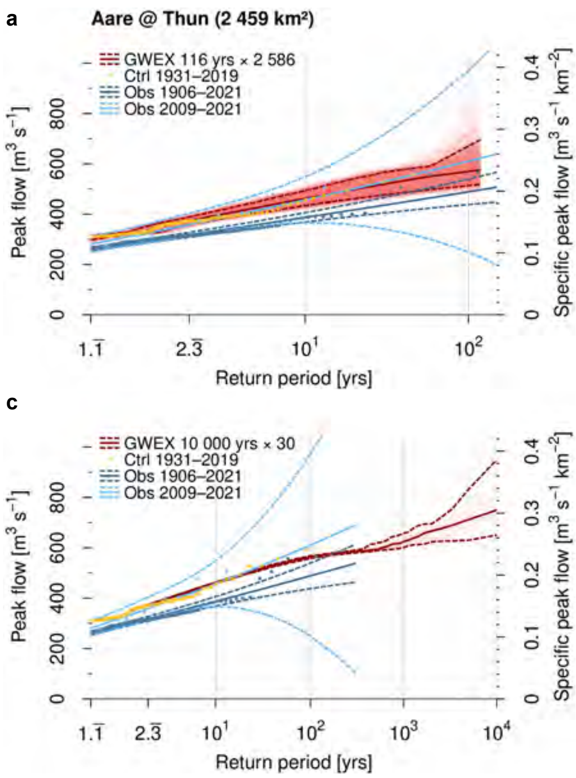

Figure 6.3: GWEX-based flood estimates for Aare at Thun, with simulations subdivided into blocks as follows: panel a, blocks similar in length to the annual peak flow record; panel b, 300 blocks of 1 000 years; panel c, 30 blocks of 10 000 years. Statistics of observed peak flows are derived from two different periods due to marked changes to the hydrological system (see main text). For interpretation and important background information see Chapter 10.

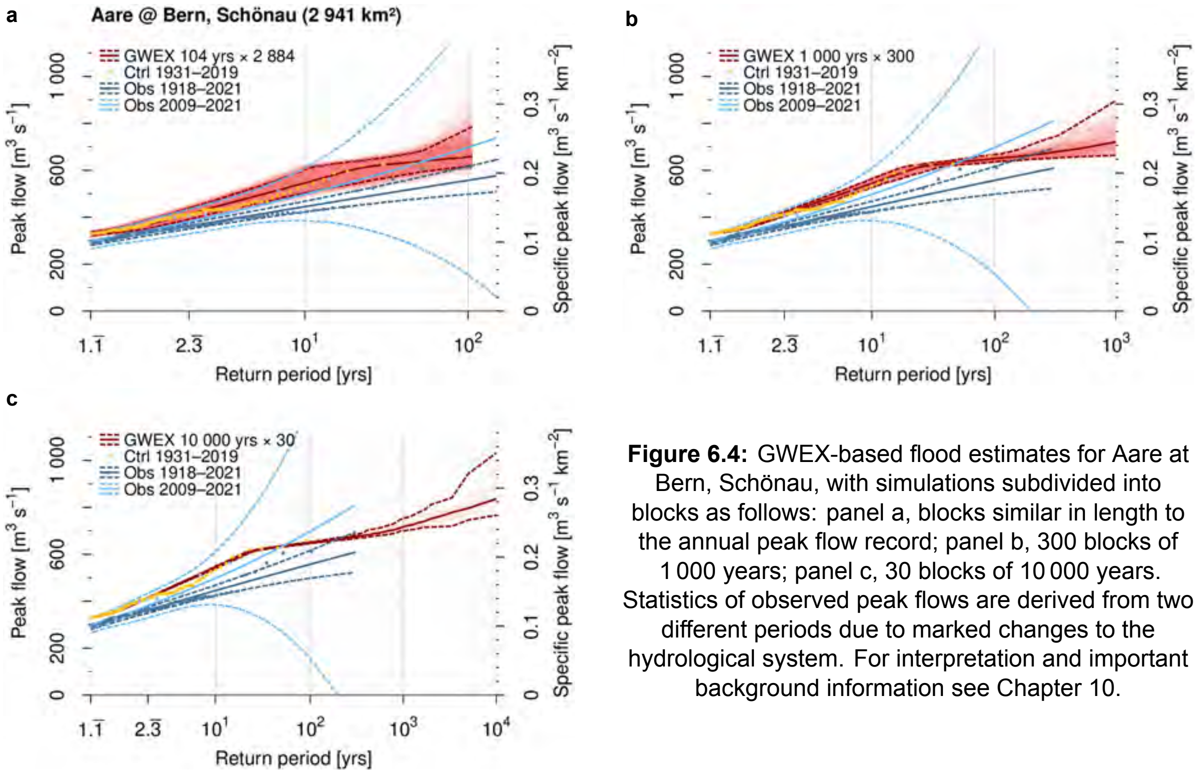

Figure 6.4: GWEX-based flood estimates for Aare at Bern, Schönau, with simulations subdivided into blocks as follows: panel a, blocks similar in length to the annual peak flow record; panel b, 300 blocks of 1 000 years; panel c, 30 blocks of 10 000 years. Statistics of observed peak flows are derived from two different periods due to marked changes to the hydrological system. For interpretation and important background information see Chapter 10.

6.2.3. Aare at Bern, Schönau

Similar to the Aare River at Thun (Section 6.2.2), flood discharges at Bern (2 941 km^2) are likely not stationary (Bundesamt für Umwelt (BAFU), 2020a), with a strong influence of the flood relief tunnel in Thun and the changes to regulation of lakes Thun and Brienz. And also here, the appropriate period for comparison of observations and the current state implemented in the simulation chain is 2009–2021. For this period, observations and control simulation agree well (Figure 6.4), especially for AMFs in the range of the mean annual flood (recurrence interval of $2.\overline{3}$ years) and higher. For peak flows exceeding approximately 590 $m^3\,s^{-1}$, inundations occur in the Belpmoos region upstream of Bern. The resulting flowing retention is depicted in the simulation chain, with RS Minerve emulating the behaviour found in more detailed 2D hydraulic simulations (see Section 3.4). The flowing retention manifests as a flattening of the exceedance curve in both the control simulation and the long continuous simulation, persisting up to recurrence intervals of approximately 500 years. The highest simulated peak flow in the 300 000-year long CS reaches ~1 100 $m^3\,s^{-1}$, which is close to the Probable Maximum Precipitation (PMP)-Probable Maximum Flood (PMF) estimate of ~1 300 $m^3\,s^{-1}$ found in the literature (see Felder and Weingartner, 2016, 2017; Zischg et al., 2018)

6.2.4. Sarine at Rossens dam

The Saane River joins the Aare River between output sites Mühleberg (not shown) and Aarberg (see Section 6.2.7). Three sites along the Saane are discussed here and in the following two sections, before continuing with the Aare further downstream.

The Rossens dam, which impounds Lake Gruyère, has a direct tributary catchment of 952 km^2. In this context, it is important to note that the weather generators developed in EXAR and refined in the present EXCH module on large catchments are primarily designed to accurately and realistically represent one- to multi-day precipitation events relevant to floods in catchments with an area of approximately 1 000 km^2 or more. Smaller catchments, such as that of the Sarine at Rossens dam, are therefore increasingly below the spatial scope of the CS implementation for large catchments in EXCH. This is because shorter-duration precipitation events become more relevant for flood generation with decreasing catchment size, especially in pre-alpine basins like the Sarine as well as in alpine basins.

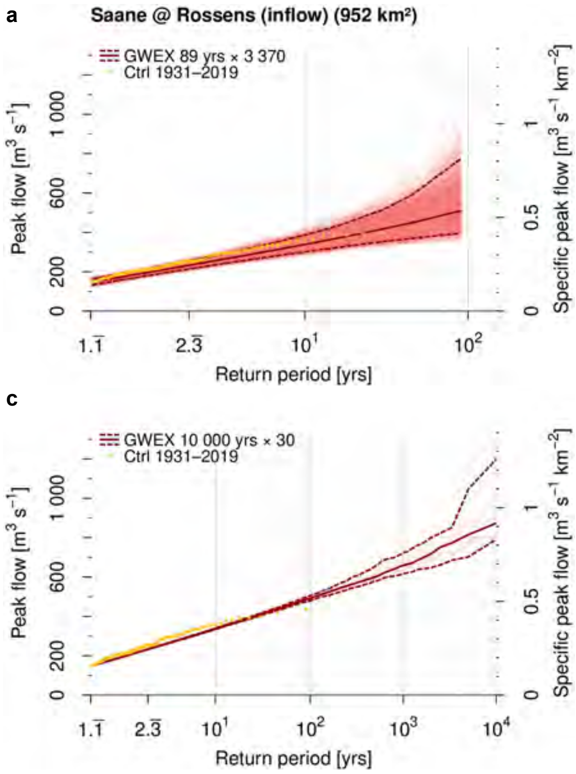

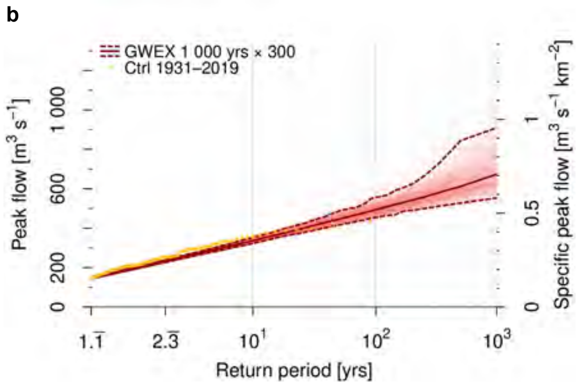

Figure 6.5: GWEX-based flood estimates for Rossens, with simulations subdivided into blocks as follows: panel a, blocks similar in length to the annual peak flow record; panel b, 300 blocks of 1 000 years; panel c, 30 blocks of 10 000 years. Note that the catchment area of this site (952 km^2) and transitions below the scope of the methods for large catchments employed in this study. Results are provided for informational purposes only. For interpretation and important background information see Chapter 10.

Such events, with more convective than synoptic characteristics, were not the main focus of the weather generators employed here (see Sections 3.1.1 and 10.2). Also, no inflow observations are available for comparison. The results shown in Figure 6.5 are therefore for informational purposes and should not be considered fully reliable for flood estimation. This is also the case for the EXAR results at Rossens (Kauzlaric et al., 2021b; Staudinger et al., 2021; Staudinger and Viviroli, 2020), which differ from those reported here for the reasons outlined in Chapter 8. As a detail, EXAR reported outflows of Rossens, whereas inflows are reported here.

Note that the EXCH module on small catchments will also provide results for Rossens, although in that module the site will be close to the upper scale limit. Varying results are expected between the small catchments and the large catchments modules of EXCH, as it is not feasible to seamlessly process all considered scales using exactly the same set of methods.

6.2.5. Maigrauge / Saane at Fribourg

The next dam in the Saane River cascade, Maigrauge, is located approximately 21 km downstream of Rossens. It has a direct tributary catchment of 1 264 km^2 – thus within scope of EXCH methods for large catchments –, and its impact on AMFs can be considered comparatively small due to the limited storage volume of 0.65 Mio. m^3. Therefore, the discharge observations at Fribourg, located just over 2 km downstream of the dam, can be used for comparison. High agreement is noted between observations, control simulation and long continuous simulation (Figure 6.6).

6.2.6. Saane at Laupen

The most downstream output site on the Saane River is Laupen, with a catchment area of 1 862 km^2. Laupen is located downstream of the three hydropower dams Rossens (see Section 6.2.4), Maigrauge (see Section 6.2.5) and Schiffenen, and the corresponding artificial lakes Gruyère, Pérolles and Schiffenen, all of which are implemented in the simulations via routing in RS Minerve. Immediately upstream of Laupen, the Sense River joins the main flow.

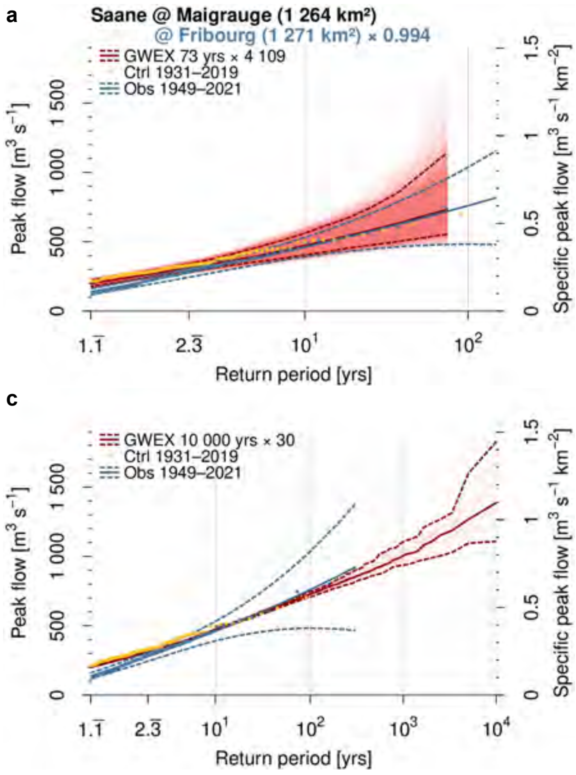

Figure 6.6: GWEX-based flood estimates for Maigrauge, with simulations subdivided into blocks as follows: panel a, blocks similar in length to the annual peak flow record; panel b, 300 blocks of 1 000 years; panel c, 30 blocks of 10 000 years. For interpretation and important background information see Chapter 10.

Good agreement is noted between control simulation and observations (Figure 6.7). In particular, the range of approximately 10 to 60 years recurrence interval is almost identical, whereas the control simulation provides slightly higher AMFs in comparison to observations for more frequent floods. The long continuous simulations with GWEX input in turn show similar behaviour to the control simulation, with a rather steady rise in the exceedance curve beyond return periods of a few hundred years.

6.2.7. Aare at Aarberg

Following the main flow of the Aare River, the Aarberg run-of-river weir is the next output site downstream, with a catchment area of 5 095 km^2. Control simulation and GWEX simulation exhibit very similar behaviour, with no marked change in the slope of the exceedance curve (Figure 6.8). A scenario that would re-activate the old course of the Aare River through a levee breach is not implemented, as per the methods defined for EXCH (see Section 3.4), even though water can overflow the banks and reach the Old Aare River in case of extreme floods. This can also impact floods downstream of Lake Biel (see Section 6.2.11).

No observations are available for comparison, and the gauge at Hagneck (Section 6.2.8 below), even though located nearby, is unsuitable for comparison due to bank overflow occurring en route.

6.2.8. Aare at Hagneck

The site Hagneck (catchment area: 5 112 km^2) is located approximately 7.5 km downstream of the Aarberg run-of-river weir (Section 6.2.7 above), and a few hundred meters upstream of the Hagneck run-of-river weir, just before the Aare River joins Lake Biel.

The control simulation yields slightly higher AMFs compared to observations, especially in the 5- to 10-year return period range (Figure 6.9). However, this discrepancy must be viewed in context of the comparatively short AMF observations, which here span 38 years only, as well as the influence of the flood relief tunnel in Thun and changes in regulation of lakes Thun and Brienz (see Section 6.2.2). Additionally, the highest observed AMF is in the same order of magnitude as the highest AMF from the control simulation.

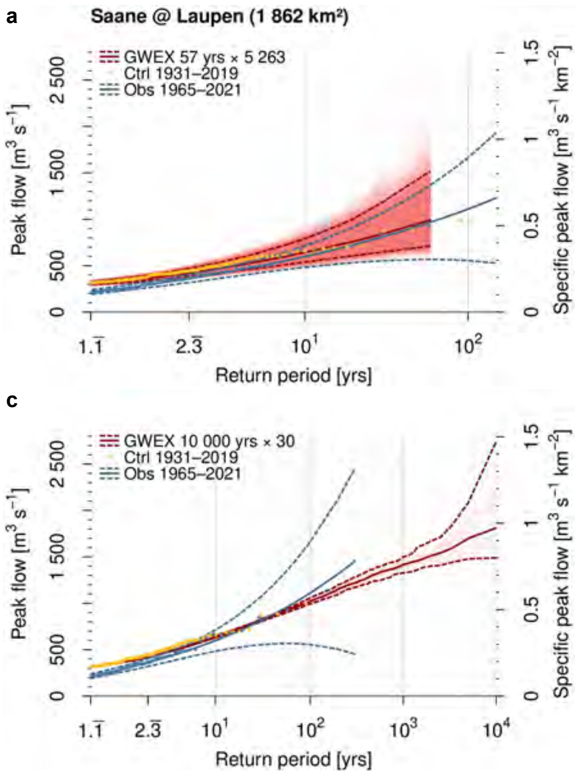

Figure 6.7: GWEX-based flood estimates for Saane at Laupen, with simulations subdivided into blocks as follows: panel a, blocks similar in length to the annual peak flow record; panel b, 300 blocks of 1 000 years; panel c, 30 blocks of 10 000 years. For interpretation and important background information see Chapter 10.

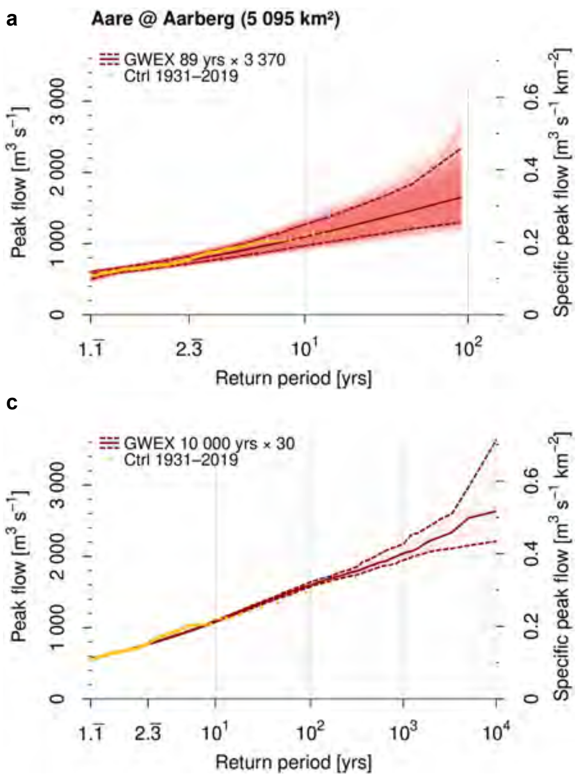

Figure 6.8: GWEX-based flood estimates for Aarberg, with simulations subdivided into blocks as follows: panel a, blocks similar in length to the annual peak flow record; panel b, 300 blocks of 1 000 years; panel c, 30 blocks of 10 000 years. For interpretation and important background information see Chapter 10.

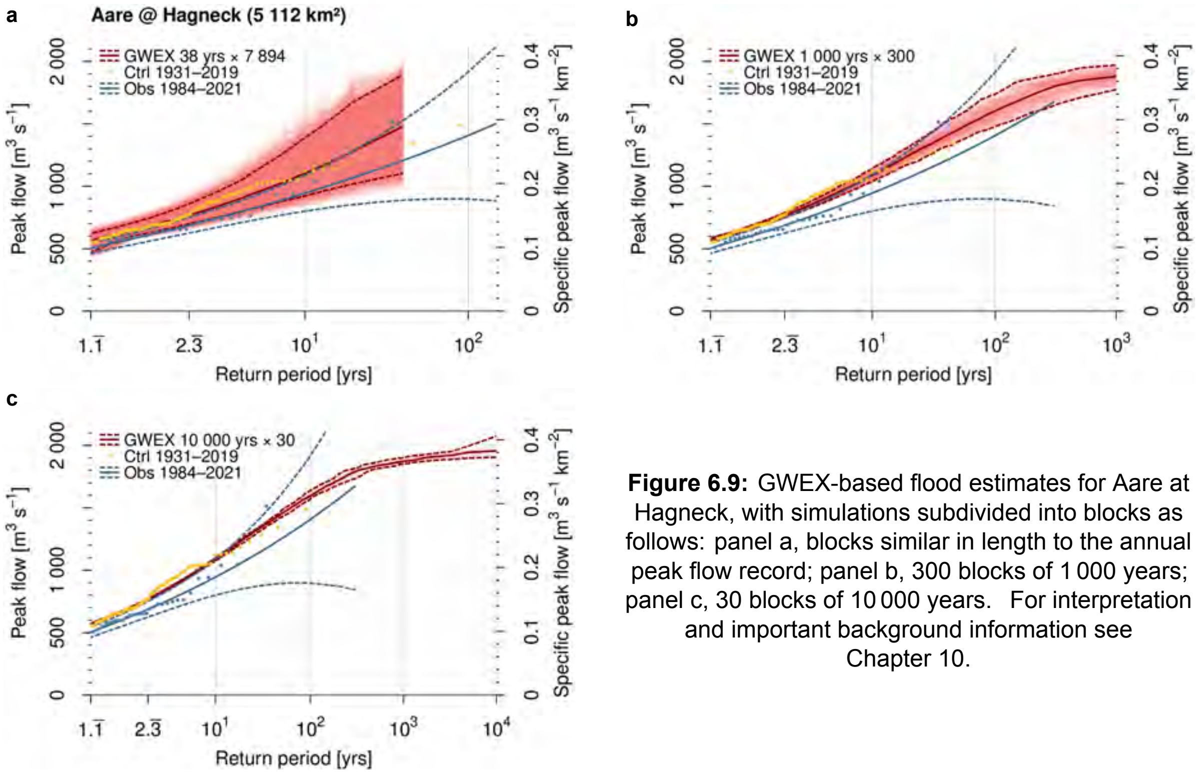

Figure 6.9: GWEX-based flood estimates for Aare at Hagneck, with simulations subdivided into blocks as follows: panel a, blocks similar in length to the annual peak flow record; panel b, 300 blocks of 1 000 years; panel c, 30 blocks of 10 000 years. For interpretation and important background information see Chapter 10.

The long continuous simulations with GWEX are very similar to the control simulation, but again noticeably higher than the observations. A distinct and sustained flattening of the flood exceedance curve is clearly visible in the GWEX-based AMFs around a discharge of 1 800 $m^3\,s^{-1}$. Starting at approximately this discharge, the Aare River begins to overflow its banks a few kilometres upstream of Hagneck, inundating the surrounding area. The result is massive retention that persists for return periods exceeding 100 000 years. This effect is absent in the observations, as the largest recorded flood only reached 1 514 $m^3\,s^{-1}$ on 23 August 2005, but it is evident in the long continuous simulations, as bank overflow and retention are implemented in the hydrological routing through RS Minerve. Simulations with SCAMP (not shown) agree better with observations at this site up to a return period of approximately 20 years, and largely follow the extrapolation of observed data. However, the SCAMP simulations show lower AMFs in comparison to the control simulation.

6.2.9. Aare at Brügg, Aegerten

Brügg (catchment area: 8 249 km^2) is located downstream of the regulated Lake Biel, just over two kilometres downstream of the weir at Port. The site is heavily influenced by the complex interplay of the three Jura lakes that was analysed extensively in EXAR (Kauzlaric et al., 2020; Pfäffli et al., 2020). Moreover, the “Murgenthal condition” must be considered, aiming to limit discharge in the Aare River downstream at Murgenthal (10 059 km^2) to 850 $m^3\,s^{-1}$. This requires accounting for inflows from additional tributaries, including the Emme River. For EXCH, the implementation of the regulation scheme at Port was further optimised, successfully eliminating most oscillations in simulated river stages and discharges that were noted in some scenarios of EXAR.

Observations, control simulation and long continuous simulation show quite similar AMFs and overall agree well (Figure 6.10). The rise of the exceedance curve around 400 years recurrence interval and the subsequent levelling off around 2 000 years recurrence interval are caused by the dynamics of lake retention and widespread inundations.

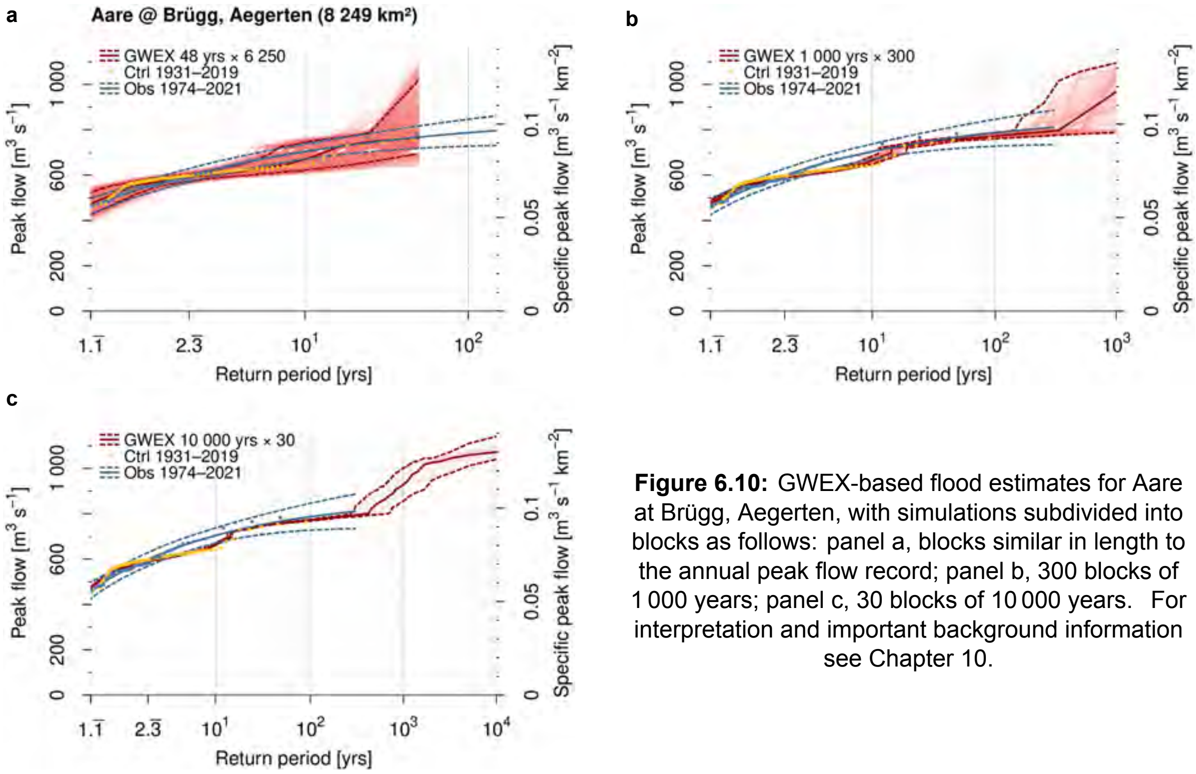

Figure 6.10: GWEX-based flood estimates for Aare at Brügg, Aegerten, with simulations subdivided into blocks as follows: panel a, blocks similar in length to the annual peak flow record; panel b, 300 blocks of 1 000 years; panel c, 30 blocks of 10 000 years. For interpretation and important background information see Chapter 10.

6.2.10. Emme at Wiler, Limpachmündung

An important tributary joining the Aare River downstream of Brügg is the Emme River. At Wiler, approximately 7.5 km upstream of its confluence, its catchment covers an area of 937 km^2 and transitions – similar to Rossens (Section 6.2.4) – below the spatial scope of the EXCH weather generator approaches for large catchments. These approaches were designed for catchments of more than approximately 1 000 km^2, focusing on the longer-duration precipitation events relevant there, rather than for smaller catchments, where limitations are particularly expected in pre-alpine and alpine regions (see Sections 3.1.1 and 10.2). It is therefore not surprising that floods at Wiler are underestimated in comparison to observations (Figure 6.11). The extent of the discrepancy is, however, exceptional, with simulated return levels between 37 % (HQ_{300}) and 45 % (HQ_{10}) lower in comparison to those derived from the observations. The underestimation remains marked when the high representative parameter set (see Section 3.3) is used. It is furthermore striking that the differences were considerably smaller in EXAR, where simulated return levels were only between 3 % (HQ_{300}) and 9 % (HQ_{10}) lower (see also juxtaposition of EXAR and EXCH return levels in Chapter 8.1).

Before examining the reasons for the discrepancies between EXAR and EXCH values, it should be emphasized that the Emme River constitutes a very challenging basin for flood hydrological simulations. Floods can result from very short summer convective storms (e.g., in 1997), short and intense precipitation events (e.g., 2006), or longer-lasting continuous rainfall (e.g., 2005). Depending on the precipitation characteristics, the resulting flood hydrographs may reach high levels over a short period (less than half a day, with very steep rise and sharp peak) or persist longer (up to one to two days, still with a steep rise but slightly more elongated, or remaining at high levels before a rapid recession). Especially during convective events, the flood waves can steepen as they travel through the upper catchment and carry notable quantities of debris and driftwood – the so-called “Anschutz” characteristic of some pre-alpine catchments, including the Emme, Kleine Emme and Lütschine rivers – , as observed during the 2014 flood. Additional factors that promote sharp floods include the steep slopes, poorly permeable subsoil, and a dense river network in the upper basin. For details, we refer to Reist et al. (2002), Bezzola and Ruf (2009), Weingartner et al. (2017) and Amt für Umwelt, Kanton Solothurn (2022). The combination of these characteristics results in the highest specific flood discharges on the northern side of the Alps and makes accurate simulation of floods particularly challenging.

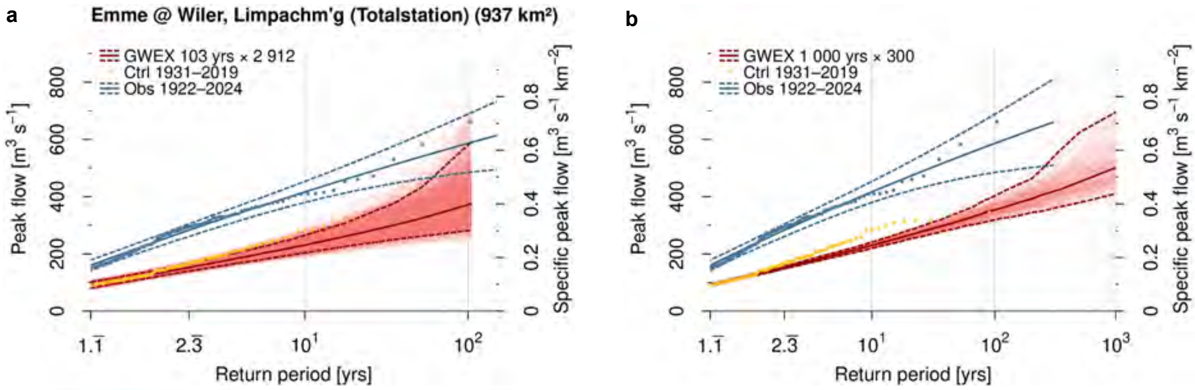

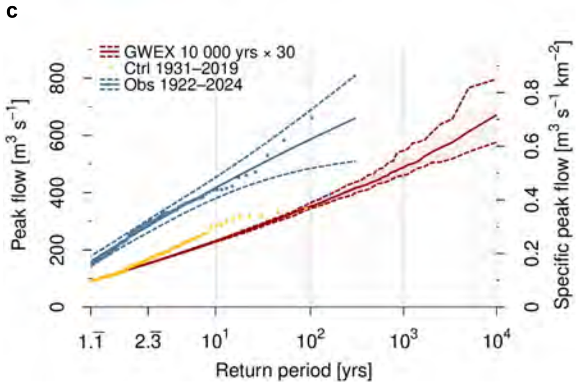

Figure 6.11: GWEX-based flood estimates for Emme at Wiler, with simulations subdivided into blocks as follows: panel a, blocks similar in length to the annual peak flow record; panel b, 300 blocks of 1 000 years; panel c, 30 blocks of 10 000 years. Note that the catchment area of this site (937 km^2) transitions below the scope of the methods for large catchments employed in this study. Results are provided for informational purposes only. For interpretation and important background information see Chapter 10.

In the context of the present CS framework, the complexities of bank overflow and retention in the lower reaches of the Emme River basin require handling the simulations with several sub-catchments and incorporating the specific hydraulic effects regarding floods into the hydrological routing of the corresponding simulations (i.e., with RS Minerve, see Section 3.4). Hence, the Emme River basin was subdivided into the gauged sub-catchments Emme at Burgdorf (673 km^2), Urtenen at Kernenried (74 km^2) and Luterbach at Oberburg (34 km^2), as well as a remaining area downstream of these sub-catchments. Consequently, the parameters of the hydrological model HBV could not be calibrated for the comparatively long continuous time series at Wiler (available at hourly resolution from 1974 onwards) and instead had to be calibrated on the observations of the sub-catchments where available. In this set-up, the influence of the sub-catchment Emme at Burgdorf, which contributes 72 % of the total basin area, is particularly strong. At the same time, continuous discharge observations at Burgdorf cover only 12 years (1979–1990), of which 8 years (1983–1990) overlap with the calibration periods defined in this project (cf. Section 3.3), based on the availability of suitably detailed meteorological forcing. No major floods occurred in this period in the sub-basin down to Burgdorf, with the largest observed AMF (recorded on 10 August 1984 at 334 m^3 s^{-1}, or 496 l s^{-1} km^{-2}) being only 44 % larger than the average AMF 1983–1990. In contrast, at Wiler, the largest observed AMF in the full series 1921–2024 (recorded on 8 August 2007 at 662 m^3 s^{-1}, or 707 l s^{-1} km^{-2}) exceeded the average by 138 %. Even though the philosophy of hydrological modelling underlying this project anticipates – and in general also successfully achieves – extrapolation well beyond flow maxima present in the calibration period, the combination of a short record and the absence of major floods therein is a limitation for parameter selection in this case. Further uncertainties of the gauge record and the rating curve must also be considered. For the rating curve alone, the 95 % uncertainty bound is 26 % at maximum flow and still 23 % for the flow exceeded 1 % of the time (Staudinger and Viviroli, 2020; Westerberg et al., 2020).

Beyond the aforementioned challenges, an important contribution to the differences arises from the improved objective function (OF) used for calibration in the present project. As a further development from EXAR, the OF used here places greater emphasis on simulating realistic hydrographs (see Section 3.3). The availability of such hydrographs is a key advantage of the CS approach and an important rationale for the EXCH project. Ensuring their realism is essential for further analyses (see, e.g., Staudinger et al.,

2021) and enhances the credibility of model behaviour under extreme conditions. Moreover, a strong emphasis on the highest peak flows was deliberately avoided in calibration due to the considerable uncertainties in the corresponding observations (Staudinger and Viviroli, 2020; Westerberg et al., 2020). Using the updated OF, the runoff hydrographs for the Emme River generally reproduce observed flow dynamics more realistically than in EXAR. However, under the specific boundary conditions of this river basin, this also led to a sizeable decrease in simulated AMFs.

Another difference between the modelling set-ups of EXAR and EXCH is that in EXAR, the intermediary catchment downstream of Burgdorf was represented as one single HBV sub-catchment with regionalised parameters, thereby including the Luterbach and Urtenen rivers. The hydrological routing downstream of Burgdorf, in contrast, is identical in both EXAR and EXCH. Finally, the GWEX weather generator was re-parametrized in EXCH using a different set of meteorological stations, resulting in some changes to the water balance of the Emme River basin (cf. Section 8.3).

Following these insights, the OF of EXAR was tentatively implemented in the current simulation framework to calibrate the gauged sub-catchments Emme at Burgdorf, Urtenen at Kernenried and Luterbach at Oberburg. This approach reduced the discrepancy for Emme at Wiler, with return levels derived from a 10 000-year test simulation ranging between 30 % (HQ_{300}) and 34 % (HQ_{10}) below those derived from observations. In consultation with FOEN and SFOE, however, this was deemed too small of an improvement to justify a re-simulation of the full 300 000 years at Wiler, which would include potentially strongly diminishing impacts further downstream while still requiring re-simulation of hydrological routing all the way down to Rhein at Basel. Further options for improvement could have included parameter regionalisation, rather than calibration, of the HBV model parameters for Emme at Burgdorf. This would in turn have required re-calibration of the respective donor catchments using the OF applied in EXAR. However, the potential for substantial improvement was considered small, and the degree of site-specific fine-tuning would have exceeded the scope of the present project.

In summary, EXCH results for the Emme River are presented and discussed here for transparency, but their use is not recommended. In cases where such results are of interest, simulations from EXAR (transfer point SSKSSD) could be used after careful consideration – keeping in mind that the corresponding hydrographs are less realistic, that the catchment transitions below the spatial scope of the weather generator approaches employed, and that the site was not within the primary focus of EXAR and therefore was not validated in detail.

Potential impacts of the underestimation for the Emme River on simulations for the Aare River further downstream can be assessed at three gauged EXCH output sites on the Aare: at Murgenthal / Ruppoldingen (not discussed in detail in this report), at Brugg / Wildegg-Brugg (Section 6.2.11), and at Untersiggenthal, Stilli / Beznau (Section 6.2.12). At Murgenthal and Untersiggenthal, the control simulations show slightly lower AMFs in comparison to observations, still falling within the confidence interval of the GEV distribution fitted to observed AMFs. At Brugg, the agreement between AMFs from control simulation and observations is high. For the long CS at all three sites, AMFs are somewhat lower for return periods up to 50 to 100 years. This should be considered also in the context of the slightly different behaviour of observations and long CS regarding the presence or absence of a tendency to level off (Section 6.2.11). In summary, both EXAR and EXCH results can be used for the Aare downstream of the Emme River confluence, depending on the objectives, and potentially also in combination. Further downstream impacts – after the confluences with the Reuss and Limmat rivers, and ultimately of the Aare with the Rhine River – can be considered small, as the areal contribution of the Emme River decreases substantially. Moreover, with increasing basin area, longer-duration flood events dominate the AMFs, during which the contribution of the Emme River becomes smaller – although superposition of its flood peaks with longer-lasting floods can still be potentially important.

6.2.11. Wildegg-Brugg / Aare at Brugg

Figure 6.12 shows exceedance curves for the SFOE output site Wildegg-Brugg (11 643 km^2), a run-of-river hydropower dam. The observed AMF values have been taken from the FOEN site Aare-Brugg (11 681 km^2) and were scaled proportionally to area, with a factor of 0.997. The simulated AMF values also refer to Wildegg-Brugg, whereas peak flows for Aare-Brugg can be inferred by scaling back proportionally to area, with a factor of 1.003 (see Table A.3). Since the difference in area is very small, the

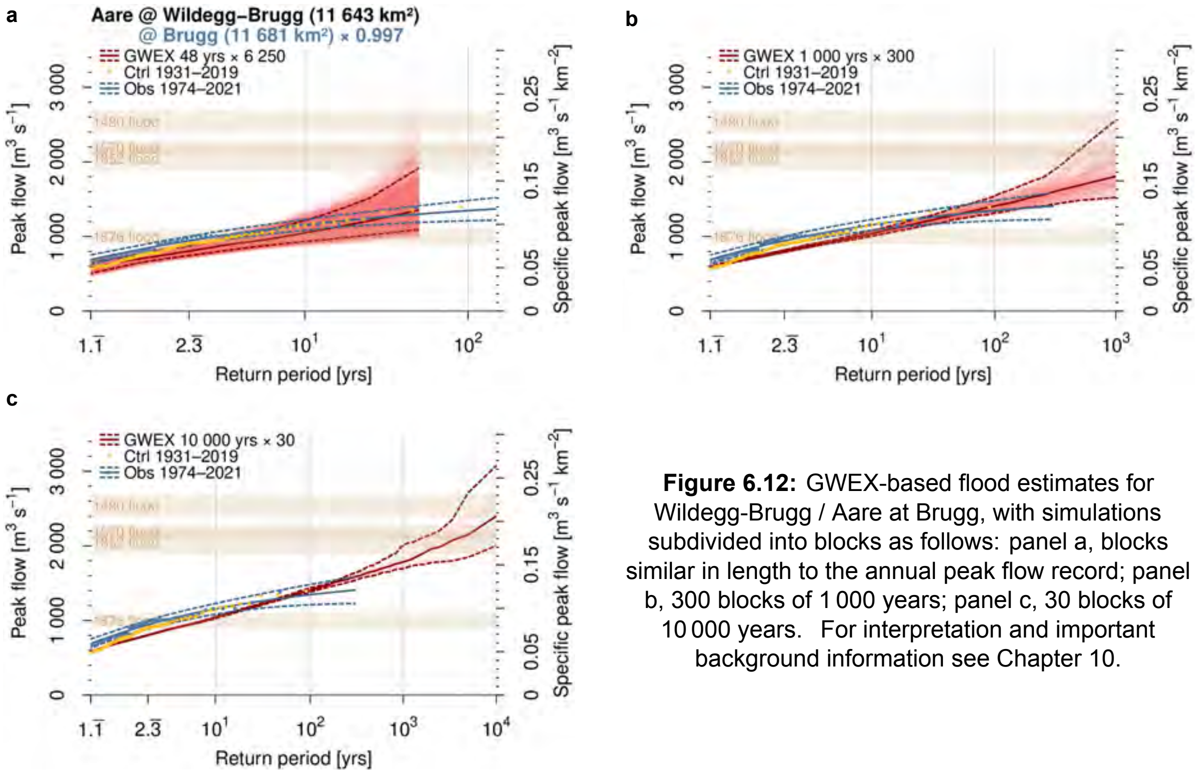

Figure 6.12: GWEX-based flood estimates for Wildegg-Brugg / Aare at Brugg, with simulations subdivided into blocks as follows: panel a, blocks similar in length to the annual peak flow record; panel b, 300 blocks of 1 000 years; panel c, 30 blocks of 10 000 years. For interpretation and important background information see Chapter 10.

specific peak flows shown in the secondary y axis can be considered valid for all data shown. As noted in the introduction to this chapter, using AMF observations before 1974 is not advisable because the second Jura water correction (1962–1973) changed the flood behaviour of the Aare River downstream of Lake Biel.

The control simulation results show good to very good agreement with observed AMFs, despite the fact that the observational period used (1974–2021) excludes over three decades covered by the control simulation (1931–2019). Consequently, the two datasets represent different samples of flood-rich and flood-poor periods (Brönnimann et al., 2022; Schmocker-Fackel and Naef, 2010a,b). The long continuous simulations using GWEX weather generator input display a relatively steady increase of AMFs in the exceedance curve. The simulated values are slightly lower than the observed values for return periods up to 20 years, and they do not exhibit the levelling off apparent in the observational data. The differences are no reason for dismissing the simulations: The weather generator explores a broad range of possible yet unobserved combinations of antecedent conditions and triggering precipitation events. This approach provides more comprehensive insights into hydrological and hydraulic behaviour beyond observed patterns, particularly in the context of a complex lake regulation system.

This site is also the only one in EXCH where estimates for historical floods conducted in EXAR (Baer and Schwab, 2020; Wetter, 2015) can be compared. As noted in Section 2.2, however, the insights possible from this comparison are very limited due to fundamental changes to the river network through major river corrections. What can be stated is that EXCH simulations contain scenarios that exceed all known historical values from the past approximately 540 years.

In this context, it should be noted that water from the Aare River can overflow into the Old Aare River at Aarberg in the simulations (see Section 6.2.7) and thus bypass the Jura lakes, even though a levee breach is not implemented into the model. Such an overflow is not captured in the observations, which partly explains why simulations show higher values for rare floods on the Aare River downstream of Lake Biel than would be expected from a straightforward extrapolation of flow observations.

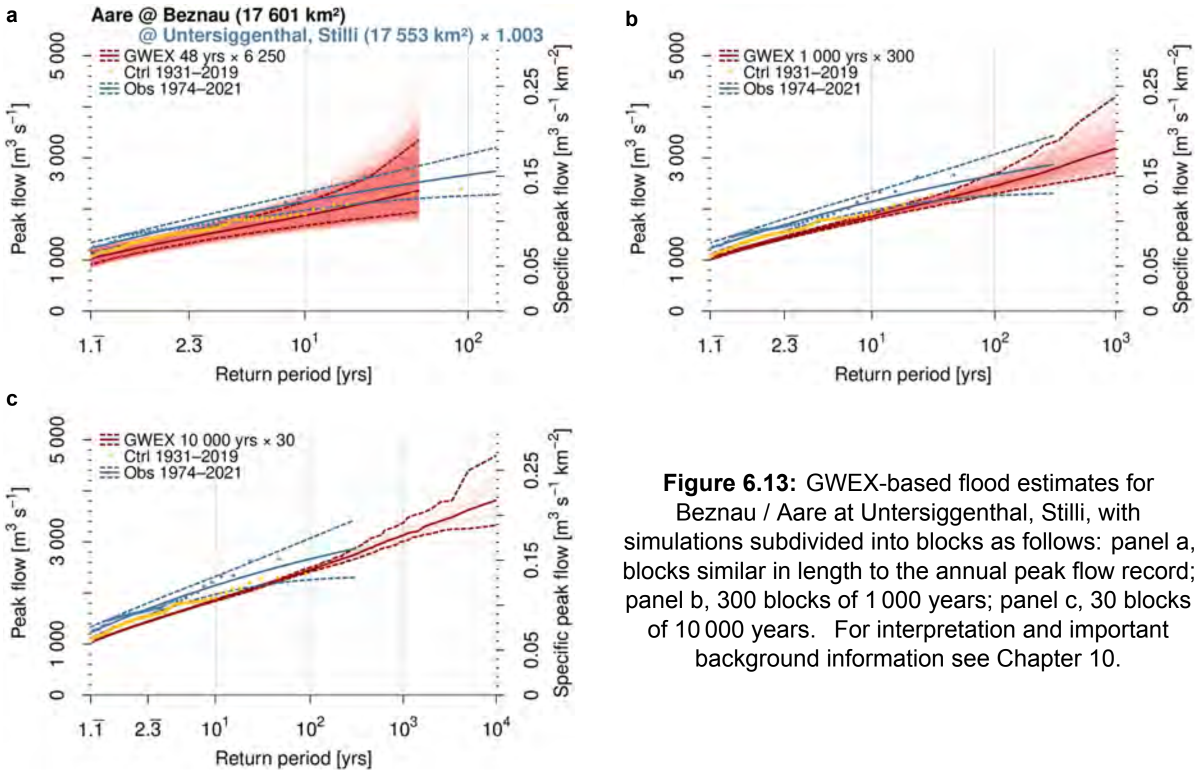

Figure 6.13: GWEX-based flood estimates for Beznau / Aare at Untersiggenthal, Stilli, with simulations subdivided into blocks as follows: panel a, blocks similar in length to the annual peak flow record; panel b, 300 blocks of 1 000 years; panel c, 30 blocks of 10 000 years. For interpretation and important background information see Chapter 10.

6.2.12. Beznau / Aare at Untersiggenthal, Stilli

Figure 6.13 shows exceedance curves for the SFOE output site Beznau (17 601 km^2), with observed AMF values from the FOEN site Untersiggenthal, Stilli scaled proportionally to area. Results from Beznau can be scaled back to FOEN Untersiggenthal, Stilli (17 553 km^2) by applying a factor of 0.997 (see Table A.3). As was the case for the Aare at Brugg / Wildegg-Brugg (Section 6.2.11), observations before 1974 are not used due to the discontinuity caused by the Jura water correction. The overall interpretation of simulation results also aligns with that of Brugg / Wildegg-Brugg. The main difference is that the control simulation here shows AMF values slightly lower than the observed ones, although they still lie within the confidence interval of the observation-based flood statistics. Also here, it has to be noted for context that the observations (1974–2021) used here contain a shorter sample than the control simulation (1931–2019) and span a different composition of flood-rich and flood-poor periods. Omitting the control simulation years before 1974 leads to an even better agreement.

6.3. Reuss River basin

6.3.1. Reuss at Luzern, Geissmattbrücke

For the Reuss River at the outflow of Lake Lucerne (2 254 km^2), observations, control simulation and continuous simulation show good agreement (Figure 6.14). It should be noted that new rules for the regulation of Lake Lucerne have been effective since 2007, and that the weir complex used to regulate lake outflow (including the needle dam) was rebuilt from 2008 to 2011. The simulations adhere to the current situation, while the observations before 2007 were recorded under slightly different conditions.

6.3.2. Reuss at Mühlau, Hünenberg

The Reuss River at Mühlau (2 902 km^2) shows a systematic underestimation (Figure 6.15), primarily due to the systematic underestimation of short, intense flood peaks in the Kleine Emme River at Emmen. The Kleine Emme joins the Reuss downstream of Lake Lucerne, which is simulated accurately (see Section 6.3.1) and attenuates its outflows due to marked lake retention. The pre-alpine Kleine

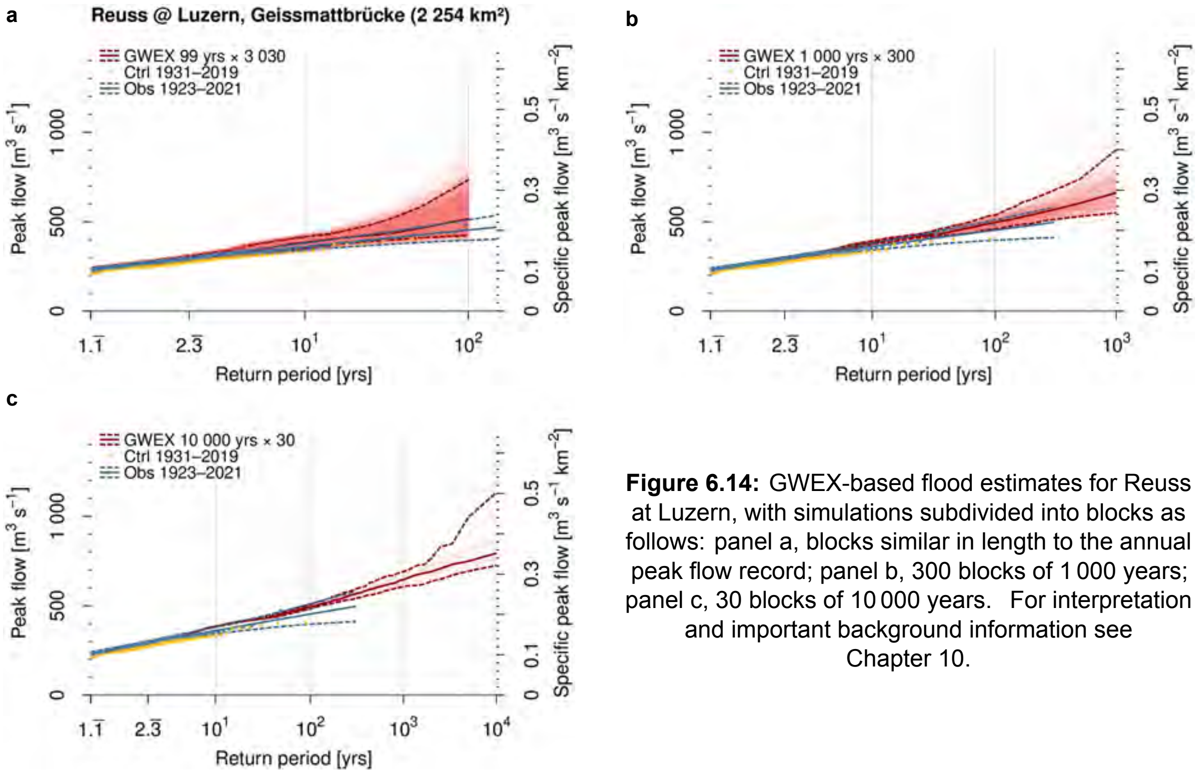

Figure 6.14: GWEX-based flood estimates for Reuss at Luzern, with simulations subdivided into blocks as follows: panel a, blocks similar in length to the annual peak flow record; panel b, 300 blocks of 1 000 years; panel c, 30 blocks of 10 000 years. For interpretation and important background information see Chapter 10.

Emme is the largest tributary to the Reuss downstream of Lake Lucerne, contributing about 74 % of the unregulated catchment area downstream of Lake Lucerne. Its flood peaks are underestimated in this project module due to its comparatively small catchment area, which with 478 km^2 clearly falls outside the target scale of the weather generators designed for large catchments. A solution could involve using results from simulations with the high representative HBV parameter set (Figure 6.16) that yields a stronger response in simulated peak flows (see Section 3.3). These align more closely with observations, although some underestimation persists.

6.3.3. Reuss at Mellingen

As already at Mühlau (see Section 6.3.2), simulation results at Mellingen (3 386 km^2) show noticeable underestimation (Figure 6.17) due to the strong influence of the Kleine Emme River, which is not adequately depicted by the weather generator for large catchments. In addition, the Lorze River, which enters the Reuss River a bit more than 3 km downstream of Mühlau, is regulated at the outlet of Lake Zug and thus also contributes attenuated flood peaks only. The Lorze River makes up 23 % of the catchment area of the Reuss River at Mellingen, whereas the Kleine Emme River still contributes 42 % of the unregulated catchment area. The same applies to the output node at Bremgarten (not shown), located approximately 15 km upstream of Mellingen, with a catchment area only 1.7 % smaller.

The exceedance curve flattens for peak discharges of more than approximately 850 $m^3\,s^{-1}$, caused by bank overflow and inundations (Figure 6.17c). The resulting flowing and standing retention effects are represented in the simulation chain, with RS Minerve emulating the behaviour found in more detailed 2D hydraulic simulations (see Section 3.4).

Like in the case of Mühlau, results of the simulations with the high representative HBV parameter set agree better with observations (Figure 6.18), albeit again with slight underestimation remaining.

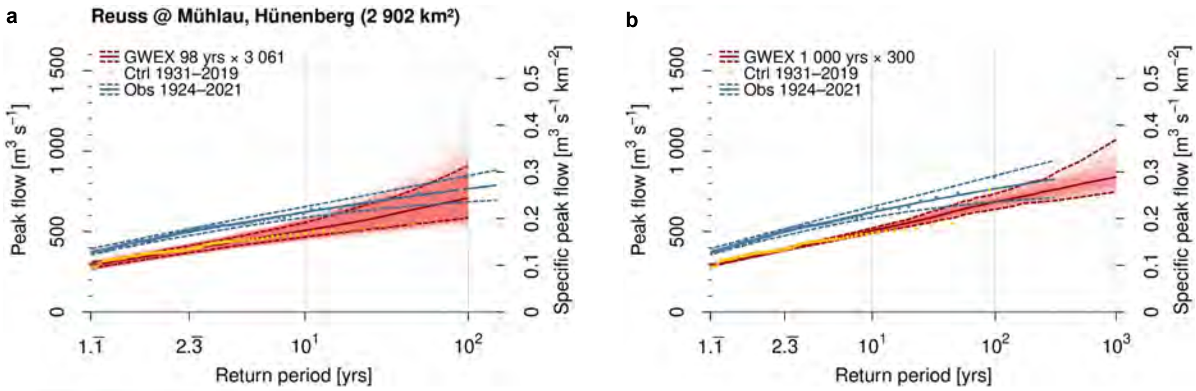

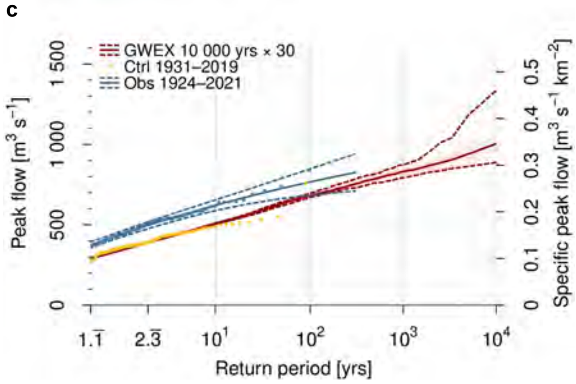

Figure 6.15: GWEX-based flood estimates for Reuss at Mühlau, Hünenberg, with simulations subdivided into blocks as follows: panel a, blocks similar in length to the annual peak flow record; panel b, 300 blocks of 1 000 years; panel c, 30 blocks of 10 000 years. For interpretation and important background information see Chapter 10.

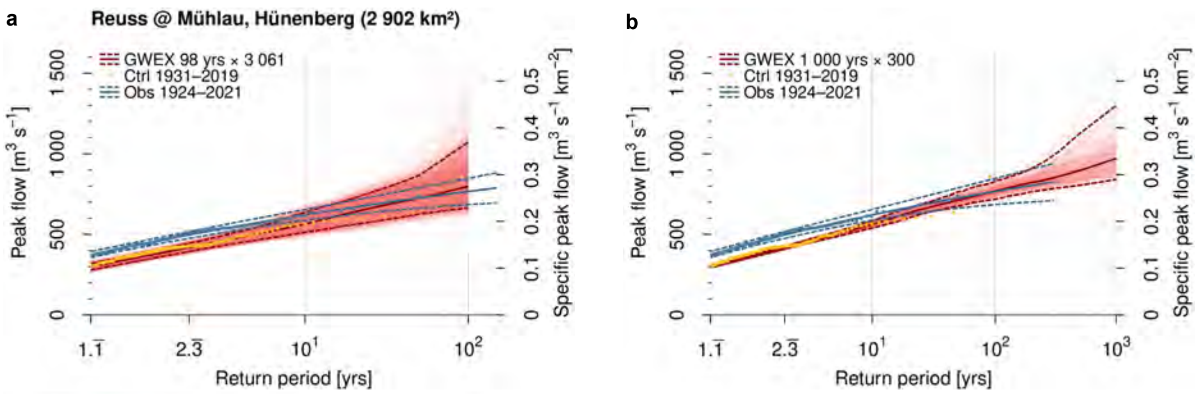

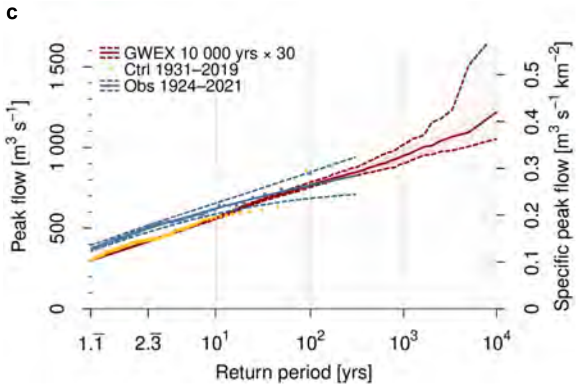

Figure 6.16: GWEX-based flood estimates for Reuss at Mühlau, Hünenberg, showing the results of the high representative parameter set, with simulations subdivided into blocks as follows: panel a, blocks similar in length to the annual peak flow record; panel b, 300 blocks of 1 000 years; panel c, 30 blocks of 10 000 years. For interpretation and important background information see Chapter 10.

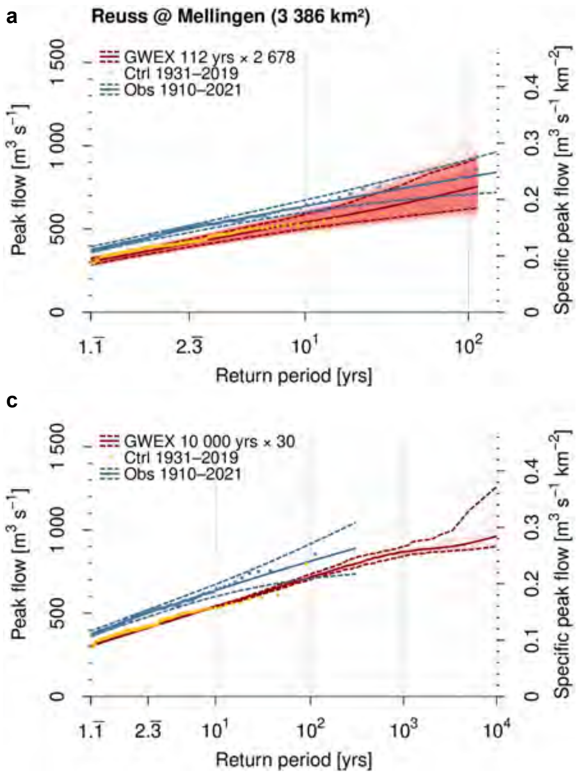

Figure 6.17: GWEX-based flood estimates for Reuss at Mellingen, with simulations subdivided into blocks as follows: panel a, blocks similar in length to the annual peak flow record; panel b, 300 blocks of 1 000 years; panel c, 30 blocks of 10 000 years. For interpretation and important background information see Chapter 10.

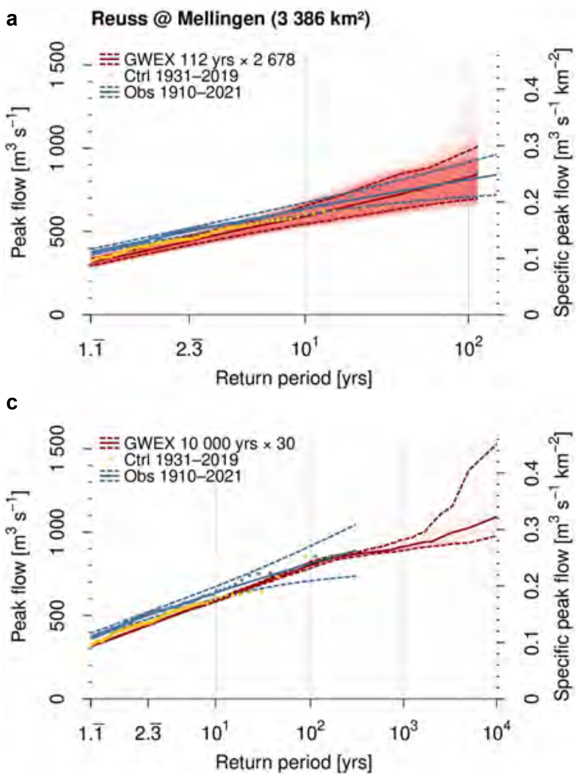

Figure 6.18: GWEX-based flood estimates for Reuss at Mellingen, showing the results of the high representative parameter set, with simulations subdivided into blocks as follows: panel a, blocks similar in length to the annual peak flow record; panel b, 300 blocks of 1 000 years; panel c, 30 blocks of 10 000 years. For interpretation and important background information see Chapter 10.

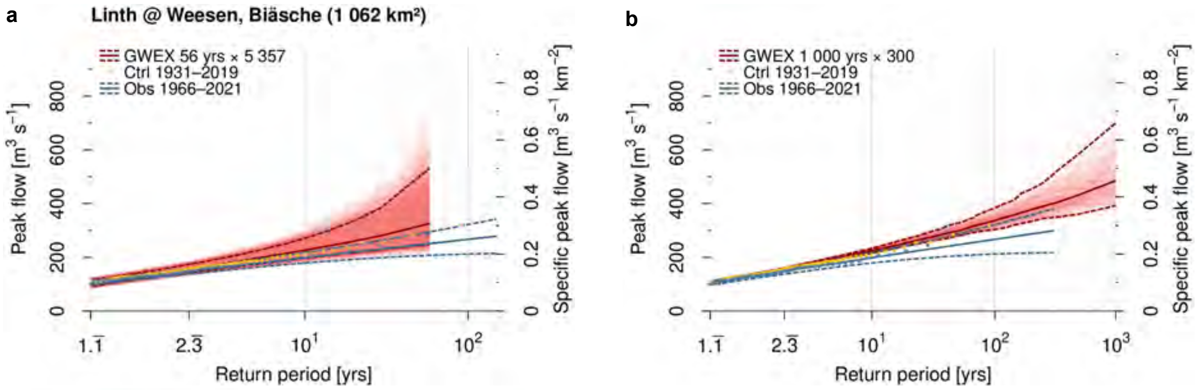

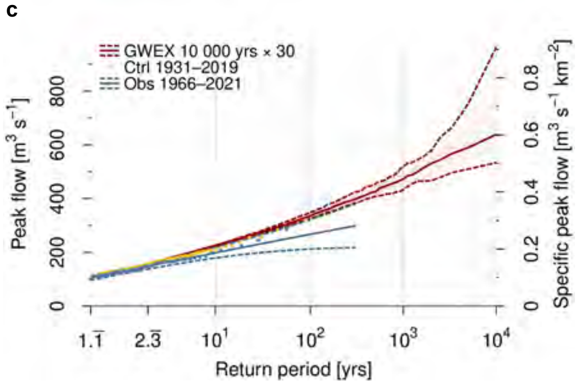

Figure 6.19: GWEX-based flood estimates for Linth at Weesen, Biäsche, with simulations subdivided into blocks as follows: panel a, blocks similar in length to the annual peak flow record; panel b, 300 blocks of 1 000 years; panel c, 30 blocks of 10 000 years. For interpretation and important background information see Chapter 10.

6.4. Limmat River basin

6.4.1. Linth at Weesen, Biäsche

The Linth River at Weesen (1 062 km^2), downstream of the unregulated Lake Walensee, shows good agreement of control simulation and observations, with simulated AMF values slightly higher than observed ones but still located around the upper confidence interval of extrapolated observations (Figure 6.19). The long continuous simulations show an exceedance curve similar to that of the control simulation, again slightly higher and just above the upper confidence interval of extrapolated observations. Despite the comparatively small area of the catchment (1 062 km^2), underestimation of AMFs is not an issue due to the retention of Lake Walensee that attenuates short floods arriving from the lake tributaries.

6.4.2. Limmat at Zürich, Unterhard

At Zürich (catchment area: 2 174 km^2), the Limmat River shows very good agreement between control simulation and observations (Figure 6.20), most likely again facilitated by lake retention, here through Lake Zürich. The long continuous simulations closely follow the lower confidence interval of observed flood statistics up to a recurrence period of approximately 20 years, after which they ascend somewhat more steeply. However, even at 300 years recurrence interval – the limit for which comparison is reasonable – they remain within the confidence interval of the extrapolated observations.

6.4.3. Wettingen / Limmat at Baden, Limmatpromenade

Also at Wettingen (catchment area: 2 376 km^2), agreement of observations, control simulation and long continuous simulation is high, and all three data sets show very similar exceedance curves (Figure 6.21). This consistency is partly due to the fact that the exceedance curve for observed AMFs does not show a tendency to level off, contrary to many other sites examined. This does not necessarily indicate different behaviour, but may be due to the randomness of the observed flood sample within the context of large internal variability (Zeder and Fischer, 2024) The Sihl River, which contributes approximately 63 % of the unregulated catchment downstream of Lake Zürich, does not appear to contribute flood

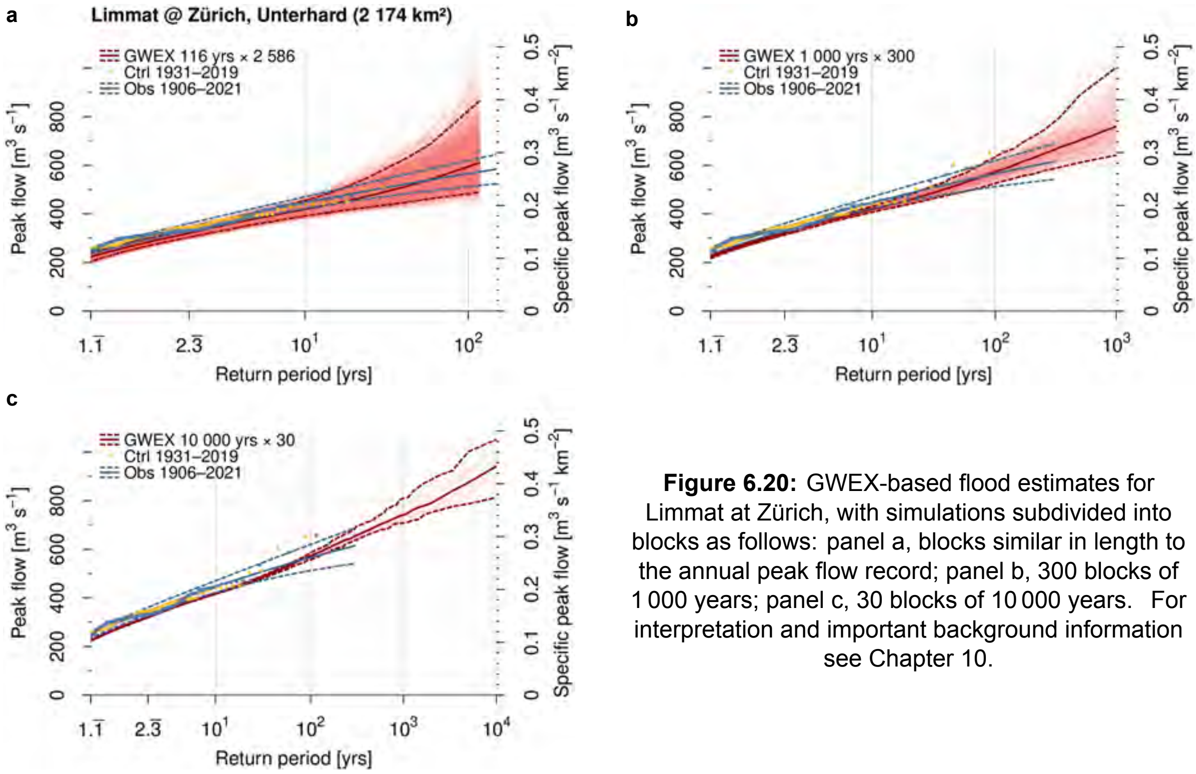

Figure 6.20: GWEX-based flood estimates for Limmat at Zürich, with simulations subdivided into blocks as follows: panel a, blocks similar in length to the annual peak flow record; panel b, 300 blocks of 1 000 years; panel c, 30 blocks of 10 000 years. For interpretation and important background information see Chapter 10.

peaks downstream of Lake Zürich that are problematic for the simulations. This is in contrast to the Reuss River downstream of Lake Lucerne, where the flashy behaviour of the Kleine Emme River – in combination with lake retention on the Reuss – led to an underestimation of AMFs (see Sections 6.3.2 and 6.3.3). One reason for the less problematic behaviour of the Sihl River might be that its headwater catchment is attenuated by Lake Sihlsee, which is regulated by a hydropower dam. This dam is implemented (in simplified form) in the modelling system via RS Minerve. The two unregulated tributaries to the Sihl River, rivers Alp and Biber, contribute only about 14 % of unregulated catchment area to the Limmat River between Zürich and Wettingen.

6.5. Rhine River basin

6.5.1. Hinterrhein at Fürstenau

The EXCH simulations for the Hinterrhein River at Fürstenau (1 577 km^2) generally show lower return levels compared to the observations (Figure 6.22). In this river basin, and also in the Vorderrhein River basin, two main challenges impact the accuracy of the simulations and the corresponding flood estimates. On the one hand, the precipitation gauge network is comparatively sparse and does not very well represent the range of elevations present. As a consequence, hydrological simulations frequently underestimate discharge, likely due to an underestimation of precipitation interpolated from the gauges. On the other hand, the observed discharges are strongly influenced by hydropower operations. As is typical for high alpine regions of Switzerland, this results in a pronounced levelling of the discharge regime and impacts on the flood regime (Margot et al., 1992; Steeb et al., 2024). These effects cannot be fully reproduced by the reservoir schemes implemented in RS Minerve (see Section 3.4), and this in turn affects model calibration. Since the exceedance curve of simulated AMFs (typically underestimated) bends noticeably upward, whereas that of observed AMFs bends very slightly downward (see Figure 6.22), the return levels for very rare simulated floods appear to align with an extrapolation of observations. However, a definitive judgment is difficult due to the large uncertainty in extrapolated discharge.

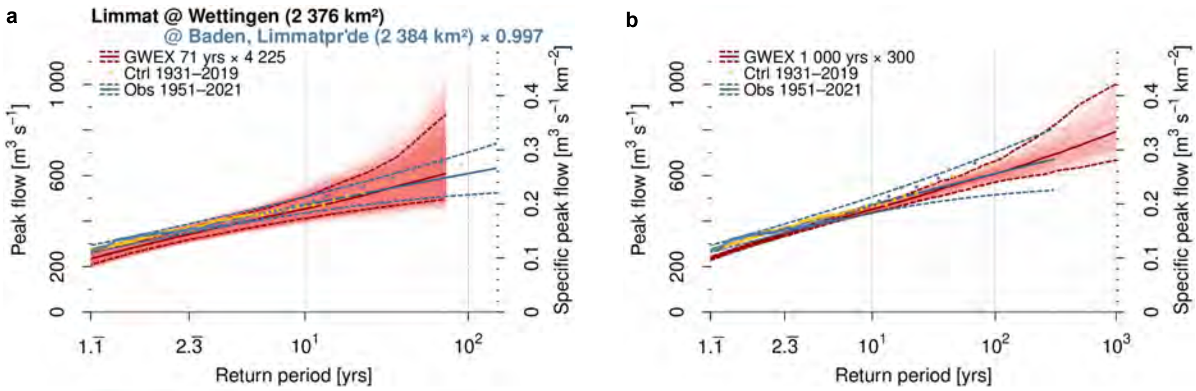

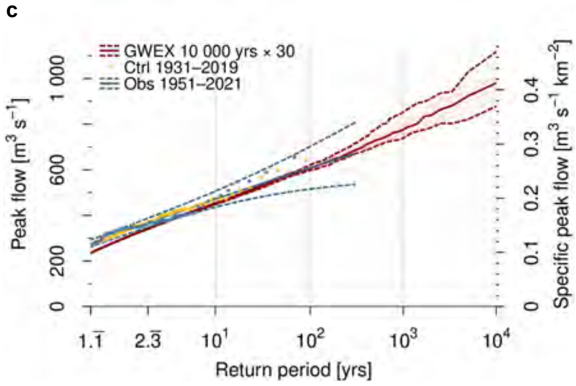

Figure 6.21: GWEX-based flood estimates for Wettingen / Limmat at Baden, Limmatpromenade, with simulations subdivided into blocks as follows: panel a, blocks similar in length to the annual peak flow record; panel b, 300 blocks of 1 000 years; panel c, 30 blocks of 10 000 years. For interpretation and important background information see Chapter 10.

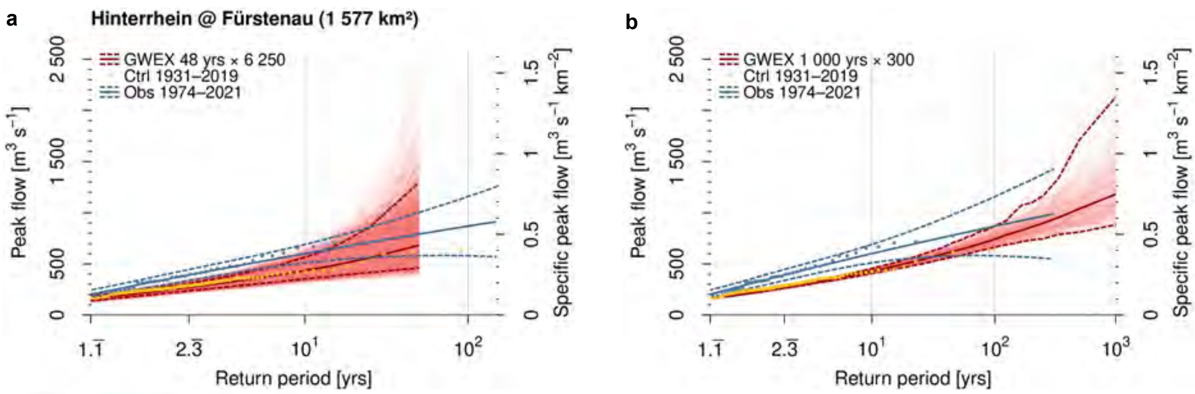

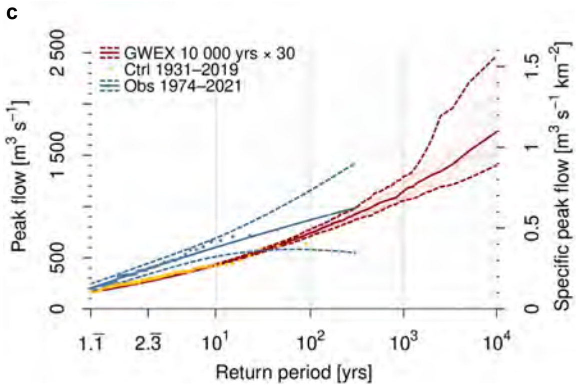

Figure 6.22: GWEX-based flood estimates for Hinterrhein at Fürstenau, with simulations subdivided into blocks as follows: panel a, blocks similar in length to the annual peak flow record; panel b, 300 blocks of 1 000 years; panel c, 30 blocks of 10 000 years. For interpretation and important background information see Chapter 10.

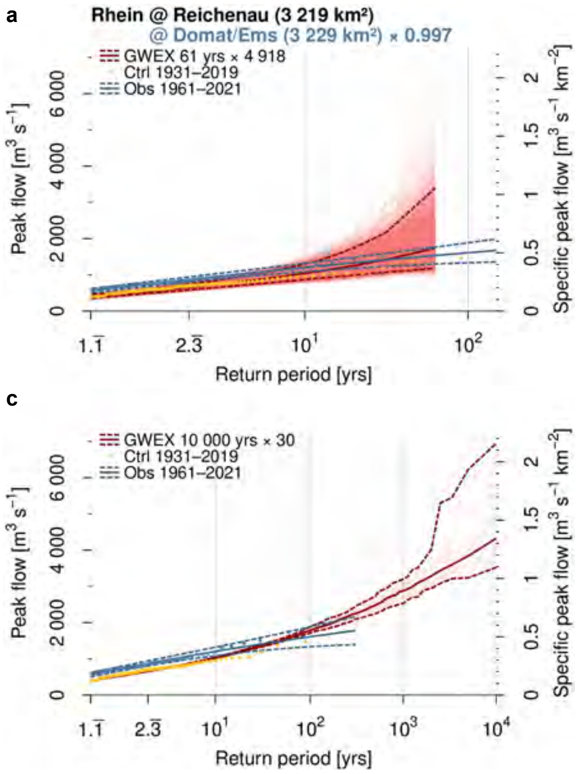

Figure 6.23: GWEX-based flood estimates for Reichenau / Rhein at Domat/Ems, with simulations subdivided into blocks as follows: panel a, blocks similar in length to the annual peak flow record; panel b, 300 blocks of 1 000 years; panel c, 30 blocks of 10 000 years. For interpretation and important background information see Chapter 10.

6.5.2. Reichenau / Rhein at Domat/Ems

At Reichenau (catchment area of 3 219 km^2), after the Hinterrhein and Vorderrhein rivers have joined, simulations can be compared to the gauge at Domat/Ems (3 229 km^2). For the reasons outlined for the Hinterrhein River at Fürstenau (Section 6.5.1 above), simulations show lower flood levels than observations, even though the underestimation is markedly less pronounced here (Figure 6.23).

6.5.3. Rhein at Diepoldsau, Rietbrücke

The site at Diepoldsau (6 299 km^2) is located approximately 15 km upstream of where the Rhine River flows into Lake Constance. Observations and simulations are relatively close to each other. The control simulation shows only slightly lower values than the observations, while the long CS with GWEX exhibits slightly better agreement with observations for return periods of 10 years and higher (Figure 6.24). Note that during the 1927 flood event, a dam failure occurred at Schaan, approximately 25 km upstream of Diepoldsau. As a result, the measured discharge peak of 2 300 m^3 s^{-1} is attenuated and thus underestimated. Combining observations and simulations, INGE Hydrologie Alpenrhein (2003) estimated a peak discharge without attenuation of 3 000 m^3 s^{-1}, agreeing very well with the GWEX-based flood estimate. With this value, the estimated 1927 discharge peak is the highest at Diepoldsau to date (see Figure 6.24). It is also noteworthy that there has also been no larger event since the end of the so-called “disaster gap” in Switzerland (Pfister, 2009), with 1987 reaching a peak of 2 661 m^3 s^{-1} and 2005 reaching a peak of 2 264 m^3 s^{-1}.

In the hydrological routing model, floodplain retention is accounted for in this region but primarily occurs downstream of Diepoldsau, resulting in no major effects being visible at this site. Note that the planned widening of the Alpine Rhine[2] will alter the hydraulic conditions around this site, leading to changes in the exceedance curve. The implementation of EXCH always reflects the current state (see Section 3.1.1).

[2] https://rhesi.org

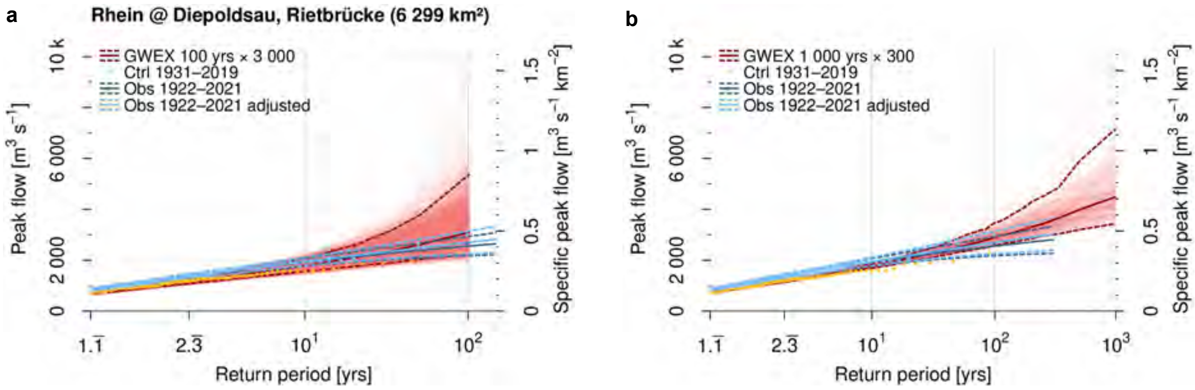

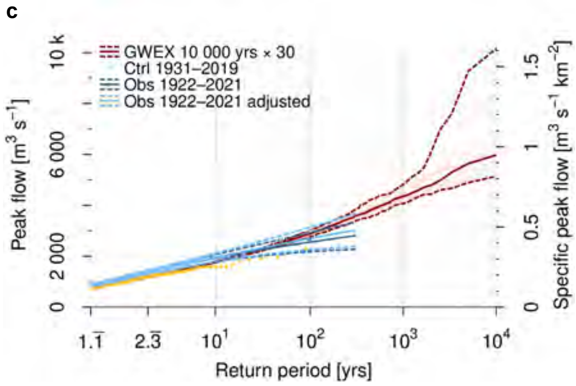

Figure 6.24: GWEX-based flood estimates for Rhein at Diepoldsau, with simulations subdivided into blocks as follows: panel a, blocks similar in length to the annual peak flow record; panel b, 300 blocks of 1 000 years; panel c, 30 blocks of 10 000 years. Observed AMFs with extrapolation and confidence intervals are here also shown in a version where the flood of 1927 was adjusted to the reconstructed value reported by INGE Hydrologie Alpenrhein (2003). For interpretation and important background information see Chapter 10.

6.5.4. Schaffhausen / Rhein at Neuhausen, Flurlingerbrücke

The run-of-river weir Schaffhausen (11 848 km^2) is located approximately 20 km downstream of where the Rhine River leaves Lake Constance. The gauging site Neuhausen, Flurlingerbrücke (11 930 km^2) is located another 1.5 km further downstream and well suited for comparison. The control simulation shows slightly higher return levels compared to those estimated from the observations, but overall, good agreement is noted (Figure 6.25). The long CS with GWEX in turn agrees well with the control simulation, even though values are increasingly higher than the observations for return periods approaching 100 years. The slope of the exceedance curve is comparatively slight due to the strong retention effect of unregulated Lake Constance.

6.5.5. Thur at Andelfingen

The Thur River is the largest tributary of the Rhine River between Lake Constance and its confluence with the Aare River. Near its outlet at Andelfingen, it has a catchment area of 1 702 km^2. The return levels of the control simulation are increasingly higher than those of the observations for return periods larger than 10 years (Figure 6.26). The disagreement is to a large part caused by the two highest simulated flood peaks in the control period. The long CS on the basis of GWEX displays very good agreement with the control simulation, with similar disagreement to observations.

In this context, it is important to note that dam breaks and inundations occurred several times before the main channel was modified until 1998 to accommodate a peak discharge of 1 400 m^3 s^{-1}. As a result, attenuation affected the recorded peak flow data. For example, the flood of 1978 was reconstructed to have a peak discharge of 1 285 m^3 s^{-1} without attenuation, instead of the observed 1 061 m^3 s^{-1}, and also the events of 1910, 1965 and 1977 would have had higher peaks without attenuation (Bundesamt für Umwelt (BAFU), 2021b; Scherrer et al., 2011). While attenuation is emulated by RS Minerve in the simulation chain based on more detailed 2D hydraulic simulations (see Section 3.4), the channel geometry used consistently reflects the current state, rather than the pre-modification state before the discharge capacity was increased. When this is considered in the comparison, the agreement between adjusted observations, control simulation and long CS is notably higher (Figure 6.26). Furthermore, the

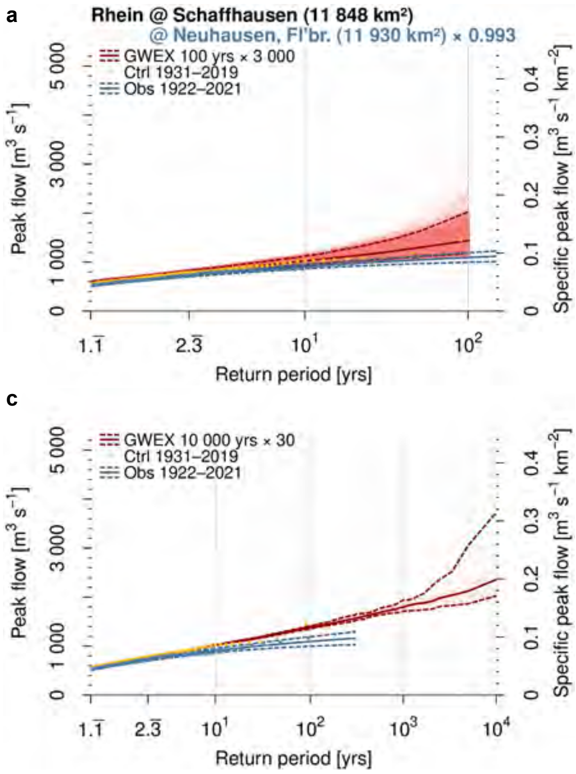

Figure 6.25: GWEX-based flood estimates for Schaffhausen / Rhein at Neuhausen, Flurlingerbrücke, with simulations subdivided into blocks as follows: panel a, blocks similar in length to the annual peak flow record; panel b, 300 blocks of 1 000 years; panel c, 30 blocks of 10 000 years. For interpretation and important background information see Chapter 10.

simulations agree well with the design discharges given in Hunziker, Zarn & Partner (2017), namely 1 200 $m^3 s^{-1}$ for HQ_{30}, 1 450 $m^3 s^{-1}$ for HQ_{100}, 1 700 $m^3 s^{-1}$ for HQ_{300} and 2 000 $m^3 s^{-1}$ for EHQ.

6.5.6. Rhein at Basel, Rheinhalle

Basel is the farthest downstream site on the Rhine River covered in EXCH and the largest catchment considered, with a catchment area of 35 878 km^2. Observations at Basel are exceptionally long-term, with daily gauge readings starting in 1808 (Wetter et al., 2011) and a limnigraph recording dating back to 1869 (Bundesamt für Umwelt (BAFU), 2017b). However, for statistical analyses, only records from 1891 onwards should be used, as the first Jura water correction (1868–1891) impacted flows even as far downstream as Basel (Bundesamt für Umwelt (BAFU), 2017b).

The agreement between the observations and the control simulation is very high (see Figure 6.27). Small discrepancies are noted for the return periods estimated for the five highest simulated events in the control period – potentially due to the considerably longer extent of observations –, while the magnitudes of these events show good agreement between observations and control simulation. Results from the long CS in turn align closely with the control simulation for the assessable return periods, and also correspond very well with observations for return periods of up to 10–20 years. For the return periods beyond the range assessable from observations, the AMFs from long CS show a steady increase with the Gumbel-scaled return period. As is the case for several other output sites, a levelling off such as noticeable in observations is not present. This is not a priori a reason to doubt the methods and results of EXCH, but rather represents an explainable difference between interpolation using hydrological records and interpolation using meteorological records.

It is noteworthy that while the simulated AMFs were generally lower than observed AMFs upstream of Lake Constance (see Sections 6.5.1, 6.5.2 and 6.5.3), this underestimation was offset by the retention effect of Lake Constance and the comparatively high simulated values for the Thur River. The latter, however, should be considered in context of attenuation affecting some recorded AMFs (see Section 6.5.5.

Several other studies have examined the flood behaviour of the Rhine River at Basel, also using reconstructed values of historical floods that occurred prior to the instrumental period. One of the main

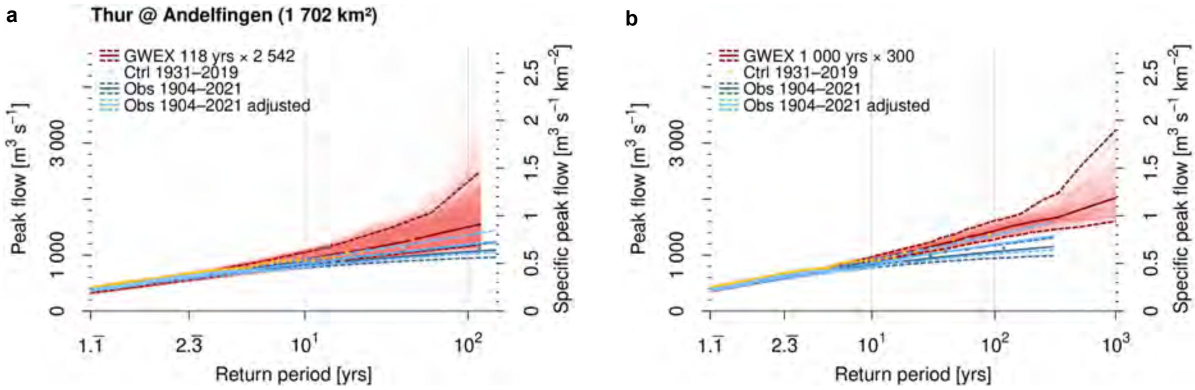

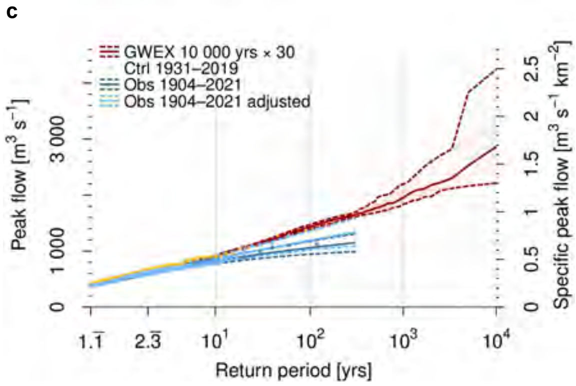

Figure 6.26: GWEX-based flood estimates for Thur at Andelfingen, with simulations subdivided into blocks as follows: panel a, blocks similar in length to the annual peak flow record; panel b, 300 blocks of 1 000 years; panel c, 30 blocks of 10 000 years. Observed AMFs with extrapolation and confidence intervals are here also shown in a version where the floods of 1910, 1965, 1977 and 1978 were adjusted to the reconstructed values reported in Kienzler and Scherrer (2018). For interpretation and important background information see Chapter 10.

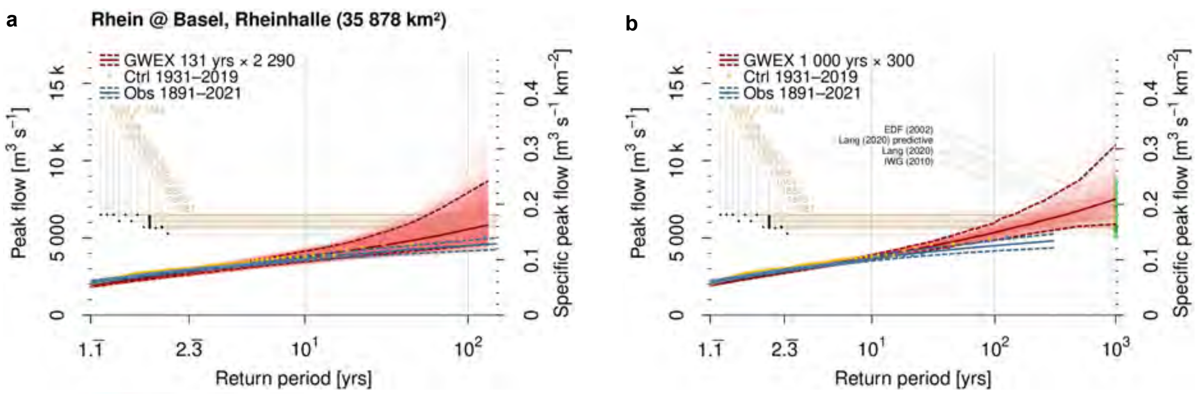

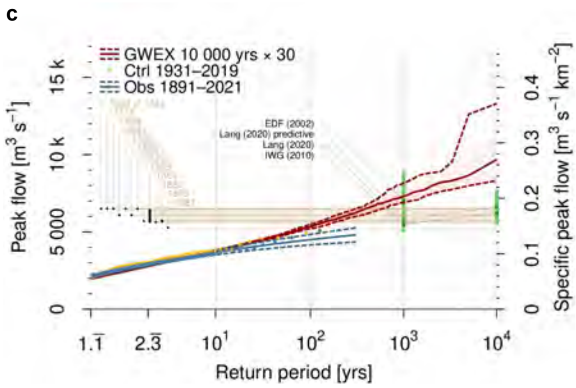

Figure 6.27: GWEX-based flood estimates for Rhein at Basel, Rheinhalle, with simulations subdivided into blocks as follows: panel a, blocks similar in length to the annual peak flow record; panel b, 300 blocks of 1 000 years; panel c, 30 blocks of 10 000 years. Historical flood estimates taken from Kienzler and Scherrer (2018) and further estimates (see Table 6.1) are included for comparison For interpretation and important background information see Chapter 10.

challenges in corresponding analyses is the impact of major river corrections: the Kander correction (1711–1714), which diverted the Kander River into Lake Thun, and the two Jura water corrections, which redirected the Aare River into Lake Biel (first correction 1868–1891) and enhanced the interconnection between the lakes of Biel, Neuchâtel and Murten (second correction 1962–1973) (Vischer, 2003). Considerable uncertainties must therefore be taken into account, also concerning the reconstruction of pre-instrumental events and the impact of floodplain retention, especially in the region of Grosses Moos (Pfäffli et al., 2020). Estimated magnitudes and probabilities of floods under current conditions should be viewed in this context.

The highest historical floods since 1268 estimated by Wetter et al. (2011) include six catastrophic events with an indicative discharge of at least 6 000 $m^3\,s^{-1}$, all of which occurred before 1700. For another six events reconstructed on the basis of vague written information, an upper range of a similar magnitude is suggested. Moreover, Wetter et al. (2011) identified 43 severe events with discharges between 5 000 and 6 000 $m^3\,s^{-1}$, with the exception of 1999 and 2007 all occurring before 1877. Figure 6.27 shows a selection of these historical floods with values as reported in Kienzler and Scherrer (2018) for visual comparison. The highest AMFs from the long CS of 300 000 years exceed all of these historical values. The extent of this exceedance appears greater than that noted for the Aare at Brugg, where estimates for historical floods are also available (Section 6.2.11). This is probably due to the influence of further rivers that join the main flow downstream of Lake Biel and did not undergo as fundamental modifications as the Aare River through the Kander correction and the Jura water correction. This reasoning particularly applies to the pre-alpine Thur River which adds relevant catchment size downstream of Lake Constance, is not attenuated by a lake, and has an increased channel capacity since 1998 (Section 6.5.5). Relevant to the observational period typically used for flood statistics, spanning from 1891 onwards, Wetter et al. (2011) note a disaster gap for floods from 1877 to 1998 – slightly extending beyond the general natural hazards disaster gap described by Pfister (2009) for 1882 to 1976. The gap may be caused not only by human intervention but also by a lack of climatic conditions that favour extreme floods (see also Zeder and Fischer, 2024).

Based on scenario considerations from observed flood events, Scherrer et al. (2006) estimated that a peak discharge of 5 000 $m^3\,s^{-1}$ has a recurrence interval of between 100 and 300 years. This is broadly consistent with EXCH results when the confidence interval is considered, even though results indicate a slightly higher return level already for a recurrence interval of 100 years. Scherrer et al. (2006) also noted that a very unfavourable combination of factors would be required today for exceeding a discharge of 6 000 $m^3\,s^{-1}$, such as a strong rise in the level of Lake Constance followed by an excessive, multi-day rainfall event on the Swiss plateau, with an unfavourable superposition of flood waves from the sub-basins. As mentioned for historical floods above, it can be assumed that the long CS indeed contains several of these very unfavourable configurations, and that exceedance of 6 000 $m^3\,s^{-1}$ is plausible.

Return levels for very rare events for Rhein at Basel were estimated by Électricité de France (EDF) (2002), Institut für Wasser und Gewässerentwicklung (IWG) (2010) as well as Lang (2020) and Lang et al. (2025), as summarised in Table 6.1. The $HQ_{1\,000}$ estimate of EDF agrees well with GWEX simulations, even though it might be rather high from the viewpoint of hydrological extreme value statistics. The other hydrology-based estimates by IWG (2010) and Lang (2020) give lower return levels compared to simulations with GWEX. For $HQ_{10\,000}$, GWEX is markedly above IWG (2010) and Lang (2020), while EDF (2002) does not give an estimate for this return period. Mind also that the hydrological extrapolations discussed here are subject to uncertainties, which in the case of EDF (2002) and Lang (2020) are quantified as a 95 % confidence interval. The confidence intervals of Lang (2020) and EXCH overlap in the case of the $HQ_{1\,000}$, but just barely do not overlap for the $HQ_{10\,000}$. In this context, it has to be stressed again that EXCH provides an extrapolation based on meteorology rather than hydrology, so that disagreement is indeed not a reason to dismiss the flood estimates (see Section 10.1).

The study by Hegnauer et al. (2014), which focusses on the 1 250-year design flood for the Rhine River at Lobith (165 000 km^2), utilizes a long CS of 50 000 years with a modelling chain somewhat similar to the one used in EXAR and EXCH. It reports that the highest flood wave at Lobith is fed by a discharge of approximately 7 500 $m^3\,s^{-1}$ at Basel. Assuming a return period of approximately 1 250 years, this is in the same order of magnitude as the EXCH and the EDF estimates. However, this value must be interpreted with particular caution due to the specific limitations of the study, which may not affect results

Table 6.1: Flood estimates for Rhein at Basel from different studies, all as reported in Lang (2020). The confidence interval (CI) is indicated where available.

Study	$HQ_{1\,000}$	95 % CI	$HQ_{10\,000}$	95 % CI
EDF (2002)	7 030	[5 760, 8 780]		
IWG (2010)	5 480		6 230	
Lang (2020)	5 520	[5 120, 6 440]	6 200	[5 580, 7 600]
Lang (2020), predictive	5 760		6 620	

at Lobith, but are relevant for the Swiss part of the Rhine River basin. These limitations include a) a daily time step that leads to poorer performances and higher uncertainties for the Swiss sub-catchments; b) a weather generator using resampling that cannot exceed the observed precipitation maxima; and c) a focus on winter floods, which are relevant for Lobith but less so for upstream areas in the Alpine region.

The flood estimates based on SCAMP weather generator input (not shown) are consistently around 10 % lower compared to those based on GWEX. This follows the general behaviour of SCAMP to produce lower flood estimates, as will be discussed in Section 9.1.

6.6. Rhone River basin (including Doubs River)

6.6.1. Rhone at Sion

The Rhone River basin is very challenging to implement in any hydrological model due to its precipitation characteristics – including strong elevation gradients, but comparatively few meteorological stations – , extensive hydropower usage, and the scarcity of long and undisturbed discharge measurements. Considerable effort was therefore put into setting up the HBV and RS Minerve models here.

As a result of these efforts, AMFs from the control simulation and observations at Sion (3 372 km^2) show good agreement (Figure 6.28a). Furthermore, the long continuous simulations using GWEX weather generator scenarios also show high agreement for frequent floods, where a comparison is feasible. For rare floods (Figures 6.28b and 6.28c), the flood exceedance curve of simulated AMFs noticeably flattens within the 100- to 200-year recurrence interval. This behaviour is due to the exhaustion of channel capacity at approximately 950 $m^3\,s^{-1}$, leading to bank overflow and surface retention. As retention becomes saturated around return periods of 300 to 500 years, the flood exceedance curve steepens again, now rising more sharply than it does for frequent floods.

6.6.2. Rhone at Porte du Scex

In addition to the hydrometeorological and hydropower challenges in the Valais, as discussed for Sion (Section 6.6.1), the flood characteristics of the Rhone River at Porte du Scex (5 238 km^2) are further influenced by the complex hydraulic conditions in the river stretch downstream of Sion. In this context, it is important to recall how the Rhone River basin was implemented in the EXCH models: For depicting river channel and floodplain, cross-sections provided by the FOEN were used, with a state representing approximately 2015. The hydraulic behaviour of river channel and floodplains was then explored with detailed 2D hydraulic simulations across all relevant return periods and then depicted in RS Minerve with simplifications. When the levees are overtopped, floodplain retention becomes active, breaking the peak wave and causing greatly delayed return flow from the plains back into the river. This is particularly relevant in the floodplain area between Sion and Martigny. Note that the levees cannot break in the model. Upstream in the side valleys, the nine largest reservoirs (Emosson / Vieux Emosson, Grande Dixence, Mattmark, Moiry, Mauvoisin, Salanfe, Les Toules, Zeuzier) are integrated into RS Minerve. Their operation was modelled on the basis of the turbining schemes in the FOEN forecast model and historical hourly turbining data. For the Mattmark and Grande Dixence reservoirs, RS Minerve does not turbinate in summer, allowing the reservoirs to fill up over summer and release sufficient water in winter (see Sections 2.2 and 3.4).

With this implementation, AMFs from control simulation and observations agree well (Figure 6.29). Winter discharges are not always well simulated as it is difficult to represent the relatively high flow from the

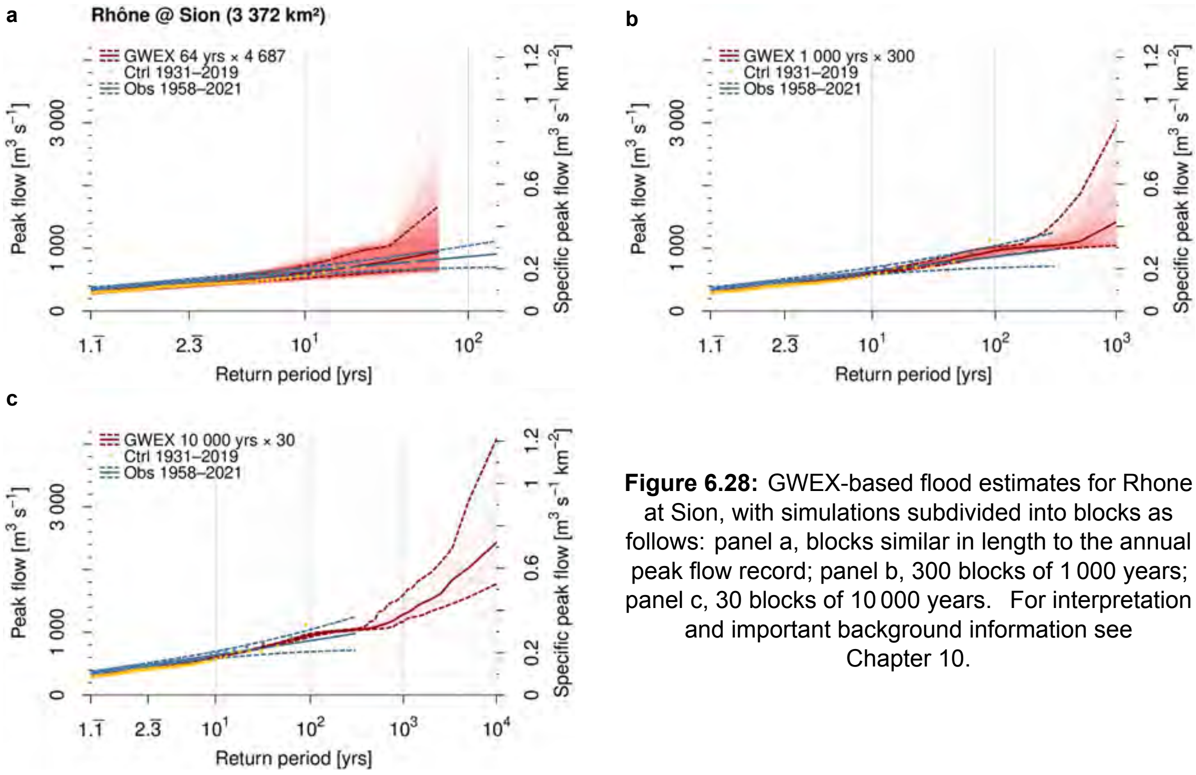

Figure 6.28: GWEX-based flood estimates for Rhone at Sion, with simulations subdivided into blocks as follows: panel a, blocks similar in length to the annual peak flow record; panel b, 300 blocks of 1 000 years; panel c, 30 blocks of 10 000 years. For interpretation and important background information see Chapter 10.

reservoirs, varying strongly around approximately 100 $m^3\,s^{-1}$. However, this does not seem to have a major impact on the flood estimates. The largest simulated flood in the control period 1931–2019 occurs on 15 October 2000, with a peak of 1 426 $m^3\,s^{-1}$. This is very close to the largest observed flood that occurred on the same day in reality, with a peak of 1 363 $m^3\,s^{-1}$. This close agreement is remarkable because the model is not calibrated for individual events, and uncertainties in observed input precipitation have to be taken into account. For the overall assessment of observed flood behaviour, it is relevant to note that major flood peaks occurred after the main time period 1958–2021 considered here, namely on 15 November 2023 (with 929 $m^3\,s^{-1}$) and on 22 and 30 June 2024 (1 047 $m^3\,s^{-1}$ and 1 193 $m^3\,s^{-1}$, respectively). These preliminary values are also shown in Figure 6.29).

The long continuous simulations show slightly higher values than observations and control simulation for return periods exceeding approximately 10 years, but still lie within the range spanned by high and low representative parameter sets of the control simulation. This behaviour is not implausible for a complex hydrological and hydraulic system, where observations of a few decades (64 years of discharge, and 89 years of meteorology driving the control simulation) might not comprehensively sample the long-term flood behaviour in time and space, with a wide range of possible combinations of antecedent conditions and triggering precipitation events. For return periods of more than 200 to 300 years, the simulations reveal marked retention where the exceedance curve flattens. This retention is exhausted only for considerably rarer floods, around 5 000 years return period, where the exceedance curve begins to rise more distinctly again.

6.6.3. Rhone at Genève, Halle de l'île

This site (catchment area: 8 000 km^2) is located around 500 m downstream of where the Rhone River leaves Lake Geneva, and around 500 m upstream of the Barrage du Seujet run-of-river weir, where the outflow of Lake Geneva is regulated. Simulating the behaviour of this site is very challenging due to the interplay of two main factors. On the one hand, lake inflows are difficult to estimate accurately because of hydrometeorological complexities, scarcity of observations, and extensive hydropower operations upstream (see Section 6.6.1). On the other hand, hydropower production at the outflow can cause repeated and strong fluctuations in lake level over the course of a day. To illustrate the potential influence of hydropower operation, it is useful to consider that the combined water storage capacity of

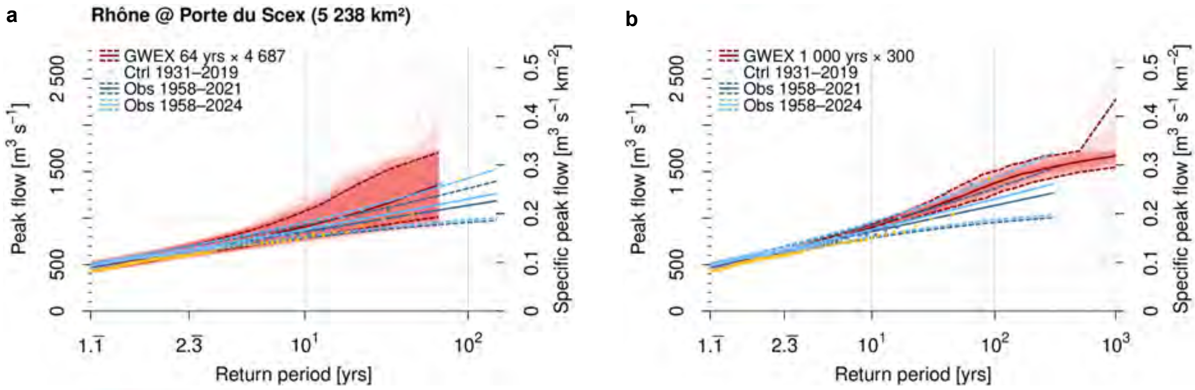

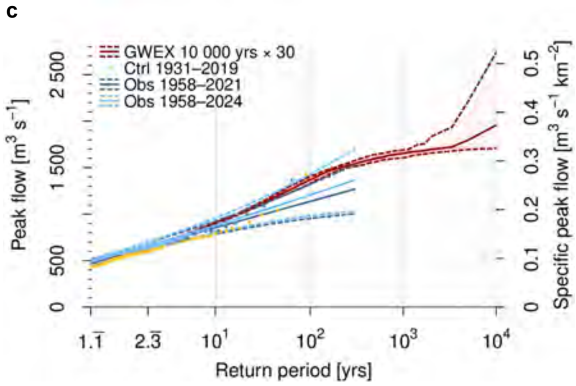

Figure 6.29: GWEX-based flood estimates for Rhone at Porte du Scex, with simulations subdivided into blocks as follows: panel a, blocks similar in length to the annual peak flow record; panel b, 300 blocks of 1 000 years; panel c, 30 blocks of 10 000 years. Observed AMFs with extrapolation and confidence intervals are here also shown in a version where the floods of years 2022–2024 are implemented from preliminary data. For interpretation and important background information see Chapter 10.

the reservoirs upstream of Lake Geneva (more than 1.3 km^3) is equivalent to well over 2 m of water level in Lake Geneva. These challenges are also discussed in Section 5.2.1.

Considerable efforts have been made to reproduce the complex behaviour of Lake Geneva, but some disagreement persists between AMFs of control simulation and observations (Figure 6.30). The exceedance curve from the long CS aligns with the control simulation for recurrence periods of less than 10 years, and then shows a steeper increase, which is closer to the observed AMFs but surpasses them. As noted at other sites, this does not necessarily indicate implausible results. In any case, caution must be applied here when interpreting return levels due to the known challenges in accurately reproducing the regulation of Lake Geneva. However, results further downstream at Chancy-Pougny (Section 6.6.5) indicate that the issues encountered here at Geneva are due to site-specific challenges rather than a fundamental problem with simulating the Rhone River.

6.6.4. Arve at Genève, Bout du Monde

The Arve River is the main tributary to the Rhone River between the outlet of Lake Geneva at Genève (Section 6.6.3) and the Swiss border near Chancy (Section 6.6.5), with a catchment area of 1 973 km^2, mostly located in the French Alps. Observations and control simulation show good agreement, and also the long CS exhibits plausible behaviour, with slightly lower return levels for very frequent floods and slightly higher return levels for floods in the order of 100 years return period. While observation-based return levels appear to level off with increasing return period, the long CS shows continued growth in flood magnitude.

6.6.5. Chancy-Pougny / Rhone at Chancy, Aux Ripes

This site on the Rhone River refers to the Chancy-Pougny weir (10 303 km^2) and can be scaled to the Chancy gauging station (10 308 km^2) with a factor of 1.001 (see Table A.3). It is located downstream of Lake Geneva, and also downstream of the confluence of the Arve River. While results for the outflow of Lake Geneva (Section 6.6.3) showed issues related to lake regulation, agreement between observations and control simulation is again high here (Figure 6.32). This re-improvement can mainly be attributed to the Arve River, which showed good agreement with observations (see Section 6.6.4

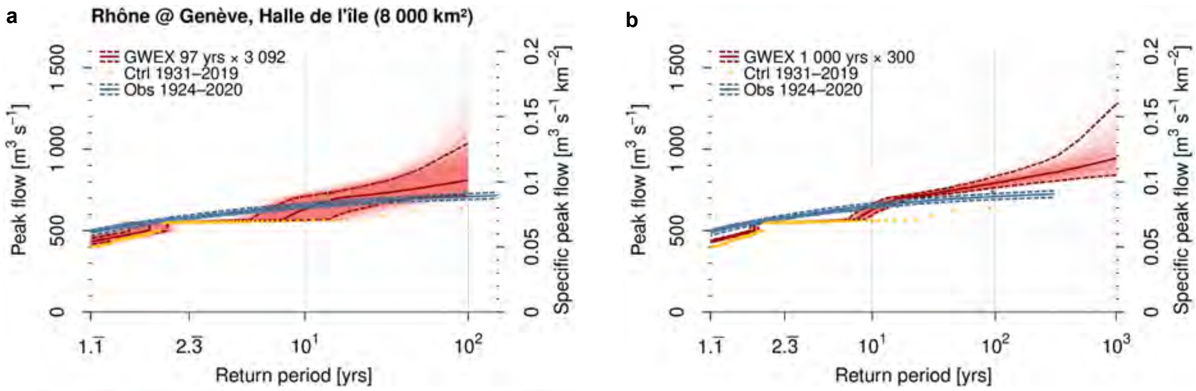

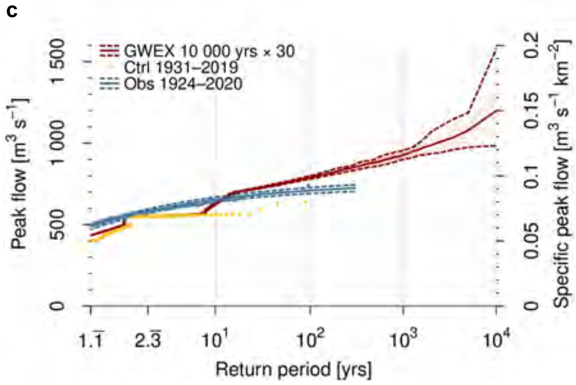

Figure 6.30: GWEX-based flood estimates for Rhone at Genève, Halle de l'île, with simulations subdivided into blocks as follows: panel a, blocks similar in length to the annual peak flow record; panel b, 300 blocks of 1 000 years; panel c, 30 blocks of 10 000 years. For interpretation and important background information see Chapter 10.

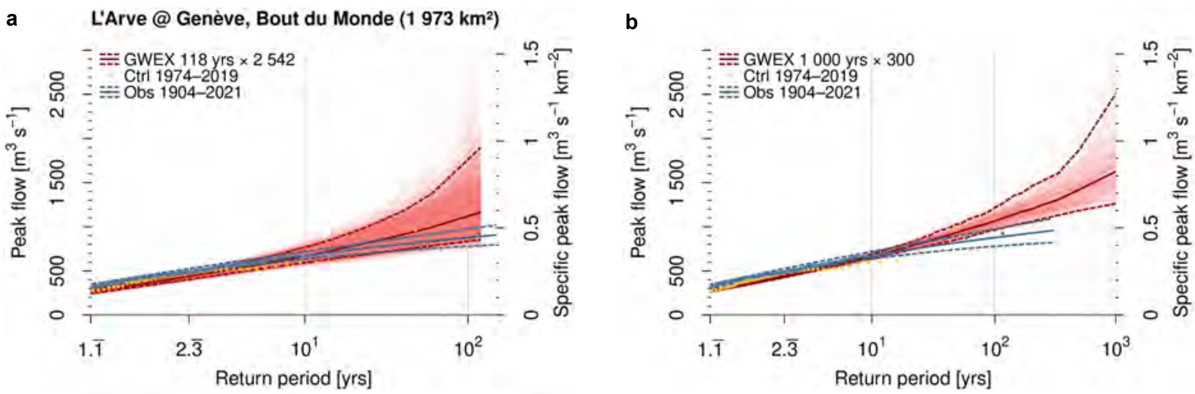

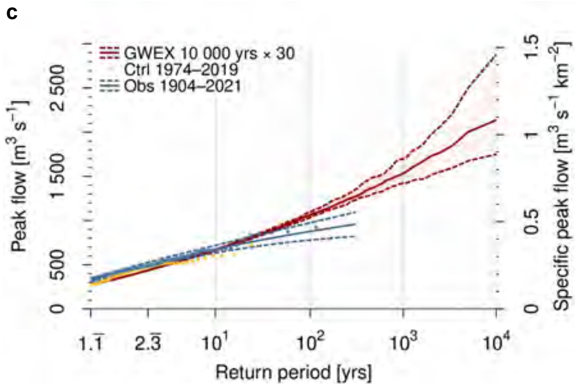

Figure 6.31: GWEX-based flood estimates for Arve at Genève, Bout du Monde, with simulations subdivided into blocks as follows: panel a, blocks similar in length to the annual peak flow record; panel b, 300 blocks of 1 000 years; panel c, 30 blocks of 10 000 years. For interpretation and important background information see Chapter 10.

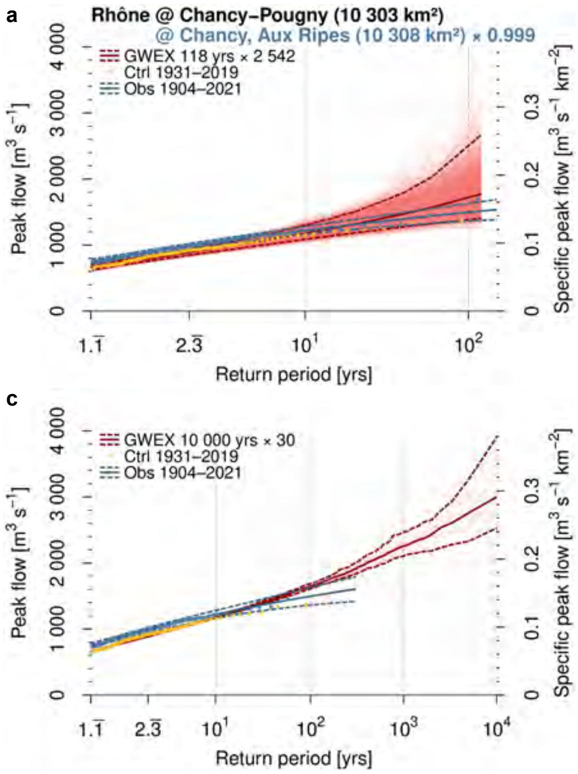

Figure 6.32: GWEX-based flood estimates for Chancy-Pougny / Rhone at Chancy, Aux Ripes, with simulations subdivided into blocks as follows: panel a, blocks similar in length to the annual peak flow record; panel b, 300 blocks of 1 000 years; panel c, 30 blocks of 10 000 years. For interpretation and important background information see Chapter 10.

above). The behaviour of the long continuous simulation for the Rhone at Chancy-Pougny is plausible as well, with a somewhat steeper increase noted for the exceedance curve above a recurrence interval of around 10 years as compared to the observation-based flood statistics.

6.6.6. Doubs at Ocourt

The Doubs River is part of the Rhone River basin, even though it joins the Rhone River – via the Saône River – only outside of Switzerland. The GWEX meteorological scenarios were therefore generated together with those for the main catchment of the Rhone River. The most downstream gauging site still located within Switzerland is Ocourt, with a catchment area of 1 275 km^2. The Doubs River is notable for widespread occurrence of karst, which can lead to irregular flow and cause process changes during flood events. Although specific karst features were not implemented explicitly in the modelling chain – among other things due to a lack of reliable data (see Section 10.2) –, the agreement between the AMFs of control simulation and observations is fair to good (Figure 6.33). Disagreement is mainly noted for return periods exceeding 10 years, where the control simulation shows slightly higher AMFs. The AMFs of the long CS generally follow the slope of the control simulation, but overall on a slightly lower level. The flood estimates derived from SCAMP (not shown) are slightly higher than those from GWEX at this site for return periods markedly exceeding 100 years. In any case, results at this site must be interpreted with particular caution.

6.7. Ticino River basin

6.7.1. Maggia at Locarno, Solduno

The Maggia at Locarno encompasses an area of 927 km^2 which, like that of the Sarine at Rossens dam (Section 6.2.4) and the Emme at Wiler (Section 6.2.10), transitions below the spatial scope of the EXCH weather generator for large catchments (see Sections 3.1.1 and 10.2). The corresponding limitations are expected to be particularly pronounced in this case due to the short and intense precipitation events characteristic of this region.

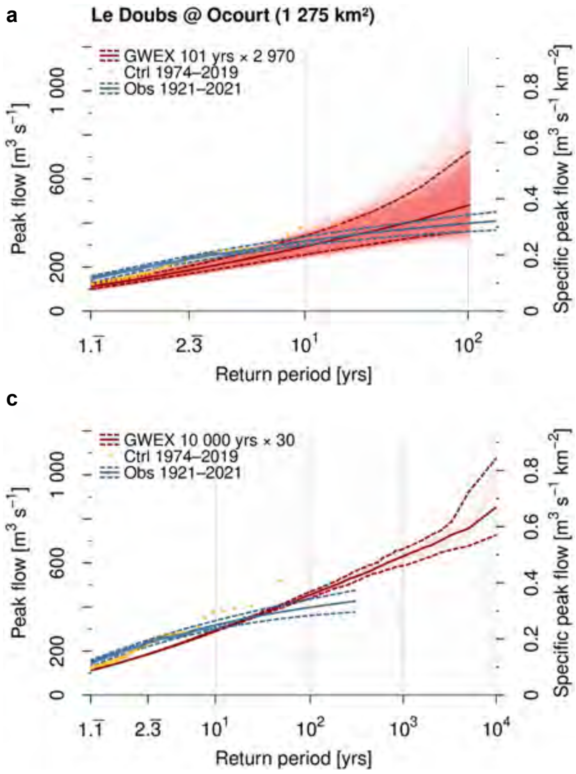

Figure 6.33: GWEX-based flood estimates for Doubs at Ocourt, with simulations subdivided into blocks as follows: panel a, blocks similar in length to the annual peak flow record; panel b, 300 blocks of 1 000 years; panel c, 30 blocks of 10 000 years. For interpretation and important background information see Chapter 10.

The control simulation forced with disaggregated meteo observations shows quite good agreement with observations, although the highest observed values are underestimated (Figure 6.34). The GWEX-based simulations are situated below observations and control simulation for return periods of 10 years and less. However, the exceedance curve of GWEX-based simulations continues rising, and extraordinarily high peak flows are reached for rare and very rare events, exceeding 10 000 $m^3\,s^{-1}$ for return periods larger than 10 000 years.

The plausibility of the exceedance curve behaviour beyond return periods of several hundreds to thousands of years is difficult to assess: As in all other cases, reliable data for comparison are not available. In this particular case, climatological and geological conditions generally favour high peak discharges, with high advection of moisture from the Mediterranean (Davolio et al., 2023) and crystalline bedrock that favours a rapid streamflow response. The range of precipitation intensities necessary to produce the highest simulated peak flow events in reality has indeed been recorded at Locarno-Monti (OTL), with 91.2 $mm\,h^{-1}$ on 28 August 1997. However, since this is a point measurement, it does not allow inference of areal precipitation intensities over the entire catchment of 927 km^2 (see Grebner et al., 1999). Extremely high precipitation sums for southern Switzerland were also reported for the 1868 flood event, with 1 118 mm over eight days at the gauge on the San Bernardino Pass, leading to widespread inundations in the Magadino Plain and on 4 October 1868 to the highest level ever recorded for Lake Maggiore (Brönnimann et al., 2018: 7).

In terms of specific peak discharge, the 1978 flood event in the Melezza River – a tributary to the Maggia River – reached an estimated value of 14.6 $m^3\,s^{-1}\,km^{-2}$ (Kienzler and Scherrer, 2018) at Palagnedra (catchment area: 137 km^2). This is approximately comparable to the lower end of the top-ten range simulated here for the Maggia River (14.9 to 26.7 $m^3\,s^{-1}\,km^{-2}$). However, the Melezza flood on 7 August 1978 was caused by a log jam at the Palagnedra reservoir, which eventually broke and released a flood wave (Stucki et al., 2017). In addition, the catchment of the Melezza River has only about one sixth of the area of the Maggia River, favouring much sharper flash floods. The Maggia River had an estimated peak of 4 500 $m^3\,s^{-1}$ (4.9 $m^3\,s^{-1}\,km^{-2}$) during this event, destroying the gauging station in Locarno. The station resumed operation only in 1985, missing the potentially large floods of 1981 and 1982. Interestingly, this observed peak of 4 500 $m^3\,s^{-1}$ mentioned for the Maggia in 1978 also amounts to one of the highest specific peak flows (4.9 $m^3\,s^{-1}\,km^{-2}$) for the Alpine climate region in the analysis

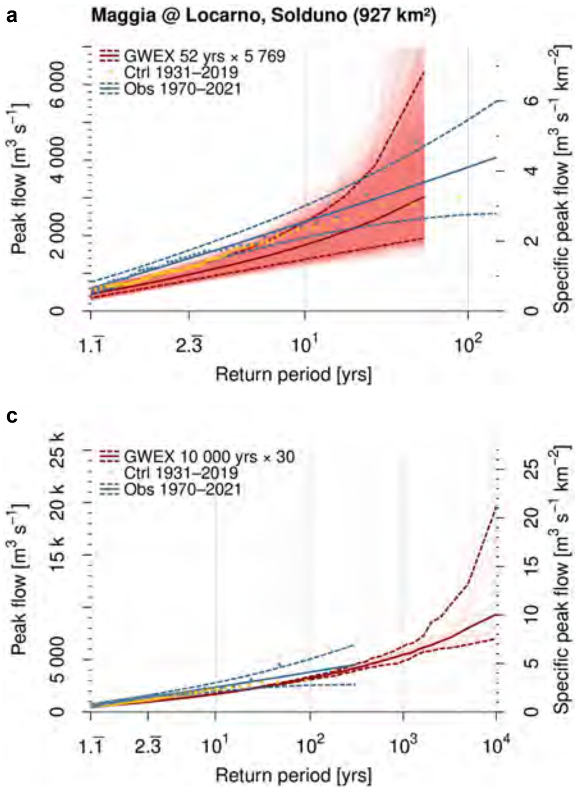

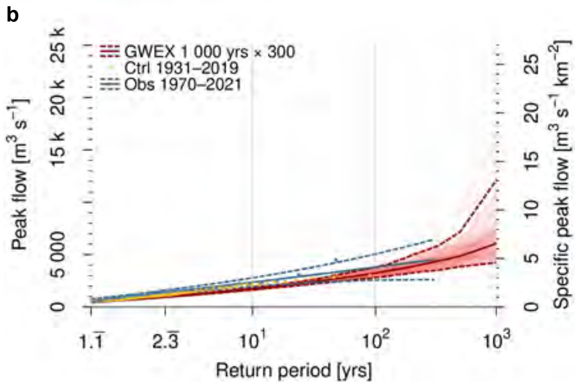

Figure 6.34: GWEX-based flood estimates for Maggia at Locarno, Solduno, with simulations subdivided into blocks as follows: panel a, blocks similar in length to the annual peak flow record; panel b, 300 blocks of 1 000 years; panel c, 30 blocks of 10 000 years. The y-axis has been truncated in panel a. Note that the catchment area of this site (927 km^2) transitions below the scope of the methods for large catchments employed in this study. Results are provided for informational purposes only. For interpretation and important background information see Chapter 10.

of extreme floods over all of Europe (Bertola et al., 2023), located on the envelope curve (see also Chapter 7).

The highest simulated discharge peaks for the Maggia River do not only exceed the envelope curve for Europe (Bertola et al., 2023) but also the value of 11 017 m^3 s^{-1} (11.9 m^3 s^{-1} km^{-2}) given as an envelope for this scale in the world catalogue of maximum observed floods by Herschy (2002; 2003) (see Chapter 7). This catalogue contains flood peaks from regions with considerably higher precipitation intensities, such as from the humid tropics, but on the other hand might still miss extraordinary events that were not recorded by a streamflow gauge somewhere. In this context, it should be noted that the longest series in the catalogue of Herschy (2002) are from markedly larger catchments than the ones considered here.

However, extremely high precipitation intensities are known in the greater region, such as reported by Davolio et al. (2023) for the Piedmont in connection with an atmospheric river. Peak intensities of more than 600 mm in 24 hours were reached on 2 October 2020 for Sambughetto in the Piedmont region, of which most occurred in the second half of the day.

Overall, it can be assumed that precipitation intensities are limited by physical constraints of water vapour transport in the atmosphere. However, it is not clear at which intensities such a plateau would be reached, even though PMP approaches aim at quantifying corresponding upper limits. During the EXAR project, this question was discussed with the accompanying expert panel, and it was concluded that if such a plateau exists, it is not yet relevant for the return periods considered (Andres et al., 2021; Kauzlaric et al., 2021b; Staudinger and Viviroli, 2020). It is important to note in this context that, due to its design, the GWEX weather generator does not provide information on the presence of a plateau. Additionally, stochastic multi-site weather generation in the Ticino region faces specific challenges including a comparatively sparse network of precipitation gauges, and comparatively short observation records that still contain some very large hourly and daily precipitation intensities. Given the substantial long-term variability in precipitation extremes, it is essential to consider that observations may underestimate the potential magnitude of such extremes (Zeder and Fischer, 2024). These challenges make it more difficult to robustly fit the shape parameter of the EGPD used in GWEX to model the extremes.

It can thus only be concluded that the GWEX weather generator follows the statistical behaviour of precipitation in the region that does not show asymptotic tendencies, and faces greater challenges for a robust fit.

Beyond the climatological considerations outlined above, simulation results from GWEX can be put into perspective by comparing them to results from SCAMP, which is structurally different from GWEX and additionally incorporates synoptic data (see Section 3.2.2), even though SCAMP also uses the observed precipitation records that were the basis for parametrizing GWEX. In the case of the Maggia River, SCAMP scenarios lead to roughly similar flood estimates, with slightly higher values as compared to GWEX for return periods up to roughly 10 000 years. The range of top-ten peaks is comparable, with SCAMP scenarios showing slightly lower values. More details are found in Section 9.1 and Figure 9.3e.

Another way of putting GWEX simulation results in perspective is by using RFs, which differ substantially from both GWEX and SCAMP regarding model structure and underlying data. Remarkably, the RF based simulations also produce exceptionally high extreme floods compared to other regions (see Section 9.2 and Figure 9.4). This suggests that the results generated by the weather generator for the Maggia River basin are not inherently unrealistic.

For all simulations, regardless of whether they use GWEX, SCAMP and RFs meteorological inputs, it is important to note that the uniform elevation-dependent adjustment factor for precipitation used for interpolation of MAP (see Section 3.3) also impacts extremes. However, its suitability for individual events is difficult to assess.

Based on the extensive considerations above, it is not possible to validate or dismiss the simulations regarding the exceptionally high peak flows or the shape of the exceedance curve. However, these considerations do not suggest that the simulated peak flows are completely unrealistic. It can thus be concluded that extremes in the range shown here might be possible, even though uncertainties of values and their return periods are considerable (see also Chapter 10).

6.7.2. Ticino at Bellinzona

For the Ticino River at Bellinzona (1 517 km^2), AMFs from control simulation and observations agree well, with the control simulations showing slightly higher return levels than the observations from roughly 10 years recurrence interval upwards (Figure 6.35). The observed AMFs level off markedly towards an apparent plateau, and the highest observed AMF is only 1.7 % and 2.3 % higher than the 2^{nd} and 3^{rd} highest AMF, respectively. This observed behaviour seems implausible and may be due to challenges with the gauging, the rating curve, or both. In contrast, the GWEX-based exceedance curve becomes steeper and reaches extraordinarily high values. As for the Maggia River at Locarno (see Section 6.7.1), simulated AMFs exceed 10 000 $m^3\,s^{-1}$, here for return periods greater than roughly 20 000 years.

The highest reconstructed peak at this site is interesting for context: It occurred on 28 September 1868, with an estimated value of 2 500 $m^3\,s^{-1}$ (Kienzler and Scherrer, 2018). This is considerably higher than expected from the 102 years of observations and their extrapolation, and suggests, in addition to challenges with observations, that possible process changes may occur during extreme floods.

Overall, the plausibility of the very rare simulated AMFs is difficult to assess also here. SCAMP-based simulations show lower AMFs for return periods larger than approximately 1 000 years (see Section 9.1 and Figure 9.3h), but it is not possible to assess whether GWEX might tend to overestimate floods or SCAMP might tend to underestimate floods.

6.7.3. Ticino at Miorina

This site at the Ticino River is located in Italy, at the outlet of Lake Maggiore. It lies approximately 2 km downstream of the Miorina dam where Lake Maggiore is regulated, and has a catchment area of 6 624 km^2. The gauge record available is short, spanning only six years from 2014 to 2019, which results in very wide confidence intervals. High agreement is noted between observations, control simulation and long continuous simulation (Figure 6.36), and the massive discharge peaks noted upstream of Lake Maggiore at Bellinzona (Ticino River, Section 6.7.2) and at Locarno (Maggia River, Section 6.7.1) are strongly attenuated by lake retention.

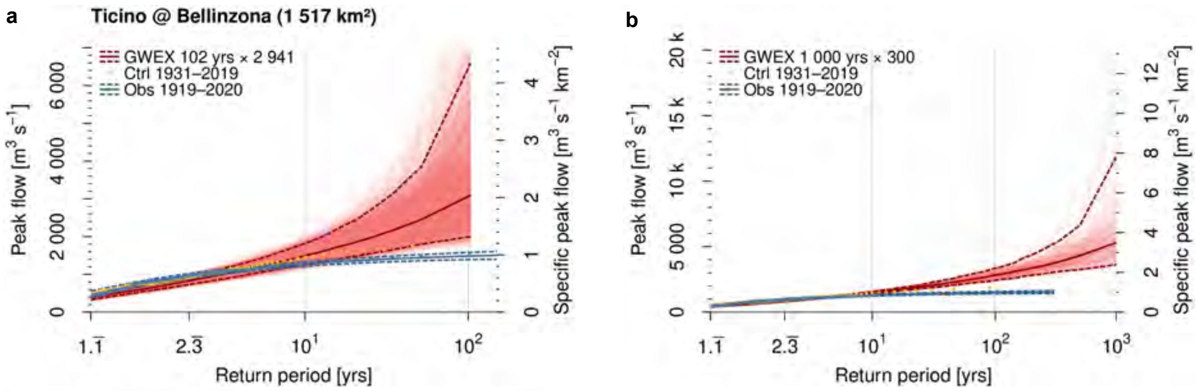

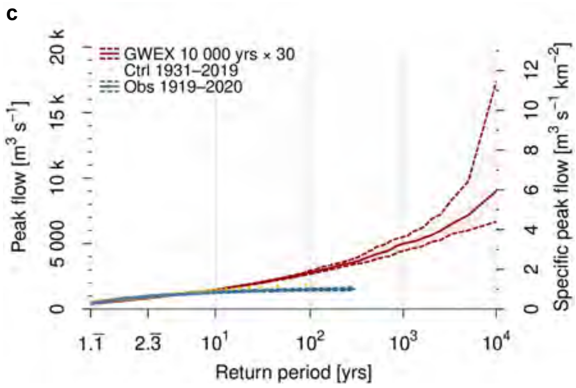

Figure 6.35: GWEX-based flood estimates for Ticino at Bellinzona, with simulations subdivided into blocks as follows: panel a, blocks similar in length to the annual peak flow record; panel b, 300 blocks of 1 000 years; panel c, 30 blocks of 10 000 years. The y-axis has been truncated in panel a. For interpretation and important background information see Chapter 10.

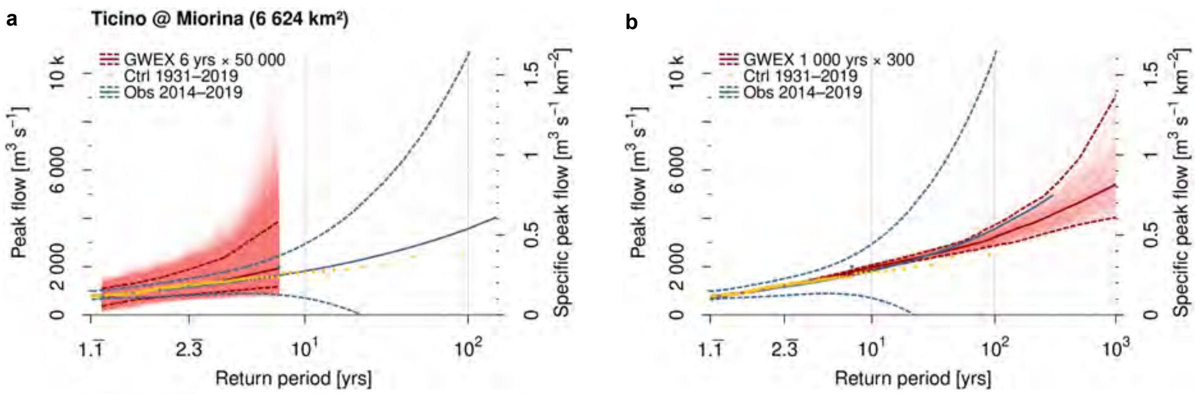

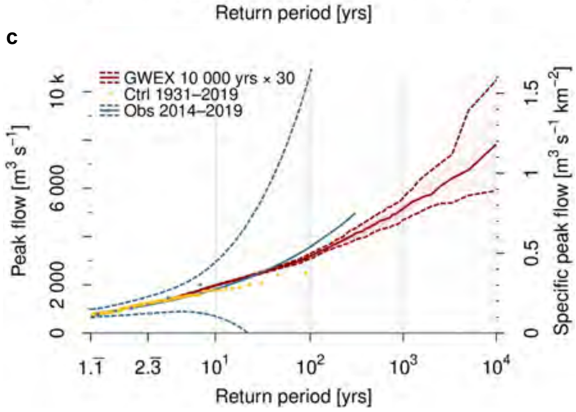

Figure 6.36: GWEX-based flood estimates for Ticino at Miorina, with simulations subdivided into blocks as follows: panel a, blocks similar in length to the annual peak flow record; panel b, 300 blocks of 1 000 years; panel c, 30 blocks of 10 000 years. For interpretation and important background information see Chapter 10.

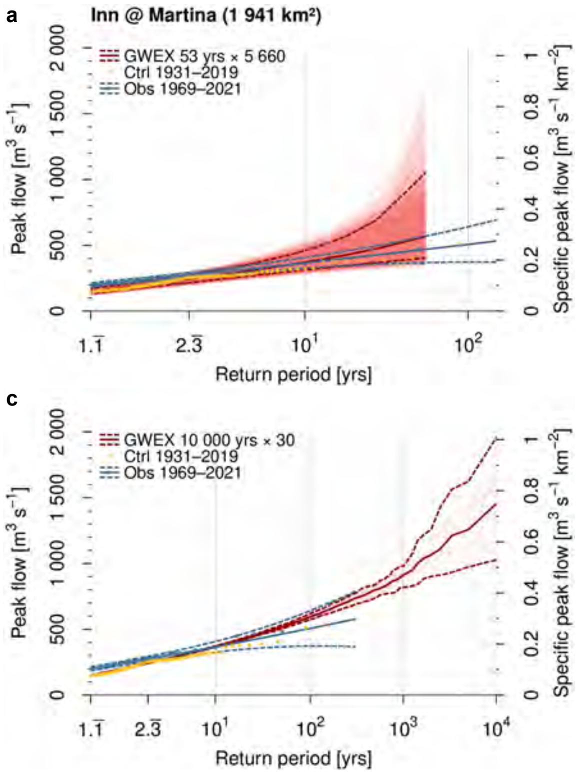

Figure 6.37: GWEX-based flood estimates for Inn at Martina, with simulations subdivided into blocks as follows: panel a, blocks similar in length to the annual peak flow record; panel b, 300 blocks of 1 000 years; panel c, 30 blocks of 10 000 years. For interpretation and important background information see Chapter 10.

6.8. Inn River basin

6.8.1. Inn at Martina

The Inn River basin, like the Rhone River basin, presents challenges for hydrological modelling due to its high elevation and the climatology of an inner-alpine dry valley, again with comparatively low density and representativeness of the meteorological gauging network. However, hydropower usage is not as widespread, and elevation gradients are somewhat less extreme.

At the only EXCH output site for large catchments in Martina (1 941 km^2), observations and control simulation agree well to very well (Figure 6.37). The long continuous simulations show behaviour that is consistent with observations and control simulation. However, they show a higher upper confidence interval in the range of observed floods (Figure 6.37a) and suggest the possibility of considerably larger floods for high return periods (Figures 6.37b and 6.37c).

7

Evaluation with envelope curves

In the following, the flood estimates derived from the hydrometeorological modelling chain are compared across different sites, and placed in context of envelope curves. Given the limited observational data, these curves provide one of the most meaningful tools for comparing and assessing flood estimates across the broad range of return periods considered. Estimates involving PMP and PMF are not considered due to incompatibilities in methods and scales. In particular, the CRUEX++ method (Fallot et al., 2017; Zeimetz et al., 2017) commonly used in Switzerland is limited to catchments smaller than 230 km^2. A more detailed discussion of this topic, along with limited juxtaposition of values, was provided in the EXAR project (Kauzlaric et al., 2021b; Staudinger and Viviroli, 2020; Viviroli et al., 2022).

The envelope curves shown in the following are based on data with different spatial scope and employ varying methods to characterise maximum observed runoff. To enhance interpretability across different applications, the figures show not only the ten highest simulated peaks, as in EXAR, but also return levels derived from the long continuous simulations. Estimates for HQ_{30}, HQ_{100} and HQ_{300} correspond to target return periods relevant for hazard mapping and hydraulic engineering, while estimates for $HQ_{1\,000}$ and $HQ_{10\,000}$ are crucial for designing and assessing the safety of critical infrastructure such as dams and weirs, as well as for evaluating the hydraulic overload scenario.

7.1. All output sites

The first comparison (Figure 7.1) shows all EXCH output sites from the large catchments module (see Appendix A) in one single graph, to give a broad overview of the flood estimates. For sites that cover both a dam under supervision of the SFOE and a gauging site of the FOEN, results are only shown for the dam, whereas the values for the corresponding FOEN site are very similar. A corresponding list with conversion factors is found in Appendix A, Table A.3.

The envelope curves shown for Switzerland (maximum and 95th percentile) are based on observed and reconstructed maximum floods reported in Kienzler and Scherrer (2018). Note that the curves computed here are based on data from all Swiss catchments with an area of 10 km^2 and more. Additionally, where a range was provided for an estimated maximum flood, the upper bound of that range was used. Overall, the maximum envelope curve is positioned quite high, determined by an extraordinary flood in the Melezza River (estimated peak flow of 2 000 m^3 s^{-1} for a catchment with an area of 137 km^2, see Section 6.7.1). This maximum envelope curve is only exceeded by the highest simulated values from the Maggia River at Locarno (including the estimated 10 000-year flood) and the Ticino River at Bellinzona. More useful in our context might be the 95th percentile envelope curve, which is in addition exceeded by the Ticino River at Miorina, despite the retention of Lake Maggiore. Further sites exceeding the 95th percentile envelope curve with their maximum simulated floods are found on the rivers Saane (at Laupen) and Rhone (at La Souste and at Sion). The three sites Rossens, Maigrauge and Schiffenen on the Saane River reach simulated maxima close to the 95th percentile envelope curve. What is striking is that comparatively more frequent return levels exceed the 95th percentile envelope curve in two cases: The Maggia River at Locarno (HQ_{30}) and the Ticino River at Bellinzona (HQ_{100}). For the remaining sites, the generic overview in Figure 7.1 shows a consistent pattern of lower estimated floods where lake retention is present, in particular also for all sites with a catchment area of 8 000 km^2 and more.

Also shown in Figure 7.1 is the envelope curve for maximum floods world-wide, sourced from the world catalogue of maximum observed floods as reported by Herschy (2003). The Maggia River at Locarno

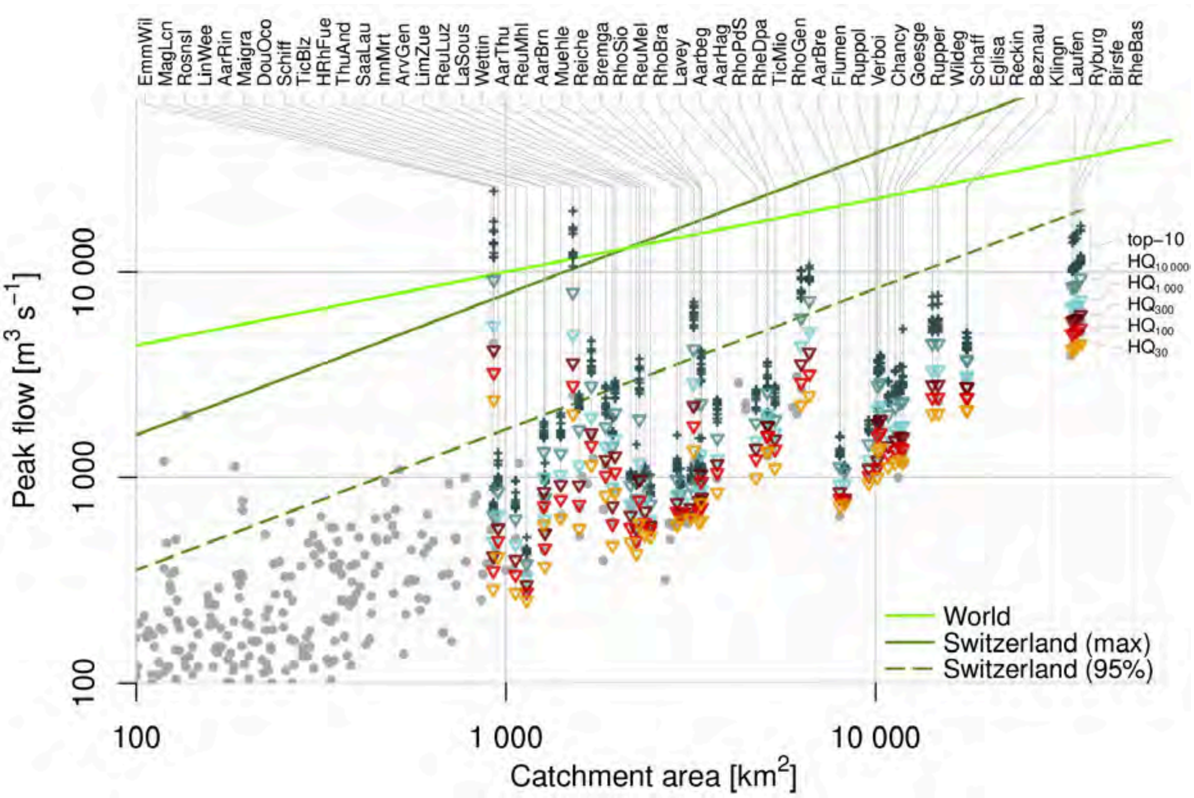

Figure 7.1: Return levels and top-10 AMFs from simulations with GWEX weather scenario input, placed in context of maximum observed floods in Switzerland (Kienzler and Scherrer, 2018) (grey dots) including a corresponding envelope curve for all data (max) and the 95th percentile (95%). Also shown is the envelope curve for maximum floods world-wide (Herschy, 2003). The abbreviations of the sites are revealed in Appendix A.

and the Ticino River at Bellinzona are the only sites that exceed this curve with their highest simulated peak flows. A more thorough discussion of this is found in the corresponding results sections 6.7.1 and 6.7.2, respectively.

7.2. Large river basins

Figure 7.2 essentially shows the same data and envelope curves as Figure 7.1, but separately for individual river basins. Also, the envelope curves were calculated from data from the river basin shown only, there again using all data referring to catchments with an area of 10 km^2 and more. The individual panels allow for a more differentiated and region-specific assessment of estimated floods.

In the Aare River basin, the influence of lake retention already mentioned in the previous Section 7.1 is clearly visible between Hagneck (AarHag) and Brügg (AarBre). Also, results of the Emme River at Wiler are lower compared to the general behaviour noted in the Aare River basin, as anticipated based on the underestimation discussed in Section 6.2.10. Apart from that, the spatial consistency of the flood estimates – a considerable advantage of EXCH – can be appreciated very well such as on the Saane River for sites Rossens (Rosnsl), Maigrauge (Maigra), Schiffenen (Schiff) and Laupen (SaaLau); and on the Aare River downstream of Lake Biel for sites Brügg (AarBre), Flumenthal (Flumen), Ruppoldingen (Ruppol), Gösgen (Goesge), Rupperswil-Auenstein (Rupper), Wildegg-Brugg (Wildeg), Beznau (Beznau) and Klingnau (Klingn).

Although some of the highest extremes in the Aare River basin reach the regional 95th percentile envelope curve, flood estimates are generally lower for the rivers Reuss (primarily due to retention through Lake Lucerne) and Limmat (primarily due to retention through Lake Walensee and Lake Zürich).

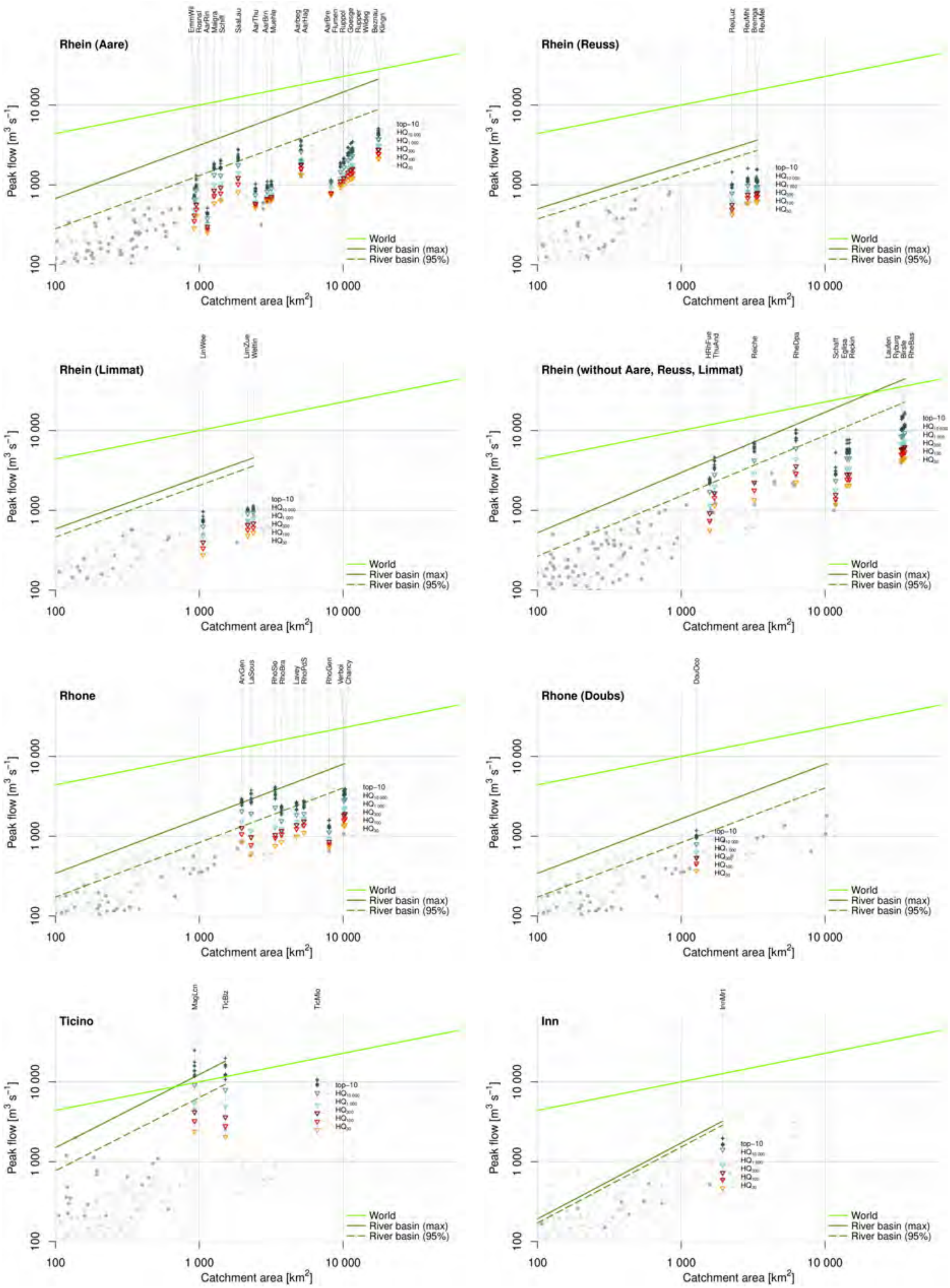

Figure 7.2: Same as Figure 7.1, but showing individual large river basins and corresponding regional envelope curves. As in Figure 7.1, dots show maximum observed floods according to Kienzler and Scherrer (2018), here in dark grey from the respective large river basin and in light grey from the rest of Switzerland.

The simulated sites on the Rhine River within the scale range of 1 000 to 10 000 km^2 display peak flow extremes that reach the envelope curve constructed from all data in this region. The retention effect of unregulated Lake Constance then causes a marked drop in return levels between Diepoldsau (RheDpa) and Schaffhausen (Schaff), with further downstream sites continuing to show values comparatively lower relative to the envelope curve.

In the Rhone River basin, all sites analysed are located along the main river, except the Arve River at Geneva (ArvGen). The attenuating effect of bank overflow and floodplain retention downstream of Sion is very well visible, leading to a drop in estimated return levels towards Branson (RhoBra) and also impacting Lavey (Lavey) and Porte du Scex (RhoPdS). It is interesting to note that the attenuation affects the high return levels much more strongly than the 30- and 100-year flood, which is compatible with the hydraulic conditions explained in Sections 6.6.1 and 6.6.2. Lake retention is then apparent at Geneva, whereas the estimated peak flows rise again at Verbois (Verboi) and Chancy-Pougny (Chancy), downstream of the confluence of the Arve River.

In the Ticino River basin, it is noteworthy that the envelope curves are steeper than those for all of Switzerland (see Figure 7.1), making the estimates from the long continuous simulation appear somewhat less extreme. To what extent the very flashy behaviour of small catchments in the Ticino River basin can be transferred to larger basins is difficult to assess, but the analysis shows that the simulated values should not easily be dismissed as implausible.

7.3. Climate regions

The envelope curves shown in Figures 7.3 and 7.4 were elaborated within a probabilistic framework as proposed by Castellarin et al. (2005, 2007), Castellarin (2007) and Vogel et al. (2007). This approach assigns an exceedance probability to the envelope curve based on AMF observations from the sites located within a region. In general, the exceedance probability assigned increases with the amount of AMF data available, whereas the data should be grouped into homogeneous regions in the sense of Hosking and Wallis (1993, 1997).

Since the approach was not used here to estimate floods at a particular site, but rather to provide an overview of flood probability across a region, slightly higher heterogeneity was accepted in favour of reasonably large regions. This also implies that the estimated recurrence intervals of the curves should be interpreted with caution and only as indicative values. In addition to AMF data, peak flow data from continuous discharge records were used where AMF data were not available. However, this was done only when the records were available at 10, 15 or 30-minute resolution, and not for 60-minute resolution.

For the present project, several regional groupings were examined, namely river basins, climate regions, biogeographical regions, regime types and flood regions. Figures 7.3 and 7.4 present an analysis by climate region (Schüepp and Gensler, 1980) as an example. Note that some climate regions do not have an EXCH output node.

The western northern slope of the Alps (Westlicher Alpennordhang) contains most of the sites of the Aare River basin (see Figure 7.2), and the probabilistic envelope curve is quite similar to the 95th percentile standard envelope curve. The estimated return period of the probabilistic envelope curve is around 3 400 years, and it is important to note that the heterogeneity is quite large, already because some sites are located downstream of large lakes and thus influenced by lake retention. Along the Saane River (Rossens, Maigrauge, Schiffenen, Laupen), the probabilistic envelope curve intersects near the 10 000-year floods estimated for these locations. Therefore, no overestimation is evident in the continuous simulations, including at the ungauged sites Rossens and Schiffenen.

The results for the Rhine River span two climate zones. All sites on the Alpine Rhine (upstream of Lake Constance) as well as the site Schaffhausen (approximately 20 km downstream of Lake Constance) are located in the northern and central Grisons (Nord- und Mittelbünden) climate zone. There, all simulated return levels fall well below the envelope curve, which has an estimated return period of approximately 1 950 years. The comparatively high position of the envelope curve can likely be attributed to peak flow observations from smaller catchments in the headwater regions. All sites on the High Rhine (i.e., downstream of Lake Constance), except Schaffhausen, are located on the northeastern central Plateau

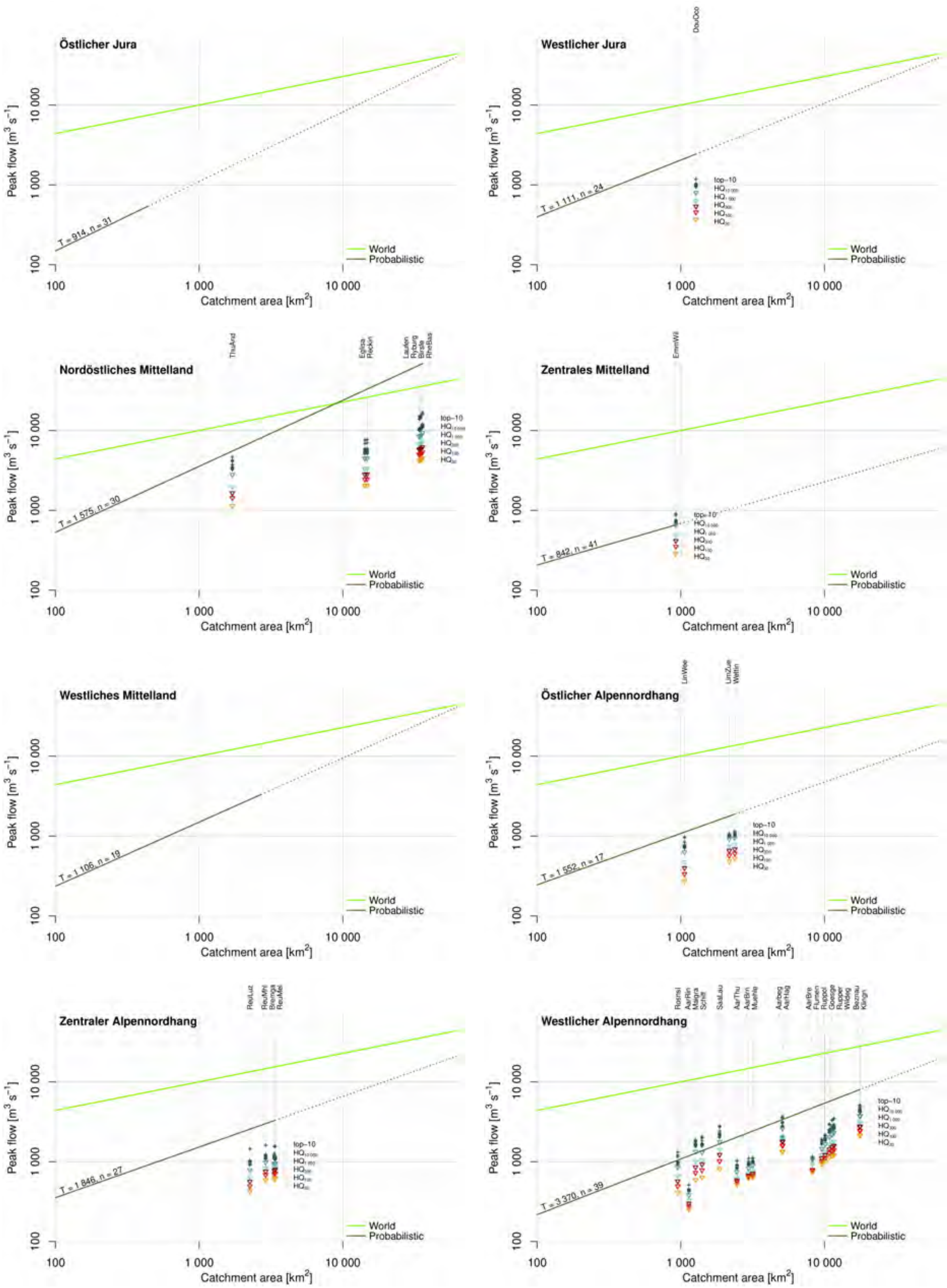

Figure 7.3: Same as Figure 7.1, but showing probabilistic envelope curves for climate regions in Switzerland. T denotes the estimated return period of the envelope curve, n denotes the number of catchments used as a basis for estimation of T per region. The figure shows the climate regions north of the Alps, for further climate regions see Figure 7.4.

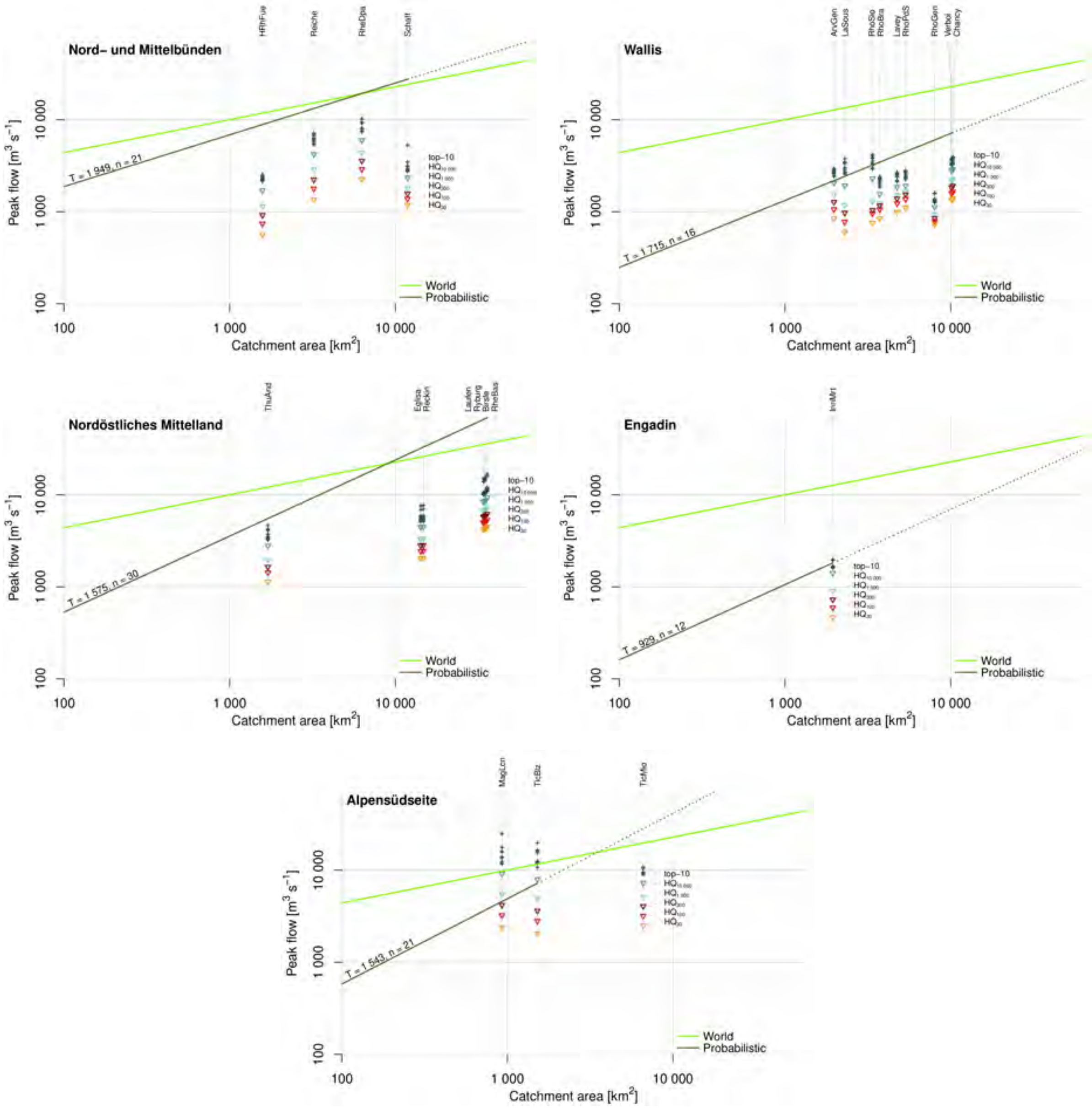

Figure 7.4: Same as Figure 7.3, but for regions in Wallis, Grisons and Ticino.

(Nordöstliches Mittelland). Their results also fall well below the envelope curve, here attributable to lake retention. The envelope curve has an estimated return period of approximately 1 600 years. In contrast, the Thur River, which does not have a major lake, reaches extremes close to the envelope curve.

For the eastern northern slope of the Alps (Östlicher Alpennordhang), where the Linth and Limmat rivers are located, simulation results again fall below the envelope curve, which has an estimated return period of approximately 1 550 years. This can be attributed to the retention effect of Lake Walensee and, in the case of the Limmat River, additionally to that of Lake Zürich. A similar interpretation applies to the central northern slope of the Alps (Zentraler Alpennordhang), where floods on the Reuss River are attenuated by Lake Lucerne.

For the Valais (Wallis), the probabilistic envelope curve has an estimated return period of over 1 700 years. Some heterogeneity arises here from the varying impact of floodplain retention and lake retention, as discussed further above and in Section 6.6. The juxtaposition does not indicate that the simulated flood estimates for the Rhone River could be too high.

Of particular interest are the results for the south side of the Alps (Alpensüdseite), where the probabilistic envelope curve shows the steepest ascent of all climate regions. Its estimated recurrence period of more than 1 500 years is well in agreement with the flood estimates for the Ticino River at Bellinzona. There, the probabilistic envelope curve intersects close to the estimated 10 000-year flood. For the Maggia River at Locarno, the envelope curve intersects between the estimated 300- and 1 000-year floods, indicating comparatively high estimates from the continuous simulation. However, this analysis also suggests that the return levels for the Ticino River basin should not be dismissed easily, even considering the limitations of the probabilistic envelope curves and the underlying data.

7.4. Extreme floods observed in Europe

This last comparison places the EXCH flood estimates in the context of an analysis over all of Europe by Bertola et al. (2023). In detail, the authors have analysed discharge records from over 8 000 sites across Europe to show that extremely high flood peaks at local scale can be anticipated from continental-scale data. Assuming that similar flood generation processes produce similar outliers, Europe was divided into five relatively large hydroclimatological regions, of which the Continental Region and the Alpine Region are the two applicable to Switzerland. This assessment is mainly interesting for extremely high flood peaks, and EXCH simulation results for the Continental Region (Figure 7.5, left) indeed appear plausible within regional context. The envelope curve indicates the possibility of even higher floods for catchments larger than approximately 5 000 km^2, although considerable retention potential of lakes (Lake Geneva in the case of the Rhone River; lakes Brienz, Thun, Murten, Biel and Neuchâtel in the case of the Aare River) has to be taken into account, in addition to surface retention in the region of Grosses Moos, proximate to the Jura lakes. Note that the highest simulated floods for Thur at Andelfingen exceed the envelope curve clearly in this climatic context, whereas they do not in the context of large river basins (Figure 7.2) and climate regions of Switzerland (Figure 7.4). For the Alpine Region (Figure 7.5, right), results for the Maggia River at Locarno and the Ticino River at Bellinzona exceed the envelope curve. This is not unexpected in view of previous discussion for these two sites (Sections 6.7.1 and 6.7.2) and in the context of other envelope curves (see Sections 7.1, 7.2, 7.3) and does not indicate fundamental issues of plausibility. Rather, the data available at continental scale might be too limited to reliably indicate extraordinary floods in this specific geological and hydroclimatological setting. For the Rhone and Inn rivers, the envelope curves indicate that considerably more extreme floods might be possible. However, the data pool from the specific hydroclimatological context – namely, inner-alpine dry valleys – may be limited in both cases.

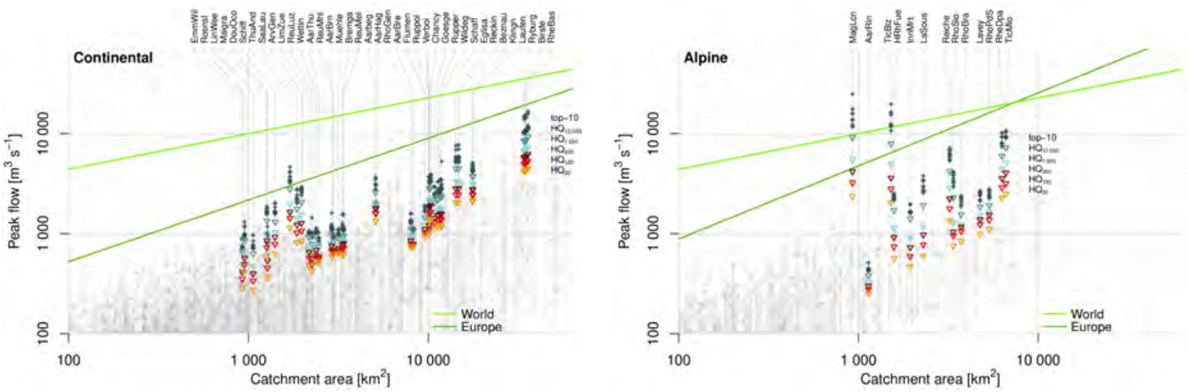

Figure 7.5: Return levels and top-10 AMFs from simulation with GWEX weather scenario input, placed in context of an assessment of megafloods for Europe (Bertola et al., 2023). The left panel shows the Continental climate region as per definition of the authors, the right panel the Alpine climate region.

8

Juxtaposition with EXAR results

The present project EXCH is a further development of the project EXAR, which was carried out between 2016 and 2021 (see Chapter 1). Although both projects were fundamentally based on similar methods, their results differ due to a number of reasons. This is explained below, along with a juxtaposition of EXAR and EXCH results.

8.1. Flood estimates

In the following, a juxtaposition of EXAR and EXCH flood estimates is presented for those sites in the Aare River basin that are reasonably comparable and have a catchment area of more than roughly 1 000 km^2. The sites Emme at Wiler and Saane at Rossens, with catchment areas of 924 and 952 km^2, respectively, are exceptions and transition below the scale range for which GWEX was developed (see Sections 3.1.1 and 10.2). Table 8.1 shows this juxtaposition for simulations using the GWEX weather generator as input. Note that only the EXCH sites ThuSee, BieSee, SSGSSH and SSHSSI are located in the focus region of EXAR and were validated in detail within EXAR.

Table 8.1: Juxtaposition of EXCH and EXAR results (EXAR final version, 2019) for sites that are reasonably comparable, using GWEX weather generator inputs in both cases. Negative values indicate smaller results for EXCH as compared to EXAR. Note that the sites ThuSee, BieSee, SSGSSH and SSHSSI, marked with an asterisk (*), are located in the focus region of EXAR, while the sites LacGru, SSKSSD, SSJSSB and VieSee were not validated in detail within EXAR.

Site (EXCH ~ EXAR)	*Area [km²]*	HQ_{10}	HQ_{30}	HQ_{100}	HQ_{300}	$HQ_{1\,000}$	$HQ_{10\,000}$
Emme @ Wiler ~ SSKSSD	924	-40%	-39%	-37%	-35%	-33%	-27%
Rossens (outflow) ~ LacGru	952	-21%	-21%	-21%	-22%	-24%	-32%
Saane @ Laupen ~ SSJSSB	1 862	-15%	-11%	-9%	-6%	-9%	-14%
Reuss @ Luzern ~ VieSee	2 254	+20%	+13%	+16%	+16%	+13%	+6%
Aare @ Thun ~ ThuSee *	2 459	-5%	-5%	-3%	-5%	-8%	-7%
Aare @ Brügg ~ BieSee *	8 248	-11%	-9%	-16%	-17%	-8%	-3%
Wildegg ~ SSGSSH *	11 643	-13%	-12%	-12%	-13%	-14%	-6%
Beznau ~ SSHSSI *	17 601	-15%	-16%	-16%	-16%	-14%	-13%

Table 8.2 presents an additional comparison with EXAR time series that have been composed to develop a method for extraction of representative hydrographs at weirs and dams (Staudinger et al., 2021). Note that the corresponding hydrographs are based on the preliminary EXAR simulations (version 2018), as only this version provided the full 289 000 years of continuous simulations required for developing and testing the extraction methods. Also, the EXAR simulations did not directly cover the sites examined, and the time series were derived by either adding up the relevant existing EXAR outputs, or by area-proportional scaling of an existing EXAR output, in both cases without site-specific routing and thus not including, for example, details of bank overflow and floodplain retention. Such effects are important for sites like Bremgarten-Zufikon, where standing retention was not well represented in EXAR because the site was outside the project's scope. Considerable work was undertaken in EXCH to improve the realism of floodplain behaviour for this and further output nodes concerned. For Bremgarten-Zufikon specifically, it should also be noted that the EXCH simulations show AMFs lower than observations, due to the strong influence of the Kleine Emme River, which is not adequately depicted by the weather generator for large catchments (see Sections 6.3.2 and 6.3.3).

Table 8.2: Juxtaposition of EXCH results and assembled EXAR preliminary results (version 2018), used for developing a representative hydrograph extraction method (Staudinger et al., 2021). Both simulations use GWEX weather generator inputs. Negative values indicate smaller results for EXCH as compared to EXAR. Note that the EXAR data here are not from output nodes but have been scaled or summed accordingly, without site-specific hydrological routing.

Site	*Area [km^2]*	HQ_{10}	HQ_{100}	$HQ_{1\,000}$
Rossens (inflow)	952	-23%	-23%	-26%
Maigrauge	1 267	-16%	-11%	-14%
Schiffenen	1 406	-12%	-7%	-14%
Wettingen	2 376	+3%	+3%	+4%
Mühleberg	3 168	-7%	-3%	-2%
Bremgarten-Zufikon	3 330	-25%	-25%	-22%
Aarberg	5 095	-14%	-11%	-13%
Flumenthal	9 582	-13%	-17%	-23%
Ruppoldingen	10 114	-14%	-16%	-22%
Gösgen	10 819	-9%	-9%	-12%
Rupperswil-Auenstein	11 298	-11%	-10%	-13%

For the sites in focus of EXAR, the EXCH simulations on the basis of GWEX generally indicate slightly lower return levels, with a median reduction of roughly 10 % depending on return period and site. An important part of this difference is due to the refined representation of the complex regulation of Lake Biel at the weir in Port, which in EXCH agrees better with observations than in EXAR. Moreover, the oscillations that occurred in some scenarios of EXAR were successfully eliminated. Furthermore, it was noted and discussed in EXAR that the Saane River exhibited quite high peak flows as compared to observations (Staudinger and Viviroli, 2020). The now refined representation of the Saane River in EXCH leads to lower return levels, which are in better agreement with observations (see Sections 6.2.5 and 6.2.6) and also influence flood peaks downstream in the Aare River. Conversely, the marked underestimation of AMFs in EXCH for the Emme River (see discussion in Section 6.2.10) to some extent contributes to lower EXCH values at Flumenthal and further downstream, with impact diminishing at sites farther along the Aare River.

For further sites not verified in detail for EXAR and beyond the scope of that project, differences in return levels range between roughly −30 % to +20 %, with the Emme River showing larger deviations. Also here, differences depend on return period and site, again with a median difference (excluding the Emme River) of roughly −10 %.

EXCH simulation results using SCAMP inputs are generally in the order of 5–10 % lower than those using GWEX inputs (see Section 9.1). In EXAR, by contrast, SCAMP inputs did not show a systematic bias in extreme peak flows as compared to GWEX inputs. However, a direct comparison is not feasible because in EXAR it was only possible to simulate 3 425 selected SCAMP scenario years containing events with high precipitation sums, due to time constraints and finite computational resources. This sample of events was biased due to the focus on precipitation and did not necessarily cover all of the largest peak flow events. Therefore, it was also not possible to estimate return periods for the corresponding flood events.

8.2. Model efficiencies

In addition to the flood estimates shown above, model efficiencies are also juxtaposed in the following. The refined and updated modelling set-up for EXCH allowed for a marked reduction in the spread of model efficiencies as compared to the version developed in the course of EXAR. Overall, the minimum Kling-Gupta efficiency (KGE) and Non-parametric Kling-Gupta efficiency (KGE-NP) in the simulation period is above 0.5 in EXCH for all of the ten sites that can be compared well in terms of model efficiencies (Figure 8.1). The lowest efficiencies are noted for the Saane at Laupen (e.g., negative NSE values). However, these values have to be interpreted with caution since the Saane River is strongly impacted by the two large hydropower dams Rossens and Schiffenen, both of which produce pronounced hydropeaking.

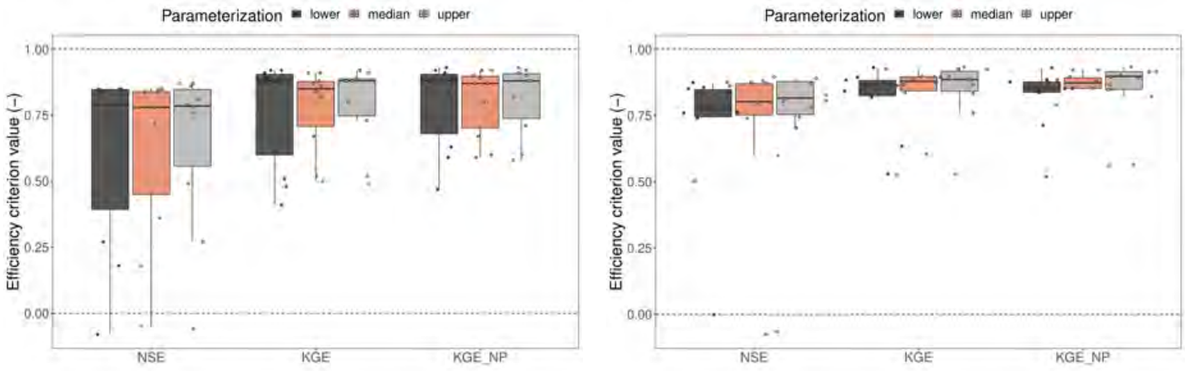

Figure 8.1: Model efficiencies at ten sites with comparable locations in both EXAR and EXCH. These include all sites listed in Table 8.1 as well as Limmat at Baden and Lorze at Frauenthal, which exhibit larger differences in routing between EXAR and EXCH. All efficiency scores (NSE, KGE, KGE-NP) have an upper bound of 1 (which means ideal performance) and are unbounded towards the bottom. The scores were computed for simulations at hourly time step over the simulation period overlapping with observations. Results from the three representative parameter sets are shown. Left panel: results from EXAR (covering 1974–2014 at most); right panel: results from EXCH (covering 1974–2019 at most).

8.3. Reasons for differences

Overall, differences for renewed simulations of the Aare River basin have been anticipated already at the end of EXAR, and are not surprising since many details of the modelling chain have been refined to meet the goals of EXCH, with additional time dedicated to fine-tuning hydrological modelling and routing. This includes, for example, more widespread and detailed depiction of bank overflow and retention areas, model calibration and parameter selection as well as lake regulation. In addition, the data basis for the weather generator and the parametrization of the hydrological model has been extended markedly, and details of the corresponding model structures have been slightly updated, to overall represent the current state of research and knowledge. Also, the weather generator has been parametrized and run for the Aare and Rhine river basins jointly in EXCH, while EXAR covered the Aare River only. For those few sites where observations exist, a closer agreement with EXCH is generally found as compared to EXAR, and model performance was further improved for the current project (see Section 8.2).

The following overview lists differences between EXAR and EXCH that are expected to contribute to the differences in results.

Meteorology:

- The GWEX weather generator has been refined for EXCH by conditioning it to weather types (Section 3.2.1).
- In EXCH, GWEX was run jointly for the Aare and Rhine river basins, whereas in EXAR, it was only run for the Aare River basin.
- In EXCH, GWEX was re-parametrized using a different set of meteorological stations, including additional stations from abroad, but with some thinning of potentially redundant stations in the Aare and Rhine river basins. The thinning out was necessary to keep the covariance matrices of GWEX numerically manageable. This may be one cause behind the underestimation of peak flows in the Emme River catchment, which performs less well than in EXAR (see Section 6.2.10).
- Slightly longer observation records were available for estimating the parameters of GWEX, namely 1930–2019, as compared to 1930–2014 in EXAR.
- A precipitation adjustment factor of +5 % per +100 m elevation was used in both EXAR and EXCH. However, in EXAR, precipitation data were first interpolated and then adjusted, while in EXCH, adjustment of station data to a reference elevation was performed first, followed by interpolation and then adjustment to mean catchment elevation.

- The temperature lapse rate in EXCH is a daily average value for each day of the year, derived from observational data. In EXAR, a uniform factor (standard atmosphere) was used throughout.

Hydrology:

- In EXAR, a full set of 289 000 years of hourly simulations was only available in a preliminary model version (2018), while the final version (2019) could only be run for 28 900 years due to time constraints in the project. 289 000 AMFs were extracted from the 2018 version and then corrected to the 2019 version, using a factor depending on return period and site. This factor was estimated by comparing 28 900 AMFs from the 2018 and 2019 versions (Viviroli and Whealton, 2020).
- In EXCH, HBV uses an improved representation of glaciers, and the glacier routine was used for catchments with a glacier cover of at least 1 % already, as compared to a threshold of 5 % used in EXAR. Also, the snow redistribution routine as per Freudiger et al. (2021) was used.
- In EXCH, HBV uses the improved runoff formation scheme (response routine) of HBV-96 (Lindström et al., 1997) instead of the the scheme of the original model (Bergström, 1972).
- Estimation of potential evapotranspiration was refined for EXCH.
- While only 49 calibrated catchments (all from the Aare River basin) were available as a basis for regionalisation of the HBV model parameters in EXAR, the calibration basis has been expanded considerably for EXCH to 463 catchments (from all of hydrological Switzerland). This has, among other improvements, enhanced parameter regionalisation for Saane River, which in EXAR subsystem SSJSSB was found to exhibit rather high peak values and high runoff coefficients (Staudinger and Viviroli, 2020).
- Calibration of the HBV model parameters has been further refined in EXCH, relying on extensive testing of different combinations of efficiency criteria for the objective function (see Section 3.3). While this generally led to more realistic simulated hydrographs, it also contributed to the underestimation of AMFs in the Emme River basin (see Section 6.2.10). Small differences also concern the selection of parameters that were calibrated versus those fixed at values determined on basis of experience from EXAR.
- The selection of the three representative parameter sets was refined.
- In EXCH, the subdivision of the Aare River into HBV catchments has been refined, with 127 HBV sub-catchments instead of 89 as in EXAR. This was done with a view to improved parameter regionalisation and based on the larger set of calibrated catchments available.

Routing:

- The representation of important floodplains has been refined considerably in cases where they were not in the scope of EXAR but become important for EXCH (e.g., Reuss River). Also, the discretization of return flows to the main river has been refined considerably.
- The complex regulation of Lake Biel has been refined.
- Regulated Lake Sihl is represented explicitly in EXCH using routing in RS Minerve, rather than implicitly in a HBV sub-catchment as in EXAR. Lake operation is dependent on the stage of Lake Zürich (see Section 3.2.3).
- For developing a hydrograph selection method for SFOE on the basis of EXAR data, the EXAR time series were summed or scaled in many cases, without adjusting and re-running hydrological routing. In EXCH, the routing was refined specifically with a view to the sites relevant for SFOE.

9

Results from alternative weather scenarios

9.1. Flood estimates using SCAMP weather generator input

The SCAMP weather generator was introduced already in the EXAR project, with the goal of having a structurally fully independent weather generator available as first link of the simulation chain. As explained in Section 3.2.2, SCAMP itself was not modified for EXCH, but its parameters were re-estimated for the project domain of EXCH.

In EXAR, only the weather scenarios from GWEX were run through the modelling chain in their entirety, spanning 300 000 years at hourly resolution. From SCAMP, only 3 425 individual years were processed due to the massive computational demand and time constraints in the project. The selection of years was based on maximum precipitation sums over different accumulation periods and with respect to different sub-basins of the Aare River. Due to this limited set, it was not possible to estimate the return periods of the corresponding flood peaks, and only the ten largest flood peaks were compared with those derived from GWEX. However, results indicated that both weather generators achieve a similar order of peak magnitude (Viviroli et al., 2022).

Also for EXCH, it was planned to only run a selection of SCAMP weather scenarios, but thanks to considerable work directed towards optimising the computational workflow, it became possible to run all 300 000 years at hourly resolution as well. With this, it also became possible to estimate the return periods of the simulated AMFs and make a comparison to results obtained using GWEX inputs.

An evaluation of all simulated sites in the context of envelope curves – similar to Figure 7.1 in Section 7.1 – is shown in Figure 9.1. To facilitate the comparison of differences, Figure 9.2 reveals the ratio between SCAMP-based and GWEX-based results. In this first full comparison, SCAMP shows slightly lower AMF values at the vast majority of output sites considered. This is compatible with the behaviour observed in validation of the flow duration curves from individual sub-catchments (see Section 5.1.2, Figure 5.12). Only for the Doubs River at Ocourt (DouOcu), SCAMP shows consistently higher return levels, and partly higher estimates are noted for Maggia at Locarno (MagLoc), Arve at Genève (ArvGen), Limmat at Zürich (LimZue) and Wettingen (Wettin). In many (but not all) cases, the differences between SCAMP and GWEX increase with increasing return period, depending on the tail behaviour of the exceedance curves derived from the simulations. Sites with a catchment area of more than approximately 10 000 km^2 show a considerably smaller spread of differences, typically constrained to a range of −10 to 0 %.

An analysis of selected individual sites – comparing some cases that are also discussed in Chapter 6 – illustrates the differences noted above: For example, Aare at Ringgenberg, Goldiswil (Figure 9.3a, Section 6.2.1) and Maigrauge (Figure 9.3g, Section 6.2.5) show SCAMP values that are in the order 10 % lower than GWEX values across a wide range of return periods. Even lower SCAMP estimates in comparison to GWEX are found, for example, for Inn at Martina (Figure 9.3c, Section 6.8.1), Rhone at Sion (Figure 9.3f, Section 6.6.1) and Ticino at Bellinzona (Figure 9.3h, Section 6.7.2). However, the extent of differences varies depending on the individual site and the return period considered. Some other sites show rather close agreement throughout, with SCAMP only having slightly lower AMF values, such as Wildegg-Brugg / Aare at Brugg (Figure 9.3b, Section 6.2.11). Only occasionally, SCAMP yields

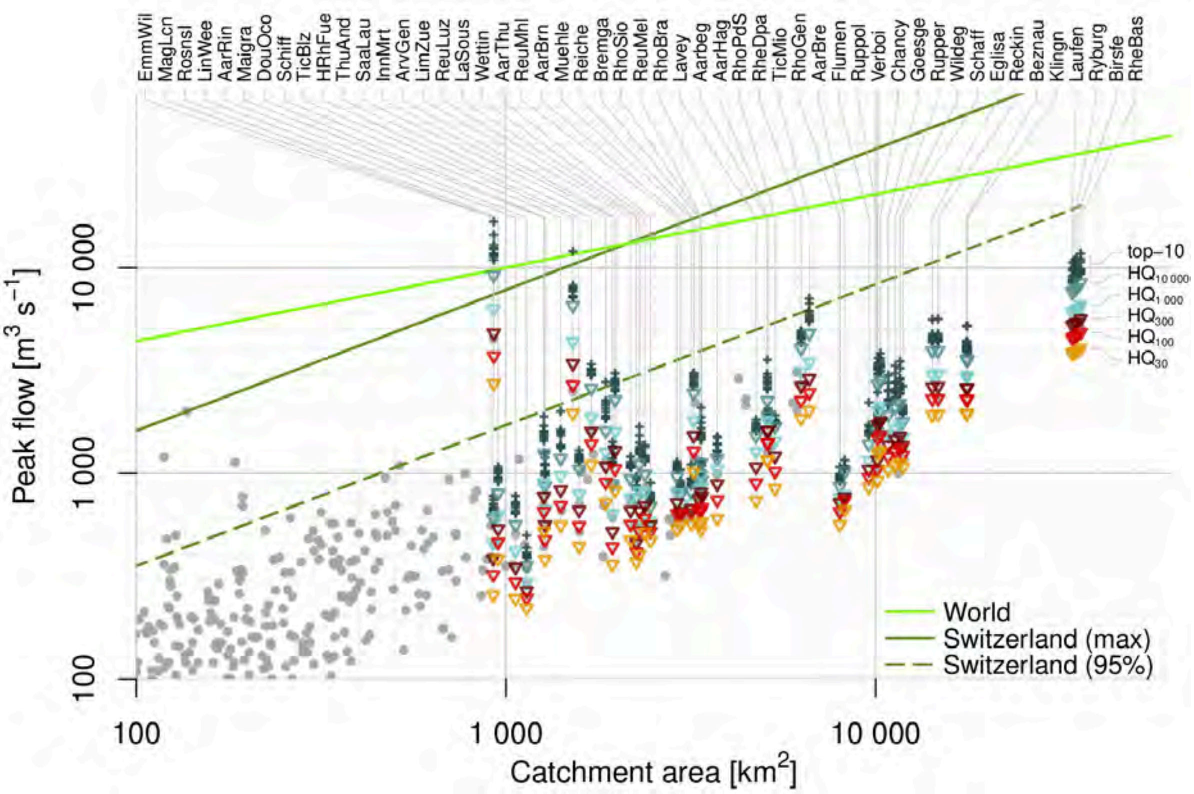

Figure 9.1: Return levels and top-10 AMFs from simulation with SCAMP weather scenario input, placed in context of maximum observed floods in Switzerland (Kienzler and Scherrer, 2018) (grey dots) including a corresponding envelope curve for all data (max) and the 95th percentile (95%). Also shown is the envelope curve for maximum floods world-wide (Herschy, 2003). The abbreviations of the sites are revealed in Appendix A. See Figure 7.1 in Section 7.1 for a similar figure based on GWEX weather scenario input.

slightly higher AMFs, such as for rare floods at Wettingen / Limmat at Baden (Figure 9.3d, Section 6.4.3), or for frequent floods at Maggia at Locarno (Figure 9.3e, Section 6.7.1).

The differences between GWEX and SCAMP based flood estimates are not straightforward to explain at first sight, as the meteorological evaluation of SCAMP 1- and 3-day precipitation sums has neither revealed major issues nor substantially worse performance in comparison to GWEX (see Section 4.3 in Mas et al., 2023). However, mean monthly precipitation sums of SCAMP were not agreeing very well with observations in many cases, especially during the summer half year. This may stem from issues with the analog approach, where it was found that the resampling is not using all observation days with similar frequency, but rather under- and oversampling certain days, which can introduce bias.

In summary, the flood exceedance curves derived from SCAMP weather scenarios show slightly lower return levels at numerous sites in comparison to those based on GWEX. This suggests that GWEX does not underestimate the range of possible floods relative to the structurally different approach used in SCAMP. However, this conclusion is tentative and limited in scope due to the apparent bias in SCAMP that was identified in the hydrological analyses above. This bias also extends to the return levels estimated, as those based on GWEX generally agree better with observations than those based on SCAMP.

9.2. Flood estimates using reforecasts

As introduced in Section 3.2.3, reforecasts (RFs) were explored within EXCH as way of achieving weather scenarios largely independent of the weather generators GWEX and SCAMP. Although the length of the RF time series feasible in the current project (approximately 10 000 years) is shorter than that of GWEX and SCAMP (300 000 years each), the RFs remain highly relevant for verifying the

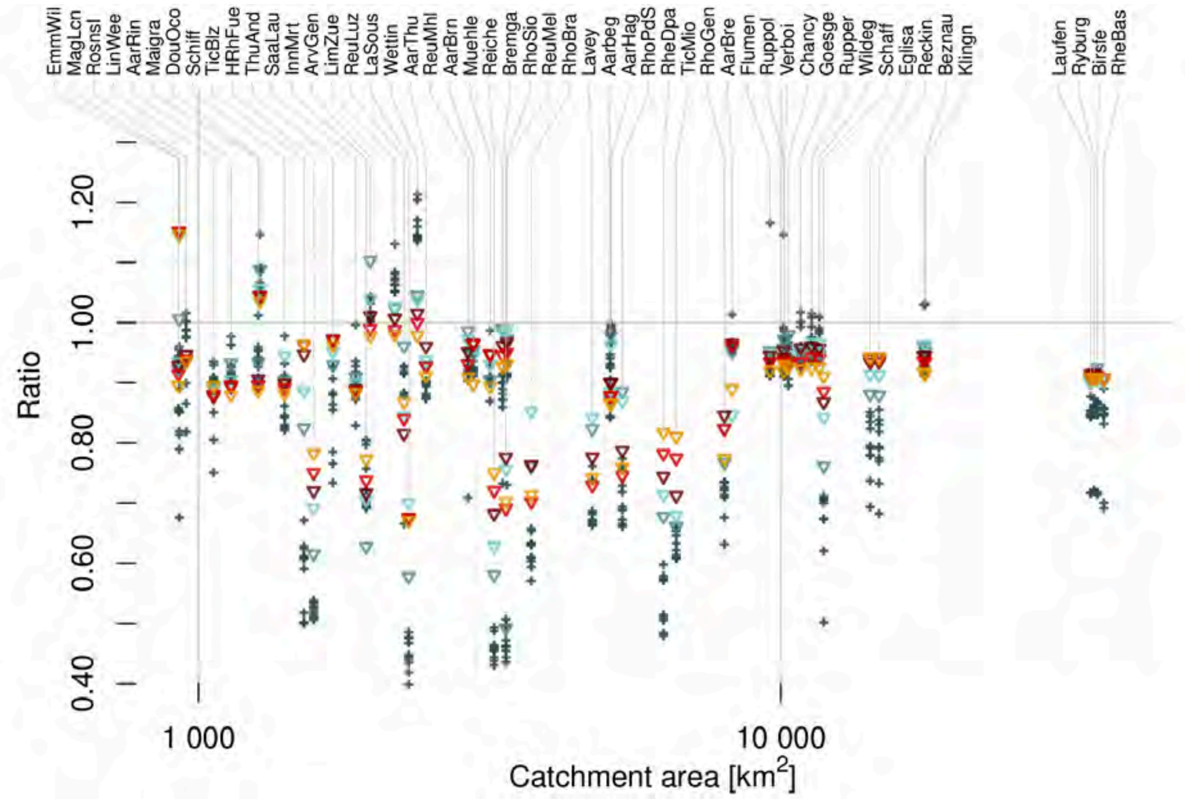

Figure 9.2: Difference in return levels and top-10 AMFs between simulation with SCAMP and GWEX weather scenario input. Values below 1 mean that SCAMP results are smaller than GWEX results. Symbols are explained in Figure 9.1, abbreviations of the sites are revealed in Annex A.

magnitude of the flood estimates based on weather generator inputs, and for assessing whether the weather generators might underestimate possible but unobserved floods. It should be noted that the use of RFs in this project was developed as a feasibility study. Moreover, results were computed for a set of test catchments only that cover a broad range of scales (approximately 20 to 3 000 km^2) and only partially overlap with the EXCH output sites.

Figure 9.4 shows an evaluation of the RF based flood estimates in the context of envelope curves, similar to Figures 7.1 and 9.1. In general, magnitude and estimated frequency of the RF based floods appear plausible, with a tendency to potentially underestimate values for smaller scales. This limitation applies to catchments where storms dominate the generation of AMFs, and thus to catchments that would require dynamical downscaling of RF – which was not feasible with the available data (see Section 3.2.3) – rather than the stochastic downscaling that was used. A comparison of top-ten values shows that RFs produce lower extremes than GWEX (note the logarithmic y-axis), which can be attributed to the shorter length of the RF series. Comparing the return levels does not indicate any systematic disagreement between GWEX and RFs. Also, the RF values for the Ticino region – Isorno at Mosogno (IsoMsg, 124.7 km^2) and Maggia at Locarno, Solduno (MagLcn, 926.9 km^2) – are notably higher than those of other regions, consistent with the findings from the GWEX results.

Exceedance curves on basis of RF meteorological inputs are shown for some selected examples in Figure 9.5. All sites except one have a catchment area larger than approximately 500 km^2, as smaller catchments are considered beyond the scope of the stochastic downscaling of RF that proved feasible. On the Aare River at Thun (Figure 9.5a), RF results align remarkably well with GWEX results and with observations (see Section 6.2.2). For the sites in the scale range of approximately 480 to 620 km^2, the RF exceedance curve in some cases lies partly higher than that of the observations (Inn at S-Chanf, Figure 9.5b; Thur at Jonschwil, Figure 9.5h), and sometimes partly lower than that of observations (Kander at Hondrich, Figure 9.5c; Kleine Emme at Emmen, Figure 9.5d). For Thur at Jonschwil, which with 493 km^2 has an area well within scope of the stochastically downscaled RF, the exceedance curve

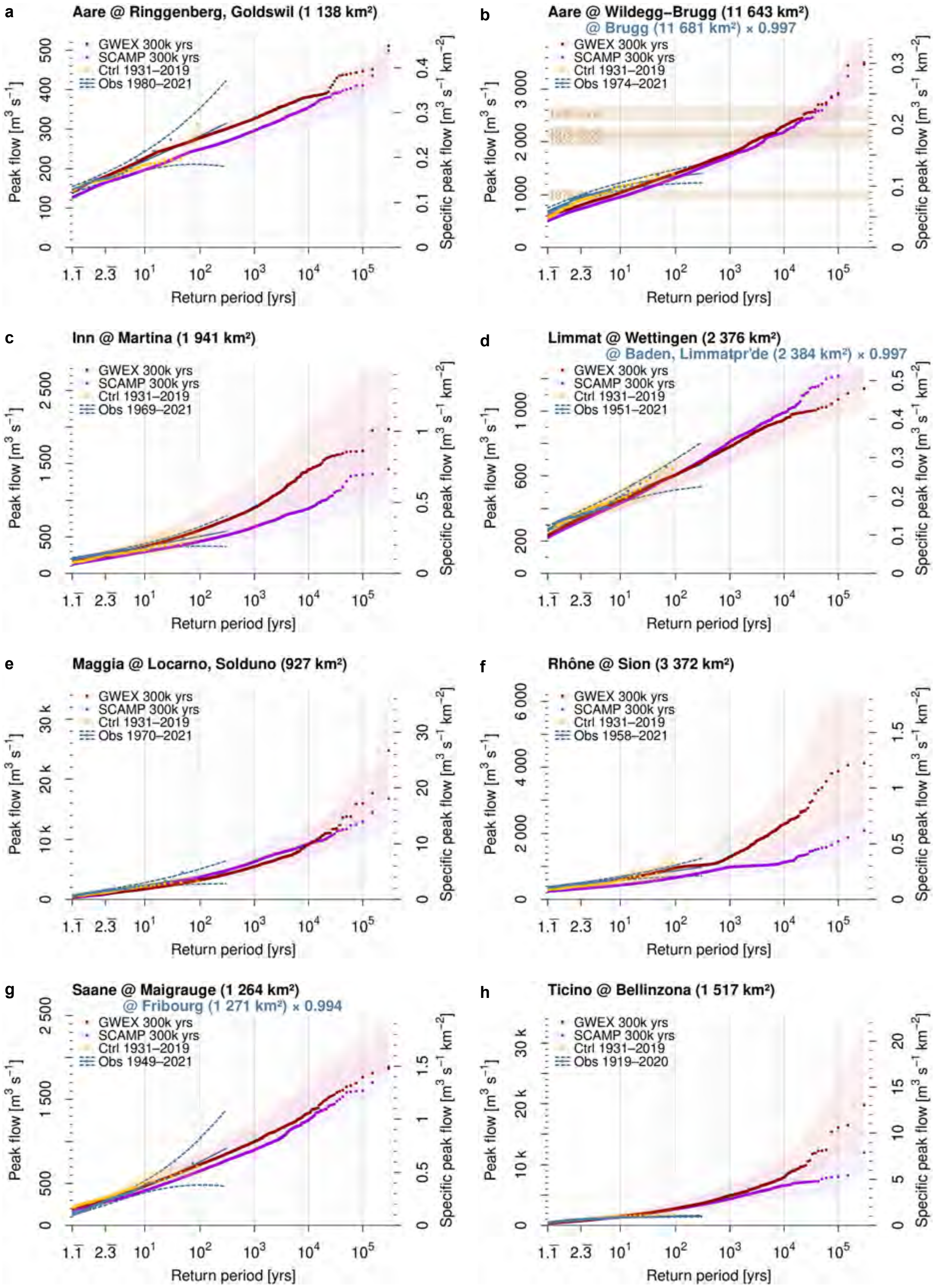

Figure 9.3: Flood estimates using SCAMP weather generator input for selected sites, showing all simulated AMFs (based on the intermediate representative parameter set) evaluated jointly. GWEX results are shown for comparison between the two approaches. The shaded area indicates the range between results obtained from the lower and the upper representative parameter sets. For details on the control simulation (Ctrl) as well as the observations (Obs) and their extrapolation, see Section 6.1.

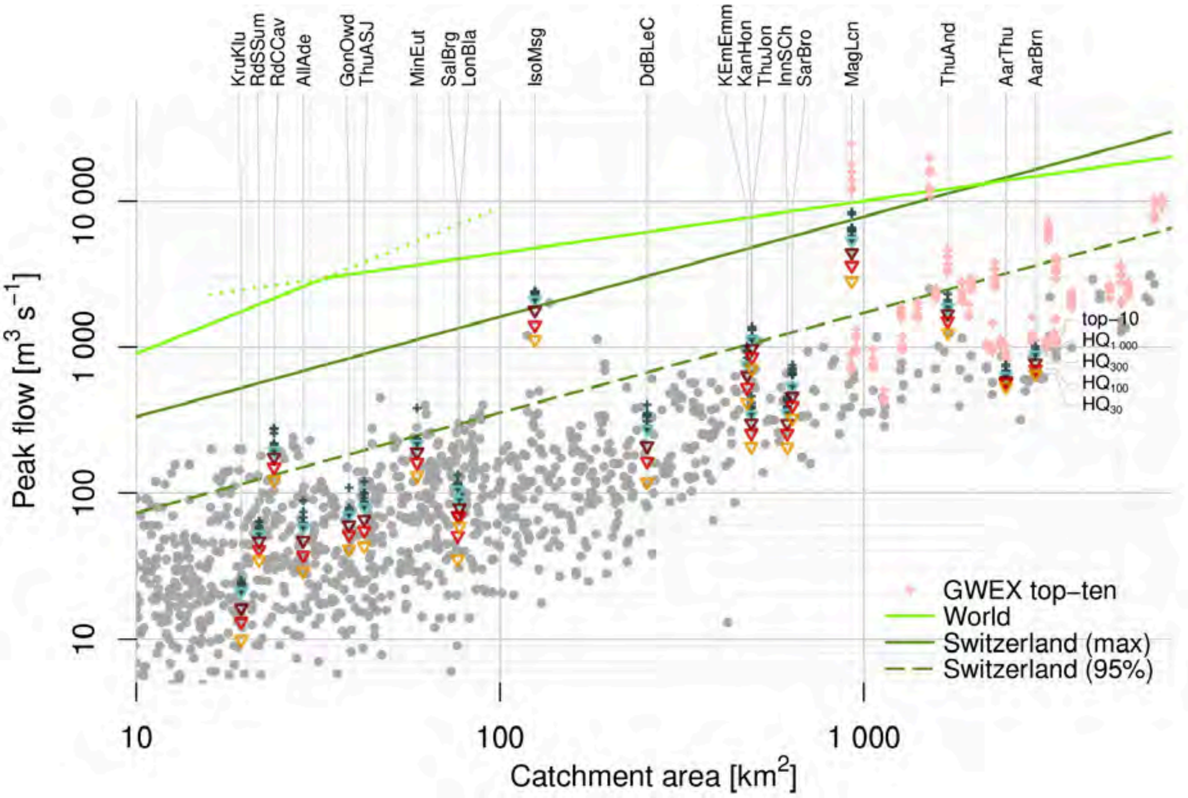

Figure 9.4: Return levels and top-10 AMFs from simulation with RF input, placed in context of maximum observed floods in Switzerland (Kienzler and Scherrer, 2018) (grey dots) including a corresponding envelope curve for all data (max) and the 95th percentile (95%). Also shown is the envelope curve for maximum floods world-wide (Herschy, 2003). The abbreviations of the sites are revealed in Table 3.1.

is markedly steeper than that of observations (Figure 9.5g), and also slightly steeper than that of the GWEX simulations (see Section 6.5.5). For the Maggia River basin, which exhibits very challenging meteorological conditions (Section 6.7.1), the RF exceedance curve agrees remarkably well with that of the observations. The highest AMFs simulated from RFs, with estimated return periods between 1 000 and 10 000 years, reach values of approximately 5 300 to 8 400 m^3 s^{-1}. The corresponding return levels estimated from GWEX are approximately 5 500 to 9 150 m^3 s^{-1}, which is higher, but not to an implausible extent. The Riale di Calneggia at Cavergno, Pontit (Figure 9.5f) is clearly beyond the scope of stochastic downscaling with a catchment area of 23.9 km^2, but is shown here as an example that occasionally good results can be achieved as well in small catchments. With the exception of Lonza at Blatten, however, all other examined test catchments with an area of less than 100 km^2 show more or less marked underestimation of return levels as compared to observations. This is expected due to the limitations of stochastic downscaling for short, intense rain events.

Note that some caution is warranted when interpreting the estimated return periods of AMFs derived from the RF simulations. Although the individual RF ensemble members are assumed independent after discarding days 1 to 15 (Jury et al., 2024), their ability to accurately represent the flood-relevant meteorological behaviour across different regions of Switzerland over extended time scales – comparable to those of the hydrometeorological observations used – has not been examined. The exceedance curves for the larger test catchments examined, however, indicate a generally plausible range when compared to observed AMFs and their extrapolation.

One interesting question where the model runs on basis of RFs can contribute crucial insights is the behaviour of the exceedance curve as the return period increases. As noted repeatedly in Chapter 6, the curves of observed AMFs sometimes exhibit a levelling off, whereas those of GWEX typically do not. Interestingly, the RF-based AMF simulations usually do not exhibit a levelling off, either, and show no tendency towards a plateau value. Moreover, the agreement between RF and GWEX-based flood

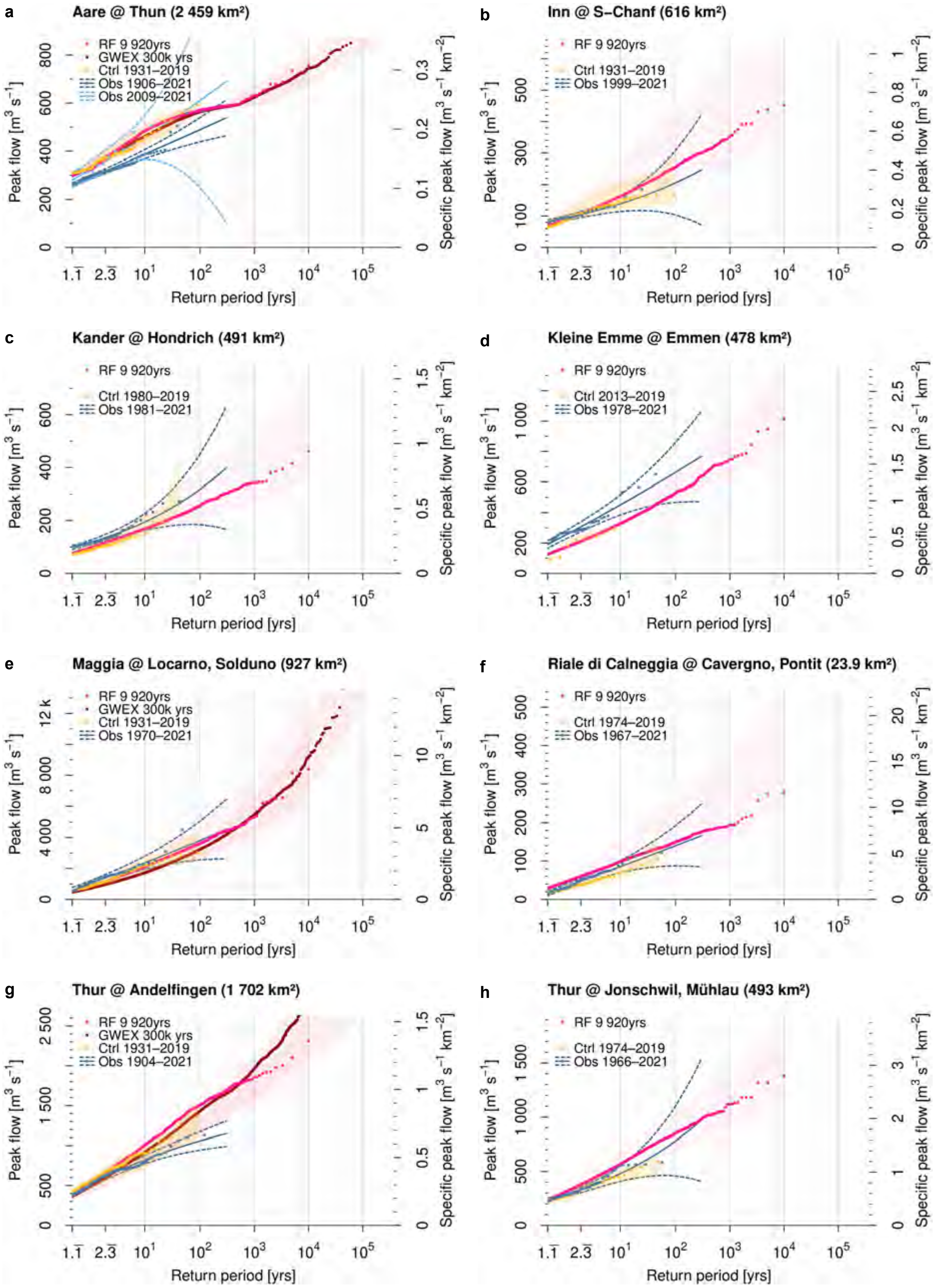

Figure 9.5: Flood estimates using RF input for selected sites, showing all simulated AMFs (based on the intermediate representative parameter set) evaluated jointly. Where available, GWEX results are shown for comparison. The shaded area indicates the range between results obtained from the lower and the upper representative parameter sets. For details on the control simulation (Ctrl) as well as the observations (Obs) and their extrapolation, see Section 6.1.

estimates in the tail is remarkably high where comparison can be made (see e.g., Figure 9.5, Panels a, e, g), particularly also in the case of the Maggia River, which shows an exceptionally heavy tail as discussed earlier. This general agreement is noteworthy because the RFs offer a more physically based approach to precipitation scenarios, whereas the GWEX weather generator employs a stochastic approach without explicit physical boundary conditions. This suggests that indeed the AMF observations – paired with extrapolation using a GEV distribution – might underestimate the potential of catchments to generate increasingly higher floods within the return periods considered in this project. This interpretation is preliminary, as the range of test catchments examined in this feasibility study to exploit RFs is limited, and the return periods covered extend only to 1 000 to 10 000 years.

Finally, it should be noted that the RFs, here available on a regular 0.5° grid (~38 km×56 km = 2 128 km^2 over Switzerland), generally offer similar information content in all grid cells. This might be advantageous for application in comparatively data-scarce regions such as Ticino, although the statistical downscaling of the RFs is impeded by low station density.

10 Advantages and limitations

10.1. Advantages

The continuous simulation (CS) approach used in this project has a number of decisive advantages over other methods of flood estimation. While some advantages have already been mentioned in Chapter 1, the following list provides a more comprehensive overview.

- The estimation of floods is carried out via extrapolation of meteorological (precipitation and temperature) data, rather than via extrapolation of hydrological (discharge) data. Meteorological observations are typically available over a longer time period than hydrological observations and can be better interpolated in space, which means that EXCH (as well as EXAR) achieve a significant overall gain in information compared to extreme value statistics of peak discharge.
- The extrapolation of meteorological conditions 1930–2019 circumvents possible challenges related to the so-called “disaster gap” of the 20th century (Pfister, 2009). The corresponding hydrological simulations contain flood extremes that clearly exceed the range covered by discharge observations and achieve orders of magnitude given in envelope curves. For the Aare River, the simulated discharges exceed those reconstructed for the past nearly 550 years.
- Assumptions about antecedent conditions and their spatial patterns are not necessary, as are assumptions about patterns of spatial and temporal development of flood-triggering meteorological conditions. Rather, a broad range of precipitation patterns possible in space and time are explored, implicitly considering a multitude of combinations of precipitation patterns with antecedent condition patterns (e.g., soil moisture, snow cover, lake levels). This reaches an extent that is not reflected in the discharge observations. As a side benefit, this also allows for more in-depth analyses concerning the role of antecedent conditions in flood generation (Staudinger et al., 2025).
- Important processes of flood generation (snow accumulation, snow melt, soil moisture storage) and routing (bank overflow, lake and floodplain retention) are conceptually represented.
- The superposition of floods from individual sub-catchments (e.g., Aare and Gürbe rivers, or Aare, Reuss and Limmat rivers), which can be decisive for the magnitude of a flood peak in a large river basin, is explored much more comprehensively, beyond what is represented in the discharge observations.
- The flood estimates are consistent in time and space across the large river basins considered and are not influenced by variations in the length of hydrological records used, or differences in the flood estimation approaches employed.
- Full continuous hydrographs are available rather than peak flow estimates only. This allows, for example, for bivariate flood statistics (Brunner et al., 2016) or identification of representative hydrograph shapes for different return periods (Staudinger et al., 2021), valuable for questions such as dam safety, levee stability or bedload transport.

Overall, the framework has been proven suitable for both estimating frequent as well as rare floods in catchments larger than roughly 1 000 km^2 (Viviroli et al., 2022), covering values required in hazard mapping and hydraulic engineering, as well as in safety assessments for critical infrastructure such as dams and weirs.

10.2. Limitations

In spite of the advantages mentioned above, the use of continuous simulations is also subject to a number of specific limitations that arise from both fundamental constraints of observational data as well as from the methods used. The following detailed overview was expanded and adapted from the the EXAR project, where a similar CS approach was used (Andres et al., 2021; Staudinger and Viviroli, 2020).

Fundamentals of the simulations:

– The hydrometeorological simulations are based on the current state of knowledge at the time of the project execution. Follow-up studies will incorporate advancements in knowledge and may lead to results that differ from those reported here.
– The simulation results are only meaningful for catchments with an area of approximately 1 000 km^2 or more. This is because the weather generators used here were developed for this scale range, with the primary aim of accurately and realistically representing of one- to multi-day precipitation events relevant to floods in large catchments. For considerably smaller catchments, where short-term precipitation events play a more important role in flood generation, the generators were neither developed nor tested in detail. A new weather generator is in development for a scale range of 10–1 000 km^2, to be used in the small catchments module of EXCH. This will be documented in a separate report.

Uncertainties in observations and their extrapolation:

– Observation networks for precipitation have a bias towards lower elevations, and measurements are subject to gauge undercatch, which is particularly marked for snow. This often calls for an elevation-dependent adjustment of precipitation, for which it is however difficult to estimate reliable and meaningful factors (see Section 3.3).
– Especially in the Ticino region, the precipitation gauge network is less dense and has shorter records than elsewhere, partly due to the characteristics of the network outside of Switzerland. At the same time, the data for this region show some exceptionally high extremes, which can be attributed to the topographical and climatological conditions. These factors limit the robustness of GWEX parameter fitting, and there remains considerable uncertainty about how rare these extremely high observations are.
– Extreme precipitation events occur very irregularly, and observed precipitation time series are only a comparatively small – and not necessarily representative – sample of what is climatologically possible. According to Zeder and Fischer (2024), there is an appreciable likelihood of decadal to centennial disaster gaps (8 % probability for no 100-year events in 250 years), whereas also event clustering may occur (11 % probability of five or more 100-year events in 250 years). The authors conclude that return levels of precipitation – the intensities associated with a specific return period – are generally underestimated.
– It is difficult to assess the realism of the precipitation patterns produced, as well as their relevance for hydrological applications. A qualitative assessment was done together with experts from MeteoSwiss within the framework of EXAR, and did not point to implausible behaviour of GWEX. However, a more formal and quantitative assessment is beyond the methods currently available. Adapting state-of-the-art methods developed for the assessment of precipitation forecasts (e.g., AghaKouchak et al., 2011; Radanovics et al., 2018) is conceivable but would require a substantial amount of development, which was beyond the possibilities of the present project.
– The time series of observed discharge contain inhomogeneities, primarily due to changing hydraulic conditions. These may be minor, repeated changes, or major, one-time alterations. A significant major change, for example, is the second Jura water correction which was completed in 1972. The flood statistics of the FOEN were updated in 2021 to take this change into account, by using only data from 1974 onwards for the Aare River downstream of Lake Biel. Another example is the flood relief tunnel on the Aare River at Thun which is operational since 2009. Caused by the higher outflow capacity of Lake Thun, the estimated return levels for floods increase for recurrence intervals of up to roughly 50–100 years.

- Estimates of the highest observed flows are subject to considerable uncertainty, not least because observed discharge is in itself based on a model, namely the stage-discharge relationship (rating curve). This relationship is poorly defined in the range of high (and low) water levels due to the rarity observations and measurement uncertainties under these conditions, leading to comparatively larger uncertainties (Westerberg et al., 2020). During large events, marked bedload transport may also influence discharge measurements. This process is not explicitly covered by hydrological models.
- For the typically available lengths of discharge observation time series, extreme value statistics are sensitive to individual events. This applies to both years with exceptionally high and exceptionally low flood discharges. In both cases, a flood estimate can change significantly with additional data points (see e.g., Klemeš, 1986). In this context, it is important to remember that also the return periods assigned to observed precipitation and discharge extremes are a statistical estimate.

Uncertainties in the simulations:

- Hydrometeorological simulations are subject to a number of uncertainties and limitations, which, due to limited computing capacities, can often only be described qualitatively. This includes model choice, model parametrization, and model calibration.
- Calibrating a hydrological model requires finding a compromise between various goals and requirements. Since the modelling chain used in this project involves unobserved weather conditions, the calibration was conducted to allow the hydrological model to reasonably simulate the entire range of flows, not only the annual peak discharges.
- Regions with widespread occurrence of karstic rock are subject to larger uncertainties, and poorer model performance must be expected. While it would be possible to implement strongly simplified karstic sources and sinks in the type of models used in this project, accurate information on the corresponding in- and outflows as well as on the recharge area – typically different from the topographical surface area – is often missing. These uncertainties and limitations are especially prevalent in the Doubs River basin, where extreme value analyses show a discontinuous behaviour (Dörfliger et al., 2004) that can hardly be reproduced in EXCH in view of the conceptual approaches used and the lack of widespread information on karst hydrology (see also Aubert et al., 2014).
- Existing information was used for determining lake regulation as far as possible. The simulations always strictly follow the implemented rules. However, the regulation handling in individual flood events cannot be fully represented, especially given that scenarios created here involve extremely rare circumstances. Deviations between regulation and actual handling are likely notable, and should be expected especially in the range of HQ_{10} to HQ_{100}.
- The uncertainties of the stage-discharge relationship mentioned above affect the calibration of the hydrological model, resulting in additional model uncertainty (Westerberg et al., 2020).
- The hydrometeorological modelling chain was validated using observed precipitation and flow events. Validation of very rare simulated extremes was not possible due to the absence of sufficiently long discharge records. However, comprehensive testing of the simulations and sensitivity analyses of the models did not indicate that the simulation results might be unrealistic.

Comparison of discharge observations and simulations:

- The flood characteristics derived from the simulation results are not directly comparable with those derived from discharge observations. The simulations are based on a weather generator that generates long series of possible precipitation and temperature patterns, which are converted into hydrographs using a catchment hydrology model. This results in an extrapolation of precipitation patterns, comprehensively exploring the climatological possibilities and translating them into discharge simulations. In contrast, flood characteristics derived from discharge observations involve an extrapolation of observed flood behaviour. Comparisons should be made cautiously, considering the uncertainties present in both observations and simulations.
- The year 2015 was used as the reference for the flow network and hydraulic structures, similar to EXAR. For example, the flood relief tunnel in Thun – which is operational since 2009 – is fully accounted for in the simulations. However, its impact on AMF exceedance curves derived from the full observational record starting 1918 remains small yet. This results in marked differences when

comparing simulated and observed exceedance curves, in this case relevant for the Aare River between lakes Thun and Biel (see Sections 6.2.2, 6.2.3 and 6.2.8).

- Meteorological observations spanning a maximum period from 1931 to 2019 were used to parametrize the weather generator. These observations do not show any levelling off or trend towards a plateau value for heavy precipitation. Consequently, neither the generated heavy precipitation scenarios nor the simulated discharge scenarios are expected to level off. The most pronounced example in this regard is the Maggia River, where this topic is discussed in more depth (see Section 6.7.1). If a plateau exists for precipitation and consequently for discharge, it should not be expected within the probability ranges examined in this project. In this context, it is important to note that the simulations on basis of reforecast, where precipitation input stems from a more physically based approach, also do not show a levelling off, at least not for the return periods of approximately 1 000 to 10 000 years that can be covered with the approach. However, observed peak flows, especially downstream of large lakes (e.g., Lake Biel), level off towards a plateau value, notably influenced by lake regulation, whereas this plateau can be broken during larger observed flood events (e.g., Aare-Murgenthal in the flood event of 2007). The same can be true for a flattening of the exceedance curve by floodplain retention, which can exhaust at discharges that have rarely been observed so far. Moreover, the choice of curve shape in extrapolating observed flows also influences the appearance of a plateau. To avoid the influence of extremely large precipitation values – of which it cannot be determined whether they fall within the range of atmospheric possibility –, Beven (2021) recommends using long CS realisations that are at least ten time times longer than the return period of interest. This rule of thumb is met in EXCH, where the long CS realisations (300 000 years) are 30 times longer than the highest return period of interest (10 000 years).
- The coincidence and superposition of flows peaks from larger rivers (e.g., Saane, Emme, Aare, Reuss, Limmat) is more comprehensively explored in the simulations than in the discharge observations. The same applies to the highly non-linear behaviour of the three Jura lakes during flood events.
- The reactivation of the Old Aare River stretch is not captured in the observational data but is included in the simulations. This partly explains why simulations show higher values for rare floods on the Aare River downstream of Lake Biel than simple extrapolation of observed AMFs would suggest.

While a comprehensive quantitative assessment of uncertainties is not feasible due to the substantial computational cost of long continuous simulations, selected aspects of uncertainty are being examined in a separate module of EXCH. In particular, two key questions are addressed for large catchments to examine some of the most relevant uncertainties: The robustness of hydrological results under changing weather generator inputs, and the robustness of the hydrological results under structural changes in the hydrological model. Results from the first question (Kritidou et al., 2024) have shown that precipitation inputs strongly contribute to the uncertainties in estimating extreme floods, whereas the sensitivity to altered precipitation inputs varies across the test catchments examined. This variability is due to differing physiographic characteristics of the catchments, although uncertainty in general increases with the return period. These and further results from this module on sensitivity will be disseminated separately.

11

Climate change and lifetime of results

The results of this project explicitly reflect current conditions. However, new hydraulic infrastructure is expected to remain in place for many decades, extending into timescales over which climate change is relevant. In addition, advances in scientific methods can be expected, potentially altering best practices and the corresponding findings. Although these challenges fundamentally affect all current flood estimates, it remains important to assess the lifetime of EXCH results, even if defining a precise time span for their validity is challenging. Climate change is a key factor in this context. The following sections outline the state of knowledge across scales, whereas it is important to note that the EXCH module presented in this report focuses on large catchments with areas of more than approximately 1 000 km^2.

Regarding heavy precipitation, both modelling and observational studies generally indicate increasing intensity and frequency across various spatial and temporal scales (Fowler et al., 2021; Sun et al., 2021; Westra et al., 2014), consistent with the Clausius-Clapeyron relationship, which describes the higher moisture-holding capacity of a warmer atmosphere (Fowler et al., 2021; Trenberth, 2011). For Switzerland, Bauer and Scherrer (2024) analysed daily and multi-day precipitation extremes from 1901 to 2023, and sub-daily to multi-day extremes from 1981 to 2023, using station data. At the decadal scale (1981–2023), they found positive trends in summer heavy precipitation intensity for short events (10 minutes to 3 hours), while the frequency of such events remained similar. In contrast, longer events (1 to 5 days) decreased in both frequency and intensity, particularly in the winter half-year. At the centennial scale (1901–2023), daily maxima and the frequency of 99^{th}-percentile events increased until the 1980s, followed by a decrease. A station-based analysis for Austria covering years 1900 to 2023 by Haslinger et al. (2025) found that over the last four decades, hourly heavy rainfall increased by 15 % (consistent with Clausius-Clapeyron scaling), while daily heavy rainfall increased by 8 % (showing alignment with atmospheric circulation indices and little correlation with air temperature).

Despite clear changes in observed precipitation, a “precipitation-flood paradox” has emerged: increases in precipitation extremes have not consistently translated into higher observed flood magnitudes worldwide (Mallakpour and Villarini, 2015; Sharma et al., 2018; Wasko et al., 2021). This apparent paradox can be resolved by differentiating by event type and flood extremeness, and accounting for other factors such as soil moisture and snow melt, which are also undergoing climate-driven changes (see, e.g., Tarasova et al., 2023). In Europe, historical records show heterogeneous trends (Blöschl et al., 2019; Hall et al., 2014; Mallakpour and Villarini, 2015), although for extreme events, increases in precipitation have been associated with larger and more consistent increases in flood magnitudes (Bertola et al., 2020; Brunner et al., 2021; Wasko et al., 2021). For Austria, a recent analysis of observations showed that floods in small catchments (<50 km^2) increased by 25 % over the past four decades, associated with the aforementioned 15 % increase in hourly heavy rainfall but showing a stronger response (Haslinger et al., 2025). By contrast, medium and large catchments (>500 km^2) in Austria experienced smaller increases of approximately 8 %, closely associated with a similar increase in daily heavy rainfall but showing little direct relationship to temperature increases and regionally modulated by soil moisture changes (Haslinger et al., 2025).

Projections for Europe show intensification of precipitation extremes across all seasons and regions, with the strongest increases in northern Europe and during winter. In southern Europe, total precipitation is projected to decline, especially in summer, while summertime extremes are projected to intensify (Rajczak and Schär, 2017). For the Alpine region, convection-permitting models recently confirmed projected decreases in mean precipitation alongside increases in hourly intensities, qualitatively agreeing with observed daily and hourly trends over recent decades (Estermann et al., 2025).

Looking at projections for floods, Brunner et al. (2021) suggested that moderately extreme events may be mitigated by reduced soil moisture due to increased evaporation, whereas very extreme events can rapidly saturate soils and generate larger floods (see also Sharma et al., 2018; Wasko et al., 2021). The strongest increases are expected for rare events that exceed the range covered by direct observations, specifically floods with return periods well above 50–100 years (Brunner et al., 2021). Palaeoflood records from the European Alps spanning up to 10 000 years also indicate a complex response of floods to warming, suggesting that a warming of 0.5–1.2 °C led to a 25–50 % decrease in the frequency of floods with return periods of 10 to 100 years, while an increase was noted for floods with return periods of 100 years or more, particularly in small alpine catchments (Wilhelm et al., 2022).

For Switzerland, Hydro-CH2018 (Bundesamt für Umwelt (BAFU), 2021a) examined projected floods with return periods of up to 30 years and did not identify a clear signal, as projected changes were uncertain in the context of strong temporal variability – particularly under a stringent climate change mitigation scenario (RCP2.6) and for rare events (see Martius et al., 2020; Molnar et al., 2020). Under high radiative forcing (RCP8.5), the projections indicated a slight but not statistically significant increase in flood frequency and intensity toward the end of the 21st century (Mülchi et al., 2020). Projections also showed considerable spatial variability: some catchments were very sensitive to changes in precipitation and air temperature and showed noticeably larger floods, while others showed negligible or even statistically significant decreasing trends, such as glaciated catchments (Molnar et al., 2020). These unclear trends reflect a complex interplay of numerous and sometimes opposing factors, limitations of the CH2018 scenarios and the strong temporal variability of flood occurrence linked to internal (irreducible) climate variability, especially for large-scale events (Bundesamt für Umwelt (BAFU), 2021a; Molnar et al., 2020; Moraga et al., 2022).

Determining an exact lifetime of EXCH results under these conditions remains challenging, not least given internal climate variability (Lehner and Deser, 2023), which strongly influences the occurrence of rare precipitation extremes (Zeder and Fischer, 2024) and associated floods. For the large catchments considered in this report, it can be assumed that over periods of approximately five to ten years, variability in regional climate – typically spanning one or more decades (Redmond et al., 2010; Schmocker-Fackel and Naef, 2010a,b) – outweighs systematic change in climate, even though this timespan should be regarded as an assessment rather than a precise estimate. Over the lifetime of new hydraulic infrastructure, however, which spans multiple decades, climate change impacts must be expected, even if they cannot yet be quantified with high confidence.

In conclusion, maintaining an up-to-date assessment of EXCH result validity requires periodic reappraisal that reflects the evolving state of knowledge and integrates the latest scientific literature. For operational purposes, such reappraisal is recommended approximately every five years and should also be aligned with major research initiatives similar to CC-Hydro (Bundesamt für Umwelt (BAFU), 2012) or Hydro-CH2018 (Bundesamt für Umwelt (BAFU), 2021a), and particularly also with the most recent CH2025 climate scenarios[1] and any hydrological studies based on them.

[1] https://www.klima-ch2025.ch

12

Summary and outlook

A comprehensive continuous simulation model chain has been presented and examined. In the vast majority of cases, control simulations have shown good agreement with observations and corresponding AMFs, and differences have been explained with changes in river engineering for some sites. However, underestimations may occur for catchments near the lower threshold of the applicable scale (approximately 1 000 km^2), and where a comparatively small tributary (considerably smaller than ~1 000 km^2) joins after a large lake. For the hydrological simulations derived from the weather scenarios, examination of results has not revealed implausible behaviour. Overall, use of the GWEX weather generator leads to best results, whereas the SCAMP weather generator tends to underestimate peak flows. The evaluation of reforecasts suggests that the range of AMFs – spanning from frequent to extreme events – simulated with GWEX is of plausible magnitude, and that the continued increase of AMFs as the return period approaches 1 000 to 10 000 years may be realistic.

The flood estimates derived in this project were shown to be valuable across a wide range of return periods, from comparatively frequent floods (recurrence intervals of around 10 years) to increasingly rare (around 100 years) and extreme floods (around 1 000 to 10 000 years), with uncertainties increasing as the recurrence interval increases. The majority of gauging sites and run-of-river dams with a catchment area greater than approximately 1 000 km^2 are covered directly or by a nearby output node. While it is possible to implement further output nodes, this would potentially require adjustments to the sub-catchment delineation and corresponding model parameters. Depending on the site, it may also require additional hydraulic simulations to determine modifications to hydrological routing.

In spite of the positive evaluation summarised above, it does not appear advisable to dismiss current flood estimates in favour of values derived from this project where available: Each approach to flood estimation has its own strengths and limitations, and it is therefore suggested to view EXCH results as an alternative that circumvents some of the limitations of common flood estimation methods while also being subject to specific limitations and uncertainties. Ideally, EXCH results should therefore be used in conjunction with other approaches. In any case, important decisions regarding design or safety values should appraise all available approaches for a given case. Where notable disagreements arise, a more detailed hydrological study should be conducted, potentially including customised sensitivity analyses of the EXCH results.

References

AghaKouchak, A., A. Behrangi, S. Sorooshian, K. Hsu, and E. Amitai (2011). Evaluation of satellite-retrieved extreme precipitation rates across the central United States. *Global Biogeochemical Cycles* 116(D2). DOI: 10.1029/2010JD014741.

Amt für Umwelt, Kanton Solothurn (2022). *Ein Fluss verbindet: Hochwasserschutz und Revitalisierung entlang der Solothurner Emme (2008–2020)*. Solothurn.

Andres, N., A. Badoux, V. Dang, B. Hingray, M. Müller, M. Pfäffli, S. Schwab, A. Sutter, D. Viviroli, and C. Hegg (2021). Diskussion der Unsicherheiten und Limitationen. In: *Grundlagen Extremhochwasser Aare*. Ed. by N. Andres, N. Steeb, A. Badoux, and C. Hegg. WSL Berichte. Birmensdorf, 222–226.

Andres, N., G. Lieberherr, I. V. Sideris, F. Jordan, and M. Zappa (2016). From calibration to real-time operations: an assessment of three precipitation benchmarks for a Swiss river system. *Meteorological Applications* 23(3), 448–461. DOI: https://doi.org/10.1002/met.1569. eprint: https://rmets.onlinelibrary.wiley.com/doi/pdf/10.1002/met.1569.

Aubert, Y., P. Arnaud, P. Ribstein, and J.-A. Fine (2014). La méthode SHYREG débit—application sur 1605 bassins versants en France métropolitaine. *Hydrological Sciences Journal* 59(5), 993–1005. DOI: 10.1080/02626667.2014.902061.

Baer, P. and S. Schwab (2020). *Extremhochwasser an der Aare: Detailbericht B Projekt EXAR. Historische Hochwasser*. Zollikofen.

Bárdossy, A. and E. J. Plate (1992). Space-time model for daily rainfall using atmospheric circulation patterns. *Water Resources Research* 28(5), 1247–1259. DOI: 10.1029/91WR02589.

Bauer, V. M. and S. C. Scherrer (2024). The observed evolution of sub–daily to multi–day heavy precipitation in Switzerland. *Atmospheric Science Letters* 25(9). DOI: 10.1002/asl.1240.

Baumgartner, E., M.-O. Boldi, C. Kan, and S. Schick (2013). Hochwasserstatistik am BAFU – Diskussion eines neuen Methodensets. *wasser, energie, luft* 105(2), 103–110.

Baumgartner, M., D. Devanthéry, and M. Kummer (2007). *Wasserentnahmen und -rückgaben*. Hydrologischer Atlas der Schweiz. Bern: Bundesamt für Umwelt BAFU, Tafel 5.10.

Beguería, S., S. M. Vicente–Serrano, M. Tomás–Burguera, and M. Maneta (2016). Bias in the variance of gridded data sets leads to misleading conclusions about changes in climate variability. *International Journal of Climatology* 36(9), 3413–3422. DOI: 10.1002/joc.4561.

Bergström, S. (1972). *Utveckling och tillämpning av en digital avrinningsmodell*. Vol. 22. SMHI Notiser och preliminära rapporter, serie HYDROLOGI. Norrköping. URL: https://www.smhi.se/polopoly_fs/1.83595!/Menu/general/extGroup/attachmentColHold/mainCol1/file/Notiser_prel_rapporter_hydrologi_22.pdf.

— (1992). *The HBV Model – its structure and applications*. Vol. 4. Reports Hydrology. Norrköping: Swedish Meteorological and Hydrological Institute (SMHI) /Sveriges Meteorologiska och Hydrologiska Institut (SMHI).

Bertola, M., A. Viglione, D. Lun, J. Hall, and G. Blöschl (2020). Flood trends in Europe: are changes in small and big floods different? *Hydrology and Earth System Sciences* 24(4), 1805–1822. DOI: 10.5194/hess-24-1805-2020.

Bertola, M. et al. (2023). Megafloods in Europe can be anticipated from observations in hydrologically similar catchments. *Nature Geoscience* 16(11), 982–988. DOI: 10.1038/s41561-023-01300-5.

Beven, K. (2021). Issues in generating stochastic observables for hydrological models. *Hydrological Processes* 35(6). DOI: 10.1002/hyp.14203.

Bezzola, G. R. and W. Ruf, eds. (2009). *Ereignisanalyse Hochwasser August 2007: Analyse der Meteo- und Abflussvorhersagen; vertiefte Analyse der Hochwasserregulierung der Jurarandgewässer*. Vol. 0927. Umwelt-Wissen. Bern: BAFU.

Blazkova, S. and K. J. Beven (2004). Flood frequency estimation by continuous simulation of subcatchment rainfalls and discharges with the aim of improving dam safety assessment in a large basin in the Czech Republic. *Journal of Hydrology* 292, 153–172.

Blöschl, G. et al. (2019). Changing climate both increases and decreases European river floods. *Nature*. ISSN: 1476-4687. DOI: 10.1038/s41586-019-1495-6.

Breinl, K. and G. Di Baldassarre (2019). Space-time disaggregation of precipitation and temperature across different climates and spatial scales. *Journal of Hydrology: Regional Studies* 21, 126–146. DOI: 10.1016/j.ejrh.2018.12.002.

Brönnimann, S., P. Stucki, J. Franke, V. Valler, Y. Brugnara, R. Hand, L. C. Slivinski, G. P. Compo, P. D. Sardeshmukh, M. Lang, and B. Schaefli (2022). Influence of warming and atmospheric circulation changes on multidecadal European flood variability. *Climate of the Past* 18(4), 919–933. DOI: 10.5194/cp-18-919-2022.

Brönnimann, S. et al. (2018). *1868 – das Hochwasser, das die Schweiz veränderte: Ursachen, Folgen und Lehren für die Zukunft*. Vol. G94. Geographica Bernensia. Bern: Geographica Bernensia.

Brunner, M. I., J. Seibert, and A.-.-C. Favre (2016). Bivariate return periods and their importance for flood peak and volume estimation. *WIREs Water* 3(6), 819–833. DOI: 10.1002/wat2.1173.

Brunner, M. I., D. L. Swain, R. R. Wood, F. Willkofer, J. M. Done, E. Gilleland, and R. Ludwig (2021). An extremeness threshold determines the regional response of floods to changes in rainfall extremes. *Communications Earth & Environment* 2(1), 173. DOI: 10.1038/s43247-021-00248-x.

Buishand, T. A. and T. Brandsma (2001). Multisite simulation of daily precipitation and temperature in the Rhine Basin by nearest-neighbor resampling. *Water Resources Research* 37(11), 2761–2776. DOI: 10.1029/2001WR000291.

Bundesamt für Energie (BFE) (2022). *Füllungsgrad der Speicherseen, Sonntag 24h, Wochenbericht Speicherinhalt*. URL: https://opendata.swiss/de/dataset/fullungsgrad-der-speicherseen-sonntag-24h-wochenbericht-speicherinhalt (visited on 2.5.2022).

Bundesamt für Landestopographie (Swisstopo) (2005). *DHM25: Das digitale Höhenmodell der Schweiz*. Wabern.

Bundesamt für Umwelt (BAFU), ed. (2012). *Auswirkungen der Klimaänderung auf Wasserressourcen und Gewässer: Synthesebericht zum Projekt "Klimaänderung und Hydrologie in der Schweiz" (CCHydro)*. Vol. 1217. Umwelt-Wissen. Bern.

— (2013). *Residual flow map*. URL: https://www.bafu.admin.ch/bafu/en/home/topics/water/state/data/residual-flow-map--requesting-data-on-the-water-withdrawn-and-re.html (visited on 2.5.2022).

— (2017a). *Hochwasserstatistik Stationsbericht Aare - Ringgenberg, Goldswil*. URL: https://www.hydrodaten.admin.ch/documents/Hochwasserstatistikberichte/2457_hq_Bericht.pdf (visited on 25.10.2024).

— (2017b). *Hochwasserstatistik Stationsbericht Rhein - Basel*. URL: https://www.hydrodaten.admin.ch/documents/Hochwasserstatistikberichte/2289_hq_Bericht.pdf (visited on 25.10.2024).

— (2017c). *Hochwasserstatistik Stationsbericht Rhône - Porte du Scex*. URL: https://www.hydrodaten.admin.ch/documents/Hochwasserstatistikberichte/2009_hq_Bericht.pdf (visited on 20.11.2024).

— (2017d). *Hochwasserstatistik Stationsbericht Rhône - Sion*. URL: https://www.hydrodaten.admin.ch/documents/Hochwasserstatistikberichte/2011_hq_Bericht.pdf (visited on 20.11.2024).

— (2020a). *Hochwasserstatistik Stationsbericht Aare - Bern*. URL: https://www.hydrodaten.admin.ch/documents/Hochwasserstatistikberichte/2135_hq_Bericht.pdf (visited on 25.10.2024).

— (2020b). *Hochwasserstatistik Stationsbericht Aare - Thun*. URL: https://www.hydrodaten.admin.ch/documents/Hochwasserstatistikberichte/2030_hq_Bericht.pdf (visited on 25.10.2024).

— ed. (2021a). *Auswirkungen des Klimawandels auf die Schweizer Gewässer: Hydrologie, Gewässerökologie und Wasserwirtschaft*. Umwelt-Wissen 2101. Bern.

— (2021b). *Hochwasserstatistik Thur - Andelfingen*. URL: https://www.hydrodaten.admin.ch/documents/Hochwasserstatistik/2044hq.pdf (visited on 8.11.2022).

— (2022). *Die 5 Gefahrenstufen für Hochwasser und Verhaltensempfehlungen*. URL: https://www.hydrodaten.admin.ch/de/die-5-gefahrenstufen-fuer-hochwasser (visited on 28.10.2024).

Castellarin, A. (2007). Probabilistic envelope curves for design flood estimation at ungauged sites. *Water Resources Research* 43(4), W04406. DOI: 10.1029/2005WR004384.
Castellarin, A., R. M. Vogel, and N. C. Matalas (2005). Probabilistic behavior of a regional envelope curve. *Water Resources Research* 41(6). DOI: 10.1029/2004WR003042.
— (2007). Multivariate probabilistic regional envelopes of extreme floods. *Journal of Hydrology* 336(3-4), 376–390. DOI: 10.1016/j.jhydrol.2007.01.007.
Chardon, J., B. Hingray, A.-C. Favre, P. Autin, J. Gailhard, I. Zin, and C. Obled (2014). Spatial Similarity and Transferability of Analog Dates for Precipitation Downscaling over France. *Journal of Climate* 27(13), 5056–5074. DOI: 10.1175/JCLI-D-13-00464.1.
Chardon, J., A.-C. Favre, and B. Hingray (2016). Effects of Spatial Aggregation on the Accuracy of Statistically Downscaled Precipitation Predictions. *Journal of Hydrometeorology* 17(5), 1561–1578.
Chardon, J., B. Hingray, and A.-C. Favre (2018). An adaptive two-stage analog/regression model for probabilistic prediction of small-scale precipitation in France. *Hydrology and Earth System Sciences* 22(1), 265–286. DOI: 10.5194/hess-22-265-2018.
Davolio, S., M. Vercellino, M. M. Miglietta, L. Drago Pitura, S. Laviola, and V. Levizzani (2023). The influence of an atmospheric river on a heavy precipitation event over the western Alps. *Weather and Climate Extremes* 39, 100542. DOI: 10.1016/j.wace.2022.100542.
Dörfliger, N., J. L. Pinault, V. Petit, and D. Jauffret (2004). *Systèmes karstiques et crues du Doubs: Rapport final: Étude réalisée dans le cadre du projet de recherche BRGM KARSTEAU*.
Électricité de France (EDF) (2002). *Calcul du débit millénal à Fessenheim par la méthode du renouvellement dans le cadre de la réactualisation de la CMS du site*.
Estermann, R., J. Rajczak, P. Velasquez, R. Lorenz, and C. Schär (2025). Projections of Heavy Precipitation Characteristics Over the Greater Alpine Region Using a Kilometer–Scale Climate Model Ensemble. *Journal of Geophysical Research: Atmospheres* 130(2). ISSN: 2169-897X. DOI: 10.1029/2024JD040901.
European Environment Agency (EEA) (2018). *European Digital Elevation Model (EU-DEM), version 1.1*. URL: https://land.copernicus.eu/pan-european/satellite-derived-products/eu-dem/eu-dem-v1.1?tab=metadata.
European Union Copernicus Land Monitoring Service (Copernicus) (2020). *CORINE Land Cover 2000 (raster 100 m)*. DOI: 10.2909/ddacbd5e-068f-4e52-a596-d606e8de7f40.
Evin, G., J. Blanchet, E. Paquet, F. Garavaglia, and D. Penot (2016). A regional model for extreme rainfall based on weather patterns subsampling. *Journal of Hydrology* 541, 1185–1198. DOI: 10.1016/j.jhydrol.2016.08.024.
Evin, G., A.-C. Favre, and B. Hingray (2018). Stochastic generation of multi-site daily precipitation focusing on extreme events. *Hydrology and Earth System Sciences* 22(1), 655–672. DOI: 10.5194/hess-22-655-2018.
— (2019). Stochastic generators of multi-site daily temperature: comparison of performances in various applications. *Theoretical and Applied Climatology* 135(3-4), 811–824. DOI: 10.1007/s00704-018-2404-x.
Evin, G., M. Le Lay, C. Fouchier, D. Penot, F. Colleoni, A. Mas, P.-A. Garambois, and O. Laurantin (2024). Evaluation of hydrological models on small mountainous catchments: impact of the meteorological forcings. *Hydrology and Earth System Sciences* 28(1), 261–281. DOI: 10.5194/hess-28-261-2024.
Fallot, J.-M., J.-A. Hertig, R. G. Receanu, F. Zeimetz, J.-M. Fallot, J.-A. HERTIG, R. G. Receanu, and F. Zeimetz (2017). Détermination des précipitations et des crues extrêmes en suisse à l'aide de la méthode PMP-PMF. *Bulletin de la Société Géographique de Liège* 68, 77–96. DOI: 10.25518/0770-7576.4556.
Fantini, A., F. Raffaele, C. Torma, S. Bacer, E. Coppola, F. Giorgi, B. Ahrens, C. Dubois, E. Sanchez, and M. Verdecchia (2018). Assessment of multiple daily precipitation statistics in ERA-Interim driven Med-CORDEX and EURO-CORDEX experiments against high resolution observations. *Climate Dynamics* 51(3), 877–900. DOI: 10.1007/s00382-016-3453-4.
Farinotti, D., S. Usselmann, M. Huss, A. Bauder, and M. Funk (2012). Runoff evolution in the Swiss Alps: projections for selected high-alpine catchments based on ENSEMBLES scenarios. *Hydrological Processes* 26(13), 1909–1924. DOI: 10.1002/hyp.8276.

Felder, G. and R. Weingartner (2016). An approach for the determination of precipitation input for worst-case flood modelling. *Hydrological Sciences Journal* 61(14), 2600–2609. DOI: 10.1080/02626667.2016.1151980.

— (2017). Assessment of deterministic PMF modelling approaches. *Hydrological Sciences Journal* 62(10), 1591–1602. DOI: 10.1080/02626667.2017.1319065.

Fernandez, C. and M. F. J. Steel (1998). On Bayesian Modeling of Fat Tails and Skewness. *Journal of the American Statistical Association* 93(441), 359–371. DOI: 10.2307/2669632.

Fowler, H. J. et al. (2021). Anthropogenic intensification of short-duration rainfall extremes. *Nature Reviews Earth & Environment* 2(2), 107–122. DOI: 10.1038/s43017-020-00128-6.

Frei, C. and F. A. Isotta (2019). Ensemble Spatial Precipitation Analysis From Rain Gauge Data: Methodology and Application in the European Alps. *Journal of Geophysical Research: Atmospheres* 121(4), 3807. DOI: 10.1029/2018JD030004.

Freudiger, D., I. Kohn, J. Seibert, K. Stahl, and M. Weiler (2017). Snow redistribution for the hydrological modeling of alpine catchments. *Wiley Interdisciplinary Reviews: Water* 15, e1232. DOI: 10.1002/wat2.1232.

Freudiger, D., M. Vis, and J. Seibert (2021). *Quantifying the contributions to discharge of snow and glacier melt: Hydro-CH2018 project*.

Fukutome, S., A. Schindler, and A. Capobianco (2018). *MeteoSwiss extreme value analyses: User manual and documentation*.

Gangopadhyay, S., M. P. Clark, B. Rajagopalan, and M. Clark (2005). Statistical downscaling using K -nearest neighbors. *Water Resources Research* 41(2), W02024. DOI: 10.1029/2004wr003444.

García Hernández, J. (2011). *Flood management in a complex river basin with a real-time decision support system based on hydrological forecasts*. Ed. by A. Schleiss. Communications du Laboratoire de Constructions Hydrauliques Communication 48. EPFL, Lausanne.

García Hernández, J., A. Foehn, J. Fluixá-Sanmartín, B. Roquier, T. Brauchli, J. Paredes Arquiola, and G. de Cesare (2020). *RS MINERVE – Technical manual, v2.25*. URL: https://crealp.ch/wp-content/uploads/2021/09/rsminerve_technical_manual_v2.25.pdf.

Gervais, M., L. B. Tremblay, J. R. Gyakum, and E. Atallah (2014). Representing Extremes in a Daily Gridded Precipitation Analysis over the United States: Impacts of Station Density, Resolution, and Gridding Methods. *Journal of Climate* 27(14), 5201–5218. DOI: 10.1175/JCLI-D-13-00319.1.

Gottardi, F., C. Obled, J. Gailhard, and E. Paquet (2012). Statistical reanalysis of precipitation fields based on ground network data and weather patterns: Application over French mountains. *Journal of Hydrology* 432-433, 154–167. DOI: 10.1016/j.jhydrol.2012.02.014.

Grebner, D., T. Roesch, and M. Schwarb (1999). *Extreme Gebietsniederschläge unterschiedlicher Dauer und Wiederkehrperioden 1981–1993*. Hydrologischer Atlas der Schweiz. Bern: Bundesamt für Umwelt BAFU, Tafel 2.5.

Gringorten, I. I. (1963). A plotting rule for extreme probability paper. *Global Biogeochemical Cycles* 68(3), 813–814. DOI: 10.1029/JZ068i003p00813.

Gupta, H. V., H. Kling, K. K. Yilmaz, and G. F. Martínez (2009). Decomposition of the mean squared error and NSE performance criteria: Implications for improving hydrological modelling. *Journal of Hydrology* 377(1–2), 80–91. DOI: 10.1016/j.jhydrol.2009.08.003.

Hall, J. et al. (2014). Understanding flood regime changes in Europe: a state-of-the-art assessment. *Hydrology and Earth System Sciences* 18(7), 2735–2772. DOI: 10.5194/hess-18-2735-2014.

Hamon, W. R. (1961). Estimating potential evapotranspiration. *Journal of the Hydraulics Division-ASCE*(87), 107–120. DOI: 10.1061/JYCEAJ.0000599.

Haslinger, K., K. Breinl, L. Pavlin, G. Pistotnik, M. Bertola, M. Olefs, M. Greilinger, W. Schöner, and G. Blöschl (2025). Increasing hourly heavy rainfall in Austria reflected in flood changes. *Nature* 639(8055), 667–672. DOI: 10.1038/s41586-025-08647-2.

Hegg, C., F. Schmid, and E. Frick (2002). *Hochwasser 2000 – Les crues 2000. Ereignisanalyse/Fallbeispiele – Analyse des événements/Cas exemplaires*. Ed. by F. O. of EnvironmentFOEN. Vol. 2. Berichte des BWG, Serie Wasser. Bern: Bundesamt für Wasser und Geologie (BWG).

Hegnauer, M., J. J. Beersma, van den Boogaard, H. F. P., T. A. Buishand, and R. H. Passchier (2014). *Generator of Rainfall and Discharge Extremes (GRADE) for the Rhine and Meuse basins: Final report of GRADE 2.0*. URL: https://publications.deltares.nl/1209424_004_0018.pdf.

Herschy, R. W. (2002). The world's maximum observed floods. *Flow Measurement and Instrumentation* 13(5-6), 231–235. DOI: 10.1016/S0955-5986(02)00054-7.
— (2003). *World Catalogue of Maximum Observed Floods*. Vol. 284. IAHS publication. Wallingford: IAHS Press. ISBN: 1-901502-47-3.
Horton, P., B. Schaefli, and M. Kauzlaric (2022). Why do we have so many different hydrological models? A review based on the case of Switzerland. *WIREs Water* 9(1), e1574. DOI: 10.1002/wat2.1574.
Hosking, J. R. M. and J. R. Wallis (1993). Some useful statistics in regional frequency analysis. *Water Resources Research* 29(2), 271–281. DOI: 10.1029/92WR01980.
— (1997). *Regional frequency analysis: An approach based on L-moments*. Cambridge: Cambridge University Press. ISBN: 0-511-52944-9. DOI: 10.1017/CBO9780511529443.
Hunziker, Zarn & Partner (2017). *Gefahrenkartierung Naturgefahren Thur: Technischer Bericht*. Aarau.
INGE Hydrologie Alpenrhein (2003). *Hydrologie Alpenrhein: Zusammenfassender Bericht*. Zürich, Domat/Ems and Sargans.
Institut für Wasser und Gewässerentwicklung (IWG) (2010). *Ermittlung von extremen Abflüssen für die Staustufen Gambsheim und Iffezheim*. Karlsruhe.
Jordan, F. (2007). *Modèle de prévision et de gestion des crues - Optimisation des opérations des aménagements hydroélectriques à accumulation pour la réduction des débits de crue*. Ed. by A. Schleiss. Communications du Laboratoire de Constructions Hydrauliques Communication 29. EPFL, Lausanne.
Jordan, F., J.-L. Boillat, J. Dubois, and A. Schleiss (2004). MINERVE, a tool for flood prediction and management of the Rhône river catchment area. In: *Wasserbauliche Mitteilungen*. Ed. by I. für Wasserbau und Technische Hydromechanik der TU Dresden. Vol. 27. Dresden, 227–236. URL: https://izw.baw.de/publikationen/dresdner-wasserbauliche-mitteilungen/0/22_Heft_27_MINERVE_a_tool_for_flood_prediction.pdf.
Jury, M. W., T. Lichtenegger, I. Kohlhauser, H. Truhetz, and D. Maraun (2024). *Reforecasts development: Final working report*.
Kauzlaric, M., L. Keller, M. Pfäffli, A. Senoner, M. Staudinger, and D. Viviroli (2020). Sensitivity and plausibility of hydrological simulations. In: *Extremhochwasser an der Aare*. Ed. by M. Staudinger and D. Viviroli. Zürich: University of Zürich, 22–95.
Kauzlaric, M., G. Nicolet, and D. Viviroli (2021a). Entwicklung hydrometeorologischer Grundlagen. In: *Grundlagen Extremhochwasser Aare*. Ed. by N. Andres, N. Steeb, A. Badoux, and C. Hegg. WSL Berichte. Birmensdorf, 29–37.
Kauzlaric, M., C. Whealton, P. Baer, and D. Viviroli (2021b). Resultate der hydrometeorologischen Grundlagen. In: *Grundlagen Extremhochwasser Aare*. Ed. by N. Andres, N. Steeb, A. Badoux, and C. Hegg. WSL Berichte. Birmensdorf, 71–80.
Kelder, T., T. I. Marjoribanks, L. J. Slater, C. Prudhomme, R. L. Wilby, J. Wagemann, and N. Dunstone (2022). An open workflow to gain insights about low–likelihood high–impact weather events from initialized predictions. *Meteorological Applications* 29(3). DOI: 10.1002/met.2065.
Kelder, T., M. Müller, L. J. Slater, T. I. Marjoribanks, R. L. Wilby, C. Prudhomme, P. Bohlinger, L. Ferranti, and T. Nipen (2020). Using UNSEEN trends to detect decadal changes in 100-year precipitation extremes. *npj Climate and Atmospheric Science* 3(1). DOI: 10.1038/s41612-020-00149-410.1029/1999WR900330.
Kienzler, P. M. and S. Scherrer (2018). *Verzeichnis grosser Hochwasserabflüsse in Schweizerischen Einzugsgebieten: Auswertung und graphische Aufbereitung*. Reinach. URL: https://www.bafu.admin.ch/bafu/de/home/themen/wasser/zustand/wasser--methoden/grosse_hochwasserabflusse-2.html.
Klemeš, V. (1986). Dilettantism in hydrology: Transition or destiny? *Water Resources Research* 22(9S), 177S–188S. DOI: 10.1029/WR022i09Sp0177S.
Klingler, C., K. Schulz, and M. Herrnegger (2021). LamaH-CE: LArge-SaMple DAta for Hydrology and Environmental Sciences for Central Europe. *Earth System Science Data* 13(9), 4529–4565. DOI: 10.5194/essd-13-4529-2021.
Kochendorfer, J., R. Rasmussen, M. Wolff, B. Baker, M. E. Hall, T. Meyers, S. Landolt, A. Jachcik, K. Isaksen, R. Brækkan, and R. Leeper (2017). The quantification and correction of wind-induced

precipitation measurement errors. *Hydrology and Earth System Sciences* 21(4), 1973–1989. DOI: 10.5194/hess-21-1973-2017.

Kritidou, E., M. Kauzlaric, M. Staudinger, G. Evin, B. Hingray, M. J. P. Vis, J. Seibert, and D. Viviroli (2024). Impact of different weather generator scenarios on extreme flood estimates in Switzerland. *Stochastic Environmental Research and Risk Assessment*. Submitted.

Lang, M. (2020). *Expertise sur l'hydrologie du Rhin sur les biefs de Gambsheim et Iffezheim*. Tech. rep. INRAE. URL: https://hal.science/hal-03295501.

Lang, M., J. Le Coz, B. Renard, and M. Darienzo (2025). Accounting for historical data uncertainty in flood frequency analysis: the Upper Rhine River. *Journal of Hydrology*, 133480. DOI: 10.1016/j.jhydrol.2025.133480.

Lavers, D. A., S. Harrigan, and C. Prudhomme (2021). Precipitation Biases in the ECMWF Integrated Forecasting System. *Journal of Hydrometeorology* 22(5), 1187–1198. DOI: 10.1175/JHM-D-20-0308.1.

Lehner, F. and C. Deser (2023). Origin, importance, and predictive limits of internal climate variability. *Environmental Research: Climate* 2(2), 023001. DOI: 10.1088/2752-5295/accf30.

Lindström, G., B. Johansson, M. Persson, M. Gardelin, and S. Bergström (1997). Development and test of the distributed HBV-96 hydrological model. *Journal of Hydrology* 201(1–4), 272–288. DOI: 10.1016/S0022-1694(97)00041-3.

Mallakpour, I. and G. Villarini (2015). The changing nature of flooding across the central United States. *Nature Climate Change* 5(3), 250–254. DOI: 10.1038/nclimate2516.

Maniak, U. (2005). *Hydrologie und Wasserwirtschaft: Eine Einführung für Ingenieure*. 5., bearbeitete und erweiterte Ausgabe. Berlin, Heidelberg, and New York: Springer. ISBN: 9783540200918.

Margot, A., B. Schädler, R. Sigg, and R. Weingartner (1992). *Beeinflussung der Fliessgewässer durch Kraftwerke (≥ 300 kW) und Seeregulierungen*. Hydrologischer Atlas der Schweiz. Bern: Bundesamt für Umwelt BAFU, Tafel 5.3.

Martius, O., D. Viviroli, O. Rössler, A. Zischg, V. Röthlisberger, F. Aemisegger, L. Schulte, M. Stuber, J. C. Pena, V. Ruiz-Villanueva, and P. Molnar (2020). Understanding flood triggering mechanisms and flood risk changes. In: *Past, current, and future changes in floods in Switzerland*. ETH Zurich, 38–50. DOI: 10.3929/ethz-b-000462775.

Mas, A., G. Evin, and B. Hingray (2023). *Simulation of MAT and MAP scenarios using the weather generators GWEX and SCAMP: EXCH Final working report – Large catchments*.

Ménégoz, M., E. Valla, N. C. Jourdain, J. Blanchet, J. Beaumet, B. Wilhelm, H. Gallée, X. Fettweis, S. Morin, and S. Anquetin (2020). Contrasting seasonal changes in total and intense precipitation in the European Alps from 1903 to 2010. *Hydrology and Earth System Sciences* 24(11), 5355–5377. DOI: 10.5194/hess-24-5355-2020.

MeteoSwiss (2013). *Daily Precipitation (final analysis): RhiresD: Documentation of MeteoSwiss Grid-Data Products*.

Mezghani, A. and B. Hingray (2009). A combined downscaling-disaggregation weather generator for stochastic generation of multisite hourly weather variables over complex terrain: Development and multi-scale validation for the Upper Rhone River basin. *Journal of Hydrology* 377(3–4), 245–260. DOI: 10.1016/j.jhydrol.2009.08.033.

Molnar, P., Y. Y. Chang, N. Peleg, S. Moraga, M. Zappa, M. I. Brunner, J. Seibert, D. Freudiger, O. Martius, and R. Mülchi (2020). Future changes in floods. In: *Past, current, and future changes in floods in Switzerland*. ETH Zurich, 51–58. DOI: 10.3929/ETHZ-B-000462778.

Montanari, A., B. Merz, and G. Blöschl (2024). HESS Opinions: The sword of Damocles of the impossible flood. *Hydrology and Earth System Sciences* 28(12), 2603–2615. DOI: 10.5194/hess-28-2603-2024.

Moraga, J. S., N. Peleg, P. Molnar, S. Fatichi, and P. Burlando (2022). Uncertainty in high–resolution hydrological projections: Partitioning the influence of climate models and natural climate variability. *Hydrological Processes* 36(10). DOI: 10.1002/hyp.14695.

Mosimann, M., M. Kauzlaric, S. Schick, O. Martius, and A. P. Zischg (2024). Evaluation of surrogate flood models for the use in impact-based flood warning systems at national scale. *Environmental Modelling & Software* 173, 105936. DOI: https://doi.org/10.1016/j.envsoft.2023.105936.

Mülchi, R., O. Rössler, J. Schwanbeck, R. Weingartner, and O. Martius (2020). *Neue hydrologische Szenarien für die Schweiz: Bericht im Auftrag des Bundesamts für Umwelt, Themenschwepunkt Hydro-CH2018*. Bern.

Näf-Huber, D., S. Scherrer, and P. Kienzler (2021). *Le grandi piene della Maggia (Ct. Ticino). Studio principale. Derivazione delle portate di piena per diversi periodi di ritorno lungo la Maggia*. Reinach.

National Center for Atmospheric Research (NCAR) (2023). *AMO Index Data provided by the Climate Analysis Section, NCAR, Boulder, USA, Trenberth and Shea (2006). Updated yearly*. URL: https://climatedataguide.ucar.edu/sites/default/files/2022-03/amo_monthly.txt (visited on 12.10.2023).

Naveau, P., R. Huser, P. Ribereau, and A. Hannart (2016). Modeling jointly low, moderate, and heavy rainfall intensities without a threshold selection. *Water Resources Research* 52(4), 2753–2769. DOI: 10.1002/2015WR018552.

Papastathopoulos, I. and J. A. Tawn (2013). Extended generalised Pareto models for tail estimation. *Journal of Statistical Planning and Inference* 143(1), 131–143. DOI: 10.1016/j.jspi.2012.07.001.

Pfäffli, M., P. Baer, A. Sutter, A. Irniger, and R. Hunziker (2020). *Extremhochwasser an der Aare: Detailbericht E Projekt EXAR. Hydraulische Modellierungen*. Zollikofen, Aarau and Bern.

Pfister, C. (2009). Die "Katastrophenlücke" des 20. Jahrhunderts und der Verlust traditionalen Risikobewusstseins. *Gaia* 18(3), 239–246. DOI: 10.14512/gaia.18.3.10.

Poli, P., H. Hersbach, D. P. Dee, P. Berrisford, A. J. Simmons, F. Vitart, P. Laloyaux, D. G. H. Tan, C. Peubey, J.-N. Thépaut, Y. Trémolet, E. V. Hólm, M. Bonavita, L. Isaksen, and M. Fisher (2016). ERA-20C: An Atmospheric Reanalysis of the Twentieth Century. *Journal of Climate* 29(11), 4083–4097. DOI: 10.1175/JCLI-D-15-0556.1.

Radanovics, S., J.-P. Vidal, and E. Sauquet (2018). Spatial Verification of Ensemble Precipitation: An Ensemble Version of SAL. *Weather and Forecasting* 33(4), 1001–1020. DOI: 10.1175/WAF-D-17-0162.1.

Rajczak, J. and C. Schär (2017). Projections of Future Precipitation Extremes Over Europe: A Multimodel Assessment of Climate Simulations. *Journal of Geophysical Research: Atmospheres* 122(20), 10, 773–10, 800. ISSN: 2169897X. DOI: 10.1002/2017JD027176.

Raynaud, D., B. Hingray, G. Evin, A.-C. Favre, and J. Chardon (2020). Assessment of meteorological extremes using a synoptic weather generator and a downscaling model based on analogues. *Hydrology and Earth System Sciences* 24(9), 4339–4352. DOI: 10.5194/hess-24-4339-2020.

Raynaud, D., B. Hingray, I. Zin, S. Anquetin, S. Debionne, and R. Vautard (2017). Atmospheric analogues for physically consistent scenarios of surface weather in Europe and Maghreb. *International Journal of Climatology* 37(4), 2160–2176. DOI: 10.1002/joc.4844.

Redmond, K. T., Y. Enzel, P. K. House, and F. Biondi (2010). Climate Variability and Flood Frequency at Decadal to Millennial Time Scales. In: *Ancient floods, modern hazards*. Ed. by P. K. House. Water Science and Application. Washington, DC: American Geophysical Union, 21–45. ISBN: 9781118665701.

Reist, T., R. Weingartner, and J. Gurtz (2002). Neue Wege bei der Beschreibung alter Hochwasser – "Die Wassernot im Emmental am 13. August 1837". *Wasser & Boden* 54(10), 50–54. DOI: 10.7892/boris.133967.

Ruelland, D. (2020). Should altitudinal gradients of temperature and precipitation inputs be inferred from key parameters in snow-hydrological models? *Hydrology and Earth System Sciences* 24(5), 2609–2632. DOI: 10.5194/hess-24-2609-2020.

Scherrer, S., R. Frauchiger, D. Näf, and G. Scheible (2011). Historische Hochwasser: Weshalb der Blick zurück ein Fortschritt bei Hochwasserabschätzungen ist. *wasser, energie, luft* 103(1), 7–13.

Scherrer, S., A. Petrascheck, and H. Hodel (2006). Extreme Hochwasser des Rheins bei Basel – Herleitung von Szenarien. *wasser, energie, luft* 98(1), 42–48.

Schmocker-Fackel, P. and F. Naef (2010a). Changes in flood frequencies in Switzerland since 1500. *Hydrology and Earth System Sciences* 14(8), 1581–1594. DOI: 10.5194/hess-14-1581-2010.

— (2010b). More frequent flooding? Changes in flood frequency in Switzerland since 1850. *Journal of Hydrology* 381(1–2), 1–8. DOI: 10.1016/j.jhydrol.2009.09.022.

Schüepp, M. and G. Gensler (1980). Klimaregionen der Schweiz. In: *Die Beobachtungsnetze der Schweizerischen Meteorologischen Anstalt*. Arbeitsberichte der Schweizerischen Meteorologischen Anstalt, 64.

Schulla, J. (2009). *Model Description WaSiM (Water balance Simulation Model)*. Tech. rep. Hydrology Software Consulting J. Schulla, 376 p.

Schulla, J. and K. Jasper (2007). *Model description WaSiM-ETH (Water balance Simulation Model ETH)*. Tech. rep., 181p. URL: %7Bhttp://www.wasim.ch/downloads/doku/wasim/wasim_2007_en.pdf%7D.

Seibert, J. (1997). Estimation of parameter uncertainty in the HBV model. *Nordic Hydrology* 28(4-5), 247–262. DOI: 10.2166/nh.1998.15.

— (2000). Multi-criteria calibration of a conceptual runoff model using a genetic algorithm. *Hydrology and Earth System Sciences* 4(2), 215–224. DOI: 10.5194/hess-4-215-2000.

Seibert, J. and S. Bergström (2022). A retrospective on hydrological catchment modelling based on half a century with the HBV model. *Hydrology and Earth System Sciences* 26(5), 1371–1388. DOI: 10.5194/hess-26-1371-2022.

Seibert, J. and M. J. P. Vis (2012). Teaching hydrological modeling with a user-friendly catchment-runoff-model software package. *Hydrology and Earth System Sciences* 16(9), 3315–3325. DOI: 10.5194/hess-16-3315-2012.

Seibert, J., M. J. P. Vis, I. Kohn, M. Weiler, and K. Stahl (2018). Technical note: Representing glacier geometry changes in a semi-distributed hydrological model. *Hydrology and Earth System Sciences* 22(4), 2211–2224. DOI: 10.5194/hess-22-2211-2018.

Shahgedanova, M., C. Adler, A. Gebrekirstos, H. R. Grau, C. Huggel, R. Marchant, N. Pepin, V. Vanacker, D. Viviroli, and M. Vuille (2021). Mountain Observatories: Status and Prospects for Enhancing and Connecting a Global Community. *Mountain Research and Development* 41(2). DOI: 10.1659/MRD-JOURNAL-D-20-00054.1.

Sharma, A., C. Wasko, and D. P. Lettenmaier (2018). If Precipitation Extremes Are Increasing, Why Aren't Floods? *Water Resources Research* 54(11), 8545–8551. DOI: 10.1029/2018WR023749.

Sideris, I. V., M. Gabella, R. Erdin, and U. Germann (2014). Real-time radar-rain-gauge merging using spatio-temporal co-kriging with external drift in the alpine terrain of Switzerland. *Quarterly Journal of the Royal Meteorological Society* 140(680), 1097–1111. DOI: 10.1002/qj.2188.

Sikorska, A. E., D. Viviroli, and J. Seibert (2015). Flood-type classification in mountainous catchments using crisp and fuzzy decision trees. *Water Resources Research* 51(10), 7959–7976. DOI: 10.1002/2015WR017326.

Sikorska-Senoner, A. E., B. Schaefli, and J. Seibert (2020). Downsizing parameter ensembles for simulations of rare floods. *Natural Hazards and Earth System Sciences* 20(12), 3521–3549. DOI: 10.5194/nhess-20-3521-2020.

Stahl, K., R. D. Moore, J. M. Shea, D. Hutchinson, and A. J. Cannon (2008). Coupled modelling of glacier and streamflow response to future climate scenarios. *Water Resources Research* 44(2), 20, 355. DOI: 10.1029/2007WR005956.

Staudinger, M., R. Furrer, and D. Viviroli (2021). *Hochwasserereignisse aus kontinuierlicher Langzeitsimulation zur Überprüfung der Sicherheit der Stauanlagen: Projektschlussbericht im Auftrag des Bundesamts für Energie (BFE)*. Zürich.

Staudinger, M., M. Kauzlaric, A. Mas, G. Evin, B. Hingray, and D. Viviroli (2025). The role of antecedent conditions in translating precipitation events into extreme floods at the catchment scale and in a large-basin context. *Natural Hazards and Earth System Sciences* 25(1), 247–265. DOI: 10.5194/nhess-25-247-2025.

Staudinger, M. and D. Viviroli, eds. (2020). *Extremhochwasser an der Aare: Detailbericht A Projekt EXAR. Hydrometeorologische Grundlagen*. Zürich.

Steeb, N., F. Lustenberger, and M. Zappa (2024). *Beurteilung der Beeinflussung des Abflusses an NAWA-Messstellen: Detailbericht des BAFU-Projekts HydCHeck*. DOI: 10.55419/wsl:37799.

Stucki, P., M. Bandhauer, U. Heikkilä, O. Rössler, M. Zappa, L. Pfister, M. Salvisberg, P. Froidevaux, O. Martius, L. Panziera, and S. Brönnimann (2018). Reconstruction and simulation of an extreme flood event in the Lago Maggiore catchment in 1868. *Natural Hazards and Earth System Sciences* 18(10), 2717–2739. DOI: 10.5194/nhess-18-2717-2018.

Stucki, P., A. Baumann, and D. Bucher (2017). The 1978 Heavy Precipitation and Flood Event in Switzerland. In: *Historical Weather Extremes in Reanalyses*. Ed. by S. Brönnimann. Geographica Bernensia. Bern, 69–80.

Sun, Q., X. Zhang, F. Zwiers, S. Westra, and L. V. Alexander (2021). A Global, Continental, and Regional Analysis of Changes in Extreme Precipitation. *Journal of Climate* 34(1), 243–258. ISSN: 0894-8755. DOI: 10.1175/JCLI-D-19-0892.1.

Swiss Committee on Dams (swissdams) (2022). *List of dams in Switzerland*. URL: https://www.swissdams.ch/en/les-barrages/liste-des-barrages-suisses (visited on 2.5.2022).

Switanek, M., D. Maraun, and E. Bevacqua (2022). Stochastic downscaling of gridded precipitation to spatially coherent subgrid precipitation fields using a transformed Gaussian model. *International Journal of Climatology* 42(12), 6126–6147. DOI: 10.1002/joc.7581.

Tarasova, L., D. Lun, R. Merz, G. Blöschl, S. Basso, M. Bertola, A. Miniussi, O. Rakovec, L. Samaniego, S. Thober, and R. Kumar (2023). Shifts in flood generation processes exacerbate regional flood anomalies in Europe. *Communications Earth & Environment* 4(1), 49. DOI: 10.1038/s43247-023-00714-8.

Thiessen, A. H. (1911). Precipitation Averages for Large Areas. *Monthly Weather Review* 39, 1082–1084. DOI: 10.1175/1520-0493(1911)39<1082b:PAFLA>2.0.CO;2.

Thompson, V., N. J. Dunstone, A. A. Scaife, D. M. Smith, J. M. Slingo, S. Brown, and S. E. Belcher (2017). High risk of unprecedented UK rainfall in the current climate. *Nature Communications* 8(1), 107. DOI: 10.1038/s41467-017-00275-3.

Trenberth, K. E. (2011). Changes in precipitation with climate change. *Climate Research* 47(1), 123–138. DOI: 10.3354/cr00953.

Trenberth, K., R. Zhang, and National Center for Atmospheric Research Staff (2023). *The Climate Data Guide: Atlantic Multi-decadal Oscillation (AMO) and Atlantic Multidecadal Variability (AMV)*. URL: https://climatedataguide.ucar.edu/climate-data/atlantic-multi-decadal-oscillation-amo (visited on 17.10.2023).

Verbunt, M., M. Zwaaftink, and J. Gurtz (2005). The hydrologic impact of land cover changes and hydropower stations in the Alpine Rhine basin. *Ecological Modelling* 187(1). Special Issue on Advances in Sustainable River Basin Management, 71–84. DOI: https://doi.org/10.1016/j.ecolmodel.2005.01.027.

Vetsch, D. et al. (2018). *System Manuals of BASEMENT, Version 2.8*. Zurich. URL: http://www.basement.ethz.ch/.

Vischer, D. L. (2003). *Die Geschichte des Hochwasserschutzes in der Schweiz: Von den Anfängen bis ins 19. Jahrhundert*. Vol. 5. Berichte des BWG, Serie Wasser. Biel: Bundesamt für Wasser und Geologie (BWG).

Viviroli, D., A. E. Sikorska-Senoner, G. Evin, M. Staudinger, M. Kauzlaric, J. Chardon, A.-C. Favre, B. Hingray, G. Nicolet, D. Raynaud, J. Seibert, R. Weingartner, and C. Whealton (2022). Comprehensive space-time hydrometeorological simulations for estimating very rare floods at multiple sites in a large river basin. *Natural Hazards and Earth System Sciences* 22(9), 2891–2920. DOI: 10.5194/nhess-22-2891-2022.

Viviroli, D. and C. Whealton (2020). Correction of inconsistency in AP2 hydrological model runs. In: *Extremhochwasser an der Aare*. Ed. by M. Staudinger and D. Viviroli. Zürich, 96–104.

Viviroli, D. et al. (2011). Climate change and mountain water resources: overview and recommendations for research, management and policy. *Hydrology and Earth System Sciences* 15(2), 471–504. DOI: 10.5194/hess-15-471-2011.

Vogel, R. M., N. C. Matalas, England Jr., John F., and A. Castellarin (2007). An assessment of exceedance probabilities of envelope curves. *Water Resources Research* 43(W07403). DOI: 10.1029/2006WR005586.

Wasko, C., R. Nathan, L. Stein, and D. O'Shea (2021). Evidence of shorter more extreme rainfalls and increased flood variability under climate change. *Journal of Hydrology* 603, 126994. DOI: 10.1016/j.jhydrol.2021.126994.

Weingartner, R. and H. Aschwanden (1992). Abflussregimes als Grundlage zur Abschätzung von Mittelwerten des Abflusses. In: *Hydrologischer Atlas der Schweiz*. Bern: Bundesamt für Umwelt BAFU, Tafel 5.2.

Weingartner, R., P. Hofer, E. Zbinden, and T. Reist (2017). Und immer wieder herrschte Wassernot. Geschichte der Hochwasser im Emmental seit 1275. In: *Emmental*. Ed. by E. Bäschlin. Vol. 65. Jahrbuch der Geographischen Gesellschaft Bern. Geographische Gesellschaft Bern, 87–109. ISBN: 978-3-9520124-6-8. DOI: 10.5169/SEALS-960364.

Westerberg, I. K., A. E. Sikorska-Senoner, D. Viviroli, M. Vis, and J. Seibert (2020). Hydrological model calibration with uncertain discharge data. *Hydrological Sciences Journal* 67(16), 2441–2456. DOI: 10.1080/02626667.2020.1735638.

Westra, S., H. J. Fowler, J. P. Evans, L. V. Alexander, P. Berg, F. Johnson, E. J. Kendon, G. Lenderink, and N. M. Roberts (2014). Future changes to the intensity and frequency of short-duration extreme rainfall. *Reviews of Geophysics* 52(3), 522–555. DOI: 10.1002/2014RG000464.

Wetter, O. (2015). *Rekonstruktion vorinstrumenteller Scheitelwasserstände der Aare – einschliesslich ihrer wichtigsten Zubringer Saane, Emme, Reuss und Limmat inklusive einer Meteoumfeldanalyse für die extremsten Hochwasser: Studie im Auftrag des Bundesamtes für Umwelt (BAFU)*. Bern.

Wetter, O., C. Pfister, R. Weingartner, J. Luterbacher, T. Reist, and J. Trösch (2011). The largest floods in the High Rhine basin since 1268 assessed from documentary and instrumental evidence. *Hydrological Sciences Journal* 56(5), 733–758. DOI: 10.1080/02626667.2011.583613.

Weusthoff, T. (2011). *Weather Type Classification at MeteoSwiss: Introduction of new automatic classification schemes*. Vol. 235. Arbeitsbericht der MeteoSchweiz. Zurich: MeteoSwiss.

Wilhelm, B. et al. (2022). Impact of warmer climate periods on flood hazard in the European Alps. *Nature Geoscience* 15(2), 118–123. DOI: 10.1038/s41561-021-00878-y.

Wilks, D. S. (1998). Multisite generalization of a daily stochastic precipitation generation model. *Journal of Hydrology* 210(1–4), 178–191. DOI: 10.1016/S0022-1694(98)00186-3.

Zarn, B., J. Schulla, C. Schreiber, and W. Sandholzer (2017). *D13 Speicherseen und Hochwasserrückhalt*. Tech. rep. Internationale Regierungskommission Alpenrhein IRKA. URL: https://www.alpenrhein.net/Portals/0/Content/Publikationen/Speicherseen_und_Hochwasserr%C3%BCckhalt_Bericht.pdf.

Zeder, J. and E. M. Fischer (2024). Decadal to centennial extreme precipitation disaster gaps — Long-term variability and implications for extreme value modelling. *Weather and Climate Extremes* 43, 100636. DOI: 10.1016/j.wace.2023.100636.

Zeimetz, F., J. Garcia Hernàndez, and F. Jordan (2017). Abschätzung von Extremhochwassern bei Talsperren nach der Methode CRUEX++. *wasser, energie, luft* 109(4), 261–270. DOI: 10.5169/SEALS-941629.

Zischg, A. P., G. Felder, R. Weingartner, N. Quinn, G. Coxon, J. Neal, J. Freer, and P. Bates (2018). Effects of variability in probable maximum precipitation patterns on flood losses. *Hydrology and Earth System Sciences* 22(5), 2759–2773. DOI: 10.5194/hess-22-2759-2018.

A
Output sites

Table A.1: Output sites that concern weirs under the supervision of SFOE.

ID12	*ID6*	*Site (river)*	*Area [km^2]*
587362209652	Aarbeg	Aarberg (Aare)	5 095
660102267770	Beznau	Beznau (Aare)	17 601
614100267800	Birsfe	Birsfelden (Rhein)	34 970
668560244020	Bremga	Bremgarten-Zufikon (Reuss)	3 330
487029113185	Chancy	Chancy-Pougny (Rhone)	10 303
677800269900	Eglisa	Eglisau (Rhein)	14 238
611458230923	Flumen	Flumenthal (Aare)	9 582
636521246104	Goesge	Gösgen (Aare)	10 819
659005273014	Klingn	Klingnau (Aare)	17 709
615324128982	LaSous	La Souste (Rhone)	2 296
645900267500	Laufen	Laufenburg (Rhein)	34 039
568770114877	Lavey_	Lavey (Rhone)	4 747
579190183120	Maigra	Maigrauge (Saane)	1 267
588310202000	Muehle	Mühleberg (Aare)	3 168
667700269300	Reckin	Reckingen AG (Rhein)	14 752
752270188970	Reiche	Reichenau (Rhein)	3 219
575046174135	Rosnsl	Rossens (inflow) (Saane)	952
651006251366	Rupper	Rupperswil-Auenstein (Aare)	11 298
633178240195	Ruppol	Ruppoldingen (Aare)	10 114
629700270700	Ryburg	Ryburg-Schwörstadt (Rhein)	34 496
689500283100	Schaff	Schaffhausen (Rhein)	11 849
581280192390	Schiff	Schiffenen (Saane)	1 406
491190116720	Verboi	Verbois (Rhone)	10 137
666560256580	Wettin	Wettingen (Limmat)	2 376
655116257810	Wildeg	Wildegg-Brugg (Aare)	11 642

Table A.2: Output sites that concern discharge gauging stations operated by the FOEN.

ID12	*ID6*	*River and site*	*Area [km^2]*
600710198000	AarBrn	Aare @ Bern, Schönau	2 965
588220219020	AarBre	Aare @ Brügg, Aegerten	8 248
580680211650	AarHag	Aare @ Hagneck	5 112
633730171510	AarRin	Aare @ Ringgenberg, Goldiswil	1 138
613230179280	AarThu	Aare @ Thun	2 459
608220223240	EmmWil	Emme @ Wiler, Limpachmündung	924
753570175730	HRhFue	Hinterrhein @ Fürstenau	1 577
830640197190	InnMrt	Inn @ Martina	1 941
501220115120	ArvGen	L'Arve @ Genève, Bout du Monde	1 973
572530244460	DouOco	Le Doubs @ Ocourt	1 275
682055249430	LimZue	Limmat @ Zürich, Unterhard	2 174
725160221380	LinWee	Linth @ Weesen, Biäsche	1 062
703100113860	MagLcn	Maggia @ Locarno, Solduno	927
665330211800	ReuLuz	Reuss @ Luzern, Geissmattbrücke	2 254
662830252580	ReuMel	Reuss @ Mellingen	3 386
672520230600	ReuMhl	Reuss @ Mühlau, Hünenberg	2 902
613400267650	RheBas	Rhein @ Basel, Rheinhalle	3 586
766280250360	RheDpa	Rhein @ Diepoldsau, Rietbrücke	6 288
573150108300	RhoBra	Rhône @ Branson	3 728
499890117850	RhoGen	Rhône @ Genève, Halle de l'île	8 000
557660133280	RhoPdS	Rhône @ Porte du Scex	5 344
593770118630	RhoSio	Rhône @ Sion	3 372
584440195300	SaaLau	Saane @ Laupen	1 862
693510272500	ThuAnd	Thur @ Andelfingen	1 702
721245117025	TicBlz	Ticino @ Bellinzona	1 518
694281061276	TicMio	Ticino @ Miorina	6 614

Table A.3: Discharge gauging stations operated by the FOEN that are located near a weir under federal supervision, i.e., a SFOE output site (see Table A.1). Also shown is the distance between FOEN and SFOE site (↑ means the FOEN site is upstream of the SFOE site, ↓ means the FOEN site is downstream of the SFOE site) and the area conversion factor (i.e., multiply results from the SFOE site with this factor to obtain results at the FOEN site).

ID12	*ID6*	*River and site (FOEN)*	*Area [km^2]*	*Weir (SFOE)*	*Distance*	*Factor*
657000259360	AarBru	Aare @ Brugg	11 681	Wildegg-Brugg	↓ 4.9 km	1.003
629665235150	AarMur	Aare @ Murgenthal	10 059	Ruppoldingen	↑ 6.8 km	0.995
659970263180	AarUnt	Aare @ Untersiggenthal	17 553	Beznau	↑ 7.1 km	0.997
665640258690	LimBad	Limmat @ Baden	2 384	Wettingen	↓ 3.5 km	1.003
753890189370	RheDEm	Rhein @ Domat/Ems	3 229	Reichenau	↓ 1.9 km	1.003
689145281975	RheNhs	Rhein @ Neuhausen	11 930	Schaffhausen	↓ 1.5 km	1.007
667060269230	RheRek	Rhein @ Rekingen AG	14 767	Reckingen	↓ 0.7 km	1.001
627190267840	RheRhe	Rhein @ Rheinfelden	34 524	Ryburg-Schwör.	↓ 4.6 km	1.001
486600112340	RhoCha	Rhône @ Chancy	10 308	Chancy-Pougny	↓ 1.0 km	1.001
579420183670	SarFri	Sarine @ Fribourg	1 271	Maigrauge	↓ 2.3 km	1.006

Table A.4: Sites that were considered but discarded.

Site	*Explanation*
Albbruck-Dogern (Rhein)	Lower priority in comparison to weir close by
Augst-Wyhlen (Rhein)	Lower priority in comparison to weir close by (Birsfelden)
Bannwil (Aare)	Lower priority in comparison to weir close by
Châtelot (Doubs)	Catchment area too small
Doubs @ Le Noirmont, La Goule	Not promising, need for parameter estimation in heavily karstic region
Fiesch (Rhone)	Catchment area too small
Gluringen (Rhone)	Catchment area too small
Höfe (Sihl)	Catchment area too small
Inn @ Tarasp	Lower priority
Massongex-Bex (Rhone, project)	Lower priority in comparison to weir close by (Lavey)
Mattsand (Matter Vispa)	Catchment area too small
Mörel (Rhone)	Catchment area too small
Niederried (Aare)	Lower priority in comparison to weir close by (Aarberg)
Pradella (Inn)	Not under federal or cantonal supervision
Rheinau (Rhein)	Lower priority in comparison to weir close by (Schaffhausen)
Rheinfelden (Rhein)	Lower priority in comparison to weir close by (Ryburg-Schwörstadt)
Säckingen (Rhein)	Lower priority in comparison to weir close by
Simmewehr (Simme)	Catchment area too small
Thur @ Halden	Lower priority
Wynau-Schwarzhäusern (Aare)	Lower priority in comparison to weir close by

B

Flood estimation results based on GWEX weather scenario input

Table B.1: Flood estimation results for all output sites as listed in Appendix A. Note that the return levels were always computed from the full, 300 000-year long continuous simulations (CSs) for consistency, and that minor differences occur compared to return levels computed from the CSs divided into blocks (see Section 6.1). All values are given in [$m^3 s^{-1}$]. For ten sites operated by the FOEN and located near a weir under federal supervision (i.e., a SFOE output site, see footnotes), results were converted using the scaling factors detailed in Table A.3, assuming similar specific discharge. For interpretation and important background information see Chapter 10, for discussion of results at selected sites see Chapter 6.

ID12	*ID6*	*River and site*	HQ_{30}	HQ_{100}	HQ_{300}	$HQ_{1\,000}$	$HQ_{10\,000}$
587362209652	Aarbeg	Aare @ Aarberg	1 340	1 601	1 792	2 044	2 591
600710198000	AarBrn	Aare @ Bern, Schönau	622	649	673	716	828
660102267770	Beznau	Aare @ Beznau	2 137	2 450	2 758	3 139	3 745
657000259360	AarBru	Aare @ Brugg[1]	1 220	1 411	1 589	1 787	2 306
588220219020	AarBre	Aare @ Brügg, Aegerten	747	772	793	928	1 070
611458230923	Flumen	Aare @ Flumenthal	934	1 022	1 107	1 216	1 456
636521246104	Goesge	Aare @ Gösgen	1 130	1 289	1 427	1 620	2 029
580680211650	AarHag	Aare @ Hagneck	1 340	1 600	1 792	1 873	1 951
659005273014	Klingn	Aare @ Klingnau	2 140	2 450	2 755	3 079	3 724
629665235150	AarMur	Aare @ Murgenthal[2]	1 001	1 110	1 208	1 333	1 646
588310202000	Muehle	Aare @ Mühleberg	638	678	712	763	901
633730171510	AarRin	Aare @ Ringgenberg, Goldswil	252	277	300	327	381
651006251366	Rupper	Aare @ Rupperswil-Auenstein	1 180	1 356	1 522	1 707	2 197
633178240195	Ruppol	Aare @ Ruppoldingen	1 006	1 115	1 214	1 340	1 655
613230179280	AarThu	Aare @ Thun	516	563	585	624	744
659970263180	AarUnt	Aare @ Untersiggenthal, Stilli[3]	2 130	2 442	2 749	3 129	3 734
655116257810	Wildeg	Aare @ Wildegg-Brugg	1 216	1 407	1 585	1 782	2 299
501220115120	ArvGen	L'Arve @ Genève, Bout du Monde	846	1 063	1 274	1 536	2 065
572530244460	DouOco	Le Doubs @ Ocourt	370	455	537	627	797
608220223240	EmmWil	Emme @ Wiler, Limpachmündung	287	352	415	490	656
753570175730	HRhFue	Hinterrhein @ Fürstenau	564	740	919	1 143	1 706
830640197190	InnMrt	Inn @ Martina	468	594	727	902	1 416
665640258690	LimBad	Limmat @ Baden, Limmatprom.[4]	528	607	687	784	949
666560256580	Wettin	Limmat @ Wettingen	527	605	685	781	946
682055249430	LimZue	Limmat @ Zürich, Unterhard	484	571	656	743	918
725160221380	LinWee	Linth @ Weesen, Biäsche	275	336	399	473	628
703100113860	MagLcn	Maggia @ Locarno, Solduno	2 386	3 235	4 175	5 488	9 159
668560244020	Bremga	Reuss @ Bremgarten-Zufikon	607	697	774	856	934
665330211800	ReuLuz	Reuss @ Luzern, Geissmattbrücke	428	494	563	643	786
662830252580	ReuMel	Reuss @ Mellingen	622	718	798	868	952
672520230600	ReuMhl	Reuss @ Mühlau, Hünenberg	588	683	755	827	979
613400267650	RheBas	Rhein @ Basel, Rheinhalle	4 473	5 340	6 217	7 313	9 335
614100267800	Birsfe	Rhein @ Birsfelden	4 323	5 129	5 935	6 936	8 636
766280250360	RheDpa	Rhein @ Diepoldsau, Rietbrücke	2 265	2 894	3 572	4 384	5 979

(continued on next page)

[1] Converted from Aare @ Wildegg-Brugg (ID12 655116257810)
[2] Converted from Aare @ Ruppoldingen (ID12 633178240195)
[3] Converted from Aare @ Beznau (ID12 660102267770)
[4] Converted from Limmat @ Wettingen (ID12 666560256580)

ID12	*ID6*	*River and site*	HQ_{30}	HQ_{100}	HQ_{300}	$HQ_{1\,000}$	$HQ_{10\,000}$
753890189370	RheDEm	Rhein @ Domat/Ems[5]	1 361	1 787	2 241	2 887	4 225
677800269900	Eglisa	Rhein @ Eglisau	2 045	2 448	2 820	3 310	4 481
645900267500	Laufen	Rhein @ Laufenburg	4 217	4 992	5 749	6 704	8 443
689145281975	RheNhs	Rhein @ Neuhausen, Flurlingerbr.[6]	1 190	1 392	1 581	1 803	2 360
667700269300	Reckin	Rhein @ Reckingen AG (SFOE)	2 053	2 459	2 836	3 332	4 487
752270188970	Reiche	Rhein @ Reichenau	1 356	1 782	2 235	2 878	4 213
667060269230	RheRek	Rhein @ Rekingen AG (FOEN)[7]	2 055	2 461	2 839	3 335	4 492
627190267840	RheRhe	Rhein @ Rheinfelden[8]	4 278	5 074	5 851	6 829	8 537
629700270700	Ryburg	Rhein @ Ryburg-Schwörstadt	4 274	5 069	5 845	6 822	8 528
689500283100	Schaff	Rhein @ Schaffhausen	1 182	1 382	1 570	1 790	2 343
573150108300	RhoBra	Rhône @ Branson	846	1 057	1 164	1 232	1 552
486600112340	RhoCha	Rhône @ Chancy, Aux Ripes[9]	1 392	1 650	1 914	2 240	2 896
487029113185	Chancy	Rhône @ Chancy-Pougny	1 391	1 648	1 912	2 238	2 893
499890117850	RhoGen	Rhône @ Genève, Halle de l'île	727	791	851	927	1 127
568770114877	Lavey_	Rhône @ Lavey	996	1 232	1 385	1 516	1 847
557660133280	RhoPdS	Rhône @ Porte du Scex	1 112	1 370	1 541	1 652	1 909
593770118630	RhoSio	Rhône @ Sion	756	957	1 041	1 296	2 289
615324128982	LaSous	Rhône @ La Souste	601	776	975	1 176	1 920
491190116720	Verboi	Rhône @ Verbois	1 343	1 585	1 836	2 151	2 796
584440195300	SaaLau	Saane @ Laupen	815	1 021	1 221	1 410	1 766
579190183120	Maigra	Saane @ Maigrauge	591	727	853	1 003	1 336
575046174135	Rosnsl	Saane @ Rossens	411	493	568	659	855
581280192390	Schiff	Saane @ Schiffenen	633	782	925	1 031	1 310
579420183670	SarFri	Sarine @ Fribourg[10]	595	731	858	1 009	1 344
693510272500	ThuAnd	Thur @ Andelfingen	1 149	1 432	1 647	1 965	2 785
721245117025	TicBlz	Ticino @ Bellinzona	2 036	2 798	3 612	4 950	7 948
694281061276	TicMio	Ticino @ Miorina	2 502	3 184	4 060	5 122	7 254

[5] Converted from Rhein @ Reichenau (ID12 752270188970)
[6] Converted from Rhein @ Schaffhausen (ID12 689500283100)
[7] Converted from Rhein @ Reckingen AG (SFOE) (ID12 667700269300)
[8] Converted from Rhein @ Ryburg-Schwörstadt (ID12 629700270700)
[9] Converted from Rhône @ Chancy-Pougny (ID12 487029113185)
[10] Converted from Saane @ Maigrauge (ID12 579190183120)

C

Hydrological data used

Table C.1: Stations with discharge records used for calibration of the hydrological model HBV.

ID12	*ID6*	*River and site*	*Area [km^2]*
661390230220	AabHit	Aabach @ Hitzkirch, Richensee	73.3
689205234400	AabKae	Aabach @ Käpfnach	12.9
655710249111	AabLen	Aabach @ Lenzburg	173.9
696925240800	AabMoe	Aabach @ Mönchaltorf	44.8
695100244725	AabNdt	Aabach @ Niederuster	62.7
715297231585	AabSkn	Aabach @ Schmerikon, Gross Allmeind	38.6
656660242051	AabSng	Aabach @ Seengen	147.4
744410268400	AacSal	Aach @ Salmsach, Hungerbühl	47.4
727229247374	AccMog	Aachbach @ Mogelsberg, Aachsäge	20.1
649930177380	AarBrw	Aare @ Brienzwiler	555.2
633730171510	AarRin	Aare @ Ringgenberg, Goldiswil	1 137.5
658780174678	AarStt	Aare @ Schattenhalb, Willigen, Aareschlucht	453.5
781060161600	AlbBgn	Albula @ Bergün, Crap Alv	6.9
763420170145	AlbTie	Albula @ Tiefencastel	529.0
798898222956	AlfKls	Alfenz @ Kloesterle	66.7
567830261200	AliBct	Allaine @ Boncourt, Frontière	212.0
608710148300	AllAde	Allenbach @ Adelboden	28.8
698640223020	AlpEin	Alp @ Einsiedeln	46.7
688560185120	ApbErs	Alpbach @ Erstfeld, Bodenberg	20.7
779268224901	AlvBue	Alvier @ Bürs (Brücke L82)	72.7
568080192860	ArbAve	Arbogne @ Avenches	71.9
554350199940	AreBou	Areuse @ Boudry	377.7
532980195880	AreStS	Areuse @ St-Sulpice	104.1
762148277486	ArgGie	Argen @ Giessen	640.4
542120186380	ArnGra	Arnon @ Grandson-Poissine	89.8
508225137730	AssNyo	Asse @ Nyon	23.8
520720147410	AubAlm	Aubonne @ Allaman, Le Coulet	105.3
619110240280	AugBal	Augstbach @ Balsthal	62.7
568100122550	AvaBeY	Avancon @ Bex	78.2
789440151320	BerPon	Berninabach @ Pontresina	106.9
744862219105	BsbWst	Berschnerbach @ Walenstadt, Berschis	11.8
701590285825	BbrBuc	Biber (TG/SH) @ Buch	144.1
694183290038	BbrThy	Biber (TG/SH) @ Thayngen	74.8
697240223280	BibBib	Biber @ Biberbrugg	31.9
580409194220	BbeGum	Bibere @ Gurmels, Obere Mühle	18.8
721735273245	KmbGru	Binnekanal/Brunnenwasser/Kemmenbach @ Grubmühle	33.3
613570263080	BirMue	Birs @ Münchenstein, Hofmatt	887.3
593139232518	BirCou	Birse @ Court, Pont de la STEP	99.2
595740237010	BirMou	Birse @ Moutier, La Charrue	185.8
596780249070	BirSoy	Birse @ Soyhières, Bois du Treuil	569.5
610278265315	BsgBin	Birsig @ Binningen	73.3
609059262511	BsgObw	Birsig @ Oberwil	54.9
785465249411	BizReu	Bizauerbach @ Reuthe	14.0
526205149690	BdMTol	Boiron-de-Morges @ Tolochenaz	34.0
712670084270	BolPCe	Bolletta @ Porto Ceresio	21.2
791574244958	BgzAu_	Bregenzerach @ Au	146.5
797333240452	BgzHop	Bregenzerach @ Hopfreben	40.6
776102261003	BgzKen	Bregenzerach @ Kennelbach	822.4
784510247740	BgzMla	Bregenzerach @ Mellau	225.8
722315078320	BgaChi	Breggia @ Chiasso, Ponte di Polenta	47.1

(continued on next page)

ID12	ID6	River and site	Area [km^2]
538000182980	BriTdG	Brinaz @ Tuileries-de-Grandson	13.8
561660187320	BroPay	Broye @ Payerne, Caserne d'aviation	415.9
558900156900	BroRgv	Broye @ Semsales, La Rogivue	29.1
726977258182	BBaObb	Brübach @ Oberbüren Brübach	13.9
642875261484	BruGip	Bruggbach @ Gipf-Oberfrick	44.6
668332237511	BueMui	Bünz @ Muri	15.5
658618250316	BueOth	Bünz @ Othmarsingen	113.2
665106242991	BueWlt	Bünz @ Waltenschwil	49.3
538928178521	BurGre	Buron @ Gressy	33.8
630535263767	BuuMai	Buuserbach @ Maisprach	10.0
729440127180	CalBsn	Calancasca @ Buseno	120.5
718010097380	CasPre	Cassarate @ Pregassona	75.8
593750235652	ChlMou	Chalière @ Moutier	17.2
534390152620	CbrCpR	Chamberonne @ Chavannes-près-Renens	41.4
703720243470	ChbWet	Chämtnerbach @ Wetzikon	13.2
791430160600	CmbLPC	Chamuerabach @ La Punt-Chamues-ch	73.4
570870194650	ChaFaR	Chandon @ Faoug, Route Salavaux	38.1
611080252330	ClbHim	Chastelbach @ Himmelried	11.3
614322190508	CsbFrA	Chiesebach @ Freimettigen, ARA	45.0
609088161522	CrlDmt	Chirel @ Diemtigen, Walki, Stierebrügg	19.2
663800199570	CScAlp	Chli Schliere @ Alpnach, Chilch Erli	21.6
609787207551	CtbKra	Chrouchtalbach @ Krauchthal, Weichel	16.0
731730100420	CucPor	Cuccio @ Porlezza	54.5
740197290947	DAaNfr	Deggenhauser Aach @ Neufrach	74.9
628131249929	DieDie	Diegterbach @ Diegten	13.0
627989257087	DieSis	Diegterbach @ Sissach	30.8
786220183370	DisDav	Dischmabach @ Davos, Kriegsmatte	42.9
607867266972	Dr1All	Dorfbach @ Allschwil	8.5
735780252528	Dr4Gos	Dorfbach @ Gossau, Niederdorf	19.3
659056238505	Dr2Mei	Dorfbach @ Meisterschwanden	7.8
634440245930	Dr3Tri	Dorfbach @ Trimbach	11.1
775345252188	DbaEnz	Dornbirnerach @ Enz	54.2
770558257676	DbaHSt	Dornbirnerach @ Hoher Steg	108.7
769017259147	DbaLah	Dornbirnerach @ Lauterach	184.6
619580239070	DueBal	Dünnern @ Balsthal	140.9
616950240055	DueLpr	Dünnern @ Laupersdorf	64.9
634330244480	DueOlt	Dünnern @ Olten, Hammermühle	233.8
560930136625	EaFRnn	Eau-Froide @ Rennaz	15.7
560875134860	EaFRoc	Eau-Froide @ Roche	14.3
631696256953	EibGel	Eibach @ Gelterkinden	27.0
635020252565	EibZeg	Eibach @ Zeglingen	12.6
615220209140	EmmBur	Emme @ Burgdorf, Lochbach	660.8
627910191180	EmmEgg	Emme @ Eggiwil, Heidbüel	124.4
623610200420	EmmEmt	Emme @ Emmenmatt Totalstation	443.0
608220223240	EmmWil	Emme @ Wiler, Limpachmündung (Totalstation)	924.1
769100249106	EmsHoh	Emsbach @ Hohenems	8.3
673555202870	EBABuo	Engelberger Aa @ Buochs, Flugplatz	228.0
616709160373	EntFru	Entschlige @ Frutigen	144.6
626294257702	ErgIti	Ergolz @ Itingen	138.4
622270259750	ErgLie	Ergolz @ Liestal	261.2
632223257702	ErgOrm	Ergolz @ Ormalingen	29.4
641884251291	ErzErl	Erzbach @ Erlinsbach	6.8
650554268983	EtzEtz	Etzgerbach @ Etzgen	25.3
702390261740	EulRat	Eulach @ Räterschen	31.1
697550261240	EulWin	Eulach @ Winterthur	64.2
694120262820	EulWue	Eulach @ Wülflingen	73.6
598396149306	FrmSSt	Färmelbach @ St. Stephan, Matten	31.0
747852264825	FeiRog	Feilenbach @ Roggwil	5.8
606529162168	FilDmt	Fildrich @ Diemtigen, Riedli	76.6
672950268189	FisFis	Fisibach @ Fisibach	15.0
667079107158	TocDom	Fiume Toce @ Domodossola	923.5
668352114756	TocPtm	Fiume Toce @ Pontemaglio	359.5
726418221919	FliWee	Flibach @ Weesen, Steingüetli	9.0
535930152400	FloCap	Flon @ Capelard	19.3
552800157760	FAvOlv	Flon-Aval @ Oron-la-ville	15.9
549075148134	FrsChY	Forestay @ Chexbres	15.3
761702259757	FreRhk	Freibach @ Rheineck, Freibach	19.4
773328236532	FruLts	Frutz @ Laterns	33.0
669910255280	FurWur	Furtbach @ Würenlos	43.9

(continued on next page)

ID12	*ID6*	*River and site*	*Area [km^2]*
582737183699	GalTaf	Galternbach (Gottéron) @ Tafers (Tavel)	38.2
697776282309	GeiWdf	Geisslibach @ Willisdorf	46.8
579333179885	GerMly	Gérine @ Marly	71.3
738553274432	HorGeu	Geusenbach @ Güttingen	4.2
784788284414	GsbLoc	Giessbach (DEU) @ Lochhammer	31.0
728812269230	GsnBgl	Giessen @ Bürglen	24.8
574220181336	GlnMtr	Glâne @ Matran	180.1
689400250280	GlaDue	Glatt @ Dübendorf	187.4
737270251290	GlaHer	Glatt @ Herisau, Zellersmühle	16.7
729243256474	GlaObb	Glatt @ Oberbüren Buechental	90.5
678040269720	GlaRhs	Glatt @ Rheinsfelden	417.4
735329181796	GleCas	Glenner @ Castrisch	380.9
753190261590	GolGol	Goldach @ Goldach, Bleiche (Totalstation)	50.4
670467153932	GonOwd	Goneri @ Oberwald	38.4
752584197209	GoePfa	Görbsbach @ Pfäfers, Vättis, Winkel	30.3
563960129860	GEaAig	Grande Eau @ Aigle	131.6
548860152970	GreFor	Grenet @ Forel	19.0
700710218125	GrbEin	Grossbach @ Einsiedeln, Gross	8.9
700750218230	GrbGro	Grossbach @ Grossbach, Säge	9.0
685500196050	GroIse	Grosstalbach @ Isenthal	43.9
658706270133	GunLeu	Guntenbach @ Leuggern	10.1
604810192680	GueBel	Gürbe @ Belp, Mülimatt	116.1
605886181875	GueBgs	Gürbe @ Burgistein Station	53.0
676370282580	HalHll	Halbach @ Hallau	11.7
674440231915	HasMas	Haselbach @ Maschwanden	18.5
622278256550	HFrBub	Hintere Frenke @ Bubendorf-Morgental	38.5
618988250562	HFrRei	Hintere Frenke @ Reigoldswil	14.4
753570175730	HRhFue	Hinterrhein @ Fürstenau	1 576.8
735480154680	HRhHi2	Hinterrhein @ Hinterrhein	53.9
733706153945	HRhHi1	Hinterrhein @ Hinterrhein, Schiessplatz	41.5
660992245344	HolVlm	Holzbach @ Villmergen	23.9
629414256456	HomTrn	Homburgerbach @ Thürnen	29.8
611341249582	IbaZul	Ibach @ Zullwil	7.2
627320198600	IlfLan	Ilfis @ Langnau	187.4
769630229979	IllBes	Ill @ Beschling	1 131.0
761970236592	IllGis	Ill @ Gisingen	1 267.3
797700168170	InnCin	Inn @ Cinuos-chel	733.5
830640197190	InnMrt	Inn @ Martina	1 941.3
795800165910	InnSCh	Inn @ S-Chanf	615.9
783910150960	InnSMo	Inn @ St. Moritzbad	155.4
707050234060	JonRue	Jona @ Rüti	57.9
675120238210	JnnZwi	Jonen @ Zwillikon	36.9
656284308578	JosHoe	Josbach @ Hölzlebruck	47.0
769855149043	JulBiv	Julia @ Bivio	60.7
645327266024	KaiKai	Kaisterbach @ Kaisten	11.9
616540158316	KanFru	Kander @ Frutigen, Eisenbahnviadukt	178.8
617790168400	KanHon	Kander @ Hondrich	490.7
618188150151	KanKan	Kander @ Kandersteg	137.1
667964236710	KazMui	Katzbach @ Muri	6.1
698245249760	KptFeh	Kempt @ Fehraltorf	22.5
696710252445	KptIll	Kempt @ Illnau	39.5
695435258750	KptWin	Kempt @ Winterthur	62.5
663700213630	KEmEmm	Kleine Emme @ Emmen	478.3
664220213200	KEmLit	Kleine Emme @ Littau, Reussbühl	478.3
647870209510	KEmWer	Kleine Emme @ Werthenstein, Chappelboden	311.5
626716285346	KWiTeg	Kleine Wiese @ Tegernau	70.0
644553244335	KoeKoe	Köllikerbach @ Kölliken	10.4
644500119420	KruKlu	Krummbach @ Klusmatten	19.4
667010248723	KueKue	Küntenerbach @ Künten	4.5
540596130874	DdAVac	La Dranse d'Abondance @ Vacheresse	168.3
534356130883	DraRey	La Dranse @ Reyvroz [Bioge]	502.1
499392114421	DriGrg	La Drize @ Grange-Collomb	22.1
509972113806	MngVMo	La Menoge @ Vétraz-Monthoux	156.4
614558108851	NavZin	La Navisence @ Zinal	76.5
545696200777	NoiNoi	La Noiraigue @ Noiraigue	0.7
503072115386	SayVlt	La Seymaz @ Villette	36.5
501899125792	VsYVer	La Versoix @ Versoix-CFF	88.7
536827195999	VArMot	La Vieille Areuse @ Môtiers	0.1
496669114794	AirCen	L'Aire @ Centenaire	66.2

(continued on next page)

ID12	*ID6*	*River and site*	*Area [km^2]*
495791114076	AirCon	L'Aire @ Confignon, Mourlaz	59.4
493958110794	AirSJG	L'Aire @ Saint-Julien-en-Genevois [Thairy]	46.6
488880119460	AldDar	L'Allondon @ Dardagny, Les Granges	119.4
765364204910	LqtFel	Landquart @ Felsenbach	613.7
791193192539	LqtKlo	Landquart @ Klosters Pardenn	99.8
779640181200	LwaDav	Landwasser @ Davos, Frauenkirch	183.7
629560219135	LanHut	Langete @ Huttwil, Häberenbad	59.9
626212221961	LanLei	Langete @ Leimiswil, Weinstegen	95.2
627513231510	LanRog	Langete @ Roggwil BE, Obere Brüel	130.3
555048085084	ArvCMB	L'Arve @ Chamonix-Mont-Blanc [Pont des Favrands]	194.7
501220115120	ArvGen	L'Arve @ Genève, Bout du Monde	1 972.9
538209087967	ArvSll	L'Arve @ Sallanches	566.6
712677264228	LauMtz	Lauche @ Matzingen	61.7
719140083880	LavRSV	Laveggio @ Riva S. Vitale	31.1
537109195889	LBMBdM	Le Bied de Môtiers @ Le Bied de Môtiers	18.3
514365179183	BfRLon	Le Bief Rouge @ Longevilles-Mont-d'Or	29.5
520649087502	BorSJS	Le Borne @ Saint-Jean-de-Sixt	66.5
523975101961	BnzBvi	Le Bronze @ Bonneville [Thuet]	28.3
557530227320	DouCdS	Le Doubs @ Combe des Sarrasins	998.5
516941197988	DouDou	Le Doubs @ Doubs	378.8
554877222803	DouFou	Le Doubs @ Fournet-Blancheroche [La Rasse]	918.8
563061235752	DouGou	Le Doubs @ Goumois	1 149.0
518076192662	DouCeM	Le Doubs @ la Cluse-et-Mijoux [Pontarlier amont]	334.3
511505180814	DouLab	Le Doubs @ Labergement-Sainte-Marie	177.4
561430231050	DouLNo	Le Doubs @ Le Noirmont, La Goule	1 046.7
505964173371	DouMte	Le Doubs @ Mouthe	92.2
572530244460	DouOco	Le Doubs @ Ocourt	1 275.4
515781189193	DouOye	Le Doubs @ Oye-et-Pallet	251.7
544560214880	DouSlB	Le Doubs @ Sortie du lac des Brenets	867.4
526829205992	DouVdP	Le Doubs @ Ville-du-Pont	640.1
504859184983	DurBvY	Le Drugeon @ Bonnevaux	41.0
515226198854	DurVlc	Le Drugeon @ Vuillecin [2]	195.9
534906194729	FleFle	Le Fleurier @ Fleurier	0.6
506016117116	ForAmb	Le Foron @ Ambilly	41.3
518579131551	ForSci	Le Foron @ Sciez	48.7
527235107858	GifMrg	Le Giffre @ Marignier [Plan Séraphin]	440.3
521260132505	RedMgc	Le Redon @ Margencel	31.2
525581109908	RisSJe	Le Risse @ Saint-Jeoire [Pont du Risse]	67.9
534368209212	TheGCC	Le Théverot @ Grand'Combe-Châteleu [Châteleu]	26.3
794634260963	LecKaw	Leckenbach @ Kaelberweide	15.0
772968267685	LeiUhs	Leiblach mit Werkskanal @ Unterhochsteg (Summenpegel)	105.5
508190128616	HrmHrm	L'Hermance @ Hermance	44.1
757750234590	LBKRug	Liechtensteiner Binnenkanal @ Ruggell	115.7
718285197310	LinLin	Linth @ Linthal, Ausgleichsbecken KLL	146.9
723985217965	LinMol	Linth @ Mollis, Linthbrücke	600.2
724290205945	LinSwa	Linth @ Schwanden	250.3
725160221380	LinWee	Linth @ Weesen, Biäsche	1 061.5
787930217330	LitSrs	Litz @ Schruns (Vonbunweg)	101.0
630530171819	LomUts	Lombach @ Unterseen, Birmse	43.8
629130140910	LonBla	Lonza @ Blatten	77.4
501445156305	OrbLCh	L'Orbe @ Le Chenit, Frontière	45.8
507710162190	OrbSen	L'Orbe @ Le Sentier	130.3
530080175560	OrbOrb	L'Orbe @ Orbe, Le Chalet	342.7
497829152612	OrbRou	L'Orbe @ Rousses	20.7
674715229845	LorFra	Lorze @ Frauenthal	261.7
680600226070	LorZug	Lorze @ Zug, Letzi	100.2
638720247930	LosLos	Lostorferbach @ Lostorf	5.9
589113146122	LouGst	Louibach @ Gstaad, Badweidli	62.9
538665133884	UgiSPC	L'Ugine @ Saint-Paul-en-Chablais	24.0
612755245090	LssBwl	Lüssel @ Beinwil	14.0
607753250488	LssBrt	Lüssel @ Breitenbach	43.8
607820246770	LssEsw	Lüssel @ Erschwil	33.2
614020209727	LtbObe	Luterbach @ Oberburg	34.1
732832232031	LtnNes	Luteren @ Nesslau, Auguet	29.2
640560226740	LutNeb	Luthern @ Nebikon	104.7
633130168200	LueGst	Lütschine @ Gsteig	380.7
784554233509	LtzGar	Lutz @ Garsella	93.5
598361252787	LzlKle	Lützel @ Kleinlützel	66.1
709784261838	LMgAad	Lützelmurg @ Aadorf	34.5

(continued on next page)

ID12	*ID6*	*River and site*	*Area [km^2]*
711994264382	LMgMtz	Lützelmurg @ Matzingen neu	43.4
594451210540	LysSpf	Lyssbach @ Schüpfen, Bundkofen	23.5
627073266038	MgbRhe	Magdenerbach @ Rheinfelden	33.1
696420124125	MagLdn	Maggia @ Lodano	514.9
711620093290	MglMag	Magliasina @ Magliaso, Ponte	34.4
719024088196	MarMar	Mara @ Maroggia	14.6
609093262473	MrbObw	Marchbach @ Oberwil	12.0
643700137290	MasBla	Massa @ Blatten bei Naters	195.5
533890153120	MebCpR	Mèbre @ Chavannes-près-Renens	21.5
690500275165	MedMth	Mederbach @ Marthalen	25.5
726988114670	MlaMlr	Melera @ Melera (Valle Morobbia)	1.1
690124112000	MelCam	Melezza @ Camedo	126.0
545440180875	MenYvo	Mentue @ Yvonand, La Mauguettaz	105.3
760770133450	MerSog	Mera @ Soglio	177.4
704425215310	MinEut	Minster @ Euthal, Rüti	59.1
732640123460	MoeGrn	Moesa @ Grono, Brücke	252.5
724765120360	MoeLum	Moesa @ Lumino, Sassello	471.9
632611265780	MhbZei	Möhlinbach @ Zeinignen	26.6
527070151675	MgsMgs	Morges @ Morges	31.8
535509179532	MujTre	Mujon @ Treycovagnes	31.7
688262206170	MuoIng	Muota @ Ingenbohl	316.6
709540269660	MurFrf	Murg @ Frauenfeld	213.3
629340233555	MurMur	Murg @ Murgenthal, Wallisil	183.4
714105261720	MurWae	Murg @ Wängi	80.1
708160277908	MueEsc	Müsbach @ Eschenz	6.8
691675264240	NaeNef	Näfbach @ Neftenbach	36.1
727110247290	NecMog	Necker @ Mogelsberg, Aachsäge	88.1
531030170390	NozOrn	Nozon @ Orny	43.1
782003283522	OArEpp	Obere Argen @ Epplings	160.8
790192280672	OArZkb	Obere Argen @ Zwirkenberg	100.7
770127269841	ORAAes	Oberreitnauer Ach @ Aeschach	28.2
619680228265	OenHei	Önz @ Heimenhausen, Hueb	86.5
622260259433	OriLie	Orisbach @ Liestal	21.0
612803220799	OesKop	Ösch @ Koppigen, Neumatt	40.8
804930174830	OdCZer	Ova da Cluozza @ Zernez	26.9
810560170790	OdFZer	Ova dal Fuorn @ Zernez, Punt la Drossa	55.3
552060161650	ParEcu	Parimbot @ Ecublens, Eschiens	6.9
566490194420	PGlVlG	Petite Glâne @ Villars-le-Grand	75.5
635481237778	PfaVor	Pfaffnern @ Vordemwald	39.1
757975191925	PleChu	Plessur @ Chur	264.4
803490130520	PosLeP	Poschiavino @ Le Prese	167.7
510080140080	ProGla	Promenthouse @ Gland, Route Suisse	119.1
705034288406	RzARie	Radolfzeller Aach @ Rielasingen	209.3
748390215074	RagMls	Ragnatscherbach @ Mels, Hof	3.6
595990236663	RauMou	Raus @ Moutier, Sous les Rives	41.5
723097219369	RtiObu	Rauti @ Oberurnen	46.3
718810167690	RdSSum	Rein da Sumvitg @ Sumvitg, Encardens	21.8
675660245430	RepBir	Reppisch @ Birmensdorf	24.7
672435251590	RepDtk	Reppisch @ Dietikon	68.5
688120166320	ReuAdm	Reuss @ Andermatt	190.2
690085193210	ReuSee	Reuss @ Seedorf	833.2
749550187758	RheBdz	Rhein @ Bonaduz Farsch	1 501.3
770292256198	RBKLus	Rheintaler Binnenkanal @ Lustenau (Hofsteig)	74.9
641340129700	RhoBrg	Rhône @ Brig	906.1
670810157200	RhoGle	Rhône @ Gletsch	39.4
661910146780	RhoRec	Rhône @ Reckingen VS	214.3
684970135960	RdCCav	Riale di Calneggia @ Cavergno, Pontit	23.9
708060123950	RdPLav	Riale di Pincascia @ Lavertezzo	44.5
733545118160	RdRRov	Riale di Roggiasca @ Roveredo, Bacino di compenso	8.1
725184238523	RicWat	Rickenbach @ Wattwil, Bleikenstrasse	16.0
760939248731	RacAst	Rietaach @ Altsätten, Eschen	33.0
718840248440	RieMos	Rietholzbach @ Mosnang, Rietholz	3.2
830800168700	RomMus	Rom @ Müstair	128.5
630257231650	RotRog	Rot @ Roggwil BE, Seijumatte	42.5
783405267018	RaATha	Rotach (AUT) @ Thal (Martinsbrücke)	84.1
754561280746	RaDFrd	Rotach (DEU) @ Friedrichshafen	125.9
751182291494	RaDFuc	Rotach (DEU) @ Fuchstobel	71.1
611860184376	RtaOpp	Rotache @ Oppligen, Rotache	35.9
748320248925	RbaBha	Rotbach (AR) @ Bühler Au	23.1

(continued on next page)

ID12	ID6	River and site	Area [km^2]
665710216710	RtbEmm	Rotbach (LU) @ Emmen, Neuhüsern	28.2
680913125677	RovCVa	Rovana @ Campo Vallemaggia	36.6
646794239350	RueSoe	Ruederchen @ Schöftland	19.1
773575267444	RugLou	Ruggbach @ Lochau	7.4
584440195300	SaaLau	Saane @ Laupen	1 861.8
571277145973	SaaRss	Saane @ Rossiniere	401.1
588569216818	SagWor	Sagibach @ Worben, Hinderfeld	14.7
642220129630	SalBrg	Saltina @ Brig	76.5
764826230699	SamAme	Samina @ Amerluegen	68.4
573520161345	SarBro	Sarine @ Broc, Château d'en bas	636.3
579420183670	SarFri	Sarine @ Fribourg	1 270.6
661460194220	SrASar	Sarner Aa @ Sarnen	269.3
703881293301	SauHau	Saubach @ Hausen	146.1
692480191800	SaeBgl	Schächen @ Bürglen, Galgenwäldli	107.9
832172202849	SlkSlk	Schalklbach @ Schalklhof	108.0
599485244150	SltVic	Scheulte @ Vicques	72.7
677155288960	ShbTal	Schleitheimerbach @ Talmühle	35.0
656739262786	StbRem	Schmittenbach @ Remigen	13.0
767294308232	SssDur	Schussen @ Durlesbach	297.2
757417282317	SssGer	Schussen @ Gerbertshaus	812.6
774883257621	SzbSwz	Schwarzach @ Schwarzach	17.5
644850163535	SLuGrG	Schwarze Lütschine @ Grindelwald, Grund	108.0
646617163555	SLuGrM	Schwarze Lütschine @ Grindelwald, Mettenberg	50.1
708129273499	SbhHue	Seebach @ Hüttwilen	21.7
735389288185	SeAUhl	Seefelder Aach @ Uhldingen	280.6
658530218290	SelNkr	Sellenbodenbach @ Neukirch	10.4
593350193020	SenTho	Sense @ Thörishaus, Sensematt	351.2
731616202785	SerMat	Sernf @ Matt	131.0
724975206204	SerSwa	Sernf @ Schwanden	210.1
559370206810	SeyVal	Seyon @ Valangin	112.3
693645225585	SihBwg	Sihl @ Blattwag, Radaraufz.	257.3
682145246890	SihZue	Sihl @ Zürich, Sihlhölzli	342.6
610680167840	SimLat	Simme @ Latterbach	563.2
602630141660	SimObd	Simme @ Oberried / Lenk	34.7
600060167090	SimObw	Simme @ Oberwil	343.7
595620155960	SimZwS	Simme @ Zweisimmen, Lischere	202.1
753806230476	SmiGms	Simmi @ GAMS Simmiwinkel	32.1
672455227153	SinSin	Sinserbach @ Sins	16.4
572420167540	SioVui	Siogne @ Vuippens, Château	43.4
594400119900	SnnSio	Sionne @ Sion	27.6
642037264717	SisEik	Sissle @ Eiken	122.6
645220261446	SisHor	Sissle @ Hornussen	37.0
749040244220	SitApp	Sitter @ Appenzell	74.4
742540253230	SitSGa	Sitter @ St. Gallen, Bruggen / Au	261.1
733496259643	SbcNdb	Sornbach @ Niederbüren, Husermüli	19.0
593520246290	SorDel	Sorne @ Delémont	213.9
645150261285	StaFrk	Staffeleggbach @ Frick	20.9
667878289182	SnaIlm	Steina @ Illmühle	47.6
750756262614	SacSac	Steinach @ Steinach, Mattenhof	25.2
721186229733	SteKal	Steinenbach @ Kaltbrunn, Steinenbrücke	18.6
732835277970	StiBot	Stichbach @ Bottighofen	16.3
714371297227	SkAWah	Stockacher Aach @ Wahlwies	236.4
639060247540	StuLos	Stüsslingerbach @ Lostorf	10.3
796455251598	SubSnb	Subersach @ Schönenbach (Hengstig)	30.8
651320223140	SuhObk	Suhre @ Oberkirch	75.6
646921233528	SuhRtn	Suhre @ Reitnau	134.5
647104246554	SuhSuh	Suhre @ Suhr	242.6
646112245970	SuhUtf	Suhre @ Unterentfelden	195.0
649632265866	SulSul	Sulzerbach @ Sulz	8.2
662342268505	SurDoe	Surb @ Döttingen	66.1
667078263737	SurLng	Surb @ Lengnau	31.9
669930262510	SurNiw	Surb @ Niederwenignen	15.7
586198221200	SuzBie	Suze, Totalabfluss @ Biel-Bienne, Hauserwehr	208.6
585519225712	SuzPer	Suze @ Péry, vigier Ciment	174.9
579810227350	SuzSon	Suze @ Sonceboz	127.2
568420223260	SuzVil	Suze @ Villeret, Pont de la STEP	59.7
669458267932	TaeWis	Tägerbach @ Wislikofen	13.2
653608255423	TalSDo	Talbach @ Schinznach-Dorf	13.4
532700173030	TltChv	Talent @ Chavronay	67.1

(continued on next page)

ID12	*ID6*	*River and site*	*Area [km²]*
741133228784	ThuASJ	Thur @ Alt St. Johann, Unterwasser, Chlostobel	42.3
693510272500	ThuAnd	Thur @ Andelfingen	1 701.6
733560263180	ThuHal	Thur @ Halden	1 085.0
723675252720	ThuJon	Thur @ Jonschwil, Mühlau	492.9
732391259249	ThuNdb	Thur @ Niederbüren, Golfplatz	690.5
736018228258	ThuSte	Thur @ Stein, Iltishag	83.2
721245117025	TicBlz	Ticino @ Bellinzona	1 517.5
716120135330	TicPol	Ticino @ Pollegio, Campagna	443.8
639979091039	AnzMac	Torrente Anza @ Macugnaga	39.5
653736092944	AnzSCa	Torrente Anza @ San Carlo	157.3
664574108152	BogPCa	Torrente Bogna @ Ponte Caddo	81.4
663354102130	OveVdo	Torrente Ovesca @ Villadossola	145.0
684260090031	SBeSan	Torrente San Bernardino @ Santino	119.7
688426088391	TSGVrb	Torrente San Giovanni @ Verbania	59.5
677233086632	StrGrv	Torrente Strona @ Gravellona	227.2
707750248010	ToeAlt	Töss @ Altlandenberg, Bauma	66.7
714210242375	ToeBei	Töss @ Beicher, Steg/Fischenthal	11.1
686005264990	ToeFre	Töss @ Freienstein	404.7
691460263820	ToeNef	Töss @ Neftenbach	343.3
703795255605	ToeRae	Töss @ Rämismühle	126.7
694260262120	ToeWue	Töss @ Wülflingen	262.7
572497160763	TrmTdT	Trême @ La Tour-de-Trême	27.0
709580092145	TrePTr	Tresa @ Ponte Tresa, Rocchetta	609.1
754664215385	TbbWar	Trübbach @ Wartau Trübbach, unteres Gufalon	8.2
631742197595	TruTru	Trueb @ Trubschachen	53.2
644830241641	UerHol	Uerke @ Holziken	25.1
796065288215	UArBeu	Untere Argen @ Beutelsau	127.7
778611286497	UArRen	Untere Argen @ Rengers	264.9
798807280563	UArSel	Untere Argen @ Seltmans	68.5
740165244800	UrnHun	Urnäsch @ Hundwil, Aeschentobel	64.6
607891213532	UrtKer	Urtenen @ Kernenried	73.9
728887257068	UzeUzw	Uze @ Uzwil, Thurau	12.6
733380164490	VlRVlP	Valserrhein @ Vals Platz	128.0
714110095680	VedAgn	Vedeggio @ Agno	99.9
532040154160	VenEcu	Venoge @ Eculbens, Les Bois	227.6
708420122920	VerLav	Verzasca @ Lavertezzo, Campiòi	185.1
554675146565	VevVev	Veveyse @ Vevey, Copet	64.5
754977215241	VWKWar	Vilterser-Wangser-Kanal @ Wartau Trübbach, Süsswinkel	56.8
621208265057	VioAug	Violenbach @ Augst	16.4
634030125900	VisVis	Vispa @ Visp	781.7
623422255512	VFrBub	Vordere Frenke @ Bubendorf-Talhaus	43.5
623463248115	VFrWal	Vordere Frenke @ Waldenburg	11.8
734997182035	VRhIla	Vorderrhein @ Ilanz	774.0
708723231762	WagRap	Wagnerbach @ Rapperswil-Jona, Rinderweid	10.5
645510185640	WEmSbg	Waldemme @ Sörenberg	23.2
588408168814	WSeSSe	Warme Sense @ Schwarzsee	20.2
786782264220	WeiKru	Weissach @ Krumbach-Zwing	198.0
793982268955	WeiObs	Weissach @ Oberstaufen	60.8
646553162656	WL2Gri	Weisse Lütschine (Schwarze Lütschine) @ Grindelwald, Gl’schlucht	45.1
635310164550	WL1Zwe	Weisse Lütschine @ Zweilütschinen	164.9
756795234005	WBKSlz	Werdenberger Binnenkanal @ Salez	182.6
611800269700	WieBas	Wiese @ Basel	441.8
630536283286	WieZel	Wiese @ Zell	207.0
641370225968	WigEgo	Wigger @ Egolzwil	180.8
637580237080	WigZof	Wigger @ Zofingen	366.2
644102252888	WilKtt	Wilenbergbach @ Küttigen	0.5
734679249995	WisDeg	Wissbach @ Degersheim Tal	14.5
665993239102	WsbBos	Wissenbach @ Boswil	11.2
671108234842	WsbMer	Wissenbach @ Merenschwand	10.0
734916229441	WThSte	Wissthur @ Stein, Büel	17.6
764716299791	WAcRai	Wolfegger Aach @ Rainpadent	158.9
641692258961	WoeWit	Wölflinswilerbach @ Wittnau	17.3
603005202455	WorItt	Worble @ Ittigen	67.1
675721300247	WutEwa	Wutach @ Ewattingen	342.5
666672275112	WutObl	Wutach @ Oberlauchringen	627.2
656516233148	WynRnc	Wyna @ Reinach	38.3
649012247534	WynSuh	Wyna @ Suhr	120.4
650860240671	WynUtk	Wyna @ Unterkulm	92.3

D

Meteorological data used

Table D.1: List of selected precipitation stations with daily data that contribute to the interpolation of MAP of at least one catchment, revealing coordinates (X, Y) and elevation (E). For details see Mas et al. (2023).

ID	*Site*	*X [m]*	*Y [m]*	*E [m a.s.l.]*
ABE	Aarberg	588 051	209 518	493
FRABD	Abondance	546 157	126 380	949
DL21	Achberg-Doberatsweiler	769 883	275 763	498
AST	Ackersand Stalden	633 630	121 150	700
COM	Acquarossa / Comprovasco	714 998	146 440	575
ABO	Adelboden	609 350	149 001	1 326
AFT	Affeltrangen	719 070	265 660	479
AIG	Aigle	560 400	130 713	381
AIR	Airolo	688 910	153 400	1 139
ALT	Altdorf	690 174	193 558	438
ALS	Altstätten, SG	759 910	250 202	430
DL146	Altusried-Muthmannshofen	799 300	296 898	730
AMW	Amriswil	741 785	268 332	420
AND	Andeer	752 687	164 035	987
AFI	Andelfingen	693 810	273 070	382
OSAND	Andelsbuch	784 054	253 121	553
ANT	Andermatt	687 444	165 044	1 438
APP	Appenzell	748 012	245 040	750
ARB	Arbon	750 520	263 110	402
FR74016001	ARCHAMPS	499 643	109 756	560
FR74056004	ARGENTIERE	560 449	92 544	1 275
ARI	Arisdorf	625 310	261 860	480
ARO	Arosa	771 030	184 825	1 878
DL7135	Aulendorf-Haslach	767 411	315 178	565
AVB	Avers am Bach	761 985	146 785	2 000
FR74024001	AYZE	522 072	103 611	449
101543	Baad	803 684	244 018	1 305
IYBAD	Baceno / Alpe Devero	663 269	129 730	1 581
BAC	Bachtel	709 440	239 140	1 110
BAD	Baden	665 490	259 140	385
DL275	Balderschwang	800 946	260 553	1 039
BAW	Barmelweid	640 160	252 380	770
BAS	Basel / Binningen	610 911	265 600	316
BAU	Baulmes	530 050	182 450	642
BAM	Bauma	710 805	247 005	667
FR74031001	BEAUMONT	496 904	105 488	690
FR39047001	BELLEFONTAINE	494 617	157 260	1 030
BEY	Bellelay	579 603	234 880	923
BLZ	Bellinzona	721 060	116 800	225
BEP	Belp	605 140	193 805	515
BER	Bern / Zollikofen	601 929	204 409	552
DL440	Bernau-Goldbach	643 962	296 215	928
BEC	Bernina-Curtinatsch	795 795	146 486	2 090
BMU	Beromünster	657 200	228 760	642
BEX	Bex	565 806	121 511	402
BZN	Beznau	659 975	267 750	327
BIA	Biasca	718 550	132 800	278
BIN	Binn	657 892	135 176	1 448
BIS	Bisisthal	705 770	200 450	785

(continued on next page)

ID	Site	X [m]	Y [m]	E [m a.s.l.]
BIV	Bivio	771 281	148 119	1 856
BIE	Bière	515 888	153 206	683
100362	Blons	783 091	233 119	772
DL548	Blumberg	682 168	299 652	707
BLU	Blumenstein	606 260	177 010	655
DL573	Bodman-Ludwigshafen	720 407	295 051	415
DL574	Bodnegg-Billen	768 419	287 532	640
FR74037002	BOEGE	519 462	118 520	750
IYPIZ	Bognanco / Pizzanco	657 131	108 328	1 089
BOT	Boltigen	596 130	164 180	855
BOS	Bosco-Gurin	680 879	130 027	1 486
BSP	Bourg-St-Pierre	582 155	88 270	1 664
BRA	Braggio	729 975	128 600	1 315
OSBRB	Brand bei Bludenz	775 069	219 936	956
BRW	Braunwald	717 942	199 651	1 299
OSBRE	Bregenz	773 841	263 492	377
DL684	Breitnau	647 636	309 977	1 001
BRZ	Brienz	647 552	176 803	567
BRI	Brig	640 567	129 069	665
BSG	Brissago	698 200	108 390	280
BRT	Bristen	696 223	180 373	784
BRP	Brusio-Piazzo	806 477	127 184	856
DL754	Buchau, Bad	762 368	325 270	585
DL758	Buchenberg	810 283	286 834	900
DL759	Buchenberg-Kreuzthal	802 034	287 660	845
BUS	Buchs / Aarau	648 389	248 365	386
BUF	Buffalora	816 494	170 225	1 968
FRE	Bullet / La Frétaz	534 221	188 081	1 205
BUD	Burgdorf	613 020	212 670	525
OSBOD	Bödele	778 795	254 888	1 103
BUE	Bülach	682 010	263 780	402
DL779	Bürchau	629 148	291 055	710
IYCAF	Carcoforo	647 490	84 143	1 237
CAV	Cavaglia	799 850	138 470	1 706
FR39085002	CERNIEBAUD	498 897	176 788	966
CEV	Cevio	689 688	130 565	417
CHZ	Cham	677 758	226 878	442
FRCHX	Chamonix	556 924	87 014	989
FRCMT	Charquemont	553 144	230 082	834
CHA	Chasseral	570 847	220 158	1 599
FR74063002	CHATEL	552 474	123 028	1 135
CHY	Chavornay	531 887	172 741	439
FR01104001	CHEZERY	481 063	122 122	700
CHU	Chur	759 471	193 157	556
CBS	Châbles	552 495	186 320	589
CHD	Château-d’Oex	577 039	147 654	1 029
CHX	Chéserex	502 600	139 350	532
CIM	Cimetta	704 433	117 452	1 661
FR74080001	CLUSAZ (LA)	521 580	83 472	1 150
FR74081002	CLUSES	532 284	103 544	500
CDM	Col des Mosses	573 817	137 852	1 412
GSB	Col du Grand St-Bernard	579 200	79 720	2 472
COL	Coldrerio	721 080	79 235	347
IYCOC	Colico	750 371	111 494	180
COG	Combe-Garot	551 220	201 450	532
FR74083002	COMBLOUX	536 964	82 681	1 183
CPS	Compesières	498 120	112 020	474
FRCTM	Contamine-sur-Arve	515 083	108 987	402
FR74085001	CONTAMINES MJ	544 826	74 767	1 180
COS	Cossonay	527 563	162 465	590
COY	Courtelary	573 622	225 597	695
COU	Couvet	540 607	198 345	728
IYCRO	Crodo	668 287	119 841	508
IYCUR	Cursolo	687 283	105 874	888
DL5688	Dachsberg-Wolpadingen	650 074	283 516	880
100263	Dalaas	796 497	223 011	951
DAV	Davos	783 514	187 457	1 594
DLDEG	Deggenhausertal	747 743	296 332	661
DEM	Delémont	593 269	244 543	439

(continued on next page)

ID	Site	X [m]	Y [m]	E [m a.s.l.]
DIE	Diessenhofen	696 730	283 130	405
DIT	Dietikon	672 870	251 875	385
DMA	Dischma	786 600	182 990	1 710
DIS	Disentis / Sedrun	708 188	173 789	1 197
FR01143001	DIVONNE	501 363	136 944	488
IYDOD	Domodossola	666 780	106 089	200
DL1018	Donaueschingen	679 652	310 737	677
100735	Doren	782 555	262 734	710
IYDRU	Druogno	676 305	109 663	779
EBK	Ebnat-Kappel	726 346	237 176	623
OSEBN	Ebnit	774 067	246 953	1 053
ECH	Echallens	537 455	160 430	603
EGO	Egolzwil	642 913	225 540	521
EIT	Eigenthal	659 340	203 880	1 114
EIN	Einsiedeln	699 983	221 068	910
DL1176	Eisenbach	662 041	312 880	976
ELM	Elm	732 265	198 425	958
DL1227	Emmingen-Liptingen	706 102	309 989	744
ENG	Engelberg	674 156	186 097	1 035
ENT	Entlebuch	647 935	204 165	768
FREPE	Epenoy	518 642	220 134	702
EPT	Eptingen	628 720	248 410	565
ERB	Erlenbach im Simmental	608 350	167 300	683
ERN	Ernen	653 160	138 025	1 000
EKO	Eschlikon	715 699	256 836	578
FR74116002	ETEAUX	510 001	101 944	805
FR74119002	EVIAN	532 923	138 723	395
EVD	Evilard / Leubringen	584 412	221 985	725
EVL	Evolène	604 720	106 510	1 375
EVO	Evolène / Villa	605 415	106 740	1 825
FAH	Fahy	562 458	252 676	596
FAI	Faido	704 950	148 266	747
DLFEB	Feldberg / Schwarzwald	642 285	302 865	1 440
OSFEK	Feldkirch	764 270	237 852	391
FEY	Fey	586 725	115 180	737
FIL	Filisur	772 250	171 320	1 030
FIO	Fionnay	589 960	97 765	1 500
FLW	Flawil	733 050	252 940	570
FLU	Flühli, LU	644 332	193 311	939
FRF	Frauenfeld	709 480	270 170	393
GRA	Fribourg / Posieux	575 182	180 076	646
DL1476	Fridingen	710 571	319 914	634
DL1510	Fronreute-Blitzenreute	760 462	303 995	584
FRC	Fruence	558 860	152 799	809
FRU	Frutigen	616 773	160 884	756
100438	Fussach	767 788	261 369	400
FR74133001	GAILLARD	505 206	114 524	400
OSGAL	Galtür	809 004	205 515	1 536
GEI	Geils	605 670	145 015	1 710
DLGEI	Geisingen	690 327	308 879	623
GEP	Gempen, SO	616 260	260 400	585
GEA	Genève-Aire	495 935	116 925	376
GVE	Genève-Cointrin	498 904	122 631	412
FR74134002	GETS (LES)	540 647	112 194	1 172
FR01173001	GEX	494 099	132 998	612
GIH	Giswil	657 320	188 980	471
GLA	Glarus	723 752	210 567	516
DL1727	Grafenhausen/Hochschwarzwald	660 640	292 008	948
FR74136003	GRAND BORNAND	522 947	91 459	1 300
GRH	Grimsel Hospiz	668 583	158 215	1 980
GWA	Grindelwald	645 793	164 458	1 158
GRO	Grono	733 016	124 090	323
GHS	Grosshöchstetten	616 015	194 885	755
GRY	Gryon	571 520	125 125	1 146
GRC	Grächen	630 738	116 062	1 605
GIN	Grüningen	701 580	236 750	520
GUS	Grüsch	766 900	204 900	590
GSG	Gsteig, Gstaad	587 680	136 130	1 196
GUG	Guglera	585 040	177 635	877

(continued on next page)

ID	Site	X [m]	Y [m]	E [m a.s.l.]
GTT	Guttannen	665 296	167 601	1 055
DL4657	Görwihl-Burg	647 871	278 862	782
GOS	Göschenen	688 477	171 926	950
GOA	Göscheneralp	681 250	166 790	1 745
GUE	Gütsch ob Andermatt	690 050	167 475	2 283
FR74140001	HABERE-POCHE	526 961	122 127	1 093
FR73132001	HAUTELUCE	537 775	69 276	1 215
HTW	Herbetswil	611 290	238 440	544
DL2146	Herdwangen-Schönach	733 528	305 197	607
HEB	Herzogenbuchsee	619 970	227 350	467
HIR	Hinterrhein	733 900	153 980	1 611
DL2241	Hochdorf-Unteressendorf	774 922	321 097	567
DL2496	Hohenfels, Kr.Konstanz-Kalkofen	725 020	303 989	635
FR74143003	HOUCHES (LES)	550 486	82 534	1 005
HER	Hérémence	597 370	114 165	1 238
DL2359	Hüfingen-Fürstenberg	683 355	305 032	786
ILZ	Ilanz	735 685	181 965	698
DL2404	Immenstadt (Wärterhaus)	808 293	269 820	935
DL2405	Immenstadt-Reute	807 752	276 670	960
OSINL	Innerlaterns	774 396	236 489	977
INN	Innerthal	712 019	218 326	903
INT	Interlaken	633 019	169 093	577
IST	Isenthal	685 460	196 110	778
JAU	Jaun	587 520	162 280	1 030
FRJOY	Joncherey	567 724	264 452	310
FR25318001	JOUGNE	519 799	179 329	988
JUS	Jussy	508 910	120 364	466
DL2513	Kandern-Sitzenkirch	617 422	287 273	416
KAS	Kandersteg	618 313	149 198	1 178
KIE	Kiental	622 110	159 075	930
KIS	Kiesen	610 270	185 510	535
FR68165001	KIFFIS	593 737	254 137	576
KIG	Kilchberg BL	634 650	252 860	570
KSE	Kleine Scheidegg	639 925	159 425	2 061
DL5866	Klettgau-Grießen	673 076	275 247	390
KLA	Klosters / Aeuja	786 857	193 366	1 186
100826	Klösterle	800 866	223 527	1 057
DLKON	Konstanz	731 513	282 223	396
OSKOP	Kops	803 552	206 007	1 778
KUB	Küblis	778 470	198 480	815
KUE	Küsnacht, ZH	686 700	240 570	412
AUB	L' Auberson	523 852	186 295	1 096
BRL	La Brévine	536 981	203 974	1 050
CDF	La Chaux-de-Fonds	550 919	214 861	1 018
CUE	La Cure	495 298	146 347	1 185
DOL	La Dôle	497 061	142 362	1 669
VST	La Valsainte	580 110	166 298	1 042
FR25320001	LABERGEMENT	511 482	181 670	858
LAC	Lachen / Galgenen	707 637	226 334	468
DL2846	Langenargen-Oberdorf	760 757	276 490	416
LAB	Langenbruck	624 250	244 720	731
LAG	Langnau i.E.	628 005	198 792	745
LAT	Latsch	777 273	166 618	1 407
OSLAU	Latschau	784 889	216 568	951
LBG	Lauenen bei Gstaad	590 910	141 700	1 250
LAF	Laufen	604 455	251 915	357
LFB	Laufenburg	646 900	267 700	330
LSN	Lausanne	538 976	153 256	601
LTB	Lauterbrunnen	635 851	160 291	815
FR74034001	LE BIOT	536 977	125 516	690
CTA	Le Châtelard	564 160	103 590	1 242
FR74136400	Le Grand Bornand	523 685	91 639	1 270
LOC	Le Locle	547 260	211 730	920
MLS	Le Moléson	567 723	155 072	1 974
FRLRS	Le Russey	547 025	223 463	845
SET	Le Sentier	506 720	161 620	1 015
FR74056003	LE TOUR	561 881	94 758	1 460
LEH	Lenzerheide	761 860	175 890	1 400
AVA	Les Avants	561 860	145 050	1 012

(continued on next page)

ID	*Site*	*X [m]*	*Y [m]*	*E [m a.s.l.]*
BNE	Les Brenets	544 675	213 685	907
FR74014002	LES CARROZ	538 464	97 319	1 160
CHB	Les Charbonnières	513 821	169 387	1 045
DIB	Les Diablerets	579 038	132 867	1 191
FR25254001	LES FOURGS	523 494	187 474	1 138
MAR	Les Marécottes	567 375	107 577	990
PSB	Les Plans-sur-Bex	572 960	122 720	1 070
PDM	Les Ponts-de-Martel	545 880	205 400	1 052
FR39470001	LES ROUSSES	494 260	148 739	1 110
LEU	Leukerbad	614 083	135 090	1 286
DL2967	Leutkirch	793 379	300 282	655
FRLEV	Levier	499 937	200 647	663
OTL	Locarno / Monti	704 160	114 350	366
LON	Longirod	509 387	150 106	900
FRLUC	Lucelle	587 142	254 185	641
LUG	Lugano	717 873	95 884	273
LUN	Lungern	655 275	181 800	740
LUT	Luthern	636 465	212 020	767
LUZ	Luzern	665 540	209 848	454
DL3041	Löffingen-Dittishausen	669 484	307 474	776
LOB	Löwenburg	587 680	251 985	738
OSLUN	Lünersee	776 073	213 155	1 966
IYMCM	Macugnaga / Passo del Moro	641 668	94 084	2 766
MAG	Magadino / Cadenazzo	715 479	113 161	203
DL3130	Maierhöfen	795 745	280 254	745
DL1492	Malsburg-Marzell-Friedrichsheim	622 195	292 415	852
MAC	Marcelin	528 774	152 105	374
IYMMR	Marienberg	835 681	177 352	1 259
DL3174	Markdorf	745 711	288 551	515
MAS	Marsens	571 758	167 316	714
MAB	Martigny / Ravoire	570 860	106 590	462
MAT	Martina	830 464	196 986	1 041
MAU	Mauvoisin	592 520	94 600	1 841
FR74173001	MEGEVE	535 484	78 528	1 080
MER	Meiringen	655 844	175 930	588
MEB	Menzberg	642 430	209 660	1 035
MEV	Mervelier	603 884	243 975	540
100503	Meschach	769 760	245 174	857
MES	Mesocco	737 850	139 825	830
FR01247003	MIJOUX	491 679	138 000	1 041
MST	Monstein	778 080	176 230	1 575
MOD	Montagne-du-Droit	561 830	222 150	1 170
MOB	Montagnier, Bagnes	583 420	102 460	848
MVE	Montana	601 706	127 482	1 427
CLA	Montreux-Clarens	558 560	143 600	405
MGI	Morgins	554 720	120 680	1 340
MMO	Mormont	569 727	254 223	535
FR25411004	MORTEAU	536 285	212 072	790
FR74191001	MORZINE	543 602	114 356	960
MSG	Mosogno	692 803	117 050	771
FR25413001	MOUTHE	506 009	173 604	940
MOU	Moutier	594 940	235 690	579
MUR	Muri, AG	667 276	235 323	577
100792	Möggers	778 799	270 591	1 010
MOE	Möhlin	633 053	269 147	344
MUE	Mürren	634 700	156 410	1 645
NAP	Napf	638 132	206 078	1 403
NEU	Neuchâtel	563 086	205 559	485
DLNEU	Neuhausen ob Eck / Unterschwandorf	716 142	312 459	615
FR74203001	NOVEL	549 955	135 400	963
CGI	Nyon / Changins	506 880	139 573	455
OBI	Oberiberg	701 841	210 464	1 075
DL3714	Oberreute	788 299	270 011	896
DL3716	Oberried-Hofsgrund	634 414	305 816	1 023
DL3717	Oberried-Sankt Wilhelm	638 514	304 174	920
OSOBV	Obervermunt	801 538	199 688	1 929
IYOGA	Oga / S. Colombano	820 248	148 717	2 248
OTN	Olten	634 530	243 750	413
FR25432001	ORCHAMPS-VENNES	530 322	219 944	761

(continued on next page)

ID	Site	X [m]	Y [m]	E [m a.s.l.]
ORS	Orsières	577 022	96 695	929
OSPAR	Partenen	799 189	205 491	980
BEH	Passo del Bernina	798 422	143 020	2 260
PAV	Payerne-Ville	561 615	187 040	448
FR74211001	PERS-JUSSY	509 377	106 800	580
PIL	Pilatus	661 910	203 410	2 106
PIO	Piotta	695 888	152 261	990
COV	Piz Corvatsch	783 150	143 521	3 302
FRPTR	Pontarlier	516 126	195 060	781
POT	Ponte Tresa	710 110	91 630	274
PON	Pontresina	788 700	151 730	1 774
ROB	Poschiavo / Robbia	801 850	136 180	1 078
PUY	Pully	540 811	151 514	455
PUD	Punt la Drossa	810 560	170 640	1 710
DL4053	Radolfzell-Markelfingen	717 144	289 518	407
FR74221001	REPOSOIR (LE)	530 249	96 151	965
RIE	Ried, Lötschen	628 275	140 370	1 500
WHF	Riedholz-Wallierhof	609 375	231 520	520
ROE	Robièi	682 587	144 091	1 896
ROM	Romont	561 476	172 622	692
SRL	S-charl	821 200	178 020	1 830
SBE	S. Bernardino	734 112	147 296	1 638
SBA	Saas Balen	637 535	112 170	1 461
SAA	Saas-Fee	637 650	106 200	1 785
SAI	Saignelégier	566 390	233 730	993
FRSTD	Saint-Dizier-lÉvêque	563 841	257 525	504
FR74256001	SALLANCHES	538 902	87 020	541
DL4358	Sallneck	625 171	285 789	610
SAM	Samedan	787 210	155 700	1 708
FR74258002	SAMOENS	544 936	103 949	749
SAR	Sargans	752 046	213 364	590
SRN	Sarnen	661 580	193 690	475
SAG	Sattel-Aegeri	690 999	215 145	790
DL4409	Saulgau, Bad-Bolstern	750 767	317 164	630
SVG	Savognin	765 387	162 663	1 172
SHA	Schaffhausen	688 698	282 796	438
SCH	Schleitheim	678 225	288 730	499
DL4620	Schopfheim-Schweigmatt	633 266	281 315	723
OSSCP	Schoppernau	794 988	243 262	791
OSSCK	Schröcken	800 337	237 940	1 195
DL4572	Schussenried, Bad-Olzreute	767 659	320 259	586
SCE	Schwarzenegg	621 130	182 730	920
SWA	Schwägalp	742 180	235 650	1 348
SCA	Schänis	719 940	225 580	415
OSSBA	Schönenbach	795 539	250 105	992
SCU	Scuol	817 135	186 393	1 303
SED	Sedrun	702 480	170 825	1 400
SIA	Segl-Maria	778 574	144 976	1 804
SPA	Sempach	657 433	220 760	532
SEM	Semsales	561 110	158 430	873
FR74266001	SERVOZ	547 923	86 836	815
SEV	Sevelen	755 605	221 302	457
SRE	Sierre	609 138	127 458	536
SIH	Sihlbrugg	686 318	230 586	549
SIO	Sion	591 630	118 575	482
SOG	Soglio	761 393	134 474	1 086
SDO	Splügen-Dorf	744 420	157 435	1 460
FR74252001	ST SIGISMOND	536 054	103 091	1 020
OSANT	St. Anton am Arlberg	814 518	223 912	1 254
SAN	St. Antönien	781 634	205 103	1 456
STU	St. Urban	631 125	230 015	491
IYVAL	St. Valentin a.d. Haide	835 955	185 172	1 448
SMM	Sta. Maria, Val Müstair	828 860	165 579	1 383
SBO	Stabio	716 050	77 966	353
SNS	Stans	668 918	202 459	438
STB	Starkenbach	737 313	227 576	897
STE	Steckborn	715 200	280 150	399
DL4881	Stockach	717 981	302 139	532
IYMOE	Stresa / Mottarone	678 806	81 620	1 452

(continued on next page)

ID	*Site*	*X [m]*	*Y [m]*	*E [m a.s.l.]*
IYSOO	Stresa / Someraro	683 315	82 499	375
STP	Stöckalp	664 320	183 550	1 070
SUS	Susch	802 002	181 593	1 416
SAE	Säntis	744 200	234 920	2 502
TAM	Tamins	750 155	188 614	667
IYTAU	Taufers i.M.	831 404	169 576	1 183
TEU	Teufen	747 810	250 410	835
FR74280001	THONES	513 375	81 304	630
FRTHO	Thonon-les-Bains	524 152	135 511	326
THU	Thun	611 200	177 640	570
THS	Thusis	753 155	175 089	672
OSTHU	Thüringen	776 724	230 239	532
DL5047	Titisee-Neustadt-Langenordnach	656 392	310 156	870
TRU	Trun	719 985	178 224	834
TST	Tschiertschen	765 538	187 679	1 273
ULR	Ulrichen	666 740	150 760	1 345
UNK	Unterkulm	650 838	241 212	454
UAG	Unterägeri	686 475	221 000	733
URB	Urnerboden	712 650	195 250	1 395
URN	Urnäsch	739 205	241 765	825
FR74286001	VACHERESSE	540 803	129 691	790
VAR	Valeyres-sous-Rances	530 230	178 350	512
VVI	Vallorbe-Ville	519 400	174 060	748
FR74290002	VALLORCINE	560 405	97 714	1 300
VLS	Vals	734 016	165 551	1 242
IYVAO	Varallo	664 916	74 560	419
IYVAZ	Varzo / San Domenico	658 178	122 299	1 255
IYPAZ	Verbania / Pallanza	686 121	86 448	152
VEV	Vevey / Corseaux	552 106	146 847	405
VIO	Vicosoprano	768 485	135 866	1 089
VIT	Villars-Tiercelin	544 198	163 650	859
VIS	Visp	631 149	128 020	639
VAE	Vättis	752 732	197 282	939
DL5318	Waldsee, Bad-Dinnenried	771 595	305 901	597
WIE	Wasen im Emmental	627 850	210 550	770
WEE	Weesen	724 983	221 383	425
DL3047	Weil am Rhein-Haltingen	613 656	273 293	273
DLWEI	Weingarten	763 437	297 359	394
WID	Widnau	766 485	248 850	411
WBR	Wil bei Rafz	680 340	273 225	406
WCH	Wilchingen	677 050	280 200	420
DL5980	Wilhelmsdorf	748 489	303 302	619
WIS	Wimmis	615 110	168 800	669
WIN	Winterthur-Seen	699 845	259 054	506
WIW	Witzwil	570 735	205 414	434
DL5666	Wolfegg (Neckenfurt)	776 167	297 927	623
DL5723	Wurzach, Bad	784 347	309 340	657
WGI	Wängi	714 200	261 900	473
YVN	Yverdon-les-Bains	539 855	181 540	433
ZER	Zermatt	624 350	97 560	1 638
ZNZ	Zernez	802 720	175 230	1 471
ZEV	Zervreila	728 780	160 000	1 738
ZUB	Zugerberg	682 975	222 000	920
ZWE	Zweisimmen	595 870	155 480	1 015
OSZUR	Zürs	806 493	228 174	1 657
DL5138	Überlingen/Bodensee	728 741	292 603	446
DL498	Ühlingen-Birkendorf	665 434	288 661	760

Table D.2: List of selected temperature stations with daily data that contribute to the interpolation of MAT of at least one catchment, revealing coordinates (X, Y) and elevation (E). For details see Mas et al. (2023).

ID	*Site*	*X [m]*	*Y [m]*	*E [m a.s.l.]*
COM	Acquarossa / Comprovasco	714 998	146 440	575
ABO	Adelboden	609 350	149 001	1 326
ALT	Altdorf	690 174	193 558	438
ANT	Andermatt	687 444	165 044	1 438
ARO	Arosa	771 030	184 825	1 878
FR74024001	AYSE (AYZE)	522 072	103 611	449
RAG	Bad Ragaz	756 909	209 350	496
BAS	Basel / Binningen	610 911	265 600	316
FR73034002	BEAUFORT (BEAUFORT-SUR-DORON)	532 205	60 308	1 030
BER	Bern / Zollikofen	601 929	204 409	552
OSBRE	Bregenz	773 841	263 492	377
BUF	Buffalora	816 494	170 225	1 968
FRBAL	Bâle / Mulhouse	605 367	273 742	214
FR74056001	CHAMONIX-MONT-BLANC (CHAMONIX)	556 469	86 590	1 042
FR25127001	CHARQUEMONT	552 763	229 952	884
CHM	Chaumont	565 060	211 006	1 136
CHU	Chur	759 471	193 157	556
CHD	Château-d’Oex	577 039	147 654	1 029
CIM	Cimetta	704 433	117 452	1 661
GSB	Col du Grand St-Bernard	579 200	79 720	2 472
FR74087001	CONTAMINE-SUR-ARVE (CONTAMINE-SUR- ARVE)	515 086	109 163	452
DAV	Davos	783 514	187 457	1 594
DEM	Delémont	593 269	244 543	439
DIS	Disentis / Sedrun	708 188	173 789	1 197
EBK	Ebnat-Kappel	726 346	237 176	623
EIN	Einsiedeln	699 983	221 068	910
ELM	Elm	732 265	198 425	958
ENG	Engelberg	674 156	186 097	1 035
FR25219001	EPENOY	518 921	220 255	742
DLFEB	Feldberg / Schwarzwald	642 285	302 865	1 440
DL1346	Feldberg/Schwarzwald	642 286	302 865	1 490
OSFEK	Feldkirch	764 270	237 852	391
GRA	Fribourg / Posieux	575 182	180 076	646
OSGAL	Galtür	809 004	205 515	1 536
GVE	Genève-Cointrin	498 904	122 631	412
GLA	Glarus	723 752	210 567	516
GRH	Grimsel Hospiz	668 583	158 215	1 980
FR74137001	GROISY (GROISY_SAPC)	502 088	96 463	670
GRO	Grono	733 016	124 090	323
GRC	Grächen	630 738	116 062	1 605
GUE	Gütsch ob Andermatt	690 050	167 475	2 283
HLL	Hallau	677 456	283 472	419
INT	Interlaken	633 019	169 093	577
FR90056002	JONCHEREY	567 201	264 021	359
JUN	Jungfraujoch	641 930	155 275	3 580
DL2559	Kempten	817 254	289 862	705
DLKLI	Klippeneck	698 042	329 166	928
BRL	La Brévine	536 981	203 974	1 050
CDF	La Chaux-de-Fonds	550 919	214 861	1 018
FR25320001	LABERGEMENT-SAINTE-MARIE (LABERGEMENT)	511 482	181 670	858
FR39275004	LAMOURA	486 238	138 789	1 124
LAG	Langnau i.E.	628 005	198 792	745
FRLRS	Le Russey	547 025	223 463	845
FR74134002	LES GETS (GETS (LES))	540 647	112 194	1 172
OTL	Locarno / Monti	704 160	114 350	366
LUG	Lugano	717 873	95 884	273
LUZ	Luzern	665 540	209 848	454
MAG	Magadino / Cadenazzo	715 479	113 161	203
IYMMR	Marienberg	835 681	177 352	1 259
FR74173001	MEGEVE	535 484	78 528	1 080
MER	Meiringen	655 844	175 930	588
MVE	Montana	601 706	127 482	1 427
FR25547001	MONTBELIARD (SOCHAUX)	553 018	261 949	318
GEN	Monte Generoso	722 503	87 456	1 600

(continued on next page)

ID	*Site*	*X [m]*	*Y [m]*	*E [m a.s.l.]*
FR25413001	MOUTHE	506 009	173 604	940
DL259	Müllheim	614 985	295 113	273
DLMUE	Müllheim	614 964	295 104	224
NAS	Naluns / Schlivera	815 374	188 987	2 400
OSNAU	Nauders	833 017	197 875	1 279
NEU	Neuchâtel	563 086	205 559	485
CGI	Nyon / Changins	506 880	139 573	455
DL3730	Oberstdorf	814 143	253 607	806
DLOBD	Oberstdorf	814 151	253 624	758
BEH	Passo del Bernina	798 422	143 020	2 260
FR25453001	PIERREFONTAINE-LES-VARANS (PIERREFONTAINE)	531 083	229 919	695
PIO	Piotta	695 888	152 261	990
COV	Piz Corvatsch	783 150	143 521	3 302
FR25462001	PONTARLIER	516 353	195 141	831
ROB	Poschiavo / Robbia	801 850	136 180	1 078
DL4175	Rheinfelden	625 099	267 640	282
ROE	Robièi	682 587	144 091	1 896
SBE	S. Bernardino	734 112	147 296	1 638
HAI	Salen-Reutenen	719 099	279 046	718
SAM	Samedan	787 210	155 700	1 708
SHA	Schaffhausen	688 698	282 796	438
OSSCP	Schoppernau	794 988	243 262	791
OSSCK	Schröcken	800 337	237 940	1 195
SCU	Scuol	817 135	186 393	1 303
SIA	Segl-Maria	778 574	144 976	1 804
DLSIG	Sigmaringen	730 847	326 083	535
DL4703	Sigmaringen-Laiz	730 854	326 082	581
SIO	Sion	591 630	118 575	482
OSANT	St. Anton am Arlberg	814 518	223 912	1 254
STG	St. Gallen	747 865	254 588	775
IYVAL	St. Valentin a.d. Haide	835 955	185 172	1 448
SMM	Sta. Maria, Val Müstair	828 860	165 579	1 383
SBO	Stabio	716 050	77 966	353
SAE	Säntis	744 200	234 920	2 502
IYTAU	Taufers i.M.	831 404	169 576	1 183
FR74280001	THONES	513 375	81 304	630
FR74281001	THONON-LES-BAINS (THONON-INRA)	524 306	135 501	376
30610	Valtournenche - Lago Cignana	612 159	80 820	2 070
30620	Valtournenche - Lago Goillet	617 375	86 685	2 471
DLVIS	Villingen-Schwenningen	676 223	322 146	674
DLWEI	Weingarten	763 437	297 359	394
DL4094	Weingarten, Kr. Ravensburg	763 437	297 349	440
WFJ	Weissfluhjoch	780 614	189 634	2 691
SMA	Zürich / Fluntern	685 116	248 065	555
KLO	Zürich / Kloten	682 710	259 338	426